Mitochondrial Function Regulates Telomere Elongation during Embryogenesis

Yasmyn Ellaynah Winstanley



Robinson Research Institute, Discipline of Obstetrics and Gynaecology, School of Medicine, Faculty of Health Sciences, The University of Adelaide, Australia

A thesis submitted to the University of Adelaide in fulfilment of the requirements for admission to the degree of Doctor of Philosophy

May 2021

Table of Contents

Abstract ..... **vi**
Declaration ..... **viii**
Acknowledgements ..... **ix**
Publications Arising During PhD Candidature ..... **x**
Abstracts Arising From This Thesis ..... **xi**
List of Figures ..... **xii**
List of Tables ..... **xvi**
Abbreviations ..... **xvii**

CHAPTER 1 LITERATURE REVIEW **1**

1.1 Introduction 2
1.2 Mammalian embryo development 3
1.2.1 Folliculogenesis and oocyte maturation 3
1.2.2 Fertilisation 6
1.2.3 Pre-implantation embryo development 6
1.2.4 Epigenetic reprogramming 10
1.2.5 Pluripotency 12
1.2.6 Pre-implantation development reprogramming impacts lifelong health 14
1.2.7 Major cellular components are inherited 16
1.3 Mitochondria 17
1.3.1 Mitochondrial structure and function 17
1.3.2 Mitochondrial localisation and utilisation during oocyte maturation and early embryogenesis 20
1.3.3 Mitochondrial DNA (mtDNA) 21
1.3.4 Mitochondrial DNA replication patterns in oocyte growth, maturation and embryogenesis 22
1.4 Telomeres 24
1.4.1 Telomere structure and function 24
1.4.2 The end replication problem 26
1.4.3 Telomere elongation mechanisms 27
1.4.4 Epigenetic regulation of telomeres 35
1.4.5 Telomeres in early development 36
1.4.6 Telomere length resetting 38

1.5 Links between mitochondria and telomeres 44
1.5.1 Mitochondrial dysfunction and telomere dysfunction display a bi-directional relationship 44
1.5.2 Mitochondria and telomeres in aging and disease 45
1.5.3 Mitochondrial metabolism intermediates can affect epigenetic regulation of gene expression 47
1.6 Summary and outline of aims 50
1.7 References 51

CHAPTER 2 DEVELOPMENT OF A QPCR "TRIPLE TEST" FOR ASSESSMENT OF TELOMERE AND mtDNA IN INDIVIDUAL OOCYTES AND EMBRYOS 84

2.1 Introduction 85
2.2 Materials and Methods 90
2.2.1 Mice 90
2.2.2 Collection, DNA extraction, and qPCR of whole ovaries 90
2.2.3 Derivation of oocytes, early embryos, and blastocysts 91
2.2.4 Extraction and purification 92
2.2.5 Agarose Gel 93
2.2.6 Sample lysis and preparation for qPCR 94
2.2.7 Triple test qPCR assay 94
2.2.8 Statistical analysis 96
2.3 Results 97
2.3.1 Validation of primer efficiencies and reference selection 97
2.3.2 Optimising established method 100
2.3.3 Optimisation of mtDNA extraction efficiency 107
2.3.4 Re-design and validation of the Triple Test qPCR 112
2.4 Discussion 117
2.5 References 119
2.6 Supplementary information 122

CHAPTER 3 TELOMERE ELONGATION AND mtDNA REGULATION DURING MOUSE PRE-IMPLANTATION EMBRYOGENESIS 127

3.1 Introduction 128
3.2 Materials and Methods 132
3.2.1 Mice 132
3.2.2 Derivation of oocytes, early embryos, and blastocysts 132

3.2.3 Blastocyst dissections 134
3.2.4 Sample collection 135
3.2.5 Sample lysis and preparation for qPCR.....136
3.2.6 Triple test qPCR assay.....136
3.2.7 Embryo sex determination.....138
3.2.8 RT-PCR for mRNA expression of telomere elongation and stability associated genes.....139
3.2.9 Immunofluorescence 140
3.2.10 Statistical analysis.....143
3.3 Results.....144
3.3.1 Telomere length and mtDNA copy number remain stable throughout oocyte maturation 144
3.3.2 Telomere elongation occurs throughout pre-implantation embryogenesis.....148
3.3.3 Telomere length is reset following fertilisation, prior to the first mitosis.....156
3.3.4 Parthenogenetically activated embryos display similar telomere dynamics to IVF embryos 158
3.3.5 Male and female embryos do not differ in telomere length or mtDNA content at the blastocyst stage.....165
3.3.6 IVF and parthenogenetically derived blastocysts display differences in cell-specific telomere elongation 167
3.3.7 Telomere elongation mechanisms are sensitive to culture conditions 170
3.4 Discussion 173
3.5 References 180
3.6 Supplementary information.....188

CHAPTER 4 ROTENONE-INDUCED MITOCHONDRIAL DYSFUNCTION DISRUPTS PRE-IMPLANTATION EMBRYO DEVELOPMENT AND TELOMERE LENGTH 193

4.1 Introduction.....194
4.2 Materials and Methods.....197
4.2.1 Mice.....197
4.2.2 Rotenone diet 197
4.2.3 Derivation of oocytes, early embryos, and blastocysts.....197
4.2.4 Blastocyst immunosurgery 198

4.2.5 Sample preparation for qPCR 199
4.2.6 Triple test qPCR assay 199
4.2.7 TMRM 201
4.2.8 Pronuclear cytosine methylation immunofluorescence 201
4.2.9 Blastocyst differential stain 202
4.2.10 Statistical analysis 202
4.3 Results 204
4.3.1 *In vivo* rotenone exposure compromises oocyte quality and telomere length 204
4.3.2 Rotenone induced mitochondrial dysfunction is present in zygotes and disrupts epigenetic reprogramming 208
4.3.3 Rotenone exposure impairs early embryogenesis and alters telomere elongation dynamics 212
4.3.4 Rotenone exposure decreases blastocyst cell numbers 214
4.3.5 Oocyte rotenone exposure correlates with decreased blastocyst telomere lengths 216
4.4 Discussion 218
4.5 References 223

CHAPTER 5 MATERNAL OBESITY OR ADVANCED MATERNAL AGE ALTERS TELOMERE LENGTH IN EMBRYOS 229

5.1 Introduction 230
5.2 Materials and Methods 233
5.2.1 Mice 233
5.2.2 Derivation of oocytes, early embryos, and blastocysts 233
5.2.3 Blastocyst Immunosurgery 234
5.2.4 Sample collection, lysis and preparation for qPCR 235
5.2.5 Triple test qPCR assay 235
5.2.6 Pronuclear cytosine methylation immunofluorescence 237
5.2.7 Statistical analysis 238
5.3 Results 239
5.3.1 C57BL/6JSfdAnu-Alms1 embryos exhibit telomere elongation and typical mtDNA characteristics 239
5.3.2 Maternal obesity reduces oocyte telomere lengths 241
5.3.3 Maternal obesity alters zygote pronuclear epigenetic reprogramming events 245

5.3.4 Maternal obesity does not impact on-time embryo development but results in shorter blastocyst telomeres 248
5.3.5 Advanced maternal age reduces oocyte telomere length and mtDNA copy number 252
5.3.6 Advanced maternal age results in perturbations to zygotic epigenetic reprogramming 257
5.3.7 Advanced maternal age does not impact on-time embryo development but results in shorter telomeres in blastocysts 260
5.4 Discussion 264
5.5 References 271

CHAPTER 6 SUMMARY AND FUTURE DIRECTIONS 277

6.1. Summary and future directions 278
6.2 References 286

Abstract

Oocytes and embryos are highly susceptible to intrinsic and extrinsic stressors. In particular, physiological cues, such as obesity and aging, are sensed by mitochondria. Mitochondria are inherited solely through the maternal lineage; meaning all mitochondria in offspring are derived from those in the mature oocyte. Therefore, oocyte mitochondria quality and quantity are of utmost importance to embryonic development and postnatal health. In parallel, telomere length is regenerated in offspring during embryogenesis to ensure viability and longevity of each new generation. Despite the importance of telomere elongation during development, little is known about this process. This thesis aims to better understand how maternal obesity and aging affects mitochondria and telomere length in the oocyte and pre-implantation embryo, and by identifying these pathways, develop strategies to enhance these early determinants of lifetime health.

First, a highly sensitive qPCR assay to analyse relative telomere lengths and mtDNA copy number in individual oocytes and embryos was developed, termed the 'Triple Test'. This assay elucidated natural variability in mtDNA and telomeric DNA content between individual oocytes and embryos. It also enabled robust and precise measurements in physiological contexts where tissue availability is limited.

Next, the Triple Test was implemented to conduct a thorough examination of telomere length kinetics throughout pre-implantation embryogenesis. This identified two elongation phases, specific to embryo type. Genes involved in telomere elongation processes and telomere protection roles were analysed throughout oocyte maturation and pre-implantation embryogenesis, and displayed dynamic regulation of expression throughout.

Mitochondrial function and telomere length are the two most well characterised markers of cellular aging, and it was hypothesised that mitochondrial activity is a key factor regulating telomere elongation. This was tested by using rotenone to induce mitochondrial dysfunction in oocytes and tracking telomere length throughout embryogenesis. Reducing mitochondrial bioenergetics decreased telomere length in MII oocytes and cells of the ICM. On a molecular level, rotenone altered global epigenetic reprogramming in zygote pronuclei. These results demonstrate that optimal

mitochondrial activity is required for numerous reprogramming processes, and indicates a functional link between mitochondria and telomeres.

Two physiological scenarios that involve perturbed oocyte mitochondrial function are advanced maternal ageing and obesity; and whether this is associated with perturbed telomere length reprogramming was investigated. While oocyte quality and embryo development were not compromised, telomere length and mtDNA copy number were decreased in oocytes and ICM. Further, treatment of females *in vivo* with BGP-15, a mitochondrial therapeutic, reversed the deficiencies seen in ICM telomere length, and normalised perturbed epigenetic reprogramming in zygotes.

Cumulatively, this work provides critical insights into the patterns of telomere elongation during pre-implantation embryogenesis, and how telomere length and epigenetic re-programming are compromised in subfertility. By manipulating mitochondrial bioenergetics, the relationship between mitochondrial function and telomere health is demonstrated. Additionally, new strategies are identified that positively modulate telomere length during development. This work has identified novel links between mitochondrial activity and telomere elongation and new information about the regulation of these mechanisms that are fundamental to the creation of a new embryo and the lifetime health of that individual.

Declaration

I certify that this work contains no material which has been accepted for the award of any other degree or diploma in my name, in any university or other tertiary institution and, to the best of my knowledge and belief, contains no material previously published or written by another person, except where due reference has been made in the text. In addition, I certify that no part of this work will, in the future, be used in a submission in my name, for any other degree or diploma in any university or other tertiary institution without the prior approval of the University of Adelaide and where applicable, any partner institution responsible for the joint-award of this degree.

I give permission for the digital version of my thesis to be made available on the web, via the University's digital research repository, the Library Search and also through web search engines, unless permission has been granted by the University to restrict access for a period of time.

I acknowledge the support I have received for my research through the provision of an Australian Government Research Training Program Scholarship.

Yasmyn Ellaynah Winstanley

14/05/2021

Acknowledgements

Firstly I would like to thank my supervisors, Professor Rebecca Robker and Professor Darryl Russell for this wonderful opportunity to complete my PhD under their guidance. This has been my biggest personal achievement and it would not have been possible without your support, advice, and guidance. You have instilled in me a passion and love for research and I am forever grateful to have had you as my supervisors and mentors throughout this journey.

I would like to acknowledge the support of the National Health and Medical Research Council for the grant funding used to undertake this work. I would also like to acknowledge the Australian Government Research Training Program for my postgraduate scholarship to support me during my studies. Thank you to all the staff in the Faculty of Health and Medical Sciences, Discipline of Obstetrics and Gynaecology, and the Robinson Research Institute for exceptional resources which I have accessed throughout my studies.

I wish to extend a special thank you to Takashi, Haley, Thao, and Macarena for your experimental and technical assistance in the lab. I want to thank Dr Sonja Frölich for teaching me so much about telomeres, your expertise was invaluable. Thank you to all lab members, past and present, for your friendship and encouragement throughout my candidature, including Carl, Haley, Alka, Macarena, Thao, Eryk, Takashi, Tim, Tasman, Atsushi, Kirsten, Elisha, and Matilda.

Thank you to my closest friends, Carl, Caitlin, Peyman, Ashlee, and Lochie for your friendship and support, and for letting me ramble on about my work. Thank you to my extended family in Doula, Wayne, Anthony, and Gillian for your love and care throughout this time.

Last, but certainly not least, thank you to my mum Lee-anne. I would not have been able to achieve this without your unwavering love and support. Also, thanks for tolerating me when I am hungry and sleep deprived! I cannot find the words to express my gratitude for everything you have done for me to allow me to dedicate so much time and energy to this thesis. I always say this but I really am so lucky to have you as my mum and am forever grateful for everything you do.

Publications Arising During PhD Candidature

1. Chen, M., Wong, S.L., Wu, L.L., **Gordon, Y.E.**, Heilbronn, L.K., Robker, R.L., 2019. Differential impacts of gonadotrophins, IVF and embryo culture on mouse blastocyst development. Reproductive BioMedicine Online 39, 372–382. https://doi.org/10.1016/j.rbmo.2019.02.007

2. Umehara, T., **Winstanley, Y.E.**, Andreas, E., Morimoto, A., Carroll, J., Febbraio, M.A., Russell, D.L., Shimada, M., Robker, R.L. Targeting mitochondrial bioenergetics reverses ovarian fibrosis due to obesity or aging and promotes ovulation. (submitted to Nature Communications).

3. Andreas, E.*, **Winstanley, Y.E.***, Robker, R.L. Effect of the ovarian environment on the developmental competence of the oocyte. (invited review submitted to Current Opinion in Endocrine and Metabolic Research).

Abstracts Arising From This Thesis

2020

GORDON, Y.E., RUSSELL, D.L., ROBKER, R.L. Telomere elongation kinetics during embryogenesis are dysregulated by maternal obesity and age, Society for Reproductive Biology Awards Symposium 2020, online **(oral)**

Finalist for the ART Laboratory Solutions Gamete and Embryo Award

GORDON, Y.E., RUSSELL, D.L., ROBKER, R.L. Telomere elongation kinetics during embryogenesis are dysregulated by maternal obesity and age, 2020 Annual Florey Postgraduate Research Conference, Adelaide, Australia **(poster)**

2019

GORDON, Y.E., GONZALEZ, M, ROSE, R.D., RUSSELL, D.L., ROBKER, R.L. Telomere elongation patterns during mouse pre-implantation embryogenesis, Australian Cell Cycle Meeting 2019, Sydney, Australia. **(poster)**

GORDON, Y.E., GONZALEZ, M, ROSE, R.D., RUSSELL, D.L., ROBKER, R.L. Telomere elongation patterns during mouse pre-implantation embryogenesis, Society for Reproductive Biology Scientific Meeting 2019, Sydney, Australia. **(poster)**

GORDON, Y.E., GONZALEZ, M, ROSE, R.D., RUSSELL, D.L., ROBKER, R.L. Telomere elongation patterns during mouse pre-implantation embryogenesis, Robinson Research Institute Symposium 2019, Adelaide, Australia **(poster and rapid-fire presentation)**

GORDON, Y.E., GONZALEZ, M, ROSE, R.D., RUSSELL, D.L., ROBKER, R.L. Telomere elongation patterns during mouse pre-implantation embryogenesis, Australian Society for Medical Research Conference 2019, Adelaide, Australia **(oral)**

List of Figures

CHAPTER 1

Figure 1. Mammalian folliculogenesis ……. 3

Figure 2. Mammalian female meiosis ……. 5

Figure 3. Mammalian pre-implantation embryogenesis and epigenetic reprogramming ……... 9

Figure 4. Mitochondrial localisation, structure, and ETC within eukaryotic cells ….. 19

Figure 5. Schematic of general mammalian telomere structure ……. 25

Figure 6. Schematic representation of telomerase extension of telomeric DNA at the 3’ end of a linear DNA strand ..……..……..…... 29

Figure 7. Telomere elongation in the Alternative Lengthening of Telomeres pathway ……..……..…… 30

Figure 8. ALT-associated PML Bodies are a key feature of the Alternative Lengthening of Telomeres pathway ……..….. 32

Figure 9. Telomere length homeostasis mechanisms involve telomere trimming processes ..…….. 34

Figure 10. Telomeres play important roles during Prophase I of gametogenesis ... 37

CHAPTER 2

Figure 1. Linear correlations of primer efficiency and normalisation telomere length and mtDNA content using candidate reference genes ……..... 99

Figure 2. Pre-amp optimisation in single MII oocytes ……..…… 103

Figure 3. Products generated using telomere primers and 18S rRNA primers together in qPCR ……..…. 106

Figure 4. mtDNA extraction optimisation in oocytes ……..……. 110

Figure 5. Lysis optimisation in oocytes and blastocysts for mtDNA and nDNA ..… 111

Figure 6. Triple test qPCR work flow and validation using oocytes and embryos .. 115

Supplementary figure 1. Primer BLAST and product alignment ……. 122

Supplementary figure 2. Reproducibility of mtDNA standard curve …….…… 123

Supplementary figure 3. Design of triple test qPCR and use on oocytes and embryos ……..…….…… 124

CHAPTER 3

Figure 1. Expression of telomere binding and extension-associated proteins throughout oocyte maturation ……..……... 146

Figure 2. Telomere length and mtDNA copy number in GV and MII oocytes …..... 147

Figure 3. Expression of telomere binding and extension associated proteins throughout pre-implantation embryogenesis ……. 152

Figure 4. Telomere elongation dynamics throughout pre-implantation embryogenesis …….. 153

Figure 5. Mitochondrial DNA dynamics throughout pre-implantation embryogenesis ……..…….. 155

Figure 6. Telomere length and mtDNA copy number following fertilisation ……. 157

Figure 7. Methylation patterns in fertilised zygotes and parthenogenetically activated once-cell embryos …….……..... 162

Figure 8. Telomere length regulation characteristics in parthenogenetic embryos ……..…….…… 163

Figure 9. Day 5 blastocyst development in IVF and parthenogenetic blastocysts ……164

Figure 10. Telomere and mtDNA content in male and female embryos …….. 166

Figure 11. Telomere and mtDNA content in blastocyst ICM and TE cell populations ……..…… 169

Figure 12. Telomere elongation and mtDNA per cell in adverse high oxygen culture conditions ……..… 172

Supplementary figure 1. Parthenogenetically activated embryos are diploid ……. 188

Supplementary figure 2. Confirmation of embryo sex and immunosurgery validation ……..…… 189

CHAPTER 4

Figure 1. Rotenone inhibits the mitochondrial electron transport chain…… 195

Figure 2. Experimental design ……..... 196

Figure 3. Oocyte quality following in vivo rotenone exposure ……... 206

Figure 4. Telomere length in MII oocytes following in vivo rotenone exposure ….. 207

Figure 5. Zygote mitochondrial membrane potential ……. 210

Figure 6. Methylation patterns in fertilised zygotes …… 211

Figure 7. Two-cell and eight-cell embryo development rates and eight-cell telomere length and mtDNA copy number ……..... 213

Figure 8. Day 5 blastocyst development ……..…… 215

Figure 9. Telomere elongation during embryogenesis and telomere length in blastocysts and ICM populations ……..…….. 217

CHAPTER 5

Figure 1. Experimental design ……... 232

Figure 2. C57BL/6JSfdAnu-Alms1 embryos display typical telomere elongation and mtDNA characteristics …… 240

Figure 3. Obesity reduces ovulation numbers but does not impact oocyte viability or maturation ……..….. 243

Figure 4. Obesity reduces MII oocyte telomere length ……..… 244

Figure 5. Maternal obesity results in alterations to zygotic epigenetic reprogramming events that are reversed by BGP-15 treatment …….. 247

Figure 6. Obesity does not impact embryo development or 8C telomere lengths ……. 250

Figure 7. Obesity reduces blastocyst and ICM telomere length ……... 251

Figure 8. Advanced maternal age reduces ovulation numbers but does not impact oocyte viability or maturation …… 254

Figure 9. Advanced maternal age is associated with reduced telomere length in MII oocytes ……..……...…… 256

Figure 10. Advanced maternal age alters zygotic epigenetic reprogramming events that is partially restored by BGP-15 treatment ……..……. 259

Figure 11. Advance maternal age does not impact embryo development or 8C telomere lengths ……..……..……..……..……... 262

Figure 12. Advanced maternal age reduces blastocyst telomere length and mtDNA copy number that is reversible by treatment with BGP-15 ……..…. 263

Figure 13. Maternal obesity and age disrupt telomere elongation events …….. 264

CHAPTER 6

Figure 1. Novel findings of mitochondrial influence on early reprogramming events ….……..……..……..……..……..……..……..……..……..……... 282

List of Tables

CHAPTER 2

Table 1. PCR and qPCR primers ……..…….. 96

Supplementary table 1. Dilutions of relevant DNA regions of interest in each sample type …… 125

CHAPTER 3

Table 1. qPCR primers ……..…….. 139

Table 2. Taqman assays …….. 140

Supplementary table 1. n-values for telomere elongation and mtDNA copy number time course …… 190

Supplementary table 2. Proportion of telomere elongation with each cell division .. 191

CHAPTER 4

Table 1. qPCR primers ……..…….. 201

CHAPTER 5

Table 1. qPCR primers ……..…….. 237

Abbreviations

αMEM	alpha minimal essential medium
Δ	delta (change in)
5hmC	5-hydroxymethylcytosine
5mC	5-methylcytosine
ALT	alternative lengthening of telomeres
APB	ALT associated PML body
ATP	adenosine triphosphate
BLM	bloom syndrome protein
cDNA	complementary DNA
Ct	cycle threshold
CTC1	CST telomere replication complex component 1
DDR	DNA damage response
DNA	deoxyribonucleic acid
DNMT	DNA methyltransferase
ETC	electron transport chain
GV	germinal vesicle
HAT	histone acetyltransferase
HDAC	histone deacetylase
HMTase	histone methyltransferase
HP1	heterochromatin protein 1
ICM	inner cell mass
IVF	*in vitro* fertilisation
LH	luteinizing hormone
MII	metaphase II
mRNA	messenger ribonucleic acid
mtDNA	mitochondrial DNA
nDNA	nuclear DNA

PCR	polymerase chain reaction
PML	promyelocytic leukaemia protein
PN	pronucleus
POLG	DNA polymerase subunit gamma
qFISH	quantitative fluorescence *in situ* hybridisation
qPCR	quantitative polymerase chain reaction
ref	reference gene
RIF1	replication timing regulatory factor 1
RNA	ribonucleic acid
rRNA	ribosomal RNA
RTEL1	regulator of telomere elongation helicase 1
ROS	reactive oxygen species
SCNT	somatic cell nuclear transfer
TE	trophectoderm
TEN1	CST complex subunit TEN1
TERC	telomerase RNA component
TERT	telomerase reverse transcriptase
TET	ten-eleven translocation
TFAM	mitochondrial transcription factor A
TRF(1/2)	telomeric repeat-binding factor (1/2)
T-SCE	telomere sister chromatid exchange
TZAP/ZBTB48	telomeric zinc-finger associated protein
ZGA	zygotic genome activation
ZSCAN4	zinc finger and scan domain containing 4

CHAPTER 1

LITERATURE REVIEW

1.1 Introduction

Formation of new life requires the coming together of a viable mature oocyte and a sperm, an event termed ‘fertilisation’. The formation of an oocyte, that is ‘developmentally competent’ to form an embryo, begins in the ovary of a female before she is even born, and finishes with the processes of nuclear and cytoplasmic maturation that are triggered by the LH surge at ovulation. Following fertilisation, early embryogenesis is a time of rapid cell divisions, and profound reprogramming events occur during this critical time in the formation of a new organism from just a single cell. Epigenetic reprogramming is perhaps the most well-known process to occur during this time, however other reprogramming events are also required to ensure the health span and life span of the offspring. One such critical event is the resetting of cellular telomere length through elongation events during pre-implantation embryogenesis. Telomere length has been established as an important determinant of cellular lifespan, and as such the regeneration of optimal telomere lengths for an organism during development is vital for lifetime health.

Oocytes and early embryos are known to be highly susceptible to both internal and external stressors. One of the primary cellular organelles that senses external stressors, and can also be responsible for internal stress, are mitochondria. Mitochondria are entirely maternally inherited, and are major players in successful embryo development, as well as disease and ageing. Importantly, both mitochondrial function and telomere length are the most well characterised markers of cellular ageing, suggesting an important link between the two that may also have implications during embryogenesis.

This review encompasses the regulatory processes controlling ovarian follicle development and production of a mature oocyte, and the orchestration of fertilisation and pre-implantation development. Further to this, the mechanisms and specifications of epigenetic reprogramming, the role of mitochondria, and the current understanding of telomere elongation during development are summarised. Lastly, the evidence that perturbations to these sensitive biological pathways can have lifelong consequences is discussed.

1.2 Mammalian embryo development

1.2.1 Folliculogenesis and oocyte maturation

Gametogenesis is a tightly controlled form of cell division that results in the production of haploid gametes (sperm and oocyte). A stark contrast between male and female mammals is that while males produce viable sperm throughout their life, females have all of the oocytes for their reproductive lifespan present in their ovaries by the time they are born. Meiosis is the highly specialised cell division that results in the production of these gametes and the timing of female meiosis is greatly different to that in males.

Oocytes originate as primordial germ cells that undergo rapid mitotic divisions and give rise to oogonia that continue to proliferate and further expand the oogonia pool (Gondos et al., 1986). Following this, follicle formation begins, where oogonia are encircled by somatic epithelial cells at which point the oogonia cease mitotic activity, enter meiosis and are then classified as primordial follicles (Fig. 1.1, Byskov, 1986; Gondos et al., 1986). An oogonia that has entered into meiosis is then termed a primary oocyte, and the somatic cells surrounding the primary oocyte give rise to the granulosa cell layer. At this point primordial follicles remain quiescent until the female reaches puberty, where these follicles will slowly be recruited into the growing follicle pool throughout the female's reproductive lifespan. When follicles are activated to continue growing, they are known as primary follicles, which then grow into secondary follicles and finally give rise to a mature antral follicle (Fig. 1.1, reviewed in Desai et al., 2017).

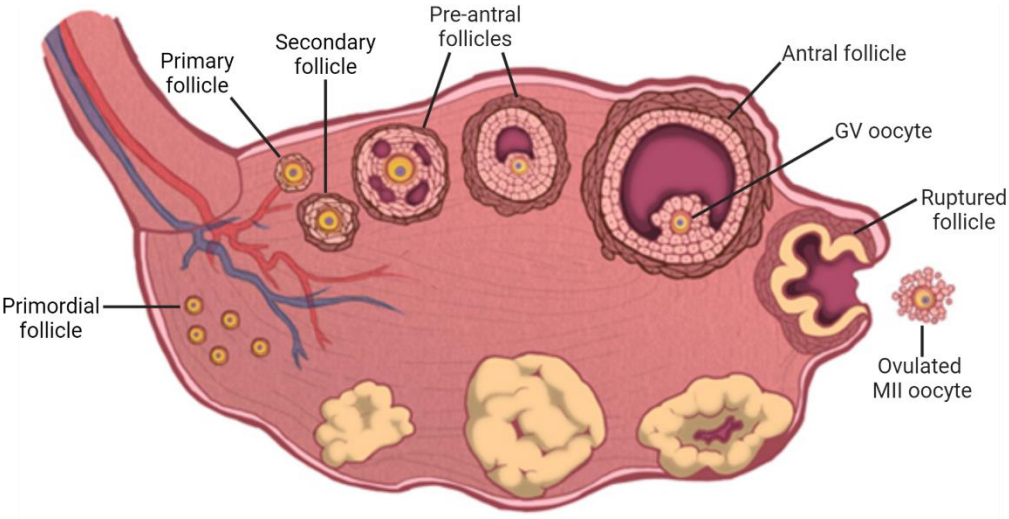


Figure 1.1 Mammalian folliculogenesis

Meiosis is unique to germ cells. In males, meiosis results in the formation of four haploid daughter cells (sperm), whereas in females the cell division is unequal and gives rise to a single haploid ovum with all other chromosomes extruded in polar bodies. Genome organisation during this time is highly specific, to allow for recombination between homologous chromosomes to occur to give rise to genetic variation between the resultant gametes. Meiosis is two-step division process that consists of Meiosis I (where homologous chromosomes are separated) and Meiosis II (where sister chromatids are separated), each with a subset of phases (prophase, metaphase, anaphase, and telophase). Before entering meiosis I, cells go through interphase, where all chromosomes are replicated, prior to prophase I entry. Prophase I, the most complicated phase of meiosis, occurs for a prolonged time (compared to mitotic prophase), and is further divided into four sub stages: leptotene, zygotene, pachytene and diplotene. In leptotene, replicated chromosomes condense, and then form synaptonemal complexes between homologous chromosomes in zygotene. During pachytene, a bivalent has formed and crossing over occurs between non-sister chromatids to allow for recombination. In diplotene, the synaptonemal complex dissociates but non-sister chromatids remain connected by the chiasma (crossover site formed in pachytene). In primordial follicles, primary oocytes are arrested at the diplotene stage of prophase in meiosis I (Borum, 1961). Oocytes are referred to as germinal vesicle (GV) oocytes at this stage.

Oocytes remain arrested in meiotic prophase I during follicle growth until the antral follicle stage. Hormonal cues at ovulation trigger GV break down, the resumption of meiosis, and ovulation (Fig. 1.1, Nagaoka et al., 2012). During metaphase I, homologous pairs line up at the metaphase plate, and homologues are separated during anaphase I, with telophase resulting in the formation of two new cells, one becoming a polar body containing half of the genetic material, and the other capable to continue onto meiosis II (Fig 1.2).

Oocytes then enter meiosis II without DNA replication. During prophase II, chromosomes condense, spindle formation begins, and chromosomes begin to be captured by microtubules. Oocytes are paused at metaphase II, ovulated from the antral follicles and await fertilisation in the oviduct, which stimulates the resumption of metaphase. Metaphase, anaphase and telophase II are then similar to during meiosis I, however this time the sister chromatids are separated to result in just one chromatid

from each maternal chromosome remaining. Telophase results in the extrusion of the second polar body and a fertilised zygote with a haploid female pro-nucleus and a haploid male pro-nucleus (Figure 1.2).

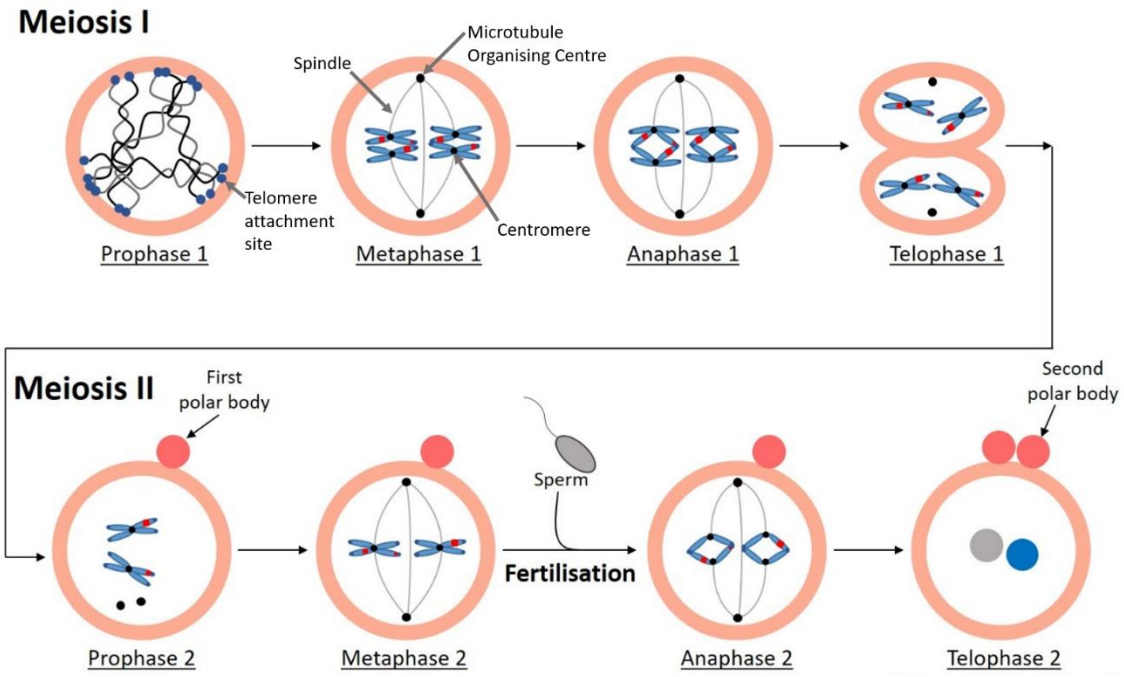


Figure 1.2. Mammalian female meiosis

The oocyte is shown in the diplotene arrest of Prophase I. Following completion of Telophase I, one daughter cell becomes highly condensed to form the first polar body. The oocyte is then arrested in Metaphase II until fertilisation occurs, resulting in completion of meiosis II and extrusion of the second polar body, resulting in a zygote, which contains a haploid maternal pronucleus, and a haploid paternal pronucleus. Black circles indicate the microtubule organising centres

1.2.2 Fertilisation

Fertilisation is the merging of two haploid gametes (oocyte and sperm) to form a diploid cell (zygote), that will go on to form a new individual. Sperm progenitor cells undergo meiotic divisions similar to those described for oocytes during their differentiation in the testis, with the exception that the cell divisions are symmetrical and four individual haploid sperm are produced, rather than polar bodies. For mature sperm to become competent to successfully penetrate the zona pellucida and fertilise an oocyte, they must first undergo capacitation and the sperm acrosome reaction. Following the penetration of the oocyte zona pellucida by a competent sperm, the cortical reaction and zona reaction occur. The cortical reaction is the release of cortical granules from the egg, which are regulatory secretory organelles that function by secreting their contents during fertilisation to block polyspermy (fertilisation by multiple sperm). The zona reaction is the modification of the zona pellucida by altering the solubility and binding properties of the zona to inhibit binding of other free-swimming sperm to the fertilised oocyte. Both the cortical and zona reactions result in the prevention of polyspermy which would result in an unviable zygote. Once the sperm has bound the egg cytoplasmic membrane, the sperm is drawn into the egg by elongation and fusion of plasma membranes in the sperm and the oocytes microvilli, resulting in the integration of the sperm nucleus into the oocyte. Following this the sperm nucleus is modified by undergoing chromatin decondensation and formation of a new nuclear envelope, resulting in the formation of the paternal pronucleus. Upon the sperm head entering the oocyte cytoplasm, meiosis II is resumed in the oocyte and the second polar body is extruded, resulting in the formation of the maternal pronucleus (Fig. 1.2). Microtubules enable migration and relocation of the paternal pronucleus to the site of the maternal pronucleus, after which the two pronuclei fuse and result in the formation of a diploid nucleus (the zygotic or embryonic genome), and the cell is now termed a zygote.

1.2.3 Pre-implantation embryo development

The period of time between zygote formation and embryo implantation in the uterus is termed pre-implantation development. During this time the zygote undergoes multiple cell cycles and cleavages to form a blastocyst containing more than 100 cells that is

competent to implant. During pre-implantation embryogenesis, each cell within an embryo is referred to as a 'blastomere'. Following zygote formation, the embryo subsequently undertakes a succession of asynchronous cell cleavages, whereby cell number increases but overall cytoplasmic volume remains constant. The first cleavage to form a 2-cell embryo takes approximately 20 hours to occur after fertilisation in mice (Artus and Cohen-Tannoudji, 2008). Until the late 2-cell stage (in mice, or 8-cell stage in humans) of development, the embryo relies upon proteins and messenger RNAs (mRNAs) retained by the oocyte that were maternally provided. At the late 2-cell stage, the zygotic genome undergoes a major burst of transcriptional activation, referred to as zygotic genome activation (ZGA) (Aoki et al., 1997). Once this activation occurs, maternally inherited mRNAs begin to be degraded, however many maternal proteins can persist throughout pre-implantation development (Johnson and McConnell, 2004). The second cleavage to form a 4-cell embryo also takes approximately 20 hours, however the subsequent cleavages are considerably faster, at approximately 12 hours (Artus and Cohen-Tannoudji, 2008). The third cleavage completes the formation of the 8-cell embryo, and begins the next major pre-implantation event, compaction, which results in an early morula stage embryo. The blastomeres of the 8-cell embryo maintain their typical spherical morphology until compaction beings, where blastomeres begin to flatten against each other and greatly increase their intercellular contact area (Fig. 1.3) and adherens junctions form at these cell-to-cell contact sites (Mihajlović and Bruce, 2017). During compaction another major event occurs, polarisation, which takes approximately 3-5 hours (Johnson and Ziomek, 1981). Polarisation establishes cell polarity, which is defined as a structurally and functionally asymmetric organisation of cellular components that is preserved and transmitted through cell divisions (reviewed in Bornens, 2008). After polarisation, many polarity proteins accumulate at the apical membrane, while others localise at the basolateral part of the cell membrane. Polarisation is important for the eventual formation of two distinct cell populations with different fates in the blastocyst (the trophectoderm and inner cell mass). The next cell cleavage results in a 16-cell morula, where cell polarisation gives rise to inner versus outer blastomeres. These two populations of blastomeres continue their divergent differentiation through the next cell cleavage, resulting in the 32-cell morula (late morula). Next, cavitation is initiated, whereby the outside cells secrete fluid into the morula, creating the fluid filled blastocoel cavity, which is key in the formation of the blastocyst. During cavitation and subsequent

blastocyst development and expansion, the embryo begins to grow in size and undergo further cell divisions. By the 64-cell stage the embryo has formed two entirely separate cell layers, signifying the first differentiation into distinct cell lineages in mammalian embryo development. Specifically, the outer cells of the morula become lineage specified as the trophectoderm, and the inner cells remain in a pluripotent state as the inner cell mass (ICM, see Fig. 1.3, pink and blue cells represent the ICM in blastocyst stages) and go on to eventually form the foetus. Following full expansion of the blastocyst to form a late blastocyst, hatching occurs, wherein the embryo breaks out of the zona pellucida to allow for implantation into the uterus. For hatching to occur, a trypsin-like protease called strypsin, located in the trophoblast cell membranes, lyses a hole in the zona pellucida and the blastocyst manoeuvres through the breach while continuing to expand. Once the blastocyst is completely free of the zona pellucida, or fully hatched, it is capable to implant and continue post-implantation development (Fig. 1.3). An important determinant of blastocyst quality that is routinely assessed is the number of cells that make up the blastocyst, particularly the ICM portion, as this has been shown to positively correlate with implantation rates (Lane and Gardner, 1997; Richter et al., 2001).

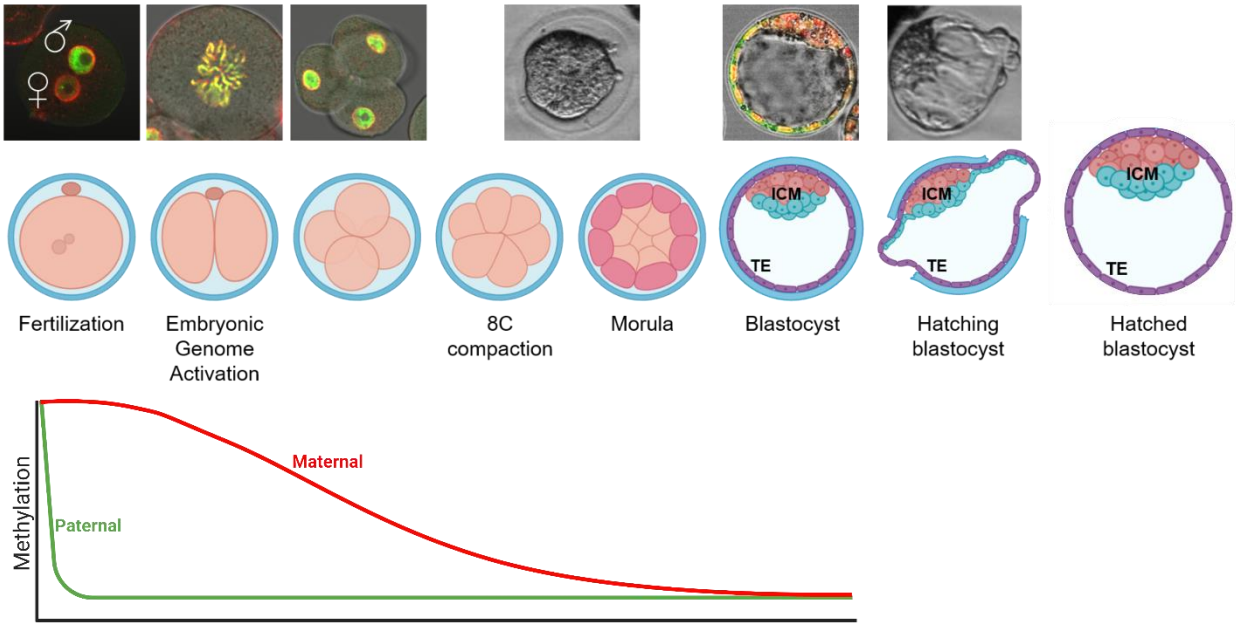


Figure 1.3. Mammalian pre-implantation embryogenesis and epigenetic reprogramming

Following fertilisation, multiple cleavages give rise to a morula stage embryo that then undergoes cavitation and cellular differentiation to form a blastocyst that hatches from its zona pellucida and implant into the uterus. Epigenetic reprogramming also occurs during this time, most noticeably, DNA methylation. The maternal PN is highly methylated (5mC, red) at fertilisation which is maintained by protection from demethylation enzymes by proteins such as STELLA. The paternal PN has actively undergone the first oxidation step in demethylation (5hmC, green) which is catalysed by TET enzymes. The maternal methylation marks are progressively diluted and lost throughout subsequent cleavages to result in a hypomethylated embryo. Fluorescent blastocyst (histone methylation) image kindly provided by Dr Deepak Adhikari.

1.2.4 Epigenetic reprogramming

Epigenetic modifications are heritable changes that alter the phenotype of a cell or organism that do not involve alterations to the DNA sequence (Goldberg et al., 2007). Epigenetic modifications include DNA methylation, histone modifications, and the formation of histone variants. As epigenetic reprogramming is a deeply complex process, only a few specific aspects will be covered in this review. Of interest are pronuclear asymmetry establishment and paternal protamine to histone transfer, both of which occur following fertilisation and before the first cell cycle, as well as histone modifications in the ICM and TE lineages. Maternally and paternally inherited DNA (derived from the oocyte and sperm, respectively) contain distinct epigenetic marks that must be reprogrammed during pre-implantation embryogenesis into an embryonic pattern. At fertilisation, the epigenetic asymmetry between the maternal and paternal pronuclei is highly evident in their DNA methylation patterns (Fig. 1.3).

DNA methylation is the result of DNA methyltransferases (DNMTs) catalysing the transfer of a methyl group to the fifth position of cytosine residues in DNA (thereby referred to as 5-methylcytosine or 5mC) (Chen and Li, 2004). The methylation of these cytosine residues on chromatin is associated with transcriptional repression (Bird and Wolffe, 1999). One of the earliest epigenetic reprogramming phenomena that takes place is imprinting. Imprinting occurs via DNA methylation of maternal or paternal alleles at imprinting control regions (Bartolomei, 2009; Ferguson-Smith, 2011) during gamete differentiation, and results in expression of imprinted genes in a parent-of-origin specific manner that is maintained throughout life. Imprinting patterns play vital roles in development and growth, and their deregulation impacts significantly on embryonic and adult phenotypes (Messerschmidt et al., 2014).

As methyl groups can be added to cytosine residues (5mC) to produce repressive chromatin marks, these marks can also be modified and result in relief from these repressive features. Cytosine methyl groups can be oxidised by ten-eleven translocation (TET) DNA demethylases to 5-hydroxymethylcytosine (5hmC), thereby removing the repressive 5mC mark, and this process is thought to aid in cell-cycle independent DNA demethylation processes (Messerschmidt et al., 2014). In particular, TET3 is highly expressed in oocytes, spermatozoa, and early pre-implantation development stages. Prior to fertilisation, the mature mouse sperm genome has the highest global DNA methylation level of any mouse cell (Popp et al., 2010). However,

after fertilisation and the formation of the paternal pronucleus, the paternal chromatin undergoes rapid demethylation via TET3 demethylase activity (Gu et al., 2011) before the onset of the first mitosis (replication independent demethylation). At fertilisation the maternal pronucleus also contains repressive 5mC chromatin marks, however, unlike paternal chromatin, the maternal chromatin maintain these 5mC marks via protection from TET3 activity by the STELLA protein (Nakamura et al., 2007). These repressive marks are abundantly maintained until the 2-cell stage of development, when the maternal genome slowly begins to be passively demethylated in a replication-dependent dilution of 5mC (Mayer et al., 2000a). This passive loss is achieved by exclusion of the DNA methyltransferase DNMT1 from the nucleus which prevents transfer of methyl groups onto newly synthesised DNA (reviewed in Messerschmidt et al., 2014). There is some controversy in the embryonic epigenetic reprogramming field about the exact timing of maternal pronucleus demethylation, with one group observing that demethylation is complete by PN5 (Li and O'Neill, 2012). However, the vast majority of the field find that the maternal genome maintains higher levels of 5mC than the paternal genome until at least the 4-cell stage (in mouse embryos), after which both inherited genomes display equivalent levels of global hypomethylation (Mayer et al., 2000b, Fig. 1.3). Irrespective of the kinetics, the active demethylation of the paternal genome and passive demethylation of the maternal genome, with the exception of imprinted genes, signify the reprogramming of the embryonic epigenetic landscape. The embryonic genome is in a hypomethylated state by the 8- to 16-cell stage, and genome-wide de novo methylation begins in the ICM of the blastocyst-stage embryo (Mann and Bartolomei, 2002). At this time DNMT3b, which is first transcribed upon ZGA, displays robust expression that is largely restricted to the ICM (Watanabe et al., 2002). DNMTs play critical roles during this time as deletion of any of several DNMT3 isoforms can result in embryonic lethality or sterility (reviewed in Messerschmidt et al., 2014).

While DNA methylation reprogramming has been most thoroughly characterised, histone modifications are also reprogrammed during pre-implantation embryogenesis. Histone modifications are covalent alterations that can also regulate gene expression. The most common histone modifications are acetylation and methylation, however there is an extensive array of other modifications that occur including phosphorylation, ubiquitylation and sumoylation (Kouzarides, 2007). Histone modifications can also

interact with DNA methylation, thereby adding another layer to epigenetic regulation. Histone acetylation marks are typically correlated with more accessible chromatin and therefore transcriptional activity. Acetylation of lysine amino acids on histones is catalysed by histone acetyltransferases (HATS), and removed by histone deacetylases (HDACs). Histone methylation is associated with less accessible chromatin and therefore transcriptional repression, and is created by histone methyltransferases (HMTases). The most noticeable difference in histone modification profiles during pre-implantation embryogenesis is between the two blastocyst cell populations (Erhardt, 2003). In particular, histone methylation is preferentially re-established in the ICM, with H3K27me1/2/3 detected, while H3K27m2/3 is only found on the inactive X in the TE cells (Erhardt, 2003). The TE and ICM have distinct cell fate differences, and as such have different epigenetic and gene expression profiles. Overall, histone modification reprogramming is more complex than DNA methylation and as such, a general model of how these processes are integrated during early embryogenesis has not yet been established. However, as with DNA methylation, histone modifications do change dynamically during pre-implantation development and these modifications are required for the precise regulation of gene expression (Shi and Wu, 2009).

Another example of a major epigenetic modification during pre-implantation embryogenesis is the use of histone variants in the sperm nucleus. In mature sperm, histones are replaced by protamines (Kimmins and Sassone-Corsi, 2005), which are responsible for generation of the densely packaged sperm chromatin. Following fertilisation and the breakdown of the sperm nuclear envelope, the protamines are replaced with acetylated histones (Wright, 1999).

Epigenetic reprogramming is critical for the cell fate determination in the ICM and TE lineages of the blastocyst, and these DNA and histone marks play imperative roles in both the maintenance of pluripotency and initiation of cellular differentiation.

1.2.5 Pluripotency

A fertilised egg is a totipotent cell, meaning that it is capable of producing all embryonic and extraembryonic cell lineages. This totipotency is retained at the 2-cell stage and in the majority of blastomeres until the 8- to 16-cell stage, at which time relative

position determines their differentiation fate (Rossant and Vijh, 1980). At the 8-cell stage, the close proximity and intracellular contact area between cells that is established during compaction provides cues for the formation of inner and outer blastomeres (Rossant, 1976; Tarkowski and Wróblewska, 1967). The outer blastomeres become biased towards forming the first extraembryonic cell lineage, which is the trophectoderm, and the inner blastomeres characteristically form the ICM. By the 16- and 32-cell stage of development, inner cells upregulate *Sox2* expression, and outer cells upregulate *Id2* expression (Guo et al., 2010). The Hippo signalling pathway is important for integrating positional information into lineage specification. In outer blastomeres, Hippo signalling is 'off', allowing Yap1 to enter the nucleus, and in combination with Tead4, prime cells towards trophectoderm differentiation by expression of TE lineage-specific master regulators such as Cdx2 and Gata3 (Guo et al., 2010; Ralston et al., 2010; Ralston and Rossant, 2008). One major epigenetic change occurring during TE differentiation is the progressive silencing of the Oct4 and Nanog genes via H3K9 methylation (Feldman et al., 2006). In the inner blastomeres, Hippo signalling is 'on' when Lats1/2 phosphorylates Yap1 (Nishioka et al., 2009). When Yap1 is excluded from the nucleus it is subsequently degraded, meaning it cannot act as a coactivator of Tead4, therefore expression of TE lineage-specific master regulators does not occur, and TE programming is not induced in the inner cells.

Early ICM cells are still considered totipotent, as ICM cells separated from early mouse blastocysts still have the ability to regenerate the trophectoderm layer (Spindle, 1978). This totipotency is gradually lost once the ICM exceeds 16-19 cells (Grabarek et al., 2012; Rossant and Lis, 1979), and cells are then considered pluripotent. Pluripotency defines the capacity of a cell to self-renew while retaining the potential for unbiased differentiation. ICM cells maintain their pluripotency by expressing master regulator pluripotency genes such as Oct4, Sox2, and Nanog (Boyer et al., 2005; Chambers et al., 2003; Guo et al., 2010).

Later in blastocyst development, another cell lineage decision is made, with a subset of ICM cells differentiating into the primitive endoderm (Fig. 1.3, blue cells in the ICM), and the others forming the epiblast (Fig. 1.3, pink cells in the ICM). The epiblast will eventually differentiate into the ectoderm and mesoderm cell layers, thus the three germ layers are derived from the ICM cell lineage.

1.2.6 Pre-implantation development reprogramming impacts lifelong health

Pre-implantation development is a critical time that directs the formation of an embryo that is able to successfully implant into the uterus so that fetal growth can be sustained throughout pregnancy. Pre-implantation embryo development is largely autonomous as the embryo relies on maternally derived cellular components and also products of its own genome once ZGA occurs. Despite this, the preimplantation embryo is susceptible to influence from factors in the external environment which can result in embryonic adaptations, or in severe cases can result in aberrant embryo development (Gao et al., 2003; Niemann and Wrenzycki, 2000; Schultz, 2005). One well characterised external influence on embryo development is *in vitro* culture conditions, which can affect implantation and even extend to fetal and postnatal development and affect disease susceptibility in the offspring (Barker, 2002; Ecker et al., 2004). Studies have shown that the environment that an oocyte is exposed to during maturation can influence the abundance of transcripts in the mature oocyte (Lonergan et al., 2003; Watson et al., 2000), and even in the blastocyst (Russell et al., 2006). However, most research indicates that culture conditions post-fertilisation are more important for determining blastocyst quality and viability (ability to establish and maintain a pregnancy) as well as mRNA abundance (Lonergan et al., 2006). One of the main conditions of *in vitro* culture that has been shown to perturb embryo gene expression is the type and contents of the culture media used (Lonergan et al., 2006; Wrenzycki et al., 2005), however the oxygen concentration of the environment has also been shown to affect the abundance of certain transcripts (Harvey et al., 2004).

Moreover, assistive reproductive technology procedures expose gamete and embryo epigenomes to external stress factors that have been shown to increase histone 3 lysine 9 acetylation (Rollo et al., 2017), and alter DNA methylation status and the establishment and maintenance of genomic imprints (DeBaun et al., 2003; Maher, 2003), which results in an association between children conceived via these procedures and imprinting disorders (Bowdin et al., 2007; Le Bouc et al., 2010). These imprinting disorders are most thoroughly linked to ovarian hyperstimulation (Denomme and Mann, 2013; Market Velker et al., 2012; Sirard, 2012), most likely from the disruption of maternally derived gene products that are essential for imprinting maintenance (Denomme et al., 2011). The most prevalent imprinting disorders that

have been associated with ART are Beckwith-Wiedemann syndrome (BWS), Silver-Russel syndrome (SRS), and Angelman syndrome (AS) (Gosden et al., 2003; Maher, 2005). BWS can involve both hyper- and hypo-methylation of the differentially methylated regions H19 and LIT1, respectively (Lennerz et al., 2010), SRS involves hypo-methylation, and AS involves aberrant methylation in 80% of patients on chromosome 15 (seen in patients with AS arising from 15q11.2-q13 deletion, paternal uniparental disomy of chromosome 15, and imprinting centre defects) (Hiura et al., 2012). Studies of phenotypes in embryos and offspring derived from ART technologies highlight the importance of optimal development conditions for an embryo (whether *in vivo* or *in vitro*) as these can significantly alter gene transcription and epigenetic landscapes which can have detrimental impacts on embryo development, implantation and pregnancy, and offspring's lifelong outcomes.

Perturbing mitochondrial function in mouse zygotes for the first 48 hours of culture with FCCP (a small molecule drug which uncouples mitochondrial oxidative phosphorylation) has also been shown to influence offspring phenotypes (Zander-Fox et al., 2015). Female pups born from zygotes that were treated with FCCP displayed decreased birthweight, and remained lighter than control pups until weaning, increased adiposity by 4 weeks of age and increased adiposity gain from there until 14 weeks of age when compared to controls (Zander-Fox et al., 2015). Further, females from FCCP treated zygotes also displayed glucose intolerance by 8 weeks of age, and insulin resistance at 14 weeks. Signifying that these very early metabolic disruptions can influence reprogramming events that significantly alter offspring phenotypes.

The successful completion of the earliest events following fertilisation and even beyond are extensively determined by the quality of the oocyte from which the embryo is derived from. One of the most easily visualised determinants of oocyte quality is whether it successfully completes maturation, as immature oocytes are unable to be fertilised. Further to this, the composition of proteins and mRNAs derived during oocyte growth and maturation are vital for facilitating the earliest reprogramming event post-fertilisation (pronucleus asymmetry establishment), and deviations to this may implicate subsequent reprogramming events.

1.2.7 Major cellular components are inherited

The mature oocyte is a considerably large and complex cell that essentially contains all biochemical components required to form a viable embryo (with the exception of the paternal genome). As such, the composition of the oocyte plays a large role in the growth of the embryo and control of cellular functions (Krisher, 2004). Vital components include maternally derived mRNAs (Olszańska and Borgul, 1993) and proteins that are required up to and even after ZGA, the nucleolus (a structure within the nucleus where rRNA is transcribed and assembled into ribosomes) (Ogushi et al., 2008), the ribosomes themselves (required for translation of maternally derived mRNAs before ZGA), and the mitochondria (Giles et al., 1980). Further to this, an embryo must also inherit all of its DNA from the maternal and paternal pronuclei, the merging of which forms the embryonic genome. As such, all genomic sequences, including telomeres, are essentially inherited from parental lineages. Telomeres are sequences present at the end of all linear chromosomes that are important for genome stability and cellular lifespan (see section 1.4). All oocytes for a female's reproductive lifespan are present in the ovary at the time of birth. As previously discussed (see section 1.2.1), by this time in development all oocytes have entered meiosis and as such do not undergo further DNA replication until after fertilisation has taken place (Borum, 1961). Therefore, the telomeres that an organism will inherit from its maternal lineage are present in the oocyte throughout the maternal reproductive span and as such will be exposed to, and are highly susceptible to, cellular stresses that occur during this period of time, which can span decades (Camlin et al., 2016; Sobinoff et al., 2010). Mitochondria, the key cellular organelles for energy production (see section 1.3) are solely maternally inherited, as any paternal mitochondria that enter the oocyte via sperm fertilisation are actively degraded (Cummins et al., 1998; Hajjar et al., 2014; Song et al., 2014). Therefore the mitochondria present in the egg are the founding mitochondria from which all subsequent mitochondria will be derived, and these will go on to control embryonic metabolism (Biggers et al., 1967; Brinster, 1965; Quinn and Wales, 1973) and apoptotic events (Zhao et al., 2015), and are major factors in determining successful embryo development.

1.3 Mitochondria

Mitochondria are unique organelles that are found in most eukaryotic cells and have key roles in energy metabolism, homeostasis, cellular differentiation, and apoptosis. Fascinatingly, mitochondria are entirely maternally inherited, therefore all of the mitochondria in an organism are derived from those that were present in the mature oocyte, highlighting the importance of preserving mitochondrial health in these cells. The number of mitochondria contained within a single cell varies greatly according to cell type (Robin and Wong, 1988). Mitochondria contain many features that are distinct from other cellular organelles, such as containing their own genome, which is attributed to their evolutionary origins as an aerobic prokaryote that was engulfed by a nucleated cell, culminating in a symbiotic relationship (Embley and Martin, 2006). Mitochondria are highly sensitive to environmental cues and possess the ability to rapidly change their functional state and energy production to meet the requirements of the cell. Their proper function is vital for health, survival, and cellular activities, with many pathologies such as cancer, Alzheimer's disease, Parkinson's disease, and multiple sclerosis involving mitochondrial dysfunction (H. Reddy and P. Reddy, 2011; Karbowski and Neutzner, 2012; Reddy, 2008; Swerdlow, 2011).

1.3.1 Mitochondrial structure and function

The primary function of mitochondria is to produce adenosine triphosphate (ATP). Mitochondria have two phospholipid membranes: the outer membrane covers the mitochondria's surface, and the inner membrane is highly folded into structures called cristae which increase the surface area. The cristae of the inner membrane contain the proteins involved in the electron transport chain (ETC), and increasing this surface area allows for greater capacity of a single mitochondrion to increase its ATP output (Figure 1.4). The ETC is a vital part of mitochondrial ATP production, overall termed aerobic respiration (Alabduladhem and Bordoni, 2021). Glucose is first converted to pyruvate in the cytoplasm of the cell through glycolysis, which produces two ATP molecules. Pyruvate is then transported to the mitochondrial matrix where it is further oxidised and covalently linked to CoA to form acetyl-CoA, before entering the Krebs cycle which results in the production of a further two ATP molecules (Leese and Barton, 1984). The final stage of aerobic respiration is the ETC, where a cluster of

proteins (Complex I, II, III and IV, CoQ or ubiquinone, Cytochrome C, and ATP synthase, Fig. 1.4) transfer electrons through the inner membrane to form a proton gradient that drives ATP production (Mazat et al., 2013). To facilitate this, the electron is released through the interaction of Complex I with high energy NADH, which is generated via production of acetyl-CoA, and malate to oxaloacetate conversion in the Krebs cycle. The ETC produces the highest yield of ATP, with 32 molecules generated per each input glucose molecule (Enderle, 2012). The cristae of mitochondria greatly increase the capacity for the inner membrane to hold many clusters of ETC proteins, and therefore make mitochondrial aerobic respiration a highly efficient way of energy production. In total, this process can produce 36 molecules of ATP (Enderle, 2012), whereas anaerobic respiration (where only glycolysis is utilised) produces just two ATP per input molecule of glucose. Therefore proper mitochondrial function is critical for efficient energy production, and as a consequence, cellular function.

Mitochondrial function and the efficiency of the ETC are known to decline with aging; in particular, aging mitochondria exhibit increased electron leakage and therefore a reduction in ATP generation (Green et al., 2011). As mitochondria become more dysfunctional they produce higher levels of reactive oxygen species (ROS) which anti-oxidant mechanisms are unable to eliminate, and as a consequence, these ROS further damage mitochondria as well as cellular proteins, lipids, and DNA, thus exacerbating biochemical dysfunction (Edgar et al., 2009; Hiona et al., 2010). Therefore mitochondrial dysfunction is considered a hallmark of aging (López-Otín et al., 2013).

Mitochondrial division occurs through the process of fission, which is independent of the cell cycle divisions of the cells in which they are contained. Mitochondrial fission is mediated by dynamin-related proteins (DRPs) and other cofactors and has been well established as a process essential for viability, as homozygous DRP1 knockout mice are embryonic lethal (Manczak et al., 2012). Mitochondrial fusion is another dynamic process that mitochondria undergo independent from other cellular events, and loss of fusion potential increases mitochondrial fragmentation (Chen et al., 2003). Further, mitochondrial fusion is essential for embryonic development, as mouse embryos with mutations in either Mfn1 or Mfn2 (mitofusion-1 or -2), rendering them unable to undergo mitochondrial fusion, die in mid-gestation (Chen et al., 2003).

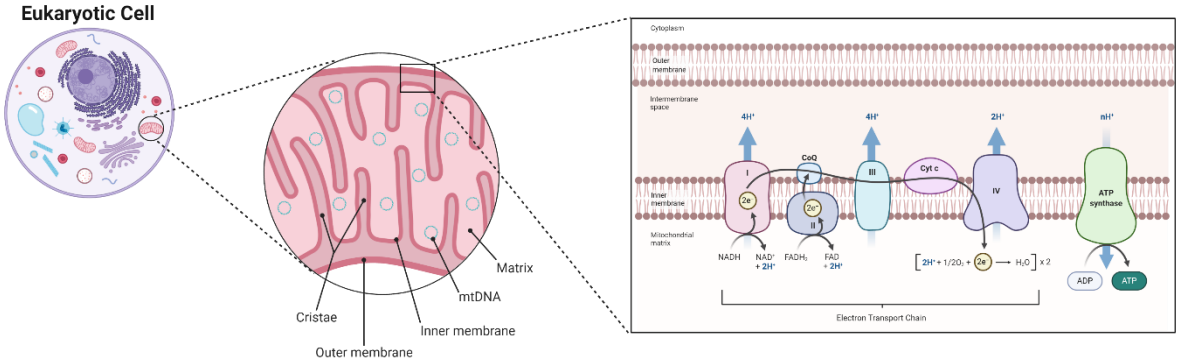


Figure 1.4. Mitochondrial localisation, structure, and ETC within eukaryotic cells

Mitochondria are membrane-bound cellular organelles with a primary role in ATP production through aerobic respiration. The inner mitochondrial membrane contains the proteins of the electron transport chain, the function of which drives ATP formation via ATP synthase, producing a high ATP yield per input glucose molecule.

The structure of mitochondria is highly adapted to maximise their efficiency in meeting the cell's energy requirements. Mitochondrial shape can also vary between cell types; for example, fibroblast mitochondria are typically long filaments, vascular smooth muscle mitochondria are rod-shaped (Dai et al., 2005), and hepatocyte mitochondria are more sphere shaped (Das et al., 2012). Oocyte and early embryo mitochondria also have a unique structure, they are typically round with relatively few cristae, and this structure is typical of stem cells (Prigione et al., 2015).

1.3.2 Mitochondrial localisation and utilisation during oocyte maturation and early embryogenesis

Mitochondrial dynamics have been thoroughly documented during oocyte maturation and pre-implantation development, including localisation and metabolism (St. John et al., 2010). During this time, mitochondria are the main ATP source, as glycolytic activity is not utilised until the blastocyst stage (Biggers et al., 1967; Dumollard et al., 2007; Leese, 1995). During oocyte maturation, oocytes are in an oxygen rich environment, with aerobic respiration and small amounts of the pentose phosphate pathway (a parallel to glycolysis) occurring (Absalón-Medina et al., 2014). In germinal vesicle oocytes, mitochondria are homogeneously distributed (Nishi et al., 2003). However, during meiotic maturation, mitochondria are heterogeneously distributed, with a heavy concentration around the developing meiotic spindle and approximately 40% of total oocyte mitochondria aggregating to this location (Dalton and Carroll, 2013, Calarco, 1995). Mitochondria play a key role in spindle formation at this time, which is evidenced by abnormal spindle formation when mitochondrial function is disrupted (Dalton and Carroll, 2013). This aggregation remains with the spindle as it migrates to the cortex, and by the time MII arrest occurs, the mitochondria are more homogenously distributed, with occasional smaller aggregations around the MII spindle (Dalton and Carroll, 2013, Calarco, 1995). Mitochondrial segregation is also highly biased in favour of the oocyte during Meiosis, minimising mitochondrial loss to the extruded polar body. Mitochondrial biogenesis does not occur until the blastocyst stage in mouse embryos (Pikó and Taylor, 1987; Thundathil et al., 2005), therefore the mitochondria contained within the oocyte must be competent to sustain early embryogenesis. Mitochondrial metabolism is heavily utilised in preimplantation embryos, with pyruvate being the most important energy substrate during early embryogenesis (Quinn and Wales, 1973). Glycolysis isn't highly utilised by embryos until after the morula stage has been achieved and glucose consumption by the embryo rises (Cagnone and Sirard, 2016; Kaneko, 2016; Wilding et al., 2009). During pre-implantation development, mitochondria are localised in the cytoplasm in 2- to 8-cell embryos, and at the periphery of nuclei in blastocysts (Basu et al., 2008; Kiyonari et al., 2019; Lee et al., 2011).

The integrity of mitochondria and their ability to function efficiently are fundamental to the formation of a fertilisable mature oocyte and the development of a viable pre-

implantation embryo (Dumollard et al., 2007). Factors that can influence mitochondrial function are substrate availability, ROS levels, and ETC protein functionality. Of particular relevance to oocytes, a key feature for the successful function of mitochondria is the mitochondrial genome (known as mitochondrial DNA, or mtDNA) because it encodes ETC proteins and thereby influences cellular metabolism (Taanman, 1999).

1.3.3 Mitochondrial DNA (mtDNA)

A feature of mitochondria that is unique from other organelles is that they possess their own genome, which is distinct from the nuclear genome. Unlike the nuclear genome which is linear chromosomes, the mitochondrial genome is circular, and small in comparison at only 16,569 base pairs in humans and 16,295 base pairs in mice, in contrast to 3.3 billion (Taanman, 1999). The mitochondrial genome is located in the matrix and contains 37 genes, which encode 13 proteins required for protein subunits of the enzymes required for aerobic respiration, as well as 22 tRNAs, and 2 rRNAs (Anderson et al., 1981; Chomyn et al., 1985; Macreadie et al., 1983). Despite this, mitochondria cannot independently produce all required proteins and as such rely on the import of nuclear gene products for many proteins required for their function. Mitochondrial DNA can be present in multiple copies in each mitochondrion, meaning many thousands of copies of mitochondrial DNA can be present in a cell, depending on the cell type (Robin and Wong, 1988). mtDNA replication occurs independently of nuclear genome replication, and utilises different proteins. TFAM (mitochondrial transcription factor A) initiates replication by binding to mtDNA and inducing structural changes that result in the initiation region being exposed. Next, mtRNA pol (mitochondrial RNA polymerase) generates an RNA that is used as a primer by POLGA (polymerase gamma A) to begin mtDNA replication (Ciesielski et al., 2016). This process is further supported by POLGB (polymerase gamma B), mtSSB (mitochondrial single-stranded binding protein), and Twinkle, which act to stabilise POLGA and mediate mtDNA unwinding (Ciesielski et al., 2016). mtDNA replication occurs independently of mitochondrial fission (Chen et al., 2010; Del Dotto et al., 2017), but is typically controlled by signals regulated by cellular energy demands.

Mitochondrial DNA has a much higher mutation rate than nuclear DNA due to a number of factors. Mitochondrial DNA replication has a lower fidelity (Shtolz and Mishmar, 2019), mtDNA has greater exposure to ROS generated during aerobic respiration, and the mitochondria also lack DNA repair mechanisms that are found in the nucleus. mtDNA copy number has been shown to decrease with age, however the burden of mtDNA mutations increase with age (Zhang et al., 2017). Increased mutation load contributes to the age associated decline in mitochondrial function because mtDNA-encoded proteins are required for proper ETC assembly and the increased mutation load can compromise the structure and function of these proteins, thus causing metabolic and other dysfunction.

The mitochondrial genome is solely maternally transmitted (Birky, 1995; Giles et al., 1980), therefore the integrity of the mitochondria and their DNA (mtDNA) in the oocyte is crucial for oocyte quality, fertilisation and subsequent embryo development, as well as lifetime health of the offspring.

1.3.4 Mitochondrial DNA replication patterns in oocyte growth, maturation and embryogenesis

Primordial germ cells, the precursors of gametes, contain approximately 200 copies of mtDNA per cell and undergo extensive mtDNA replication during oogenesis to form a fertilisable MII oocyte (Sun and St. John, 2016). Mitochondrial DNA copy number plays a crucial role in creating a viable MII oocyte, and a critical threshold of at least 100,000 copies for mice (Pikó and Taylor, 1987), humans (Santos et al., 2006), and pigs (El Shourbagy et al., 2006) has been established.

Following fertilisation, mtDNA replication does not occur to any appreciable extent until the embryo reaches the blastocyst stage. As such, the total quantity of mtDNA within a developing pre-implantation embryo does not increase from the oocyte to the early blastocyst (Pikó and Taylor, 1987) and remains relatively constant, sometimes exhibiting slight decreases during the early cleavage stages (Thundathil et al., 2005). Comparison of mtDNA copy number from *in vivo* or *in vitro* produced rat zygotes, early- and late-2C, and 8C embryos found no differences in copy numbers, however at the morula and blastocyst stage, embryos cultured *in vitro* had significantly higher mtDNA copy number than those derived *in vivo* (Kameyama et al., 2007). This indicates that

the *in vitro* culture environment can influence mtDNA replication during the later stages of pre-implantation embryogenesis. While the total mtDNA content of the embryo remains somewhat stable, it is distributed as the mitochondria are segregated between blastomeres with each cleavage, therefore the number of mtDNA molecules per cell is continuously diluted (Thundathil et al., 2005). mtDNA replication resumes at the blastocyst stage, at first in the trophectoderm lineage, then the inner cell mass (Sun and St. John, 2016). The trophectoderm are the first of the two cell types to undergo differentiation and as such lose pluripotency and begin to express lineage specific markers, which coincides with replication initiation (May-Panloup et al., 2005; McConnell and Petrie, 2004; Spikings et al., 2007). Unlike the TE, the ICM maintains its pluripotency, and as such continues to limit mtDNA replication, thus further reducing the mtDNA copy number per cell.

The reduction in mtDNA copy number per cell is key to establishing the mtDNA set point, which is required for cell lineage commitment. The mtDNA set point is characterised by a low mtDNA copy number, typically ranging from 20-200 copies per cell, (Cree et al., 2008) which is similar to that in primordial germ cells. It is believed that a low mtDNA copy number is required for the maintenance of the naïve state displayed by pluripotent cells (Facucho-Oliveira et al., 2007). The mtDNA set point provides the starting point from which cells increase their mtDNA copy number in a cell-specific manner with the resumption of mtDNA replication as they differentiate into mature, functional cells (Kelly et al., 2012). Differentiation also coincides with an increase in the number of mitochondria per cell, greater reliance on aerobic respiration, and a change in mitochondrial morphology from a rounded, stem cell-like form to displaying the typical elongated structure with defined cristae and dense matrices (Prigione et al., 2015).

While mitochondrial function and dynamics are well characterised during pre-implantation embryogenesis, there is another profound DNA change during this time that is less understood, telomere elongation.

1.4 Telomeres

1.4.1 Telomere structure and function

Telomeres are repetitive DNA sequences that cap the ends of eukaryotic linear chromosomes (Figure 1.5) and thereby maintain chromosomal length and protect genome integrity. Telomeric DNA consists of the duplex TTAGGG sequence repeated for many kilobases (ranging from approximately 5kb to 15kb in humans (Samassekou et al., 2010)) and terminates in a 3' single-strand overhang which is folded into the distal-most telomere DNA duplex (Griffith et al., 1999) resulting in the formation of a T-loop structure at the end of each chromosome (Griffith et al., 1999; M.Stansel, 2001, Figure 1.5). The 3' overhang exists due to the inability of the DNA replication machinery (i.e. polymerase) to generate double stranded DNA at the terminal ends of the template (known as the 'end replication problem') (Olovnikov, 1973). Thus, this T-loop is important because it prevents this single-stranded sequence from being recognised as damaged DNA by the cell's DNA-damage response (DDR) pathway machinery, which would then potentially lead to cell cycle arrest and/or apoptosis (Greider, 1999; Griffith et al., 1999; Karlseder, 1999).

The ability of telomeres to form these protective T-loops is enabled by the presence of a highly specific assembly of proteins that bind along the telomere repeat sequence that are collectively known as the shelterin complex (Bombarde et al., 2010; Karlseder et al., 2004). This complex comprises of proteins including RAP1, TIN2, TPP1, and POT1 (reviewed in (Xin et al., 2008), and importantly, two specialised and related proteins that bind directly to the telomeric DNA, the Telomere Repeat Binding Factor (TRF) proteins, TRF1 and TRF2 (Hanaoka et al., 2009), Figure 1). Both TRF1 and TRF2 bind to the double stranded telomeric DNA, with TRF1 binding more strongly in the major groove than TRF2 (Hanaoka et al., 2009). TRF1, with its interacting protein TIN2, has been shown to be an important regulator of telomere length (Kim et al., 1999; van Steensel and de Lange, 1997), likely by regulating telomerase access (Scherthan et al., 2000), with disruptions in TRF1 binding to telomeres resulting in inappropriate telomeric growth in telomerase positive cell lines (Smith and de Lange, 2000). Tankyrase, a telomere-associated poly-ADP ribose polymerase (PARP) interacts with telomeres via TRF1 (Smith, 1998; Smith and de Lange, 1999) and is responsible for removal of TRF1 from telomeres to allow for lengthening to occur

(Smith and de Lange, 2000, 1999); therefore, tankyrase overexpression results in similar effects to TRF1 binding disruption or knock-down (Smith and de Lange, 2000). TRF2 is well established as one of the main factors controlling telomere length, and as a key factor in telomere integrity and protection, by mediating T-loop formation (Griffith et al., 1999). TRF2 is vital for the integrity of telomeres, as TRF2 knock-downs in human fibrosarcoma cells decreased telomere lengths, chromosome end-end fusions (van Steensel and de Lange, 1997), and p53-dependent apoptosis, which all result from the TRF2-depleted telomeres being recognised as damaged DNA by the cell's DDR pathway (Karlseder, 1999). TRF2 and POT1 also aid in telomere protection by inhibiting the signalling of DNA damage-sensing proteins ATM and ATR, respectively (Karlseder et al., 2004; Zimmermann et al., 2014).

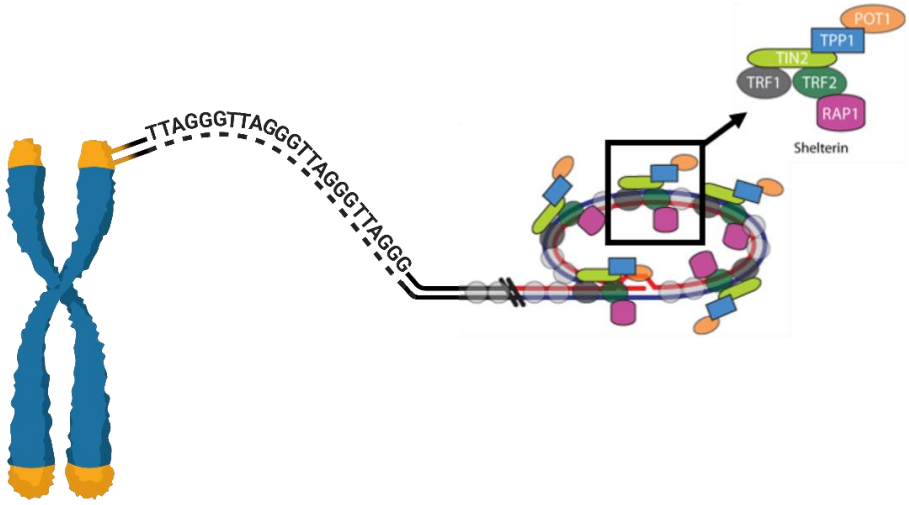


Figure 1.5. Schematic of general mammalian telomere structure

Nuclear chromosomes are capped by repetitive DNA sequences called telomeres. These sequences are bound by a specific complex of proteins, called the shelterin complex, which enable the formation of protective T-loops.

Interestingly, telomere length displays a highly variable nature. Telomere lengths within a population of cells and/or individuals are known to vary greatly. For example in humans (Eisenberg et al., 2011), telomere lengths varied from 5.1kb to 18.64kb in men aged 18-28 years old in Europe, likely due to a mix of genetic and environmental factors. Even telomere lengths in individual spermatozoa from the same male differ (Baird et al., 2006; Santiso et al., 2010), for example, Baird *et al*. (2006) found individual sperm telomere lengths from a single male could range from 8.86kb to 17.29kb. However, the cellular mechanisms responsible for these differences are not well understood.

While telomeres are essential protectors of genome integrity and stability, their length decreases with every cell division, reducing their protective roles. This continual telomere length attrition is primarily due to limitations in linear DNA replication, known as the 'end replication problem'. Further to this, telomeres are also susceptible to shortening via ROS induced damage (Oikawa and Kawanishi, 1999; von Zglinicki et al., 1995).

1.4.2 The end replication problem

The 'end replication problem' is the inability of telomeres to be completely replicated during mitosis, resulting in progressive shortening of telomeres with each round of cell division (Blackburn, 1984; Olovnikov, 1973). Telomere length will progressively shorten until the Hayflick limit (the finite number of times a cell can divide until division stops, governed by telomere shortening) is reached and cells undergo senescence (Hayflick and Moorhead, 1961). If cells surpass the Hayflick limit and continue to divide, telomere lengths decrease to a point where they can no longer form t-loops or be bound by the shelterin complex, and the DDR and apoptosis pathways are activated (Frias, 2012). Telomere length and the Hayflick limit provide a tightly regulated mechanism for cells to enter senescence at the right time to avoid undergoing apoptosis while maintaining genome integrity.

Because telomere lengths decrease with each cell division, telomeres progressively shorten with aging, and as such, short telomeres are one of the major hallmarks of aging. Short telomeres have not only been linked to aging phenotypes, but also chronic diseases (Rudolph et al., 1999). Mice have very long telomeres in comparison

to humans, and unlike humans, mice also have active telomerase in their somatic tissues, therefore they typically do not display the same aging characteristics as humans. Studies of telomerase deficient mice reveal premature aging characteristics that are similar to those in humans, such as hair greying and alopecia (hair loss), decreased body weight and a diminished fat cell layer between the dermis and skeletal muscles (Rudolph et al., 1999). The premature telomere shortening in these mice was also associated with shortened life spans, a reduced capacity to respond to stresses such as wound healing and hematopoietic ablation, as well as an increased incidence of spontaneous malignancies (Rudolph et al., 1999). Diseases in humans that are associated with, or result from short telomeres include bone marrow failure, dyskeratosis congenita (which commonly manifests as abnormal skin pigmentation, leucoplakia and nail dystrophy, and premature aging, among other symptoms), acquired aplastic anaemia, pulmonary fibrosis, and liver disease, all of which are associated with mutations in telomerase components (TERT, TERC or DKC1). Accelerated telomere attrition is also linked to cancer (Calado and Young, 2009).

To counteract the effects of gradual telomere shortening on the lifespan of subsequent generations, telomere lengths must be reset at the outset of each new generation to ensure that healthspan and lifespan do not progressively decline. Telomere elongation is known to occur via two well characterised mechanisms: telomerase and alternative lengthening of telomeres.

1.4.3 Telomere elongation mechanisms

Telomere elongation occurs in very few cell types. These are embryonic stem cells (Hiyama and Hiyama, 2007), adult stem cells (Marión and Blasco, 2010), proliferating spermatogonia (Ozturk, 2015), epidermal cells (Harle-Bachor and Boukamp, 1996), activated T-cell (Barsov, 2011) and B-cell lymphocytes (Bougel et al., 2010), and some cancers. There are two mechanisms of telomere elongation, telomerase and Alternative Lengthening of Telomeres (ALT), both of which are known to be utilised by, and best characterised in, cancer cells.

Telomerase is a ribonucleoprotein enzyme that consists of the components human telomerase reverse transcriptase (hTERT), telomerase RNA (hTERC), and dyskerin (DKC1) (Cohen et al., 2007). This complex adds telomere repeat sequence to the 3’

end of telomeres in an RNA template-dependent manner concurrent with DNA replication and cell division. Telomerase is a DNA polymerase with an RNA template to prime template-directed synthesis of telomeric DNA on the leading DNA strand (Greider and Blackburn, 1989), while DNA polymerase-α synthesises the complementary telomeric DNA of the lagging strand (Figure 1.6). Telomerase has the capacity to add approximately 50-100 base pairs of DNA per cell cycle (Cristofari and Lingner, 2006), and is therefore an efficient mechanism to minimise telomere shortening throughout frequent divisions, but it cannot achieve large scale extensions rapidly.

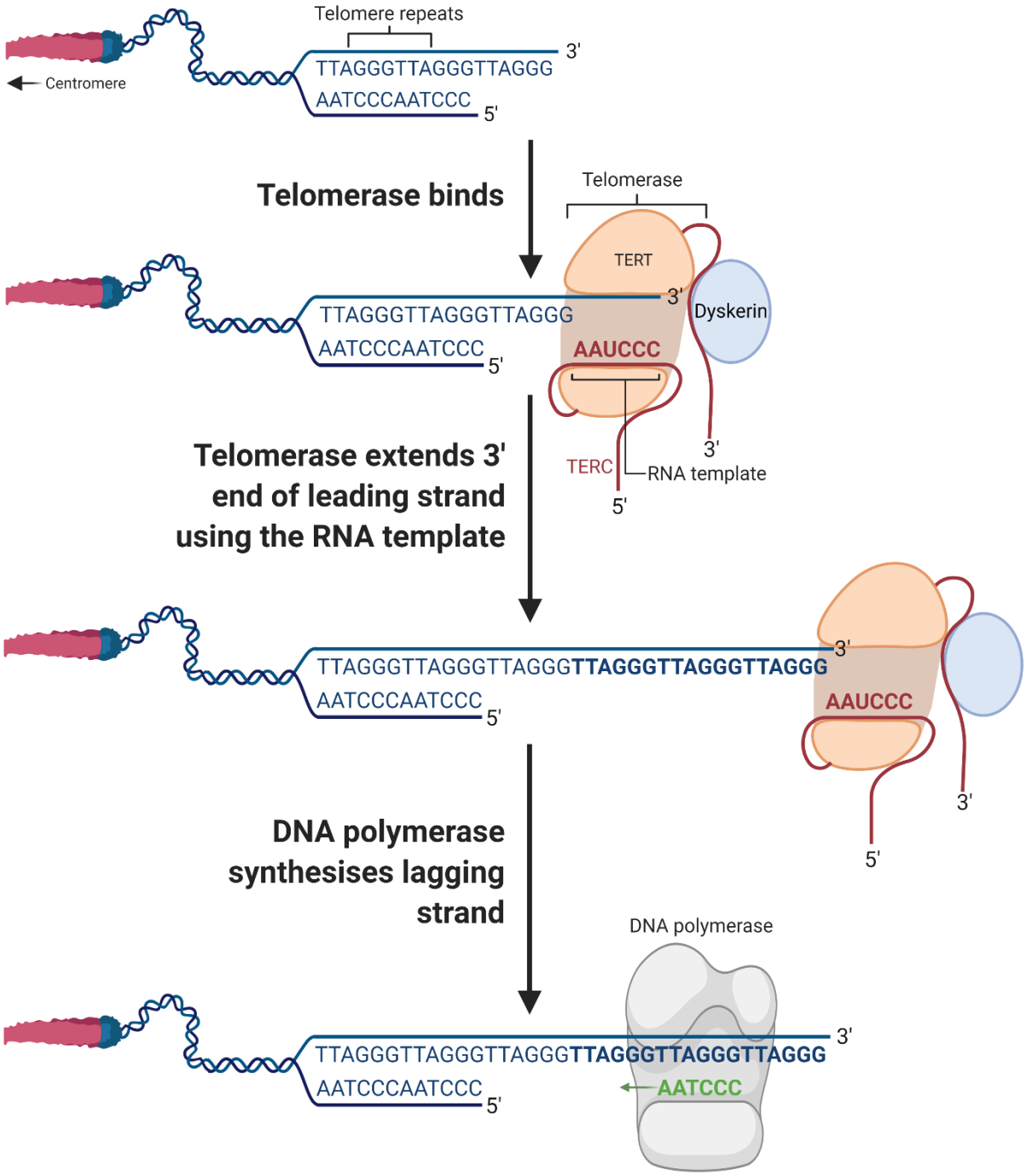


Figure 1.6. Schematic representation of telomerase extension of telomeric DNA at the 3' end of a linear DNA strand

Telomere extension by the enzyme telomerase utilises an RNA template to enable synthesis of new telomeric DNA.

A second, less widely-known mechanism of telomere elongation is Alternative Lengthening of Telomeres, commonly referred to as ALT, which is defined as any telomerase-independent mechanism that results in overall telomere lengthening. Unlike telomerase, which is an enzymatic elongation process, ALT has been shown to involve recombination (Figure 1.7 A, Pickett and Reddel, 2015), with the resultant ability to add up to approximately 1kb of DNA to telomeres in one cell cycle. This recombination occurs between sister chromatids, with telomere sister chromatid exchanges (T-SCE) being commonly observed in ALT-utilising cells (Henson and Reddel, 2010). Due to ALT's reliance on recombination and its dramatic elongation potential, ALT characteristically produces heterogeneous telomere lengths within a cell (Henson et al., 2002, Figure 1.7 B).

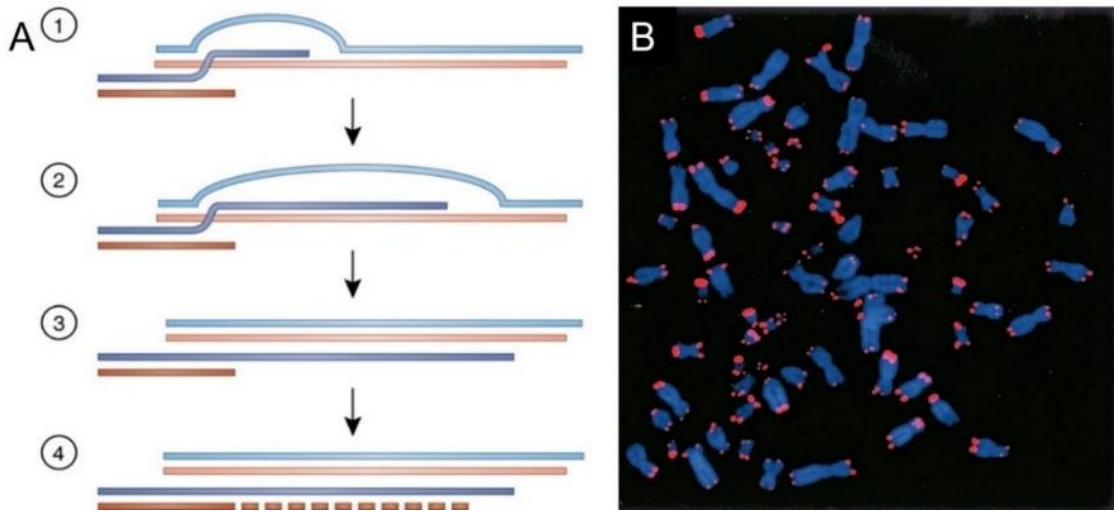


Figure 1.7. Telomere elongation in the Alternative Lengthening of Telomeres pathway

(A) Telomere lengthening via homologous recombination. One strand of DNA can be seen invading that of a homologous chromosome in (1) and using it as a template for large scale extension in (2) and (3). The newly extended telomere in (4) is then used as a template to extend the telomere of the other chromosome. (B) Cancer cell telomeres (labelled red by Fluorescence In Situ Hybridisation (FISH)) elongated by ALT display heterogeneous lengths. Image (A) adapted from Pickett and Reddel (2015), (B) adapted from Henson *et al* (2002).

One of the most defining characteristics of the ALT mechanism are APBs (ALT-associated Promyelocytic Leukemia Bodies), which are specialised nuclear structures consisting of the PML (Promyelocytic Leukemia) protein, telomeric DNA, telomere binding proteins (Yeager et al., 1999), and many other proteins involved in recombination and repair, such as BLM (Yankiwski et al., 2000). Many of the protein components of APBs are involved in recombination pathways and for this reason it is believed that telomere elongation occurs within APB's (Draskovic et al., 2009; Fasching et al., 2007, 2005); however, their definitive functions are yet to be elucidated. PML is one of the most predominant proteins in APBs and forms a large component of the shell of the APB complex (Lang et al., 2010), however PML is normally found in cells in PML nuclear bodies (Lang et al., 2010). Here it co-localises and interacts with a large number of proteins with diverse functions that give PML bodies roles in cell cycle control, tumour suppressor action, chromatin organisation, transcription, DNA replication, senescence, and apoptosis (Bernardi and Pandolfi, 2007; Borden, 2008; Dellaire and Bazett-Jones, 2004; Lang et al., 2010; Salomoni et al., 2008; Takahashi et al., 2004). While the Bloom syndrome protein (BLM) is also a key protein within APBs (Yankiwski et al., 2000), it is also found within cell nuclei that are not undergoing telomere elongation (Bernardi and Pandolfi, 2007); this is due to it being a RecQ helicase which unwinds G4-quadruplex DNA (G4-DNA) found at G-rich sequences of the genome, like telomeres (Ellis et al., 1995; Sun et al., 1998). BLM also is involved in homologous recombination (Wright, 2001; Wu et al., 2001) and has been shown to interact with TRF2 in ALT competent cancer cells to promote telomeric DNA synthesis (Stavropoulos, 2002). Therefore it is important to identify defining features of ALT, such as TSCEs and APBs, when looking for ALT activity in cells, as many of the proteins involved in this pathway have additional non-ALT associated functions within a cell.

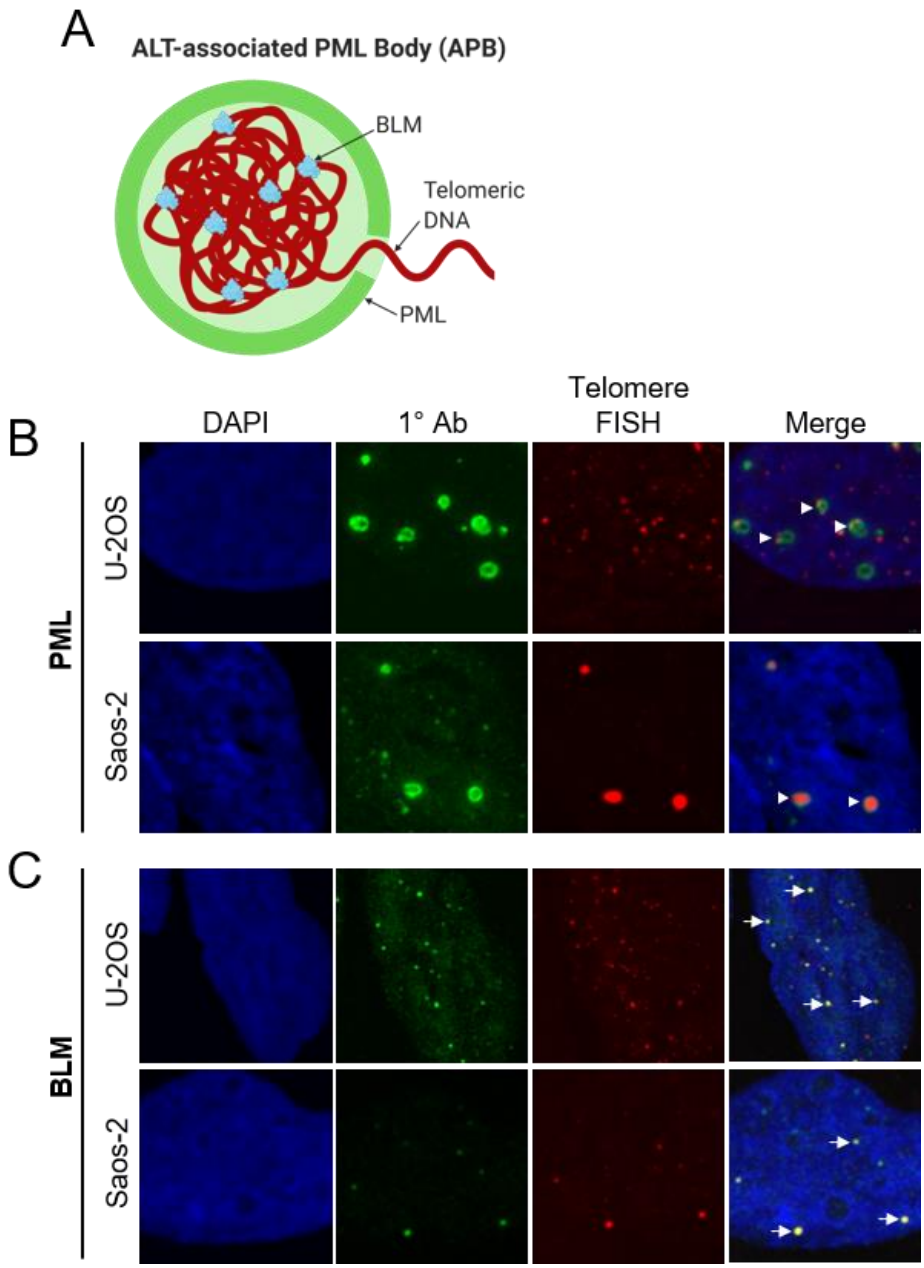


Figure 1.8. ALT-associated PML Bodies are a key feature of the Alternative Lengthening of Telomeres pathway

(A) Schematic of an ALT-associated PML body (APB), showing a PML shell (green), with telomeric DNA (red) localised inside, and BLM protein (blue) localised to telomeres. Example images of PML (B, green) and BLM (C, green) localised to telomeres (red) in two well characterised ALT-positive cell lines, the U-2OS and Saos-2 osteosarcomas. PML can be seen forming the shape of the APB shell with telomeres localising to, and within it (B, arrow heads). Multiple co-localisations between BLM and telomere foci are also observed (C, arrows).

Telomere length maintenance is a dynamic process that also involves length reduction, referred to as telomere trimming. This is distinguished from the conventional telomere shortening that happens with each round of cell replication as telomere trimming is targeted based on telomere length and requires specific proteins, such as *zbtb48* (named “TZAP”). This trimming results in the deletion of large segments of telomeric DNA, however it does not produce telomere signal-free chromosome ends (detected using FISH analysis) and also does not result in telomere dysfunction (Pickett et al., 2009), indicating a high level of regulation. Interestingly, a set proportion of shelterin complex is available for each telomere, and this quantity does not increase with telomere length (Takai et al., 2010), therefore long telomeres have a lower density of shelterin complex than short telomeres (Cristofari and Lingner, 2006). This appears to be an identifying factor for telomeres that are due to undergo trimming, as TZAP has been shown to readily localise to long telomeres (20kb), which would have low shelterin density (Figure 1.9), while no localisation was detected in cells with short (5kb) telomeres and high shelterin density (J. S. Z. Li et al., 2017). Telomere trimming is heavily utilised in embryonic stem cells to maintain length homeostasis, and an absence of TZAP in these cells allows for significant telomere elongation (J. S. Z. Li et al., 2017). Upon formation of the T-loop, the 3’ overhang inserts into the telomeric duplex and forms a D-loop (Griffith et al., 1999; Moyzis et al., 1988), and a recombination intermediate is formed at the site of this insertion. Telomere trimming involves the resolution of this recombination intermediate, which results in a sudden loss of telomere length equivalent to at least that of the T-loop, and this is detectable as extrachromosomal telomeric DNA, named telomere circles (t-circles, see Fig. 1.9) (Pickett et al., 2011, 2009). As such, the delicate process of telomere elongation is apparently also regulated by telomere trimming in order to prevent the accumulation of aberrantly long telomeres.

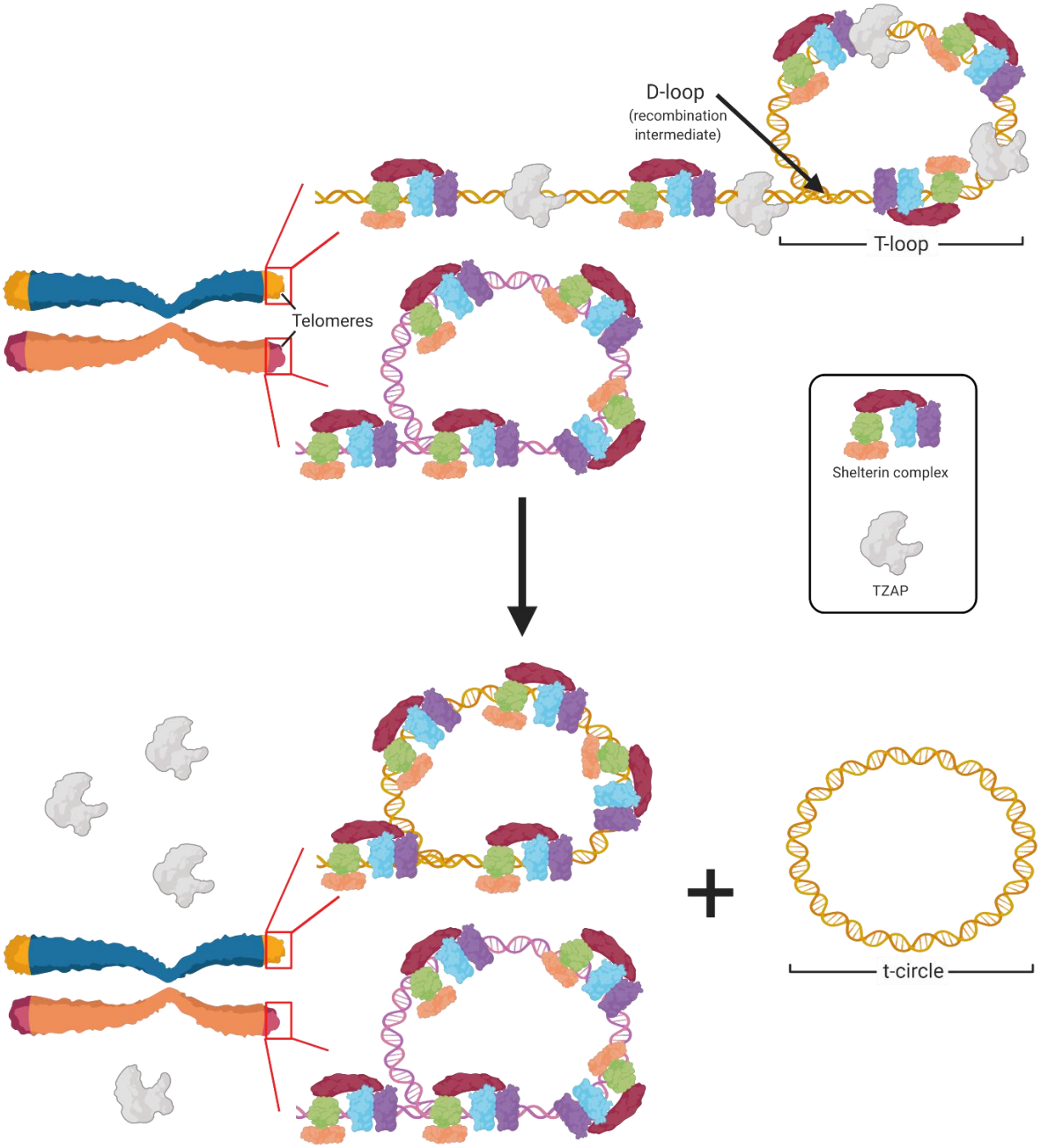


Figure 1.9. Telomere length homeostasis mechanisms involve telomere trimming processes

TZAP directed telomere trimming prevents the accumulation of aberrantly long telomeres by binding to telomeres with low shelterin density and initiating shortening processes. Trimming occurs by resolution of the recombination intermediate that is formed when the 3' overhang invades the double-stranded telomeric DNA to form the D-loop. The result of telomere trimming is shortened telomeres and t-circles, which are detectable for analysis.

1.4.4 Epigenetic regulation of telomeres

The repetitiveness and G-richness of telomeric DNA sequence enables telomeres to form highly condensed heterochromatin structures. The formation of heterochromatin is dependent on binding of heterochromatin protein (HP1) isoforms, as well as epigenetic modifications to both the DNA and histones. In heterochromatin, such as telomeres, DNMTs are responsible for methylation of cytosine residues to form 5 methyl-cytosine (5mC), while HMTases methylate lysine residues on histones 3 and 4 leading to enrichment of H3K9me3 and H4K20me3. Particularly, the histone variant H3.3 has been shown to be deposited at telomeres by ATRX for targeted K9 tri-methylation and heterochromatin formation in mouse embryonic stem cells (Udugama et al., 2015). Further, this process has been shown to be regulated by the PML protein (Chang et al., 2013; Delbarre et al., 2017; Ivanauskiene et al., 2014), providing a critical role for PML function in the maintenance of telomeric chromatin integrity in pluripotent cells by regulation of histone epigenetic modifications. These epigenetic modifications are critical to telomere length maintenance, as disruptions correlate with loss of telomere-length control (García-Cao et al., 2004, 2002; Gonzalo et al., 2006, 2005). In particular, primary cells derived from mice that were null for histone methyltransferases (both Suv39h1 and Suv39h2) had decreased levels of H3K9 di- and tri-methylation, and abnormally long telomeres compared to wild-type controls (García-Cao et al., 2004). Further to this, mouse embryonic stem cells or fibroblasts that are deficient for DNA methyltransferases (DNMT1, or DNMT-3a and -3b) or retinoblastoma proteins (RB1, RBL1, and RBL2, and single-, double-, and triple-knockouts) also exhibited decreased methylation levels and dramatically long telomeres compared to control cells (García-Cao et al., 2002; Gonzalo et al., 2006, 2005). Telomerase-null mice (lacking in the TERC component) which are unable to undergo telomere length extension exhibit short telomeres, decreased tri-methylation at both H3K9 and H4K20, and HP1 binding, while exhibiting increased density of histone acetylation marks, which are associated with more ‘open’ DNA structures (Benetti et al., 2007), further highlighting the relationship between telomere length and epigenetic modifications. It is hypothesised that these changes in epigenetic markers on short telomeres may act to help recruit telomerase to the shortest telomeres for preferential elongation, which results in a restoration of these marks (reviewed in Blasco, 2007). This notion is supported by studies where cells deficient in proteins vital

for histone or DNA methylation exhibited abnormally long telomeres when compared to control cells (García-Cao et al., 2004, 2002; Gonzalo et al., 2006, 2005). While epigenetic modifications play key roles in telomere length regulation and stability, the function and potential modifications of these epigenetic marks in pre-implantation embryogenesis telomere elongation is currently unknown.

1.4.5 Telomeres in early development

Telomere behaviour during meiosis has been thoroughly documented, however much of the molecular mechanisms behind the control of telomere elongation during pre-implantation embryo development is unknown.

Genome organisation during meiosis is highly specific to allow for recombination between homologous chromosomes to occur and give rise to genetic variation between the resultant gametes; and telomeres play a significant role in chromosome organisation throughout (Scherthan et al., 2000). Telomeres have a particularly important function during prophase of Meiosis I, which is also commonly referred to as the ‘bouquet stage’ (Reig-Viader et al., 2016). Telomeres attach chromosomes to the nuclear envelope via TRF2 (Dolnik et al., 2007, 2003; Podgornaya et al., 2000), with the rest of the chromosome looping within the nucleus resulting in an arrangement like flower petals (Scherthan et al., 2000, Figure 1.10). This telomere attachment to the nuclear envelope is initiated in leptotene and is maintained through zygotene stages of meiosis, with telomere attachment to the nuclear envelope essential for proper synapsis between homologues and for proper resolution of recombination events (Boateng et al., 2013; Link et al., 2013). Then during pachytene, sister-chromatids begin to separate, while crossing over occurs between non-sister chromatids. Non-sister chromatids then begin to separate, but are still connected by the chiasma (cross-over site formed during exchange in pachytene) which is eventually resolved via displacement of the chiasmata (named terminalisation). From late pachytene to the beginning of diplotene, bouquet dissolution occurs but telomeric attachment to the nuclear membrane remains (Nagaoka et al., 2012). Thus, telomere attachment is important for the facilitation of homologous pairing, synapsis initiation and chiasmata formation. Reduced synapsis and recombination is observed in oocytes of female mice with shortened telomeres (due to telomerase deficiency) (Liu et al., 2004), further

highlighting the importance of adequate telomere length for normal meiosis progression. In oocytes, the leptotene, zygotene and pachytene stages take place during fetal life and oocytes are arrested in the diplotene stage until the breakdown of the GV, triggered by hormones at ovulation, initiates the resumption of meiosis (reviewed in Nagaoka et al., 2012).

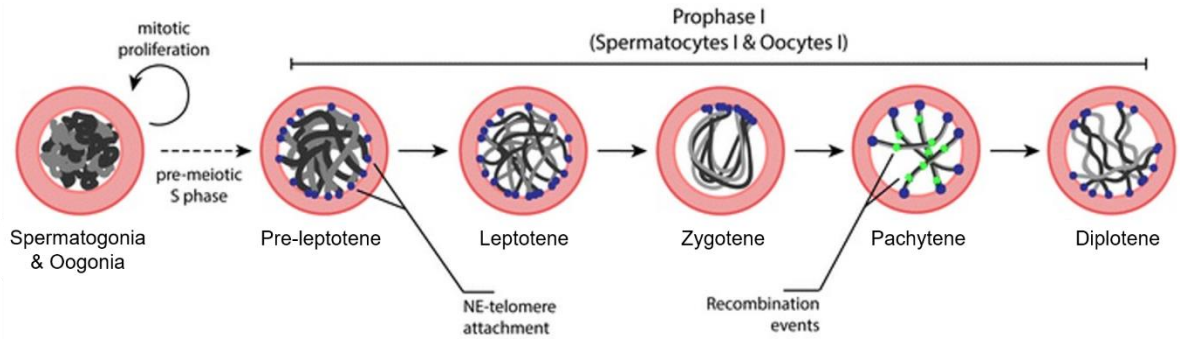


Figure 1.10. Telomeres play important roles during Prophase I of gametogenesis

Telomeres attach to the nuclear envelope and these attachments are critical for facilitating recombination events during this time. Figure adapted from Reig-Viader et al. (2016).

During metaphase I, homologous pairs line up at the metaphase plate, and then homologues are separated during anaphase I, followed by telophase which ends with the formation of two new cells. In female meiosis, meiosis I results in the formation of the first polar body, and a daughter cell (oocyte) which continues on to meiosis II, and overall telomere lengths in the oocyte and polar body are similar (Wang et al., 2013). Oocytes then continue into meiosis II without DNA replication. During prophase II, chromosomes condense, spindle formation begins, and chromosomes begin to be captured by microtubules. Oocytes are then paused at metaphase II until fertilisation occurs which resumes metaphase. Metaphase, anaphase and telophase II are then similar to that of meiosis I, however this time the sister chromatids are separated to result in gametes with just one chromatid from each chromosome. Telophase

culminates in the extrusion of the second polar body from the fertilised zygote, which then contains a haploid female pro-nucleus and a haploid male pro-nucleus.

Telomeres play vital roles throughout meiosis, aiding in proper chromosome orientation and alignment. Following fertilisation telomeres are also essential for chromosome stability during the mitotic cell divisions that characterise the earliest phases of cell division. Importantly, telomeres lengthen during pre-implantation development (L. Liu et al., 2002; Liu et al., 2007; Wang et al., 2013), and this appears to be a major mechanism by which telomere length is reset across generations. Telomere lengthening during mouse pre-implantation embryogenesis has been studied using qPCR and quantitative telomere Fluorescence In Situ Hybridisation (FISH), with significant increases between successive stages observed (L. Liu et al., 2002; Liu et al., 2007; Wang et al., 2013). However the exact mechanisms of this lengthening remain unconfirmed.

1.4.6 Telomere length resetting

As telomere length is an important determinant of health span and life span, it must be regenerated at the outset of each new generation to ensure the continuation of a species. During embryogenesis, a 'new' organism forms from a single cell (zygote) which is comprised of a haploid maternal genome and a haploid paternal genome, which are modified to endow the offspring with appropriate telomeric DNA to ensure genome integrity.

In mice, sperm telomere lengths decline with age (de Frutos et al., 2016), and as such paternal age and embryo telomere length display a negative correlation. Two cell embryos and offspring from older male mice exhibited shorter telomeres than those from younger males that had been mated with a female of the same age (de Frutos et al., 2016). Conversely, in humans, sperm telomere length increases with age, and as such aging has been associated with a higher mean sperm telomere length in older men than younger (Antunes et al., 2015, Baird et al., 2006; Eisenberg et al., 2011; Kimura et al., 2008). This increased telomere length in sperm is reflected in offspring leukocyte telomere length (Aston et al., 2012; De Meyer et al., 2007; Eisenberg et al., 2012; Gibbons, 2012; Kimura et al., 2008; Njajou et al., 2007; Sartorius and Nieschlag, 2010).

Oocyte telomere shortening with advanced reproductive age is conserved between human and mice (Henderson and Edwards, 1968; Keefe et al., 2006; Yamada-Fukunaga et al., 2013), however sperm show opposite trends between the two species with aging. Despite this, major regulatory pathways in mammalian telomere elongation during pre-implantation embryogenesis are thought to be largely conserved with some subtle species-specific differences. Much of our understanding of telomere biology during pre-implantation embryogenesis has come from primarily mice, as well as bovines.

In mice, telomere lengths have been shown to be increased consistently in 2-cell embryos, and sometimes in zygotes (depending on the strain) when compared to oocytes (Liu et al., 2007). Further to this, another study found that telomere length increases with each successive stage between zygotes, 2-cell, and 4-cell mouse embryos (Wang et al., 2013). While blastocyst telomere lengths have also been shown to be significantly longer than in oocytes, they were not different to that of a 2-cell embryo by qPCR analysis (Liu et al., 2007). Other work has found an increase in telomere length between the morula and blastocyst, however this study did not analyse any earlier stages of development (Varela et al., 2011). Telomere dynamics have been investigated further in blastocyst stage embryos, where in mice, it has been found that the cells of the ICM have longer telomeres than those of the TE (Iqbal et al., 2011). Further to this, telomere lengths did not increase during post-implantation development (Schaetzlein et al., 2004), indicating blastocyst telomere length is the maximum telomere length of an individual, and as such it has been deemed the telomere ‘set point’.

While much of our understanding of telomere length dynamics in pre-implantation embryogenesis has come from work done in mice, a large knowledge gap still remains. There is yet to be a comprehensive analysis of multiple pre-implantation stages using a single analysis method for all stages for consistency. The type of telomere elongation mechanisms occurring during this time are also not fully confirmed. Telomerase activity assays have indicated that while activity is higher in GV oocytes than MII oocytes (Liu et al., 2007), it is overall relatively low in oocytes through to the 4-cell stage, with levels greatly increasing at the blastocyst stage (Liu et al., 2002; Liu et al., 2007; Turner et al., 2010; Wright, 2001). This increase in telomerase activity at the blastocyst stage is supported by evidence in telomerase-null mice, which showed an

absence of elongation at the morula and blastocyst stages of development when compared to wild-type embryos (Schaetzlein et al., 2004). Further, when compared to oocytes, telomere elongation occurred in zygotes and 2-cell embryos of first- and even third-generation telomerase knock-out mice (Liu et al., 2007), indicating that while telomerase activity is required for telomere elongation later in development, elongation in the earliest stages occurs independently of this. Interestingly, telomere lengths were notably shorter in oocytes from first generation telomerase knock-out mice when compared to wild-type controls, and even more so in third generation mice (Liu et al., 2007), suggesting that either telomerase activity in follicles and oocytes contributes to MII oocyte telomere length, or that the primordial germ cells that the oocytes were derived from contained with shorter telomeres.

While it is becoming widely accepted that ALT is the elongation mechanism responsible for telomere elongation in the earliest stages of pre-implantation embryogenesis, much of the major defining characteristics are yet to be identified. To date, the body of work in support of this theory has arisen from just one study by Liu et al. (2007). In this report they characterised telomere elongation in zygotes and 2-cell embryos including from telomerase-null mice, however telomere length at each stage was calculated relative to MII oocyte telomere lengths, and as such this study adds no insight into telomere elongation events after the first cleavage. It also documented telomere sister chromatid exchanges (TSCE's) occurring at higher frequencies in zygotes and 2-cell embryos than blastocysts, yet whether this results in recombination and/or telomere extension is not clear. Lastly, protein expression of two APB proteins (RAD50, BLM) was analysed in mature oocytes, zygotes and 2-cells. Rad50 protein level was shown to be decreased in blastocysts and co-localised with TRF1 signal in 2-cell embryos but this was reduced in blastocysts (Liu et al., 2007). BLM however was not localised to telomeres. While these observations are a promising start, the localisation of these proteins to telomeres (with the exception of Rad50), along with other defining hallmarks, is yet to be reported. Therefore, significant advances in elucidating pre-implantation telomere lengthening mechanisms are still needed for even a basic understanding of how telomere length is established in offspring and maintained across generations.

Another animal model used to further interrogate telomere elongation during embryogenesis is the bovine. During bovine folliculogenesis, telomerase activity is

highest in oocytes within primordial follicles and lowest in those within antral follicles, with telomere length showing an inverse relationship to this, with telomeres being longest in oocytes contained within antral follicles (Betts and King, 1999; Russo et al., 2006). During oocyte maturation, telomerase activity is highest in immature (GV) oocytes, and gradually declines during maturation, reaching its lowest level in MII oocytes, despite no change in TERC expression levels (Betts and King, 1999). As for telomere length during this time, there is a discrepancy between studies, with one finding longer telomeres in GV oocytes than MII oocytes (Gilchrist et al., 2015), while another observed no differences in telomere length between stages (Meerdo et al., 2005). In contrast to mice, bovine sperm telomeres are significantly shorter than in both immature and mature oocytes (Meerdo et al., 2005). During embryogenesis, mature bovine oocytes had significantly longer telomeres than 2-8-cell embryos, which significantly lengthened at the morula stage, but decreased again by the blastocyst stage such that they were not different than in 2-8-cell stage embryos (Meerdo et al., 2005). Following the decrease in telomerase activity during oocyte maturation, activity has been shown to remain consistently low in MII oocytes through to 8-cell embryos, with great upregulation in activity in morula and blastocyst embryos when compared to the previous stages (Betts and King, 1999; Xu and Yang, 2001). In bovine blastocysts, the opposite trend to mouse embryos is seen with telomere lengths in the distinct cell populations, with the trophectoderm cells exhibiting longer telomeres than the inner cell mass (Iqbal et al., 2011).

Telomere lengths have been studied using two techniques that rely on oocyte factors for reprogramming: somatic cell nuclear transfer, and parthenogenesis. Somatic cell nuclear transfer (SCNT) is a technique that involves implanting the nucleus of a somatic (differentiated) cell into an enucleated oocyte to generate a viable embryo. Telomere lengths in animals generated by SCNT show varying results when compared to either the cell line used for SCNT, or to age-matched control animals. Of interest, the majority of studies analysing telomere length in cattle and pigs generated by SCNT have found relative telomere lengths to be of normal length or longer when compared to controls, while in sheep and goat the majority of studies have found SCNT animals to have shorter telomere lengths than controls (reviewed by Burgstaller and Brem, 2017). One study analysed telomerase activity in bovine blastocysts generated by SCNT and found that telomeres were able to be successfully reprogrammed to that of

IVF generated blastocysts, and subsequently found no difference in telomere lengths of resulting cattle (Betts, 2001). There are multiple factors in these studies that may contribute to the discrepancies in telomere lengths such as the type of somatic cell used for the donor nucleus, quality of the enucleated oocytes, nuclear transfer technique, embryo culture conditions, and of course, the efficiency of reprogramming of the somatic nucleus. Two studies have analysed telomere length in SCNT-generated mice, and both of these have found normal telomere lengths compared to controls, and astonishingly, these normal telomere lengths were maintained even after re-cloning of 25 generations (Wakayama et al., 2013, 2000). Parthenogenesis is a reproductive strategy where the oocyte is able to develop into an embryo without fertilisation or any genetic contribution from a male gamete. While parthenogenesis is common among lower plant and invertebrate animals (including aphids, ants, wasps, and bees) and quite rare in higher vertebrates, it can be induced in some higher species (commonly mice and bovine) using chemical manipulation in an ex vivo setting. Significant telomere elongation by the 2-cell stage of development has been confirmed in mouse parthenogenetic embryos when compared to MII oocytes, using both q-FISH and crude qPCR assays (de Frutos et al., 2016; Liu et al., 2007), and in blastocysts compared to MII oocytes, once again using a relatively crude qPCR assay (Liu et al., 2007). These studies indicate that parthenogenetic embryos are better able to undergo telomere length reprogramming than those generated by SCNT, however there are many complexities of SCNT that may account for these differences. Despite this, these studies are compelling evidence for the ability of oocyte derived factors to regulate telomere length reprogramming.

Telomere biology in human gametes and embryos is not well documented and there are only a few reports. Human oocyte telomere lengths decrease during oocyte maturation (Turner and Hartshorne, 2013), while GV oocytes and blastocysts have similar telomere lengths, which are significantly longer than the intervening oocyte and embryo stages (Turner et al., 2010; Wright, 2001). Similar to telomere length, telomerase activity levels are similar between GV oocytes and blastocysts, and again much higher than the intervening developmental stages (Wright, 2001). There are many shortcomings in the studies of oocytes and embryos obtained from humans as these are donated by IVF (*in-vitro* fertilisation) patients at the end of their treatment (Turner et al., 2010). Humans are highly variable, not only in genetics but also

environmental factors. The fact that the patients required IVF to conceive already suggests inherent defects in the quality of these oocytes and embryos, meaning that these samples may not reflect normal healthy material. Further to this, the donated samples are typically of poor quality as the highest quality oocytes and embryos are used for patient treatment. The limited amount of oocyte and embryo material available from humans and the associated ethical issues also means that the number of oocytes and embryos studied is very small, thus limiting the conclusions that can be made from these relatively preliminary observations. However, it is vital that this knowledge is expanded upon and made more robust as telomeres and telomerase are associated with human fertility issues (Keefe et al., 2005; Mania et al., 2014; Treff et al., 2011).

Relationships between fertility, oocyte telomere length and maternal age are consistent between humans and mice, where both fertility and telomere length decrease with age (Kalmbach et al., 2013; Keefe et al., 2006; Yamada-Fukunaga et al., 2013). Interestingly, telomeres are shorter in oocytes from women who experienced IVF failure or recurrent miscarriage (Mania et al., 2014) and conversely, patients with longer oocyte telomeres are more likely to successfully conceive when undergoing IVF (Keefe, 2007). Shorter oocyte telomeres have also been found in oocytes from patients that produced higher numbers of fragmented (Keefe et al., 2005) or aneuploidy embryos (Treff et al., 2011), analysed using q-FISH on chromosome spreads from an average of two oocytes per patient. Further to this, a close relationship has been demonstrated between short telomere lengths and in some cases a lack of telomerase activity in granulosa cells with female infertility caused by ovarian aging, PCOS (Y. Li et al., 2017), and premature ovarian failure (Butts et al., 2009).

While telomere elongation during pre-implantation embryogenesis is crucial for the offspring's health span and lifespan, there is surprisingly little understanding of the mechanisms behind this process in mice and most importantly humans, and significant advancements are needed. Further it is important to better understand how short telomeres result in or are associated with infertility phenotypes, so that we can better mitigate infertility risk factors and develop new therapeutic strategies.

1.5 Links between mitochondria and telomeres

Both telomere length and mitochondrial function decline with age and as such are both classified as major hallmarks of aging (López-Otín et al., 2013). As such telomere length and mtDNA copy number in blood leukocytes display a positive correlation (Kim et al., 2013; Qiu et al., 2015; Tyrka et al., 2015). However, mitochondria and telomeres are also linked in other contexts, including in states of cellular dysfunction, and some of which are only emerging.

1.5.1 Mitochondrial dysfunction and telomere dysfunction display a bi-directional relationship

The relationship between mitochondria and telomeres extends beyond their shared characteristic of aging-related decline to functional associations, which are bi-directional. Perhaps the most logical direction of this relationship is mitochondrial function inducing telomere damage, and indeed this is the most characterised and well documented. As a consequence of producing ATP for the cell, mitochondria also produce the majority of intracellular reactive oxygen species ((ROS), Y. Liu et al., 2002). In the context of normal respiration, cells have defence mechanisms to prevent these ROS inflicting any damage to the cell; but in cases of mitochondrial stress and/or dysfunction, levels of ROS production increase and can damage, via oxidation, both mtDNA (Cottrell and Turnbull, 2000) and nuclear DNA, leading to an accumulation of mutations in these genomes which can contribute to cellular dysfunction, cellular senescence, or apoptosis. Mutations in mtDNA can further exacerbate mitochondrial dysfunction and thus feedforward into a continuous cycle. When ROS enter the nucleus they result in oxidative damage and alterations to that intra-cellular micro-environment, which culminate in the dissociation of proteins from DNA, alterations to molecular regulatory mechanisms, and damage throughout the genome including both single and double strand DNA breaks (Sohal et al., 1994). Telomeres are guanine-rich sequences and as such are particularly susceptible to ROS induced damage, resulting in an increased rate of telomere shortening (Oikawa and Kawanishi, 1999; von Zglinicki et al., 1995).

Telomere dysfunction likely contributes to mitochondrial dysfunction and decreased mitochondrial biosynthesis through DNA damage response pathways. Studies in T cells where TRF2 was either silenced, or a mutant TRF2 protein was over expressed, resulted in increased γH2AX, and as such telomeric DNA damage (Nguyen et al., 2018). More specifically, the loss of TRF2 in mammalian cells resulted in the activation of the ATM-dependent DNA damage response pathway which in turn up-regulated p53 which leads to cell cycle arrest (Celli and de Lange, 2005; Karlseder, 1999). This telomere dysfunction related p53 activation has been shown to result in the repression of peroxisome proliferator-activated receptor gamma coactivator-1 alpha and beta (*PGC-1α* and *PGC-1β*), which are master transcriptional regulators of mitochondrial biogenesis and metabolism (Sahin et al., 2011). As such, telomere dysfunction was associated with impaired mitochondrial biogenesis and increased mitochondrial dysfunction and therefore ROS production (Sahin et al., 2011). Both mitochondrial and telomeric dysfunction are implicated in disease and ageing, likely in a bi-directional cyclic exacerbation of phenotypes.

1.5.2 Mitochondria and telomeres in aging and disease

Mitochondrial function and telomere length are both implicated as major hallmarks of aging when they decline, and modulating either of these parameters has been shown to effect the other, as well as having consequences on health span and life span.

A recent study showed that mice generated to have hyper-long telomeres maintained long telomeres in metabolic-related tissues (liver, white and brown adipose tissue) throughout their lifespan and had less cellular senescence in the liver at 100 weeks of age than control mice (Muñoz-Lorente et al., 2019). Hyper-long telomere mice also displayed less metabolic aging at 50, 75, and 100 weeks of age, and improved mitochondrial function when compared to control mice at 100-110 weeks of age (Muñoz-Lorente et al., 2019). Improved mitochondrial function was defined as higher mtDNA copy number, higher mRNA expression of oxidative phosphorylation genes (Cytochrome C, ATP synthase, and Cytochrome C subunits 6 and 5α), higher mRNA expression of PGC1-α and –β as well as PGC1 targets ERRα (involved in mitochondrial biogenesis, glucose utilisation, and enhanced fatty acid oxidation) and PPARα (enhanced fatty acid oxidation) (Muñoz-Lorente et al., 2019). These hyper-

long telomere mice also showed a 12.75% increase in median lifespan and 8.4% increase in maximum lifespan compared to controls (Muñoz-Lorente et al., 2019), further connecting telomere length and mitochondrial function with lifespan. Of interest, hyper-long telomere mice were also observed to be leaner due to lower fat accumulation, to maintain longer telomeres in both proliferative and non-proliferative tissues (skin, intestines, brain), and to have lower levels of DNA damage and telomere-specific DNA damage, and less spontaneous cancer occurrence than in control mice (Muñoz-Lorente et al., 2019). Cumulatively, these observations demonstrate that longer telomeres and lower rates of mitochondrial aging have implications for overall health span.

Studies assessing the disruption of telomere length or mitochondrial function on health and aging have shown similar phenotypes. In telomerase deficient mice (null for either the TERT or TERC component of telomerase), short telomeres were associated with impaired mitochondrial biogenesis and progressive tissue atrophy resulting from impaired mitochondrial function and increased ROS, stem cell depletion, organ system failure, and impaired tissue response to injury (Sahin et al., 2011), all of which are common aging phenotypes. Mice that contain a mutated version of mtDNA PolG (polymerase gamma, the catalytic subunit of mitochondrial DNA polymerase) have significantly more mtDNA mutations per 1000 nucleotides than wild-type PolG mice (Safdar et al., 2015). These mutations lead to increased mitochondrial dysfunction, and activity of two key mitochondrial proteins involved in clearing ROS (SOD2 and catalase) was significantly decreased in heart and muscle tissues in these mutant mice (Safdar et al., 2015). Telomere length in the heart, hematopoietic stem and progenitor cells, and satellite cells of these mutant mice were significantly shorter than wild-type mice (Safdar et al., 2015). By 7.5 months of age, PolG mutant mice showed premature onset of aging characteristics such as a progressive reduction in body size, increased kyphosis (hunchback), loss of hair pigmentation and alopecia, and ultimately had a reduced lifespan of 12 months (Safdar et al., 2015). This study further establishes the relationship between mitochondrial dysfunction and telomere length as an important regulator of lifespan.

Many human diseases also present associations between mitochondrial dysfunction and telomere length. Diseases that have mitochondrial dysfunction and increased mitochondrial ROS production as a hallmark have been associated with shorter

leukocyte telomere lengths. These include mitochondrial diabetes which results from a mtDNA mutation (m.3243A>G) (Zhou et al., 2015), primary mitochondrial dysfunction disorders such as mitochondrial myopathy, encephalopathy, lactic acid, stroke, and Leber hereditary optic neuropathy (Oexle and Zwirner, 1997), and Friedreich's Ataxia where affected people also display accelerated telomere shortening with disease progression (Castaldo et al., 2013). Interestingly, decreased leukocyte telomere lengths have also been documented in individuals with psychological disorders that are associated with mitochondrial dysfunction (Irie et al., 2003, 2001; Morris and Berk, 2015), such as major depressive disorder, bipolar disorder, anxiety, and post-traumatic stress disorder (Lindqvist et al., 2015; Simon et al., 2006). Other diseases associated with mitochondrial dysfunction and shorter telomeres in leukocytes include type I and II diabetes, cardiovascular diseases, atherosclerosis, Parkinson's disease, and Alzheimer's disease (Brouilette et al., 2003; Fitzpatrick et al., 2006; Guan et al., 2008; Matthews et al., 2006; Mikhed et al., 2015; Olivieri et al., 2009; Panossian, 2003; Ryan et al., 2015; Sampson et al., 2006; Swerdlow, 2011; Thomas et al., 2008; Uziel et al., 2007; Ward et al., 2013). These studies all strengthen the links between mitochondria and telomeres in disease and aging processes.

1.5.3 Mitochondrial metabolism intermediates can affect epigenetic regulation of gene expression

Mitochondrial metabolites are produced as intermediates of the Krebs cycle from enzymatic reactions and are required for cell growth and signalling processes that are produced during mitochondrial metabolism. These metabolites have been shown to not only be important for biosynthesis of macromolecules (such as nucleotides, lipids, and proteins) , but are also used as substrates and co-factors for a variety of enzymes that are important in epigenome modifications (Harvey, 2019; Reid et al., 2017). Examples of key metabolites that participate in epigenetic regulation are acetyl-CoA, succinate, α-ketoglutarate, and L-2-hydroxyglutarate. Mitochondria are highly responsive to the environment, therefore metabolites enable the ability for direct communication about environmental changes to the chromatin state (Cavalli and Heard, 2019), enabling rapid adaptations in gene expression to form an appropriate

cellular response. The list of known histone modifications is extensive, and many of these are influenced by metabolites, however for the purpose of this review histone acetylation and methylation will be addressed due to their importance in pre-implantation embryogenesis (see sections 1.2.4), along with DNA methylation.

Cytosine methyl modifications are added to DNA and histones by methyltransferases and erased by TET DNA demethylases. The metabolism of the essential amino acid methionine facilitates this modification. Methionine is first converted into S-adenosylmethionine (SAM, Sanderson et al., 2019) which is a metabolite that is able to be used as a methyl-donor. Following methyl donation, S-adenosylhomocysteine (SAH) is produced, which competitively inhibits methyltransferases. Changes in methionine availability or metabolism has been shown to affect SAM and SAH concentrations, resulting in changes in histone- and DNA-methylation levels (Mattocks et al., 2017; Zhang, 2018), which have been directly shown to alter levels of epigenetic modifications in a variety of cell types (reviewed in Dai et al., 2020) correlating with gene expression changes. Similarly, metabolism intermediates can also affect the activity of enzymes responsible for the removal of methylation marks, such as the TET family of DNA demethylases and histone demethylases, including JmjC-domain containing demethylases (JHDMs, Kohli and Zhang, 2013; Shi, 2007). The essential metabolite substrate for TETs and JHDMs is α-ketoglutarate (αKG). Structural analogs of αKG, such as succinate, fumarate, and 2-hydroxyglutarate (2-HG, an onco-metabolite) are also metabolism derivatives and act to inhibit TET and JHDM activity (Dai et al., 2020).

Another interesting angle in the metabolic control of methyl epigenetic modifications may be the production of ROS. ROS production can induce DNA damage (see section 1.5.1), however a study in C. *elegans* analysing ROS generation during early development revealed that the ROS was associated with inhibition of certain H3K4 methyltransferases, resulting in a global reduction in H3K4me3 levels (Bazopoulou et al., 2019). This finding should be replicated in other cell and organismal contexts, but suggests that ROS production may also influence histone methylation epigenetic modifications.

Histone acetyltransferases (HATS) catalyse the transfer of an acetyl group from the metabolite acetyl-CoA (Bannister and Kouzarides, 2011). Acetyl-CoA is derived from the supply of extracellular glucose into the mitochondrial metabolic pathway to

produce citrate, which is then further processed within the cytoplasm to generate acetyl-CoA (Wellen et al., 2009). As acetyl-CoA is directly required for acetylation, glucose availability and glycolytic activity to produce acetyl-CoA can directly influence global levels of histone acetylation (Cluntun et al., 2015; Wellen et al., 2009). Although metabolites facilitate the addition of acetylation, they also mediate the removal of these acetyl groups. Histone deacetylases (HDACS) are inhibited by metabolites that are produced from fatty acid oxidation or ketogenesis, which are butyrate and β-hydroxybutyrate (Shimazu et al., 2013). Another class of HDACS, sirtuins, are sensitive to intracellular NAD+ levels as they utilise NAD+ for deacetylation catalysis (Chalkiadaki and Guarente, 2012). NAD functions as a coenzyme in many of the reactions required for major energy production pathways, including glycolysis, the Krebs cycle, and fatty acid oxidation (Yaku et al., 2018). Therefore, not only can the availability of NAD directly mediate the activity of sirtuins, it can also influence many other metabolic enzymes, which can therefore alter the availability of other metabolites, including acetyl-CoA, isocitrate, and α-ketoglutarate, required for epigenetic modifications.

Thus mitochondria are inherently sensitive and produce a wide range of metabolites in response to signals from the intracellular and extracellular environment. In particular, over- and under-nutrition and/or metabolic dysfunction as well as normal physiological aging cause mitochondrial changes that alter metabolite supply. This in turn, via activating epigenetic regulators, alters gene expression; making mitochondria a cellular nexus between physiological signals and DNA modifications that elicit cellular adaptations. How these mechanisms regulate events during embryo formation and reprogramming is only beginning to be understood. Further, understanding how situations of nutrition, aging and metabolic dysfunction can perturb epigenetic homeostasis, therefore gene expression and even developmental reprogramming of the epigenome is crucial for furthering knowledge of the full implications of situations of perturbed embryo development and consequences for the lifetime health of offspring.

1.6 Summary and outline of aims

Pre-implantation embryogenesis is a rapid, complex, and highly dynamic time of development. Many of the processes occurring during this time have lifelong implications for the offspring, and are also highly vulnerable to perturbations. Of particular interest here are epigenetic and telomere length reprogramming events, and the roles mitochondria play in the facilitation of these. While epigenetic reprogramming mechanisms and mitochondrial localisation and utilisation have been thoroughly characterised, there is much that is still unknown about telomere elongation events occurring during preimplantation development, and how healthy mitochondrial function supports this process. As discussed in this review, there is a complex and intricate web of interactions between mitochondria, telomeres, and epigenetic modifications, which almost certainly have implications for embryo development, successful implantation and pregnancy, and offspring health trajectories.

This thesis aimed to further the understanding of telomere elongation during pre-implantation embryogenesis. Based on the information presented above, it was hypothesised that mitochondrial function plays a key role in telomere elongation events during early embryogenesis. Therefore, if mitochondria are dysfunctional then these embryos will exhibit disrupted telomere elongation, evidenced by shorter telomere lengths, and this can be rescued by modulating mitochondria function. Further, as mitochondrial metabolites are key regulators of epigenetic modifications, if mitochondria are dysfunctional then establishment of epigenetic asymmetry in zygotes will be disordered, and improving mitochondrial function can rescue this.

To address these hypotheses, this thesis focussed on the following aims:

Aim 1: To define telomere elongation kinetics and regulators during pre-implantation embryogenesis.

Aim 2: To determine if oocyte mitochondrial dysfunction, in oocytes exposed to environmental perturbations such as obese and old mothers, impacts telomere lengthening processes in embryos.

Aim 3: To determine the ability of a mitochondrial activator compound (BGP-15) to restore telomere length in oocytes and embryos from old and obese mothers.

1.7 References

Figures 1.3, 1.4, 1.5, 1.6, 1.8 A, and 1.9 created with BioRender.com.

Absalón-Medina, V.A., Butler, W.R., Gilbert, R.O., 2014. Preimplantation embryo metabolism and culture systems: experience from domestic animals and clinical implications. Journal of Assisted Reproduction and Genetics 31, 393–409. https://doi.org/10.1007/s10815-014-0179-2

Alabduladhem, T.O., Bordoni, B., 2021. Physiology, Krebs Cycle, in: StatPearls. StatPearls Publishing, Treasure Island (FL).

Anderson, S., Bankier, A.T., Barrell, B.G., de Bruijn, M.H.L., Coulson, A.R., Drouin, J., Eperon, I.C., Nierlich, D.P., Roe, B.A., Sanger, F., Schreier, P.H., Smith, A.J.H., Staden, R., Young, I.G., 1981. Sequence and organization of the human mitochondrial genome. Nature 290, 457–465. https://doi.org/10.1038/290457a0

Aoki, F., Worrad, D.M., Schultz, R.M., 1997. Regulation of Transcriptional Activity during the First and Second Cell Cycles in the Preimplantation Mouse Embryo. Developmental Biology 181, 296–307. https://doi.org/10.1006/dbio.1996.8466

Artus, J., Cohen-Tannoudji, M., 2008. Cell cycle regulation during early mouse embryogenesis. Molecular and Cellular Endocrinology 282, 78–86. https://doi.org/10.1016/j.mce.2007.11.008

Bannister, A.J., Kouzarides, T., 2011. Regulation of chromatin by histone modifications. Cell Research 21, 381–395. https://doi.org/10.1038/cr.2011.22

Barker, D.J.P., 2002. EDITORIAL: The developmental origins of adult disease. European Journal of Epidemiology 18, 733–736. https://doi.org/10.1023/A:1025388901248

Barsov, E.V., 2011. Telomerase and primary T cells: biology and immortalization for adoptive immunotherapy. Immunotherapy 3, 407–421. https://doi.org/10.2217/imt.10.107

Bartolomei, M.S., 2009. Genomic imprinting: employing and avoiding epigenetic processes. Genes & Development 23, 2124–2133. https://doi.org/10.1101/gad.1841409

Basu, B., Desai, R., Balaji, J., Chaerkady, R., Sriram, V., Maiti, S., Panicker, M.M., 2008. Serotonin in pre-implantation mouse embryos is localized to the mitochondria and can modulate mitochondrial potential. REPRODUCTION 135, 657–669. https://doi.org/10.1530/REP-07-0577

Bazopoulou, D., Knoefler, D., Zheng, Y., Ulrich, K., Oleson, B.J., Xie, L., Kim, M., Kaufmann, A., Lee, Y.-T., Dou, Y., Chen, Y., Quan, S., Jakob, U., 2019. Developmental ROS individualizes organismal stress resistance and lifespan. Nature 576, 301–305. https://doi.org/10.1038/s41586-019-1814-y

Benetti, R., García-Cao, M., Blasco, M.A., 2007. Telomere length regulates the epigenetic status of mammalian telomeres and subtelomeres. Nature Genetics 39, 243–250. https://doi.org/10.1038/ng1952

Bernardi, R., Pandolfi, P.P., 2007. Structure, dynamics and functions of promyelocytic leukaemia nuclear bodies. Nature Reviews Molecular Cell Biology 8, 1006–1016. https://doi.org/10.1038/nrm2277

Betts, D.H., 2001. Reprogramming of telomerase activity and rebuilding of telomere length in cloned cattle. Proceedings of the National Academy of Sciences 98, 1077–1082. https://doi.org/10.1073/pnas.031559298

Betts, D.H., King, W.A., 1999. Telomerase activity and telomere detection during early bovine development. Developmental Genetics 25, 397–403. https://doi.org/10.1002/(SICI)1520-6408(1999)25:4<397::AID-DVG13>3.0.CO;2-J

Biggers, J.D., Whittingham, D.G., Donahue, R.P., 1967. The pattern of energy metabolism in the mouse oocyte and zygote. Proceedings of the National Academy of Sciences 58, 560–567. https://doi.org/10.1073/pnas.58.2.560

Bird, A.P., Wolffe, A.P., 1999. Methylation-Induced Repression— Belts, Braces, and Chromatin. Cell 99, 451–454. https://doi.org/10.1016/S0092-8674(00)81532-9

Birky, C.W., 1995. Uniparental inheritance of mitochondrial and chloroplast genes: mechanisms and evolution. Proceedings of the National Academy of Sciences 92, 11331–11338. https://doi.org/10.1073/pnas.92.25.11331

Blackburn, E.H., 1984. Telomeres: Do the ends justify the means? Cell 37, 7–8. https://doi.org/10.1016/0092-8674(84)90295-2

Blasco, M.A., 2007. The epigenetic regulation of mammalian telomeres. Nature Reviews Genetics 8, 299–309. https://doi.org/10.1038/nrg2047

Boateng, K.A., Bellani, M.A., Gregoretti, I.V., Pratto, F., Camerini-Otero, R.D., 2013. Homologous Pairing Preceding SPO11-Mediated Double-Strand Breaks in Mice. Developmental Cell 24, 196–205. https://doi.org/10.1016/j.devcel.2012.12.002

Bombarde, O., Boby, C., Gomez, D., Frit, P., Giraud-Panis, M.-J., Gilson, E., Salles, B., Calsou, P., 2010. TRF2/RAP1 and DNA–PK mediate a double protection against joining at telomeric ends. The EMBO Journal 29, 1573–1584. https://doi.org/10.1038/emboj.2010.49

Borden, K.L.B., 2008. Pondering the puzzle of PML (promyelocytic leukemia) nuclear bodies: Can we fit the pieces together using an RNA regulon? Biochimica et Biophysica Acta (BBA) - Molecular Cell Research 1783, 2145–2154. https://doi.org/10.1016/j.bbamcr.2008.06.005

Bornens, M., 2008. Organelle positioning and cell polarity. Nature Reviews Molecular Cell Biology 9, 874–886. https://doi.org/10.1038/nrm2524

Borum, K., 1961. Oogenesis in the mouse. Experimental Cell Research 24, 495–507. https://doi.org/10.1016/0014-4827(61)90449-9

Bowdin, S., Allen, C., Kirby, G., Brueton, L., Afnan, M., Barratt, C., Kirkman-Brown, J., Harrison, R., Maher, E.R., Reardon, W., 2007. A survey of assisted reproductive technology births and imprinting disorders. Human Reproduction 22, 3237–3240. https://doi.org/10.1093/humrep/dem268

Boyer, L.A., Lee, T.I., Cole, M.F., Johnstone, S.E., Levine, S.S., Zucker, J.P., Guenther, M.G., Kumar, R.M., Murray, H.L., Jenner, R.G., Gifford, D.K., Melton, D.A., Jaenisch, R., Young, R.A., 2005. Core Transcriptional Regulatory Circuitry in Human Embryonic Stem Cells. Cell 122, 947–956. https://doi.org/10.1016/j.cell.2005.08.020

Brinster, R.L., 1965. Studies on the development of mouse embyrosin vitro. II. The effect of energy source. Journal of Experimental Zoology 158, 59–68. https://doi.org/10.1002/jez.1401580106

Brouilette, S., Singh, R.K., Thompson, J.R., Goodall, A.H., Samani, N.J., 2003. White Cell Telomere Length and Risk of Premature Myocardial Infarction. Arteriosclerosis,

Thrombosis, and Vascular Biology 23, 842–846. https://doi.org/10.1161/01.ATV.0000067426.96344.32

Burgstaller, J.P., Brem, G., 2017. Aging of Cloned Animals: A Mini-Review. Gerontology 63, 417–425. https://doi.org/10.1159/000452444

Butts, S., Riethman, H., Ratcliffe, S., Shaunik, A., Coutifaris, C., Barnhart, K., 2009. Correlation of Telomere Length and Telomerase Activity with Occult Ovarian Insufficiency. The Journal of Clinical Endocrinology & Metabolism 94, 4835–4843. https://doi.org/10.1210/jc.2008-2269

Byskov, A.G., 1986. Differentiation of mammalian embryonic gonad. Physiological Reviews 66, 71–117. https://doi.org/10.1152/physrev.1986.66.1.71

Cagnone, G., Sirard, M.-A., 2016. The embryonic stress response to in vitro culture: insight from genomic analysis. Reproduction 152, R247–R261. https://doi.org/10.1530/REP-16-0391

Calado, R.T., Young, N.S., 2009. Telomere Diseases. New England Journal of Medicine 361, 2353–2365. https://doi.org/10.1056/NEJMra0903373

Calarco, P.G., 1995. Polarization of mitochondria in the unfertilized mouse oocyte. Developmental Genetics 16, 36–43. https://doi.org/10.1002/dvg.1020160108

Camlin, N.J., Sobinoff, A.P., Sutherland, J.M., Beckett, E.L., Jarnicki, A.G., Vanders, R.L., Hansbro, P.M., McLaughlin, E.A., Holt, J.E., 2016. Maternal Smoke Exposure Impairs the Long-Term Fertility of Female Offspring in a Murine Model1. Biology of Reproduction 94. https://doi.org/10.1095/biolreprod.115.135848

Castaldo, I., Vergara, P., Pinelli, M., Filla, A., De Michele, G., Cocozza, S., Monticelli, A., 2013. Can Telomere Shortening in Human Peripheral Blood Leukocytes Serve as a Disease Biomarker of Friedreich's Ataxia? Antioxidants & Redox Signaling 18, 1303–1306. https://doi.org/10.1089/ars.2012.5009

Cavalli, G., Heard, E., 2019. Advances in epigenetics link genetics to the environment and disease. Nature 571, 489–499. https://doi.org/10.1038/s41586-019-1411-0

Celli, G.B., de Lange, T., 2005. DNA processing is not required for ATM-mediated telomere damage response after TRF2 deletion. Nature Cell Biology 7, 712–718. https://doi.org/10.1038/ncb1275

Chalkiadaki, A., Guarente, L., 2012. Sirtuins mediate mammalian metabolic responses to nutrient availability. Nature Reviews Endocrinology 8, 287–296. https://doi.org/10.1038/nrendo.2011.225

Chambers, I., Colby, D., Robertson, M., Nichols, J., Lee, S., Tweedie, S., Smith, A., 2003. Functional Expression Cloning of Nanog, a Pluripotency Sustaining Factor in Embryonic Stem Cells. Cell 113, 643–655. https://doi.org/10.1016/S0092-8674(03)00392-1

Chang, F.T.M., McGhie, J.D., Chan, F.L., Tang, M.C., Anderson, M.A., Mann, J.R., Andy Choo, K.H., Wong, L.H., 2013. PML bodies provide an important platform for the maintenance of telomeric chromatin integrity in embryonic stem cells. Nucleic Acids Research 41, 4447–4458. https://doi.org/10.1093/nar/gkt114

Chen, H., Detmer, S.A., Ewald, A.J., Griffin, E.E., Fraser, S.E., Chan, D.C., 2003. Mitofusins Mfn1 and Mfn2 coordinately regulate mitochondrial fusion and are essential for embryonic development. Journal of Cell Biology 160, 189–200. https://doi.org/10.1083/jcb.200211046

Chen, H., Vermulst, M., Wang, Y.E., Chomyn, A., Prolla, T.A., McCaffery, J.M., Chan, D.C., 2010. Mitochondrial fusion is required for mtDNA stability in skeletal muscle and tolerance of mtDNA mutations. Cell 141, 280–289. https://doi.org/10.1016/j.cell.2010.02.026

Chen, T., Li, E., 2004. Structure and Function of Eukaryotic DNA Methyltransferases, in: Current Topics in Developmental Biology. Elsevier, pp. 55–89. https://doi.org/10.1016/S0070-2153(04)60003-2

Chomyn, A., Mariottini, P., Cleeter, M.W.J., Ragan, C.I., Matsuno-Yagi, A., Hatefi, Y., Doolittle, R.F., Attardi, G., 1985. Six unidentified reading frames of human mitochondrial DNA encode components of the respiratory-chain NADH dehydrogenase. Nature 314, 592–597. https://doi.org/10.1038/314592a0

Ciesielski, G.L., Oliveira, M.T., Kaguni, L.S., 2016. Animal Mitochondrial DNA Replication. Enzymes 39, 255–292. https://doi.org/10.1016/bs.enz.2016.03.006

Cluntun, A.A., Huang, H., Dai, L., Liu, X., Zhao, Y., Locasale, J.W., 2015. The rate of glycolysis quantitatively mediates specific histone acetylation sites. Cancer & Metabolism 3. https://doi.org/10.1186/s40170-015-0135-3

Cohen, S.B., Graham, M.E., Lovrecz, G.O., Bache, N., Robinson, P.J., Reddel, R.R., 2007. Protein Composition of Catalytically Active Human Telomerase from Immortal Cells. Science 315, 1850–1853. https://doi.org/10.1126/science.1138596

Cottrell, D.A., Turnbull, D.M., 2000. Mitochondria and ageing: Current Opinion in Clinical Nutrition and Metabolic Care 3, 473–478. https://doi.org/10.1097/00075197-200011000-00009

Cree, L.M., Samuels, D.C., de Sousa Lopes, S.C., Rajasimha, H.K., Wonnapinij, P., Mann, J.R., Dahl, H.-H.M., Chinnery, P.F., 2008. A reduction of mitochondrial DNA molecules during embryogenesis explains the rapid segregation of genotypes. Nature Genetics 40, 249–254. https://doi.org/10.1038/ng.2007.63

Cristofari, G., Lingner, J., 2006. Telomere length homeostasis requires that telomerase levels are limiting. The EMBO Journal 25, 565–574. https://doi.org/10.1038/sj.emboj.7600952

Cummins, J.M., Wakayama, T., Yanagimachi, R., 1998. Fate of microinjected spermatid mitochondria in the mouse oocyte and embryo. Zygote 6, 213–222. https://doi.org/10.1017/S0967199498000148

Dai, J., Kuo, K.-H., Leo, J.M., van Breemen, C., Lee, C.-H., 2005. Rearrangement of the close contact between the mitochondria and the sarcoplasmic reticulum in airway smooth muscle. Cell Calcium 37, 333–340. https://doi.org/10.1016/j.ceca.2004.12.002

Dai, Z., Ramesh, V., Locasale, J.W., 2020. The evolving metabolic landscape of chromatin biology and epigenetics. Nature Reviews Genetics. https://doi.org/10.1038/s41576-020-0270-8

Dalton, C.M., Carroll, J., 2013. Biased inheritance of mitochondria during asymmetric cell division in the mouse oocyte. Journal of Cell Science 126, 2955–2964. https://doi.org/10.1242/jcs.128744

Das, S., Hajnóczky, N., Antony, A.N., Csordás, G., Gaspers, L.D., Clemens, D.L., Hoek, J.B., Hajnóczky, G., 2012. Mitochondrial morphology and dynamics in hepatocytes from normal and ethanol-fed rats. Pflügers Archiv - European Journal of Physiology 464, 101–109. https://doi.org/10.1007/s00424-012-1100-4

de Frutos, C., López-Cardona, A.P., Fonseca Balvís, N., Laguna-Barraza, R., Rizos, D., Gutierrez-Adán, A., Bermejo-Álvarez, P., 2016. Spermatozoa telomeres determine

telomere length in early embryos and offspring. Reproduction 151, 1–7. https://doi.org/10.1530/REP-15-0375

Del Dotto, V., Mishra, P., Vidoni, S., Fogazza, M., Maresca, A., Caporali, L., McCaffery, J.M., Cappelletti, M., Baruffini, E., Lenaers, G., Chan, D., Rugolo, M., Carelli, V., Zanna, C., 2017. OPA1 Isoforms in the Hierarchical Organization of Mitochondrial Functions. Cell Rep 19, 2557–2571. https://doi.org/10.1016/j.celrep.2017.05.073

Delbarre, E., Ivanauskiene, K., Spirkoski, J., Shah, A., Vekterud, K., Moskaug, J.Ø., Bøe, S.O., Wong, L.H., Küntziger, T., Collas, P., 2017. PML protein organizes heterochromatin domains where it regulates histone H3.3 deposition by ATRX/DAXX. Genome Research 27, 913–921. https://doi.org/10.1101/gr.215830.116

Dellaire, G., Bazett-Jones, D.P., 2004. PML nuclear bodies: dynamic sensors of DNA damage and cellular stress. BioEssays 26, 963–977. https://doi.org/10.1002/bies.20089

Denomme, M.M., Mann, M.R.W., 2013. Maternal control of genomic imprint maintenance. Reproductive BioMedicine Online 27, 629–636. https://doi.org/10.1016/j.rbmo.2013.06.004

Denomme, M.M., Zhang, L., Mann, M.R.W., 2011. Embryonic imprinting perturbations do not originate from superovulation-induced defects in DNA methylation acquisition. Fertility and Sterility 96, 734-738.e2. https://doi.org/10.1016/j.fertnstert.2011.06.055

Desai, N., Ludgin, J., Sharma, R., Anirudh, R.K., Agarwal, A., 2017. Female and Male Gametogenesis, in: Falcone, T., Hurd, W.W. (Eds.), Clinical Reproductive Medicine and Surgery. Springer International Publishing, Cham, pp. 19–45. https://doi.org/10.1007/978-3-319-52210-4_2

Dolnik, A., Pochukalina, G., Parfenov, V., Karpushev, A., Podgornaya, O., Voronin, A., 2007. Dynamics of satellite binding protein CENP-B and telomere binding protein TRF2/MTBP in the nuclei of mouse spermatogenic line. Cell Biology International 31, 316–329. https://doi.org/10.1016/j.cellbi.2007.01.017

Dolnik, A.V., Kuznetsova, I.S., Voronin, A.P., Podgornaya, O.I., 2003. Telomere-Binding TRF2/MTBP Localization during Mouse Spermatogenesis and Cell Cycle of

the Mouse Cells L929. Journal of Anti-Aging Medicine 6, 107–121. https://doi.org/10.1089/109454503769684784

Draskovic, I., Arnoult, N., Steiner, V., Bacchetti, S., Lomonte, P., Londoño-Vallejo, A., 2009. Probing PML body function in ALT cells reveals spatiotemporal requirements for telomere recombination. Proceedings of the National Academy of Sciences 106, 15726–15731. https://doi.org/10.1073/pnas.0907689106

Dumollard, R., Duchen, M., Carroll, J., 2007. The Role of Mitochondrial Function in the Oocyte and Embryo, in: Current Topics in Developmental Biology. Elsevier, pp. 21–49. https://doi.org/10.1016/S0070-2153(06)77002-8

Ecker, D.J., Stein, P., Xu, Z., Williams, C.J., Kopf, G.S., Bilker, W.B., Abel, T., Schultz, R.M., 2004. Long-term effects of culture of preimplantation mouse embryos on behavior. Proceedings of the National Academy of Sciences 101, 1595–1600. https://doi.org/10.1073/pnas.0306846101

Edgar, D., Shabalina, I., Camara, Y., Wredenberg, A., Calvaruso, M.A., Nijtmans, L., Nedergaard, J., Cannon, B., Larsson, N.-G., Trifunovic, A., 2009. Random Point Mutations with Major Effects on Protein-Coding Genes Are the Driving Force behind Premature Aging in mtDNA Mutator Mice. Cell Metabolism 10, 131–138. https://doi.org/10.1016/j.cmet.2009.06.010

Eisenberg, D.T.A., Salpea, K.D., Kuzawa, C.W., Hayes, M.G., Humphries, S.E., on Behalf of the European Atherosclerosis Research Study II Group, 2011. Substantial variation in qPCR measured mean blood telomere lengths in young men from eleven European countries. American Journal of Human Biology 23, 228–231. https://doi.org/10.1002/ajhb.21126

El Shourbagy, S.H., Spikings, E.C., Freitas, M., St John, J.C., 2006. Mitochondria directly influence fertilisation outcome in the pig. Reproduction 131, 233–245. https://doi.org/10.1530/rep.1.00551

Ellis, N.A., Groden, J., Ye, T.-Z., Straughen, J., Lennon, D.J., Ciocci, S., Proytcheva, M., German, J., 1995. The Bloom's syndrome gene product is homologous to RecQ helicases. Cell 83, 655–666. https://doi.org/10.1016/0092-8674(95)90105-1

Embley, T.M., Martin, W., 2006. Eukaryotic evolution, changes and challenges. Nature 440, 623–630. https://doi.org/10.1038/nature04546

Enderle, J.D., 2012. Biochemical Reactions and Enzyme Kinetics, in: Introduction to Biomedical Engineering. Elsevier, pp. 447–508. https://doi.org/10.1016/B978-0-12-374979-6.00008-3

Erhardt, S., 2003. Consequences of the depletion of zygotic and embryonic enhancer of zeste 2 during preimplantation mouse development. Development 130, 4235–4248. https://doi.org/10.1242/dev.00625

Facucho-Oliveira, J.M., Alderson, J., Spikings, E.C., Egginton, S., St. John, J.C., 2007. Mitochondrial DNA replication during differentiation of murine embryonic stem cells. Journal of Cell Science 120, 4025–4034. https://doi.org/10.1242/jcs.016972

Fasching, C.L., Bower, K., Reddel, R.R., 2005. Telomerase-Independent Telomere Length Maintenance in the Absence of Alternative Lengthening of Telomeres–Associated Promyelocytic Leukemia Bodies. Cancer Research 65, 2722–2729. https://doi.org/10.1158/0008-5472.CAN-04-2881

Fasching, C.L., Neumann, A.A., Muntoni, A., Yeager, T.R., Reddel, R.R., 2007. DNA Damage Induces Alternative Lengthening of Telomeres (ALT) Associated Promyelocytic Leukemia Bodies that Preferentially Associate with Linear Telomeric DNA. Cancer Research 67, 7072–7077. https://doi.org/10.1158/0008-5472.CAN-07-1556

Feldman, N., Gerson, A., Fang, J., Li, E., Zhang, Y., Shinkai, Y., Cedar, H., Bergman, Y., 2006. G9a-mediated irreversible epigenetic inactivation of Oct-3/4 during early embryogenesis. Nature Cell Biology 8, 188–194. https://doi.org/10.1038/ncb1353

Ferguson-Smith, A.C., 2011. Genomic imprinting: the emergence of an epigenetic paradigm. Nature Reviews Genetics 12, 565–575. https://doi.org/10.1038/nrg3032

Fitzpatrick, A.L., Kronmal, R.A., Gardner, J.P., Psaty, B.M., Jenny, N.S., Tracy, R.P., Walston, J., Kimura, M., Aviv, A., 2006. Leukocyte Telomere Length and Cardiovascular Disease in the Cardiovascular Health Study. American Journal of Epidemiology 165, 14–21. https://doi.org/10.1093/aje/kwj346

Gao, S., Chung, Y.G., Williams, J.W., Riley, J., Moley, K., Latham, K.E., 2003. Somatic Cell-Like Features of Cloned Mouse Embryos Prepared with Cultured Myoblast Nuclei1. Biology of Reproduction 69, 48–56. https://doi.org/10.1095/biolreprod.102.014522

García-Cao, M., Gonzalo, S., Dean, D., Blasco, M.A., 2002. A role for the Rb family of proteins in controlling telomere length. Nature Genetics 32, 415–419. https://doi.org/10.1038/ng1011

García-Cao, M., O'Sullivan, R., Peters, A.H.F.M., Jenuwein, T., Blasco, M.A., 2004. Epigenetic regulation of telomere length in mammalian cells by the Suv39h1 and Suv39h2 histone methyltransferases. Nature Genetics 36, 94–99. https://doi.org/10.1038/ng1278

Gilchrist, G., Kurjanowicz, P., Mereilles, F., King, W., LaMarre, J., 2015. Telomere Length and Telomerase Activity in Bovine Pre-implantation Embryos *In Vitro*. Reproduction in Domestic Animals 50, 58–67. https://doi.org/10.1111/rda.12449

Giles, R.E., Blanc, H., Cann, H.M., Wallace, D.C., 1980. Maternal inheritance of human mitochondrial DNA. Proceedings of the National Academy of Sciences 77, 6715–6719. https://doi.org/10.1073/pnas.77.11.6715

Goldberg, A.D., Allis, C.D., Bernstein, E., 2007. Epigenetics: A Landscape Takes Shape. Cell 128, 635–638. https://doi.org/10.1016/j.cell.2007.02.006

Gondos, B., Westergaard, L., Byskov, A.G., 1986. Initiation of oogenesis in the human fetal ovary: Ultrastructural and squash preparation study. American Journal of Obstetrics and Gynecology 155, 189–195. https://doi.org/10.1016/0002-9378(86)90109-2

Gonzalo, S., García-Cao, M., Fraga, M.F., Schotta, G., Peters, A.H.F.M., Cotter, S.E., Eguía, R., Dean, D.C., Esteller, M., Jenuwein, T., Blasco, M.A., 2005. Role of the RB1 family in stabilizing histone methylation at constitutive heterochromatin. Nature Cell Biology 7, 420–428. https://doi.org/10.1038/ncb1235

Gonzalo, S., Jaco, I., Fraga, M.F., Chen, T., Li, E., Esteller, M., Blasco, M.A., 2006. DNA methyltransferases control telomere length and telomere recombination in mammalian cells. Nature Cell Biology 8, 416–424. https://doi.org/10.1038/ncb1386

Gosden, R., Trasler, J., Lucifero, D., Faddy, M., 2003. Rare congenital disorders, imprinted genes, and assisted reproductive technology. The Lancet 361, 1975–1977. https://doi.org/10.1016/S0140-6736(03)13592-1

Grabarek, J.B., Zyzynska, K., Saiz, N., Piliszek, A., Frankenberg, S., Nichols, J., Hadjantonakis, A.-K., Plusa, B., 2012. Differential plasticity of epiblast and primitive

endoderm precursors within the ICM of the early mouse embryo. Development 139, 129–139. https://doi.org/10.1242/dev.067702

Green, D.R., Galluzzi, L., Kroemer, G., 2011. Mitochondria and the Autophagy-Inflammation-Cell Death Axis in Organismal Aging. Science 333, 1109–1112. https://doi.org/10.1126/science.1201940

Greider, C.W., 1999. Telomeres Do D-Loop–T-Loop. Cell 97, 419–422. https://doi.org/10.1016/S0092-8674(00)80750-3

Greider, C.W., Blackburn, E.H., 1989. A telomeric sequence in the RNA of Tetrahymena telomerase required for telomere repeat synthesis. Nature 337, 331–337. https://doi.org/10.1038/337331a0

Griffith, J.D., Comeau, L., Rosenfield, S., Stansel, R.M., Bianchi, A., Moss, H., de Lange, T., 1999. Mammalian Telomeres End in a Large Duplex Loop. Cell 97, 503–514. https://doi.org/10.1016/S0092-8674(00)80760-6

Gu, T.-P., Guo, F., Yang, H., Wu, H.-P., Xu, G.-F., Liu, W., Xie, Z.-G., Shi, L., He, X., Jin, S., Iqbal, K., Shi, Y.G., Deng, Z., Szabó, P.E., Pfeifer, G.P., Li, J., Xu, G.-L., 2011. The role of Tet3 DNA dioxygenase in epigenetic reprogramming by oocytes. Nature 477, 606–610. https://doi.org/10.1038/nature10443

Guan, J.Z., Maeda, T., Sugano, M., Oyama, J. -i., Higuchi, Y., Suzuki, T., Makino, N., 2008. A Percentage Analysis of the Telomere Length in Parkinson's Disease Patients. The Journals of Gerontology Series A: Biological Sciences and Medical Sciences 63, 467–473. https://doi.org/10.1093/gerona/63.5.467

Guo, G., Huss, M., Tong, G.Q., Wang, C., Li Sun, L., Clarke, N.D., Robson, P., 2010. Resolution of Cell Fate Decisions Revealed by Single-Cell Gene Expression Analysis from Zygote to Blastocyst. Developmental Cell 18, 675–685. https://doi.org/10.1016/j.devcel.2010.02.012

H. Reddy, P., P. Reddy, T., 2011. Mitochondria as a Therapeutic Target for Aging and Neurodegenerative Diseases. Current Alzheimer Research 8, 393–409. https://doi.org/10.2174/156720511795745401

Hajjar, C., Sampuda, K.M., Boyd, L., 2014. Dual roles for ubiquitination in the processing of sperm organelles after fertilization. BMC Developmental Biology 14, 6. https://doi.org/10.1186/1471-213X-14-6

Hanaoka, S., Nagadoi, A., Nishimura, Y., 2009. Comparison between TRF2 and TRF1 of their telomeric DNA-bound structures and DNA-binding activities. Protein Science 14, 119–130. https://doi.org/10.1110/ps.04983705

Harle-Bachor, C., Boukamp, P., 1996. Telomerase activity in the regenerative basal layer of the epidermis inhuman skin and in immortal and carcinoma-derived skin keratinocytes. Proceedings of the National Academy of Sciences 93, 6476–6481. https://doi.org/10.1073/pnas.93.13.6476

Harvey, A.J., 2019. Mitochondria in early development: linking the microenvironment, metabolism and the epigenome. Reproduction 157, R159–R179. https://doi.org/10.1530/REP-18-0431

Harvey, A.J., Kind, K.L., Pantaleon, M., Armstrong, D.T., Thompson, J.G., 2004. Oxygen-Regulated Gene Expression in Bovine Blastocysts1. Biology of Reproduction 71, 1108–1119. https://doi.org/10.1095/biolreprod.104.028639

Hayflick, L., Moorhead, P.S., 1961. The serial cultivation of human diploid cell strains. Exp. Cell Res. 25, 585–621.

Henderson, S.A., Edwards, R.G., 1968. Chiasma Frequency and Maternal Age in Mammals. Nature 218, 22–28. https://doi.org/10.1038/218022a0

Henson, J.D., Neumann, A.A., Yeager, T.R., Reddel, R.R., 2002. Alternative lengthening of telomeres in mammalian cells. Oncogene 21, 598–610. https://doi.org/10.1038/sj.onc.1205058

Henson, J.D., Reddel, R.R., 2010. Assaying and investigating Alternative Lengthening of Telomeres activity in human cells and cancers. FEBS Lett. 584, 3800–3811. https://doi.org/10.1016/j.febslet.2010.06.009

Hiona, A., Sanz, A., Kujoth, G.C., Pamplona, R., Seo, A.Y., Hofer, T., Someya, S., Miyakawa, T., Nakayama, C., Samhan-Arias, A.K., Servais, S., Barger, J.L., Portero-Otín, M., Tanokura, M., Prolla, T.A., Leeuwenburgh, C., 2010. Mitochondrial DNA Mutations Induce Mitochondrial Dysfunction, Apoptosis and Sarcopenia in Skeletal Muscle of Mitochondrial DNA Mutator Mice. PLoS ONE 5, e11468. https://doi.org/10.1371/journal.pone.0011468

Hiura, H., Okae, H., Miyauchi, N., Sato, F., Sato, A., Van De Pette, M., John, R.M., Kagami, M., Nakai, K., Soejima, H., Ogata, T., Arima, T., 2012. Characterization of

DNA methylation errors in patients with imprinting disorders conceived by assisted reproduction technologies. Human Reproduction 27, 2541–2548. https://doi.org/10.1093/humrep/des197

Hiyama, E., Hiyama, K., 2007. Telomere and telomerase in stem cells. British Journal of Cancer 96, 1020–1024. https://doi.org/10.1038/sj.bjc.6603671

Iqbal, K., Kues, W.A., Baulain, U., Garrels, W., Herrmann, D., Niemann, H., 2011. Species-Specific Telomere Length Differences Between Blastocyst Cell Compartments and Ectopic Telomere Extension in Early Bovine Embryos by Human Telomerase Reverse Transcriptase. Biology of Reproduction 84, 723–733. https://doi.org/10.1095/biolreprod.110.087205

Irie, M., Asami, S., Ikeda, M., Kasai, H., 2003. Depressive state relates to female oxidative DNA damage via neutrophil activation. Biochemical and Biophysical Research Communications 311, 1014–1018. https://doi.org/10.1016/j.bbrc.2003.10.105

Irie, M., Asami, S., Nagata, S., Miyata, M., Kasai, H., 2001. Relationships between perceived workload, stress and oxidative DNA damage. International Archives of Occupational and Environmental Health 74, 153–157. https://doi.org/10.1007/s004200000209

Ivanauskiene, K., Delbarre, E., McGhie, J.D., Küntziger, T., Wong, L.H., Collas, P., 2014. The PML-associated protein DEK regulates the balance of H3.3 loading on chromatin and is important for telomere integrity. Genome Research 24, 1584–1594. https://doi.org/10.1101/gr.173831.114

Johnson, M.H., McConnell, J.M.., 2004. Lineage allocation and cell polarity during mouse embryogenesis. Seminars in Cell & Developmental Biology 15, 583–597. https://doi.org/10.1016/j.semcdb.2004.04.002

Johnson, M.H., Ziomek, C.A., 1981. Induction of polarity in mouse 8-cell blastomeres: specificity, geometry, and stability. The Journal of Cell Biology 91, 303–308. https://doi.org/10.1083/jcb.91.1.303

Kalmbach, K.H., Fontes Antunes, D.M., Dracxler, R.C., Knier, T.W., Seth-Smith, M.L., Wang, F., Liu, L., Keefe, D.L., 2013. Telomeres and human reproduction. Fertility and Sterility 99, 23–29. https://doi.org/10.1016/j.fertnstert.2012.11.039

Kameyama, Y., Filion, F., Yoo, J.G., Smith, L.C., 2007. Characterization of mitochondrial replication and transcription control during rat early development in vivo and in vitro. Reproduction 133, 423–432. https://doi.org/10.1530/REP-06-0263

Kaneko, K.J., 2016. Metabolism of Preimplantation Embryo Development, in: Current Topics in Developmental Biology. Elsevier, pp. 259–310. https://doi.org/10.1016/bs.ctdb.2016.04.010

Karbowski, M., Neutzner, A., 2012. Neurodegeneration as a consequence of failed mitochondrial maintenance. Acta Neuropathologica 123, 157–171. https://doi.org/10.1007/s00401-011-0921-0

Karlseder, J., 1999. p53- and ATM-Dependent Apoptosis Induced by Telomeres Lacking TRF2. Science 283, 1321–1325. https://doi.org/10.1126/science.283.5406.1321

Karlseder, J., Hoke, K., Mirzoeva, O.K., Bakkenist, C., Kastan, M.B., Petrini, J.H.J., Lange, T. de, 2004. The Telomeric Protein TRF2 Binds the ATM Kinase and Can Inhibit the ATM-Dependent DNA Damage Response. PLoS Biology 2, e240. https://doi.org/10.1371/journal.pbio.0020240

Keefe, D.L., 2007. Telomeres and meiosis in health and disease. Cellular and Molecular Life Sciences 64, 115–116. https://doi.org/10.1007/s00018-006-6462-3

Keefe, D.L., Franco, S., Liu, L., Trimarchi, J., Cao, B., Weitzen, S., Agarwal, S., Blasco, M.A., 2005. Telomere length predicts embryo fragmentation after in vitro fertilization in women—Toward a telomere theory of reproductive aging in women. American Journal of Obstetrics and Gynecology 192, 1256–1260. https://doi.org/10.1016/j.ajog.2005.01.036

Keefe, D.L., Marquard, K., Liu, L., 2006. The telomere theory of reproductive senescence in women: Current Opinion in Obstetrics and Gynecology 18, 280–285. https://doi.org/10.1097/01.gco.0000193019.05686.49

Kelly, R.D.W., Mahmud, A., McKenzie, M., Trounce, I.A., St John, J.C., 2012. Mitochondrial DNA copy number is regulated in a tissue specific manner by DNA methylation of the nuclear-encoded DNA polymerase gamma A. Nucleic Acids Research 40, 10124–10138. https://doi.org/10.1093/nar/gks770

Kim, J.-H., Kim, H.K., Ko, J.-H., Bang, H., Lee, D.-C., 2013. The Relationship between Leukocyte Mitochondrial DNA Copy Number and Telomere Length in Community-Dwelling Elderly Women. PLoS ONE 8, e67227. https://doi.org/10.1371/journal.pone.0067227

Kim, S., Kaminker, P., Campisi, J., 1999. TIN2, a new regulator of telomere length in human cells. Nature Genetics 23, 405–412. https://doi.org/10.1038/70508

Kimmins, S., Sassone-Corsi, P., 2005. Chromatin remodelling and epigenetic features of germ cells. Nature 434, 583–589. https://doi.org/10.1038/nature03368

Kiyonari, H., Kaneko, M., Abe, T., Shioi, G., Aizawa, S., Furuta, Y., Fujimori, T., 2019. Dynamic organelle localization and cytoskeletal reorganization during preimplantation mouse embryo development revealed by live imaging of genetically encoded fluorescent fusion proteins. genesis 57, e23277. https://doi.org/10.1002/dvg.23277

Kohli, R.M., Zhang, Y., 2013. TET enzymes, TDG and the dynamics of DNA demethylation. Nature 502, 472–479. https://doi.org/10.1038/nature12750

Kouzarides, T., 2007. Chromatin Modifications and Their Function. Cell 128, 693–705. https://doi.org/10.1016/j.cell.2007.02.005

Krisher, R.L., 2004. The effect of oocyte quality on development. J Anim Sci 82 E-Suppl, E14-23. https://doi.org/10.2527/2004.8213_supplE14x

Lane, M., Gardner, D.K., 1997. Differential regulation of mouse embryo development and viability by amino acids. Reproduction 109, 153–164. https://doi.org/10.1530/jrf.0.1090153

Lang, M., Jegou, T., Chung, I., Richter, K., Munch, S., Udvarhelyi, A., Cremer, C., Hemmerich, P., Engelhardt, J., Hell, S.W., Rippe, K., 2010. Three-dimensional organization of promyelocytic leukemia nuclear bodies. Journal of Cell Science 123, 392–400. https://doi.org/10.1242/jcs.053496

Le Bouc, Y., Rossignol, S., Azzi, S., Steunou, V., Netchine, I., Gicquel, C., 2010. Epigenetics, genomic imprinting and assisted reproductive technology. Annales d'Endocrinologie 71, 237–238. https://doi.org/10.1016/j.ando.2010.02.004

Lee, S.-E., Hwang, K.-C., Sun, S.-C., Xu, Y.-N., Kim, N.-H., 2011. Modulation of autophagy influences development and apoptosis in mouse embryos developing in

vitro. Molecular Reproduction and Development 78, 498–509. https://doi.org/10.1002/mrd.21331

Leese, H., 1995. Metabolic control during preimplantation mammalian development. Human Reproduction Update 1, 63–72. https://doi.org/10.1093/humupd/1.1.63

Leese, H.J., Barton, A.M., 1984. Pyruvate and glucose uptake by mouse ova and preimplantation embryos. Reproduction 72, 9–13. https://doi.org/10.1530/jrf.0.0720009

Lennerz, J.K., Timmerman, R.J., Grange, D.K., DeBaun, M.R., Feinberg, A.P., Zehnbauer, B.A., 2010. Addition of H19 “loss of methylation testing” for Beckwith-Wiedemann syndrome (BWS) increases the diagnostic yield. J Mol Diagn 12, 576–588. https://doi.org/10.2353/jmoldx.2010.100005

Li, J.S.Z., Miralles Fusté, J., Simavorian, T., Bartocci, C., Tsai, J., Karlseder, J., Lazzerini Denchi, E., 2017. TZAP: A telomere-associated protein involved in telomere length control. Science 355, 638–641. https://doi.org/10.1126/science.aah6752

Li, Y., Deng, B., Ouyang, N., Yuan, P., Zheng, L., Wang, W., 2017. Telomere length is short in PCOS and oral contraceptive does not affect the telomerase activity in granulosa cells of patients with PCOS. Journal of Assisted Reproduction and Genetics 34, 849–859. https://doi.org/10.1007/s10815-017-0929-z

Li, Y., O’Neill, C., 2012. Persistence of cytosine methylation of DNA following fertilisation in the mouse. PLoS One 7, e30687. https://doi.org/10.1371/journal.pone.0030687

Lindqvist, D., Epel, E.S., Mellon, S.H., Penninx, B.W., Révész, D., Verhoeven, J.E., Reus, V.I., Lin, J., Mahan, L., Hough, C.M., Rosser, R., Bersani, F.S., Blackburn, E.H., Wolkowitz, O.M., 2015. Psychiatric disorders and leukocyte telomere length: Underlying mechanisms linking mental illness with cellular aging. Neuroscience & Biobehavioral Reviews 55, 333–364. https://doi.org/10.1016/j.neubiorev.2015.05.007

Link, J., Jahn, D., Schmitt, J., Göb, E., Baar, J., Ortega, S., Benavente, R., Alsheimer, M., 2013. The Meiotic Nuclear Lamina Regulates Chromosome Dynamics and Promotes Efficient Homologous Recombination in the Mouse. PLoS Genetics 9, e1003261. https://doi.org/10.1371/journal.pgen.1003261

Liu, L., Bailey, S.M., Okuka, M., Muñoz, P., Li, C., Zhou, L., Wu, C., Czerwiec, E., Sandler, L., Seyfang, A., Blasco, M.A., Keefe, D.L., 2007. Telomere lengthening early in development. Nature Cell Biology 9, 1436–1441. https://doi.org/10.1038/ncb1664

Liu, L., Blasco, M.A., Trimarchi, J.R., Keefe, D.L., 2002. An Essential Role for Functional Telomeres in Mouse Germ Cells during Fertilization and Early Development. Developmental Biology 249, 74–84. https://doi.org/10.1006/dbio.2002.0735

Liu, L., Franco, S., Spyropoulos, B., Moens, P.B., Blasco, M.A., Keefe, D.L., 2004. Irregular telomeres impair meiotic synapsis and recombination in mice. Proceedings of the National Academy of Sciences 101, 6496–6501. https://doi.org/10.1073/pnas.0400755101

Liu, Y., Fiskum, G., Schubert, D., 2002. Generation of reactive oxygen species by the mitochondrial electron transport chain. Journal of Neurochemistry 80, 780–787. https://doi.org/10.1046/j.0022-3042.2002.00744.x

Lonergan, P., Fair, T., Corcoran, D., Evans, A.C.O., 2006. Effect of culture environment on gene expression and developmental characteristics in IVF-derived embryos. Theriogenology 65, 137–152. https://doi.org/10.1016/j.theriogenology.2005.09.028

Lonergan, P., Gutiérrez-Adán, A., Rizos, D., Pintado, B., De La Fuente, J., Boland, M.P., 2003. Relative messenger RNA abundance in bovine oocytes collected in vitro or in vivo before and 20 hr after the preovulatory luteinizing hormone surge: GENE EXPRESSION IN BOVINE OOCYTES. Molecular Reproduction and Development 66, 297–305. https://doi.org/10.1002/mrd.10357

López-Otín, C., Blasco, M.A., Partridge, L., Serrano, M., Kroemer, G., 2013. The Hallmarks of Aging. Cell 153, 1194–1217. https://doi.org/10.1016/j.cell.2013.05.039

Macreadie, I.G., Novitski, C.E., Maxwell, R.J., John, U., Ooi, B.-G., McMullen, G.L., Lukins, H.B., Linnane, A.W., Nagley, P., 1983. Biogenesis of mitochondria: the mitochondrial gene (aap1) coding for mitochondrial ATPase subunit 8 in Saccharomyces cerevisiae. Nucleic Acids Research 11, 4435–4451. https://doi.org/10.1093/nar/11.13.4435

Maher, E.R., 2005. Imprinting and assisted reproductive technology. Human Molecular Genetics 14, R133–R138. https://doi.org/10.1093/hmg/ddi107

Manczak, M., Sesaki, H., Kageyama, Y., Reddy, P.H., 2012. Dynamin-related protein 1 heterozygote knockout mice do not have synaptic and mitochondrial deficiencies. Biochimica et Biophysica Acta (BBA) - Molecular Basis of Disease 1822, 862–874. https://doi.org/10.1016/j.bbadis.2012.02.017

Mania, A., Mantzouratou, A., Delhanty, J.D.A., Baio, G., Serhal, P., Sengupta, S.B., 2014. Telomere length in human blastocysts. Reproductive BioMedicine Online 28, 624–637. https://doi.org/10.1016/j.rbmo.2013.12.010

Mann, M.R., Bartolomei, M.S., 2002. Epigenetic reprogramming in the mammalian embryo: struggle of the clones. Genome Biol 3, reviews1003.1. https://doi.org/10.1186/gb-2002-3-2-reviews1003

Marión, R.M., Blasco, M.A., 2010. Telomeres And Telomerase in Adult Stem Cells and Pluripotent Embryonic Stem Cells, in: Meshorer, E., Plath, K. (Eds.), The Cell Biology of Stem Cells. Springer US, Boston, MA, pp. 118–131. https://doi.org/10.1007/978-1-4419-7037-4_9

Market Velker, B.A., Denomme, M.M., Mann, M.R.W., 2012. Loss of Genomic Imprinting in Mouse Embryos with Fast Rates of Preimplantation Development in Culture1. Biology of Reproduction 86. https://doi.org/10.1095/biolreprod.111.096602

Matthews, C., Gorenne, I., Scott, S., Figg, N., Kirkpatrick, P., Ritchie, A., Goddard, M., Bennett, M., 2006. Vascular Smooth Muscle Cells Undergo Telomere-Based Senescence in Human Atherosclerosis: Effects of Telomerase and Oxidative Stress. Circulation Research 99, 156–164. https://doi.org/10.1161/01.RES.0000233315.38086.bc

Mattocks, D.A.L., Mentch, S.J., Shneyder, J., Ables, G.P., Sun, D., Richie, J.P., Locasale, J.W., Nichenametla, S.N., 2017. Short term methionine restriction increases hepatic global DNA methylation in adult but not young male C57BL/6J mice. Experimental Gerontology 88, 1–8. https://doi.org/10.1016/j.exger.2016.12.003

Mayer, W., Niveleau, A., Walter, J., Fundele, R., Haaf, T., 2000a. Demethylation of the zygotic paternal genome. Nature 403, 501–502. https://doi.org/10.1038/35000656

Mayer, W., Smith, A., Fundele, R., Haaf, T., 2000b. Spatial Separation of Parental Genomes in Preimplantation Mouse Embryos. Journal of Cell Biology 148, 629–634. https://doi.org/10.1083/jcb.148.4.629

May-Panloup, P., Vignon, X., Chrétien, M.-F., Heyman, Y., Tamassia, M., Malthièry, Y., Reynier, P., 2005. [No title found]. Reprod Biol Endocrinol 3, 65. https://doi.org/10.1186/1477-7827-3-65

Mazat, J.-P., Ransac, S., Heiske, M., Devin, A., Rigoulet, M., 2013. Mitochondrial energetic metabolism-some general principles. IUBMB Life 65, 171–179. https://doi.org/10.1002/iub.1138

McConnell, J.M., Petrie, L., 2004. Mitochondrial DNA turnover occurs during preimplantation development and can be modulated by environmental factors. Reproductive BioMedicine Online 9, 418–424. https://doi.org/10.1016/S1472-6483(10)61277-1

Meerdo, L.N., Reed, W.A., White, K.L., 2005. Telomere-to-Centromere Ratio of Bovine Clones, Embryos, Gametes, Fetal Cells, and Adult Cells. Cloning and Stem Cells 7, 62–73. https://doi.org/10.1089/clo.2005.7.62

Messerschmidt, D.M., Knowles, B.B., Solter, D., 2014. DNA methylation dynamics during epigenetic reprogramming in the germline and preimplantation embryos. Genes & Development 28, 812–828. https://doi.org/10.1101/gad.234294.113

Mihajlović, A.I., Bruce, A.W., 2017. The first cell-fate decision of mouse preimplantation embryo development: integrating cell position and polarity. Open Biology 7, 170210. https://doi.org/10.1098/rsob.170210

Mikhed, Y., Daiber, A., Steven, S., 2015. Mitochondrial Oxidative Stress, Mitochondrial DNA Damage and Their Role in Age-Related Vascular Dysfunction. International Journal of Molecular Sciences 16, 15918–15953. https://doi.org/10.3390/ijms160715918

Morris, G., Berk, M., 2015. The many roads to mitochondrial dysfunction in neuroimmune and neuropsychiatric disorders. BMC Medicine 13. https://doi.org/10.1186/s12916-015-0310-y

Moyzis, R.K., Buckingham, J.M., Cram, L.S., Dani, M., Deaven, L.L., Jones, M.D., Meyne, J., Ratliff, R.L., Wu, J.R., 1988. A highly conserved repetitive DNA sequence,

(TTAGGG)n, present at the telomeres of human chromosomes. Proc Natl Acad Sci U S A 85, 6622–6626. https://doi.org/10.1073/pnas.85.18.6622

M.Stansel, R., 2001. T-loop assembly in vitro involves binding of TRF2 near the 3' telomeric overhang. The EMBO Journal 20, 5532–5540. https://doi.org/10.1093/emboj/20.19.5532

Muñoz-Lorente, M.A., Cano-Martin, A.C., Blasco, M.A., 2019. Mice with hyper-long telomeres show less metabolic aging and longer lifespans. Nature Communications 10. https://doi.org/10.1038/s41467-019-12664-x

Nagaoka, S.I., Hassold, T.J., Hunt, P.A., 2012. Human aneuploidy: mechanisms and new insights into an age-old problem. Nat. Rev. Genet. 13, 493–504. https://doi.org/10.1038/nrg3245

Nakamura, T., Arai, Y., Umehara, H., Masuhara, M., Kimura, T., Taniguchi, H., Sekimoto, T., Ikawa, M., Yoneda, Y., Okabe, M., Tanaka, S., Shiota, K., Nakano, T., 2007. PGC7/Stella protects against DNA demethylation in early embryogenesis. Nature Cell Biology 9, 64–71. https://doi.org/10.1038/ncb1519

Nguyen, L.N., Zhao, J., Cao, D., Dang, X., Wang, L., Lian, J., Zhang, Y., Jia, Z., Wu, X.Y., Morrison, Z., Xie, Q., Ji, Y., Zhang, Z., El Gazzar, M., Ning, S., Moorman, J.P., Yao, Z.Q., 2018. Inhibition of TRF2 accelerates telomere attrition and DNA damage in naïve CD4 T cells during HCV infection. Cell Death & Disease 9. https://doi.org/10.1038/s41419-018-0897-y

Niemann, H., Wrenzycki, C., 2000. Alterations of expression of developmentally important genes in preimplantation bovine embryos by in vitro culture conditions: Implications for subsequent development. Theriogenology 53, 21–34. https://doi.org/10.1016/S0093-691X(99)00237-X

Nishi, Y., Takeshita, T., Sato, K., Araki, T., 2003. Change of the Mitochondrial Distribution in Mouse OoplasmDuring In Vitro Maturation. Journal of Nippon Medical School 70, 408–415. https://doi.org/10.1272/jnms.70.408

Nishioka, N., Inoue, K., Adachi, K., Kiyonari, H., Ota, M., Ralston, A., Yabuta, N., Hirahara, S., Stephenson, R.O., Ogonuki, N., Makita, R., Kurihara, H., Morin-Kensicki, E.M., Nojima, H., Rossant, J., Nakao, K., Niwa, H., Sasaki, H., 2009. The Hippo Signaling Pathway Components Lats and Yap Pattern Tead4 Activity to Distinguish

Mouse Trophectoderm from Inner Cell Mass. Developmental Cell 16, 398–410. https://doi.org/10.1016/j.devcel.2009.02.003

Oexle, K., Zwirner, A., 1997. Advanced Telomere Shortening in Respiratory Chain Disorders. Human Molecular Genetics 6, 905–908. https://doi.org/10.1093/hmg/6.6.905

Ogushi, S., Palmieri, C., Fulka, H., Saitou, M., Miyano, T., Fulka, J., 2008. The Maternal Nucleolus Is Essential for Early Embryonic Development in Mammals. Science 319, 613–616. https://doi.org/10.1126/science.1151276

Oikawa, S., Kawanishi, S., 1999. Site-specific DNA damage at GGG sequence by oxidative stress may accelerate telomere shortening. FEBS Letters 453, 365–368. https://doi.org/10.1016/S0014-5793(99)00748-6

Olivieri, F., Lorenzi, M., Antonicelli, R., Testa, R., Sirolla, C., Cardelli, M., Mariotti, S., Marchegiani, F., Marra, M., Spazzafumo, L., Bonfigli, A.R., Procopio, A., 2009. Leukocyte telomere shortening in elderly Type2DM patients with previous myocardial infarction. Atherosclerosis 206, 588–593. https://doi.org/10.1016/j.atherosclerosis.2009.03.034

Olovnikov, A.M., 1973. A theory of marginotomy. Journal of Theoretical Biology 41, 181–190. https://doi.org/10.1016/0022-5193(73)90198-7

Olszańska, B., Borgul, A., 1993. Maternal RNA content in oocytes of several mammalian and avian species. Journal of Experimental Zoology 265, 317–320. https://doi.org/10.1002/jez.1402650313

Ozturk, S., 2015. Telomerase Activity and Telomere Length in Male Germ Cells. Biology of Reproduction 92. https://doi.org/10.1095/biolreprod.114.124008

Panossian, L., 2003. Telomere shortening in T cells correlates with Alzheimer's disease status. Neurobiology of Aging 24, 77–84. https://doi.org/10.1016/S0197-4580(02)00043-X

Pickett, H.A., Cesare, A.J., Johnston, R.L., Neumann, A.A., Reddel, R.R., 2009. Control of telomere length by a trimming mechanism that involves generation of t-circles. EMBO J 28, 799–809. https://doi.org/10.1038/emboj.2009.42

Pickett, H.A., Henson, J.D., Au, A.Y.M., Neumann, A.A., Reddel, R.R., 2011. Normal mammalian cells negatively regulate telomere length by telomere trimming. Hum Mol Genet 20, 4684–4692. https://doi.org/10.1093/hmg/ddr402

Pickett, H.A., Reddel, R.R., 2015. Molecular mechanisms of activity and derepression of alternative lengthening of telomeres. Nat. Struct. Mol. Biol. 22, 875–880. https://doi.org/10.1038/nsmb.3106

Pikó, L., Taylor, K.D., 1987. Amounts of mitochondrial DNA and abundance of some mitochondrial gene transcripts in early mouse embryos. Dev. Biol. 123, 364–374.

Podgornaya, O.I., Bugaeva, E.A., Voronin, A.P., Gilson, E., Mitchell, A.R., 2000. Nuclear envelope associated protein that binds telomeric DNAs. Molecular Reproduction and Development 57, 16–25. https://doi.org/10.1002/1098-2795(200009)57:1<16::AID-MRD4>3.0.CO;2-8

Popp, C., Dean, W., Feng, S., Cokus, S.J., Andrews, S., Pellegrini, M., Jacobsen, S.E., Reik, W., 2010. Genome-wide erasure of DNA methylation in mouse primordial germ cells is affected by AID deficiency. Nature 463, 1101–1105. https://doi.org/10.1038/nature08829

Prigione, A., Ruiz-Pérez, M.V., Bukowiecki, R., Adjaye, J., 2015. Metabolic restructuring and cell fate conversion. Cellular and Molecular Life Sciences 72, 1759–1777. https://doi.org/10.1007/s00018-015-1834-1

Qiu, C., Enquobahrie, D., Gelaye, B., Hevner, K., Williams, M., 2015. The Association between Leukocyte Telomere Length and Mitochondrial DNA Copy Number in Pregnant Women: A Pilot Study. Clinical Laboratory 61. https://doi.org/10.7754/Clin.Lab.2014.140313

Quinn, P., Wales, R.G., 1973. UPTAKE AND METABOLISM OF PYRUVATE AND LACTATE DURING PREIMPLANTATION DEVELOPMENT OF THE MOUSE EMBRYO IN VITRO. Reproduction 35, 273–287. https://doi.org/10.1530/jrf.0.0350273

Ralston, A., Cox, B.J., Nishioka, N., Sasaki, H., Chea, E., Rugg-Gunn, P., Guo, G., Robson, P., Draper, J.S., Rossant, J., 2010. Gata3 regulates trophoblast development downstream of Tead4 and in parallel to Cdx2. Development 137, 395–403. https://doi.org/10.1242/dev.038828

Ralston, A., Rossant, J., 2008. Cdx2 acts downstream of cell polarization to cell-autonomously promote trophectoderm fate in the early mouse embryo. Developmental Biology 313, 614–629. https://doi.org/10.1016/j.ydbio.2007.10.054

Reddy, P.H., 2008. Mitochondrial Medicine for Aging and Neurodegenerative Diseases. NeuroMolecular Medicine 10, 291–315. https://doi.org/10.1007/s12017-008-8044-z

Reid, M.A., Dai, Z., Locasale, J.W., 2017. The impact of cellular metabolism on chromatin dynamics and epigenetics. Nature Cell Biology 19, 1298–1306. https://doi.org/10.1038/ncb3629

Reig-Viader, R., Garcia-Caldés, M., Ruiz-Herrera, A., 2016. Telomere homeostasis in mammalian germ cells: a review. Chromosoma 125, 337–351. https://doi.org/10.1007/s00412-015-0555-4

Richter, K.S., Harris, D.C., Daneshmand, S.T., Shapiro, B.S., 2001. Quantitative grading of a human blastocyst: optimal inner cell mass size and shape. Fertility and Sterility 76, 1157–1167. https://doi.org/10.1016/S0015-0282(01)02870-9

Robin, E.D., Wong, R., 1988. Mitochondrial DNA molecules and virtual number of mitochondria per cell in mammalian cells. Journal of Cellular Physiology 136, 507–513. https://doi.org/10.1002/jcp.1041360316

Rollo, C., Li, Y., Jin, X.L., O'Neill, C., 2017. Histone 3 lysine 9 acetylation is a biomarker of the effects of culture on zygotes. Reproduction 154, 375–385. https://doi.org/10.1530/REP-17-0112

Rossant, J., 1976. Postimplantation development of blastomeres isolated from 4- and 8-cell mouse eggs. J Embryol Exp Morphol 36, 283–290.

Rossant, J., Lis, W.T., 1979. Potential of isolated mouse inner cell masses to form trophectoderm derivatives in vivo. Developmental Biology 70, 255–261. https://doi.org/10.1016/0012-1606(79)90022-8

Rossant, J., Vijh, K.M., 1980. Ability of outside cells from preimplantation mouse embryos to form inner cell mass derivatives. Developmental Biology 76, 475–482. https://doi.org/10.1016/0012-1606(80)90395-4

Rudolph, K.L., Chang, S., Lee, H.W., Blasco, M., Gottlieb, G.J., Greider, C., DePinho, R.A., 1999. Longevity, stress response, and cancer in aging telomerase-deficient mice. Cell 96, 701–712.

Russell, D.F., Baqir, S., Bordignon, J., Betts, D.H., 2006. The impact of oocyte maturation media on early bovine embryonic development. Molecular Reproduction and Development 73, 1255–1270. https://doi.org/10.1002/mrd.20553

Russo, V., Berardinelli, P., Martelli, A., Giacinto, O.D., Nardinocchi, D., Fantasia, D., Barboni, B., 2006. Expression of Telomerase Reverse Transcriptase Subunit (TERT) and Telomere Sizing in Pig Ovarian Follicles. Journal of Histochemistry & Cytochemistry 54, 443–455. https://doi.org/10.1369/jhc.4A6603.2006

Ryan, B.J., Hoek, S., Fon, E.A., Wade-Martins, R., 2015. Mitochondrial dysfunction and mitophagy in Parkinson's: from familial to sporadic disease. Trends in Biochemical Sciences 40, 200–210. https://doi.org/10.1016/j.tibs.2015.02.003

Safdar, A., Khrapko, K., Flynn, J.M., Saleem, A., De Lisio, M., Johnston, A.P.W., Kratysberg, Y., Samjoo, I.A., Kitaoka, Y., Ogborn, D.I., Little, J.P., Raha, S., Parise, G., Akhtar, M., Hettinga, B.P., Rowe, G.C., Arany, Z., Prolla, T.A., Tarnopolsky, M.A., 2015. Exercise-induced mitochondrial p53 repairs mtDNA mutations in mutator mice. Skeletal Muscle 6. https://doi.org/10.1186/s13395-016-0075-9

Sahin, E., Colla, S., Liesa, M., Moslehi, J., Müller, F.L., Guo, M., Cooper, M., Kotton, D., Fabian, A.J., Walkey, C., Maser, R.S., Tonon, G., Foerster, F., Xiong, R., Wang, Y.A., Shukla, S.A., Jaskelioff, M., Martin, E.S., Heffernan, T.P., Protopopov, A., Ivanova, E., Mahoney, J.E., Kost-Alimova, M., Perry, S.R., Bronson, R., Liao, R., Mulligan, R., Shirihai, O.S., Chin, L., DePinho, R.A., 2011. Telomere dysfunction induces metabolic and mitochondrial compromise. Nature 470, 359–365. https://doi.org/10.1038/nature09787

Salomoni, P., Ferguson, B., Wyllie, A., Rich, T., 2008. New insights into the role of PML in tumour suppression. Cell Research 18, 622–640. https://doi.org/10.1038/cr.2008.58

Samassekou, O., Gadji, M., Drouin, R., Yan, J., 2010. Sizing the ends: Normal length of human telomeres. Annals of Anatomy - Anatomischer Anzeiger 192, 284–291. https://doi.org/10.1016/j.aanat.2010.07.005

Sampson, M.J., Winterbone, M.S., Hughes, J.C., Dozio, N., Hughes, D.A., 2006. Monocyte Telomere Shortening and Oxidative DNA Damage in Type 2 Diabetes. Diabetes Care 29, 283–289. https://doi.org/10.2337/diacare.29.02.06.dc05-1715

Sanderson, S.M., Gao, X., Dai, Z., Locasale, J.W., 2019. Methionine metabolism in health and cancer: a nexus of diet and precision medicine. Nature Reviews Cancer 19, 625–637. https://doi.org/10.1038/s41568-019-0187-8

Santos, T.A., El Shourbagy, S., St John, J.C., 2006. Mitochondrial content reflects oocyte variability and fertilization outcome. Fertil. Steril. 85, 584–591. https://doi.org/10.1016/j.fertnstert.2005.09.017

Schaetzlein, S., Lucas-Hahn, A., Lemme, E., Kues, W.A., Dorsch, M., Manns, M.P., Niemann, H., Rudolph, K.L., 2004. Telomere length is reset during early mammalian embryogenesis. Proceedings of the National Academy of Sciences 101, 8034–8038. https://doi.org/10.1073/pnas.0402400101

Scherthan, H., Jerratsch, M., Li, B., Smith, S., Hultén, M., Lock, T., de Lange, T., 2000. Mammalian Meiotic Telomeres: Protein Composition and Redistribution in Relation to Nuclear Pores. Molecular Biology of the Cell 11, 4189–4203. https://doi.org/10.1091/mbc.11.12.4189

Schultz, R.M., 2005. From egg to embryo: a peripatetic journey. Reproduction 130, 825–828. https://doi.org/10.1530/rep.1.00902

Shi, L., Wu, J., 2009. Epigenetic regulation in mammalian preimplantation embryo development. Reproductive Biology and Endocrinology 7. https://doi.org/10.1186/1477-7827-7-59

Shi, Y., 2007. Histone lysine demethylases: emerging roles in development, physiology and disease. Nature Reviews Genetics 8, 829–833. https://doi.org/10.1038/nrg2218

Shimazu, T., Hirschey, M.D., Newman, J., He, W., Shirakawa, K., Le Moan, N., Grueter, C.A., Lim, H., Saunders, L.R., Stevens, R.D., Newgard, C.B., Farese, R.V., de Cabo, R., Ulrich, S., Akassoglou, K., Verdin, E., 2013. Suppression of Oxidative Stress by -Hydroxybutyrate, an Endogenous Histone Deacetylase Inhibitor. Science 339, 211–214. https://doi.org/10.1126/science.1227166

Shtolz, N., Mishmar, D., 2019. The Mitochondrial Genome–on Selective Constraints and Signatures at the Organism, Cell, and Single Mitochondrion Levels. Frontiers in Ecology and Evolution 7. https://doi.org/10.3389/fevo.2019.00342

Simon, N.M., Smoller, J.W., McNamara, K.L., Maser, R.S., Zalta, A.K., Pollack, M.H., Nierenberg, A.A., Fava, M., Wong, K.-K., 2006. Telomere Shortening and Mood Disorders: Preliminary Support for a Chronic Stress Model of Accelerated Aging. Biological Psychiatry 60, 432–435. https://doi.org/10.1016/j.biopsych.2006.02.004

Sirard, M.-A., 2012. Factors Affecting Oocyte and Embryo Transcriptomes: Factors Affecting Oocyte and Embryo Transcriptomes. Reproduction in Domestic Animals 47, 148–155. https://doi.org/10.1111/j.1439-0531.2012.02069.x

Smith, S., 1998. Tankyrase, a Poly(ADP-Ribose) Polymerase at Human Telomeres. Science 282, 1484–1487. https://doi.org/10.1126/science.282.5393.1484

Smith, S., de Lange, T., 2000. Tankyrase promotes telomere elongation in human cells. Current Biology 10, 1299–1302. https://doi.org/10.1016/S0960-9822(00)00752-1

Smith, S., de Lange, T., 1999. Cell cycle dependent localization of the telomeric PARP, tankyrase, to nuclear pore complexes and centrosomes. J. Cell. Sci. 112 (Pt 21), 3649–3656.

Sobinoff, A.P., Pye, V., Nixon, B., Roman, S.D., McLaughlin, E.A., 2010. Adding Insult to Injury: Effects of Xenobiotic-Induced Preantral Ovotoxicity on Ovarian Development and Oocyte Fusibility. Toxicological Sciences 118, 653–666. https://doi.org/10.1093/toxsci/kfq272

Sohal, R.S., Ku, H.-H., Agarwal, S., Forster, M.J., Lal, H., 1994. Oxidative damage, mitochondrial oxidant generation and antioxidant defenses during aging and in response to food restriction in the mouse. Mechanisms of Ageing and Development 74, 121–133. https://doi.org/10.1016/0047-6374(94)90104-X

Song, W.-H., Ballard, J.W.O., Yi, Y.-J., Sutovsky, P., 2014. Regulation of Mitochondrial Genome Inheritance by Autophagy and Ubiquitin-Proteasome System: Implications for Health, Fitness, and Fertility. BioMed Research International 2014, 1–16. https://doi.org/10.1155/2014/981867

Spikings, E.C., Alderson, J., John, J.C.S., 2007. Regulated Mitochondrial DNA Replication During Oocyte Maturation Is Essential for Successful Porcine Embryonic Development. Biology of Reproduction 76, 327–335. https://doi.org/10.1095/biolreprod.106.054536

Spindle, A.I., 1978. Trophoblast regeneration by inner cell masses isolated from cultured mouse embryos. Journal of Experimental Zoology 203, 483–489. https://doi.org/10.1002/jez.1402030315

St. John, J.C., Facucho-Oliveira, J., Jiang, Y., Kelly, R., Salah, R., 2010. Mitochondrial DNA transmission, replication and inheritance: a journey from the gamete through the embryo and into offspring and embryonic stem cells. Human Reproduction Update 16, 488–509. https://doi.org/10.1093/humupd/dmq002

Stavropoulos, D.J., 2002. The Bloom syndrome helicase BLM interacts with TRF2 in ALT cells and promotes telomeric DNA synthesis. Human Molecular Genetics 11, 3135–3144. https://doi.org/10.1093/hmg/11.25.3135

Sun, H., Karow, J.K., Hickson, I.D., Maizels, N., 1998. The Bloom's Syndrome Helicase Unwinds G4 DNA. Journal of Biological Chemistry 273, 27587–27592. https://doi.org/10.1074/jbc.273.42.27587

Sun, X., St. John, J.C., 2016. The role of the mtDNA set point in differentiation, development and tumorigenesis. Biochemical Journal 473, 2955–2971. https://doi.org/10.1042/BCJ20160008

Swerdlow, R.H., 2011. Brain aging, Alzheimer's disease, and mitochondria. Biochimica et Biophysica Acta (BBA) - Molecular Basis of Disease 1812, 1630–1639. https://doi.org/10.1016/j.bbadis.2011.08.012

Taanman, J.-W., 1999. The mitochondrial genome: structure, transcription, translation and replication. Biochimica et Biophysica Acta (BBA) - Bioenergetics 1410, 103–123. https://doi.org/10.1016/S0005-2728(98)00161-3

Takahashi, Y., Lallemand-Breitenbach, V., Zhu, J., de Thé, H., 2004. PML nuclear bodies and apoptosis. Oncogene 23, 2819–2824. https://doi.org/10.1038/sj.onc.1207533

Takai, K.K., Hooper, S., Blackwood, S., Gandhi, R., de Lange, T., 2010. *In Vivo* Stoichiometry of Shelterin Components. Journal of Biological Chemistry 285, 1457–1467. https://doi.org/10.1074/jbc.M109.038026

Tarkowski, A.K., Wróblewska, J., 1967. Development of blastomeres of mouse eggs isolated at the 4- and 8-cell stage. J Embryol Exp Morphol 18, 155–180.

Thomas, P., O' Callaghan, N.J., Fenech, M., 2008. Telomere length in white blood cells, buccal cells and brain tissue and its variation with ageing and Alzheimer's disease. Mechanisms of Ageing and Development 129, 183–190. https://doi.org/10.1016/j.mad.2007.12.004

Thundathil, J., Filion, F., Smith, L.C., 2005. Molecular control of mitochondrial function in preimplantation mouse embryos. Molecular Reproduction and Development 71, 405–413. https://doi.org/10.1002/mrd.20260

Treff, N.R., Su, J., Taylor, D., Scott, R.T., 2011. Telomere DNA Deficiency Is Associated with Development of Human Embryonic Aneuploidy. PLoS Genetics 7, e1002161. https://doi.org/10.1371/journal.pgen.1002161

Turner, S., Hartshorne, G.M., 2013. Telomere lengths in human pronuclei, oocytes and spermatozoa. Molecular Human Reproduction 19, 510–518. https://doi.org/10.1093/molehr/gat021

Turner, S., Wong, H.P., Rai, J., Hartshorne, G.M., 2010. Telomere lengths in human oocytes, cleavage stage embryos and blastocysts. Mol. Hum. Reprod. 16, 685–694. https://doi.org/10.1093/molehr/gaq048

Tyrka, A.R., Carpenter, L.L., Kao, H.-T., Porton, B., Philip, N.S., Ridout, S.J., Ridout, K.K., Price, L.H., 2015. Association of telomere length and mitochondrial DNA copy number in a community sample of healthy adults. Experimental Gerontology 66, 17–20. https://doi.org/10.1016/j.exger.2015.04.002

Udugama, M., Chang, F.T.M., Chan, F.L., Tang, M.C., Pickett, H.A., McGhie, J.D.R., Mayne, L., Collas, P., Mann, J.R., Wong, L.H., 2015. Histone variant H3.3 provides the heterochromatic H3 lysine 9 tri-methylation mark at telomeres. Nucleic Acids Research gkv847. https://doi.org/10.1093/nar/gkv847

Uziel, O., Singer, J.A., Danicek, V., Sahar, G., Berkov, E., Luchansky, M., Fraser, A., Ram, R., Lahav, M., 2007. Telomere dynamics in arteries and mononuclear cells of

diabetic patients: Effect of diabetes and of glycemic control. Experimental Gerontology 42, 971–978. https://doi.org/10.1016/j.exger.2007.07.005

van Steensel, B., de Lange, T., 1997. Control of telomere length by the human telomeric protein TRF1. Nature 385, 740–743. https://doi.org/10.1038/385740a0

Varela, E., Schneider, R.P., Ortega, S., Blasco, M.A., 2011. Different telomere-length dynamics at the inner cell mass versus established embryonic stem (ES) cells. Proceedings of the National Academy of Sciences 108, 15207–15212. https://doi.org/10.1073/pnas.1105414108

von Zglinicki, T., Saretzki, G., Döcke, W., Lotze, C., 1995. Mild Hyperoxia Shortens Telomeres and Inhibits Proliferation of Fibroblasts: A Model for Senescence? Experimental Cell Research 220, 186–193. https://doi.org/10.1006/excr.1995.1305

Wakayama, S., Kohda, T., Obokata, H., Tokoro, M., Li, C., Terashita, Y., Mizutani, E., Nguyen, V.T., Kishigami, S., Ishino, F., Wakayama, T., 2013. Successful Serial Recloning in the Mouse over Multiple Generations. Cell Stem Cell 12, 293–297. https://doi.org/10.1016/j.stem.2013.01.005

Wakayama, T., Shinkai, Y., Tamashiro, K.L.K., Niida, H., Blanchard, D.C., Blanchard, R.J., Ogura, A., Tanemura, K., Tachibana, M., Perry, A.C.F., Colgan, D.F., Mombaerts, P., Yanagimachi, R., 2000. Cloning of mice to six generations. Nature 407, 318–319. https://doi.org/10.1038/35030301

Wang, F., Pan, X., Kalmbach, K., Seth-Smith, M.L., Ye, X., Antumes, D.M.F., Yin, Y., Liu, L., Keefe, D.L., Weissman, S.M., 2013. Robust measurement of telomere length in single cells. Proc. Natl. Acad. Sci. U.S.A. 110, E1906-1912. https://doi.org/10.1073/pnas.1306639110

Ward, M.S., Fotheringham, A.K., Cooper, M.E., Forbes, J.M., 2013. Targeting advanced glycation endproducts and mitochondrial dysfunction in cardiovascular disease. Current Opinion in Pharmacology 13, 654–661. https://doi.org/10.1016/j.coph.2013.06.009

Watanabe, D., Suetake, I., Tada, T., Tajima, S., 2002. Stage- and cell-specific expression of Dnmt3a and Dnmt3b during embryogenesis. Mechanisms of Development 118, 187–190. https://doi.org/10.1016/S0925-4773(02)00242-3

Watson, A.J., De Sousa, P., Caveney, A., Barcroft, L.C., Natale, D., Urquhart, J., Westhusin, M.E., 2000. Impact of Bovine Oocyte Maturation Media on Oocyte Transcript Levels, Blastocyst Development, Cell Number, and Apoptosis1. Biology of Reproduction 62, 355–364. https://doi.org/10.1095/biolreprod62.2.355

Wellen, K.E., Hatzivassiliou, G., Sachdeva, U.M., Bui, T.V., Cross, J.R., Thompson, C.B., 2009. ATP-Citrate Lyase Links Cellular Metabolism to Histone Acetylation. Science 324, 1076–1080. https://doi.org/10.1126/science.1164097

Wilding, M., Coppola, G., Dale, B., Di Matteo, L., 2009. Mitochondria and human preimplantation embryo development. REPRODUCTION 137, 619–624. https://doi.org/10.1530/REP-08-0444

Wrenzycki, C., Herrmann, D., Lucas-Hahn, A., Korsawe, K., Lemme, E., Niemann, H., 2005. Messenger RNA expression patterns in bovine embryos derived from in vitro procedures and their implications for development. Reproduction, Fertility and Development 17, 23. https://doi.org/10.1071/RD04109

Wright, D.L., 2001. Characterization of telomerase activity in the human oocyte and preimplantation embryo. Molecular Human Reproduction 7, 947–955. https://doi.org/10.1093/molehr/7.10.947

Wright, S.J., 1999. 5 Sperm Nuclear Activation during Fertilization, in: Current Topics in Developmental Biology. Elsevier, pp. 133–178. https://doi.org/10.1016/S0070-2153(08)60328-2

Wu, L., Davies, S.L., Levitt, N.C., Hickson, I.D., 2001. Potential Role for the BLM Helicase in Recombinational Repair via a Conserved Interaction with RAD51. Journal of Biological Chemistry 276, 19375–19381. https://doi.org/10.1074/jbc.M009471200

Xin, H., Liu, D., Songyang, Z., 2008. The telosome/shelterin complex and its functions. Genome Biology 9, 232. https://doi.org/10.1186/gb-2008-9-9-232

Xu, J., Yang, X., 2001. Telomerase Activity in Early Bovine Embryos Derived from Parthenogenetic Activation and Nuclear Transfer1. Biology of Reproduction 64, 770–774. https://doi.org/10.1095/biolreprod64.3.770

Yaku, K., Okabe, K., Nakagawa, T., 2018. NAD metabolism: Implications in aging and longevity. Ageing Research Reviews 47, 1–17. https://doi.org/10.1016/j.arr.2018.05.006

Yamada-Fukunaga, T., Yamada, M., Hamatani, T., Chikazawa, N., Ogawa, S., Akutsu, H., Miura, T., Miyado, K., Tarín, J.J., Kuji, N., Umezawa, A., Yoshimura, Y., 2013. Age-associated telomere shortening in mouse oocytes. Reprod. Biol. Endocrinol. 11, 108. https://doi.org/10.1186/1477-7827-11-108

Yankiwski, V., Marciniak, R.A., Guarente, L., Neff, N.F., 2000. Nuclear structure in normal and Bloom syndrome cells. Proc. Natl. Acad. Sci. U.S.A. 97, 5214–5219. https://doi.org/10.1073/pnas.090525897

Yeager, T.R., Neumann, A.A., Englezou, A., Huschtscha, L.I., Noble, J.R., Reddel, R.R., 1999. Telomerase-negative immortalized human cells contain a novel type of promyelocytic leukemia (PML) body. Cancer Res. 59, 4175–4179.

Zander-Fox, D.L., Fullston, T., McPherson, N.O., Sandeman, L., Kang, W.X., Good, S.B., Spillane, M., Lane, M., 2015. Reduction of Mitochondrial Function by FCCP During Mouse Cleavage Stage Embryo Culture Reduces Birth Weight and Impairs the Metabolic Health of Offspring1. Biology of Reproduction 92. https://doi.org/10.1095/biolreprod.114.123489

Zhang, N., 2018. Role of methionine on epigenetic modification of DNA methylation and gene expression in animals. Animal Nutrition 4, 11–16. https://doi.org/10.1016/j.aninu.2017.08.009

Zhang, R., Wang, Y., Ye, K., Picard, M., Gu, Z., 2017. Independent impacts of aging on mitochondrial DNA quantity and quality in humans. BMC Genomics 18. https://doi.org/10.1186/s12864-017-4287-0

Zhao, N., Zhang, Y., Liu, Q., Xiang, W., 2015. Mfn2 Affects Embryo Development via Mitochondrial Dysfunction and Apoptosis. PLOS ONE 10, e0125680. https://doi.org/10.1371/journal.pone.0125680

Zhou, M.-C., Min, R., Ji, J.-J., Zhang, S., Tong, A.-L., Xu, J., Li, Z.-Y., Zhang, H.-B., Li, Y.-X., 2015. Analysis of association among clinical features and shorter leukocyte telomere length in mitochondrial diabetes with m.3243A>G mitochondrial DNA mutation. BMC Medical Genetics 16. https://doi.org/10.1186/s12881-015-0238-2

Zimmermann, M., Kibe, T., Kabir, S., de Lange, T., 2014. TRF1 negotiates TTAGGG repeat-associated replication problems by recruiting the BLM helicase and the

TPP1/POT1 repressor of ATR signaling. Genes & Development 28, 2477–2491. https://doi.org/10.1101/gad.251611.114

CHAPTER 2

DEVELOPMENT OF A QPCR "TRIPLE TEST" FOR ASSESSMENT OF TELOMERE AND mtDNA IN INDIVIDUAL OOCYTES AND EMBRYOS

2.1 Introduction

Telomeres are repetitive DNA sequences that cap the ends of linear chromosomes and play major roles in cellular lifespan, genomic stability, and cell cycle control (Hayflick and Moorhead, 1961; Rudolph et al., 1999). Due to the 'end replication problem', telomeres shorten with each cell division (Olovnikov, 1973), and consequently with age; therefore their length needs to be reset at the outset of each generation. While it is known that telomere length is set during the pre-implantation embryogenesis period (Ozturk et al., 2014; Schaetzlein et al., 2004), there are still significant advances to be made in understanding the elongation patterns and mechanisms controlling this. One significant challenge however has been a lack of robust assays to measure telomere length in individual oocytes and embryos.

To date, the majority of assays for telomere length have relied on having pools of oocytes or embryos for analysis. Some, such as the gold standard telomere restriction fragment (TRF) assay, require relatively large amounts of starting material such that they are not feasible for use in oocytes or embryos. Further, analysing pools of oocytes or embryos would mask variation, for instance between oocytes from an individual female or embryos from different females. qPCR is widely used to measure telomere DNA, and recent work has shown that telomere quantification determined by qPCR analysis correlates well with whole genome sequencing-based telomere length measurement techniques: *Motif_counter*, *TelSeq*, *Computel*, and *qMotif* (Lee et al., 2017). Importantly, telomere primers used for qPCR deviate from the consensus telomere sequence of TTAGGG to eliminate the risk of primer-dimer derived products from having forward and reverse primers that are able to bind due to complementary sequences (Cawthon, 2002). Previously, a qPCR method to analyse telomere length in single cells was developed (Wang et al., 2013) and published in a high impact journal (Proceedings of the National Academy of Sciences of the United States of America, PNAS), and has accumulated more than 8,700 downloads from publication in May 2013 to October 2020. While 36B4 (gene name Rplp0) is the conventional reference gene used for telomere qPCR quantification when analysing DNA from cell populations (Cawthon, 2002), authors found that this was unable to be robustly and accurately amplified from the nDNA of a single cell (Wang et al., 2013). To overcome this, authors utilised multi-copy genes as the reference, including *Alu* for human samples, *B1* for mouse samples, *18S rRNA* for both human and mouse samples

(Wang et al., 2013). Given that *Alu* and *B1* SINEs are non-coding, repetitive, transposable elements in the human and mouse genomes, respectively, we have opted not to use either of these as the reference for this assay. While *18S ribosomal RNA* is also a repetitive element, it is a eukaryotic cytosolic homologue of *16S rRNA* in prokaryotes and mitochondria, and is the structural RNA for the 40S component of cytoplasmic ribosomes. Given its function, *18S rRNA* is a vital, basic component of eukaryotic cells and therefore requires a large degree of sequence homology for function, this has been selected as the reference going forward. Due to the low quantity of DNA within a single cell (Dolezel et al., 2003), Wang et al. (2013) first collected single cells in a minimal volume (1µL), and lysed the cell in an equivalent volume of lysis buffer, which did not use any enzyme (such as proteinase K) to digest proteins, to give cell lysate in a final volume of 2µL. Following this, authors utilised a pre-amplification (pre-amp) step which multiplexed the telomere and reference primers, and determined the optimal pre-amp cycle number to be 16 for mouse cells (Wang et al., 2013). Pre-amp products were then purified using the Zymo Research DNA clean and concentrator-5 kit according to manufacturer's instructions and final purified products were eluted in 64µL (Wang et al., 2013). The same primer sequences used for pre-amp were again used for qPCR, however the primers were separated based on target sequence (telomere or *18S rRNA*) to allow for quantification of these sequences and a telomere ratio (telomere/reference) to be calculated for analysis (Wang et al., 2013). Authors then used this protocol to directly compare single cell telomere lengths in a variety of cell contexts, leading to conclusions including: telomere length in sister blastomeres from 2-cell mouse embryos were not different, nor were those from human oocytes and the respective polar body, and further, that telomere length increases between the zygote, 2-cell and 4-cell stages of mouse embryonic development (Wang et al., 2013), which have been accepted as key findings within the field. A study comparing differences in telomere length in pools of 2 mouse oocytes or zygotes, or individual 2-cell embryos fertilised by young or old males also used *18S rRNA* as a reference gene, however different primers were used to the study above, gave a 91bp fragment size, and were termed *Rn18S* in this study (de Frutos et al., 2016). The use of primers targeting the *18S rRNA* region of the nuclear genome in two studies using low nDNA quantity samples indicate that this is likely a suitable multi-copy reference gene for these analyses.

Another key determinant of cellular lifespan is mitochondrial function. Mitochondrial DNA (mtDNA) copy number is a critical component of overall mitochondrial function and cellular physiology, with low copy number linked to multiple diseases (Memon et al., 2017; Pyle et al., 2016; Yoon et al., 2016). In contrast, higher mtDNA copy number in cells is associated with better health and survival amongst elderly humans (Mengel-From et al., 2014). Mitochondrial function and mtDNA copy number play crucial roles in the early stages of embryogenesis, with a critical mtDNA copy number threshold required in mature mammalian oocytes for successful post-implantation development (Pikó and Taylor, 1987; Santos et al., 2006; Wai et al., 2010). Mitochondria, and consequently, mtDNA, are inherited solely through the maternal lineage; meaning all mitochondria in the resulting offspring are generated by replication of the mitochondria present in the mature oocyte. For that reason the quality and quantity of oocyte mitochondria are of utmost importance.

Due to the large quantity of mtDNA present in oocytes, they do not present the same challenges for quantification in individual oocytes to that of nuclear DNA. A qPCR-based assay to quantify the total mtDNA copy number in single oocytes and embryos using a standard curve method has been developed (Thundathil et al., 2005) and is commonly used in many studies, including those by Kameyama et al., (2010, 2007), Wu et al. (2015), and Pasquariello et al., (2019). This protocol requires that samples are frozen in less than 5µL, and DNA is purified using the Qiagen QIAamp DNA Micro kit according to manufacturer's instructions (Kameyama et al., 2007). This kit utilises proteinase K in the cell lysis step, as well as various buffers of undisclosed composition, and a silica-based column with 5 column centrifugation steps to give a purified DNA component. Due to the large quantity of mtDNA within an oocyte, the purified product was able to be eluted in a large volume, undergo further dilution, and still able to be reliably detected using qPCR (Kameyama et al., 2010, 2007). Further, this assay applies a standard curve with defined input target copies to allow for calculation of total mtDNA copy number in the oocyte and embryo samples. The standard curve is generated using a plasmid that contains an 1186bp fragment of the *12S rRNA* region of mouse liver mtDNA in serial dilutions ranging from 10^7 copies to 10^1 copies (refer to Kameyama et al., 2010, 2007 for further information). For qPCR, 2µL of each standard curve dilution and sample were used, along with primers targeting the *12S rRNA* region of the mitochondrial genome, however these targeted

a much smaller fragment of the region, giving a 273bp product (Kameyama et al., 2007). Ct values obtained were used to generate the standard curve and the associated linear equation (y=m*x* + C, where y is the Ct value of the sample, m is the slope of the line, *x* is the number of mtDNA copies present in the 2µL sample, and C is the y-intercept). Following calculation of *x*, the total mtDNA copy number present in the sample was calculated as: total mtDNA copy number = (10^{x})*dilution factor (for example, if the DNA from a single oocyte was eluted in 50µL the initial dilution factor is 50, 2µL of this eluent is used in the qPCR reaction, therefore the dilution factor is halved, giving a final dilution factor of 25).

While there are separate published assays analysing telomere length and mtDNA copy number in individual oocytes, there is yet to be a single assay that is able to measure both of these parameters. This is likely due to the relatively high quantity of mtDNA in a single oocyte or embryo (reaching above 10^6 copies) compared to the nuclear genomic DNA (nDNA), especially in oocytes and early cleavage stage embryos, where there are few copies of the nuclear genome. As such, measuring both mtDNA and nDNA in the same sample is technically challenging. Therefore I set out to utilise the basic principles of both of these single cell assays to create one sensitive, robust assay appropriate for making comparisons of telomere length and mtDNA copy number in individual oocytes and cleavage stage embryos.

In this study, I sought to develop a method for analysing single oocytes and embryos through qPCR. Throughout this process, critical flaws were identified in the published methods, which required extensive experimental re-design to overcome. The resulting technique was termed the “Triple Test” because it applies three assays to allow for quantification of two nuclear DNA sequences and the mitochondrial genome within a single oocyte or embryo. The method utilises quantitative amplification of mitochondrial DNA, in parallel with a standard curve, to allow for total copy number to be determined. Simultaneously, telomere sequence is amplified as well as a multi-copy reference gene (*Rn18S*) for normalisation to nuclear DNA, which is reflective of cell number. This allows three quantitative outputs to be generated per individual sample – total mtDNA copy number, mtDNA relative to nuclear DNA and telomere content relative to nuclear DNA. Due to the use of a reference gene, it is also possible to determine any relative changes in overall cell number, for instance in blastocysts. The future applications of this Triple Test assay demonstrates the value of this method.

It enables the study of telomeres and mtDNA in cases of normal versus perturbed embryo development, and thus further understanding of the underlying intrinsic oocyte and embryo deficiencies that result in lowered fertility, and how these may be responsible for observed offspring phenotypes.

2.2 Materials and Methods

2.2.1 Mice

Female C57BL/6 mice at six weeks of age were obtained from the Western Australian Animal Resources Centre (ARC). CBA male and female mice at six weeks of age were obtained from the University of Adelaide's Laboratory Animal Services. Young and aged wild-type or heterozygous *Blobby* mice (3-4 or 12-14 months old) were generated from a breeding colony maintained at the University of Adelaide's Laboratory Animal Services. All mice were maintained in 12h/12h light/dark conditions and given water and 10% fat rodent chow *ad libitum*. All animal experiments were approved by the University of Adelaide's Animal Ethics Committee and conducted in accordance with the Australian Code of Practice for the Care and Use of Animals for Scientific Purposes.

2.2.2 Collection, DNA extraction, and qPCR of whole ovaries

One whole ovary from a PMSG and hCG (see 2.2.3) stimulated 6 week old C57BL/6 female mouse was isolated 14.5 hours after hCG administration, cleaned of fat, snap frozen in LN_2 in a 1.7mL microcentrifuge tube (Axygen, MCT-175-C-S) and stored at -80°C. DNA was extracted using QIAamp DNA Micro Kit (Qiagen, #56304) as per manufacturer's instructions for 'Isolation of Genomic DNA from Tissues' and eluted in a final volume of 50µL of ultra-pure water (Water for Injection BP, AstraZeneca, referred to as H_2O). DNA concentration and purity were quantified by NanoDrop One Microvolume UV-Vis Spectrophotometer (Thermo Fisher) and diluted to 12ng/µL. Five 1:2 serial dilutions were created to give final concentrations of 6ng/µL, 3ng/µL, 1.5ng/µL, 0.75ng/µL, and 0.375ng/µL.

qPCR was performed using Power SYBR Green PCR Master Mix (Applied Biosystems, #4367659), MicroAmp Fast Optical 96-well Reaction Plates (Life Technologies, #4346906), and custom-made primers (Sigma, forward and reverse primer sequences outlined in Table 2.1), using a Quantstudio 12K Flex system (ThermoFisher). Cycling conditions for all primers were set at 95°C for 10 minutes, followed by 40 cycles of 94°C for 10s, 60°C annealing for 30s and extension at 72°C for 30s, followed by standard melt curve cycling. A single reaction consisted of 10µL

of SYBR Green, 0.5µL of both the forward and reverse primer for telomere, *36B4*, *18S rRNA* or *Rn18S* (stocks at 10µM), 4µL of H_2O, and 5µL of DNA. Three repeat reactions were performed for each primer pair for each sample.

2.2.3 Derivation of oocytes, early embryos, and blastocysts

For isolation of oocytes for analysis of DNA targets, or in vitro fertilisation (IVF), 6 week old CBA and C57BL/6 female mice were given 7.5IU pregnant mare's serum gonadotropin (PMSG, National Hormone and Pituitary Program) and female mice from the *Blobby* colony were given 5IU/12g body weight of PMSG, followed by the equivalent dose of human chorionic gonadotropin (hCG, Pregnyl) 47.5 hours later, each via intraperitoneal (ip) injection. Mice were culled via cervical dislocation 15 - 15.5h post-hCG administration, and ovaries and oviducts collected and placed in pre-warmed (37°C) αMEM-HEPES handling media (Life Technologies, #12000-014), supplemented with 1% FCS. Meiosis II (MII) oocytes were isolated by puncturing the oviducts using a 30G needle.

For individual oocyte analysis, complete cumulus cell removal was achieved via treatment with hyaluronidase (Seikagaku, #100741) for 15 minutes at 37°C, followed by aspiration using a glass pipette (VWR, #612-4897) pulled to an appropriate diameter.

For two-cell embryo (2C) and blastocyst analysis, whole cumulus-oocyte complex (COC) clusters obtained from oviduct puncture were gently washed twice in pre-warmed (37°C) fertilisation media (Vitro Fertilisation; Cook Australia, Brisbane, Australia), before being placed in a 100uL fertilisation drop containing the equivalent of 10µL of capacitated sperm (the time at which oocytes and sperm are placed in the drop is referred to as 'fertilisation time'), before being returned to the incubator (37°C, 5% O_2, 6% CO_2) for 4 hours. Following this, fertilised oocytes were cleaned of all excess sperm and cumulus cells via gentle aspiration and transferred to a culture dish containing cleave media (Vitro Cleave; Cook Australia, Brisbane, Australia) (10 embryos per 20µL cleave media drop) and returned to the incubator until 24 hours post fertilisation time. At this time, the number of embryos that successfully reached the 2C state were scored by visual assessment under a dissecting microscope and a proportion (approximately one third) collected for analysis, the rest were returned to

the incubator until 96 hours post fertilisation time, where the number of embryos that had successfully reached the blastocyst stage were scored and all were collected for analysis.

Oocyte and blastocyst samples derived from wild type (WT) or *Tfam* knock out (KO) mice were kindly supplied by Dr Deepak Adhikari (Monash University).

When collecting for analysis, single oocyte and embryo samples were first washed three times in phosphate buffered saline (PBS) containing 1mg/ml polyvinylpyrrolidone (PVP, Sigma) and transferred in 1µL to an 0.5mL PCR tube (Axygen, #PCR-05-C), snap frozen in liquid nitrogen (LN_2), and stored at -80°C until use.

2.2.4 Extraction and purification

Two methods of DNA extraction and purification were tested for use in this assay but deemed unsuitable. The methodology used is outlined below.

2.2.4.1 Pre-amp and column purification

Each oocyte sample (in 1µL) was briefly centrifuged and 1µL of lysis buffer (100mM Tris-HCl pH7.4, 300mM NaCl, 0.8mM EDTA, 2% vol/vol Nonidet P-40, 5mM DTT) was added (final volume of 2µL), and heated at 75°C for 5 minutes. This lysis method is referred to as the NE (no enzyme) method in 2.3.3, and Fig. 2.5.

Pre-amp was performed using TaKaRa DNA Polymerase Hotstart Version, 10x PCR buffer, 2.5mM dNTP (TaKaRa, #R007A), and custom made telomere and *18S rRNA* primers (Sigma, forward and reverse primer sequences outlined in Table 2.1), using a GeneAmp PCR 9700 System (Applied Biosystems). Each reaction contained a final volume of 4µL 10x PCR buffer, 4µL 2.5mM dNTP, 0.25µL DNA polymerase, 1µL of each of the four primers (telomere forward and reverse, *18S rRNA* forward and reverse, stocks at 10µM), 25.75µL sterile H_2O, and the sample (2µL volume), to give a total reaction volume of 40µL. Cycling conditions for all primers were set at 95°C for 5 minutes, followed by 8-14 cycles of 95°C for 15 seconds (s), 60°C annealing for 30s and extension at 72°C for 30s, with a final extension of 72°C for 10 minutes.

Following pre-amp, products were purified using the DNA Clean and Concentrator-5 kit (Zymo Research, D4004) according to manufacturer's instructions, with all centrifuge steps done at 8,000 rpm, and final products eluted in 64µL of sterile H_2O.

Components for a single qPCR reaction were 10µL Power SYBR Green PCR master mix (Applied Biosystems, #4367659), 0.5µL each of the forward and reverse primer for the desired sequence (i.e. telomere or *18S rRNA*, see Table 2.1 for sequences), 4µL of H_2O, and 5µL of the purified pre-amp product, set up in MicroAmp Fast Optical 96-well Reaction Plates (Life Technologies, #4346906), using a Quantstudio 12K Flex system (ThermoFisher). Reaction volumes for mtDNA primers were the same as above, except 7µL of H_2O and 2µL of purified pre-amp product was used. Cycling conditions for all primers were set at 95°C for 10 minutes, followed by 40 cycles of 95°C for 10s, 60°C annealing for 30s and extension at 72°C for 30s, followed by standard melt curve cycling.

2.2.4.2 Qiagen QIAamp DNA Micro Kit

Our group has previously used the QIAamp DNA Micro Kit (Qiagen, #56304) for mtDNA extraction. Samples for this kit were prepared and frozen as stated in 2.3.2, however they were frozen in 5µL PBS-PVP. DNA was extracted according to manufacturer's instructions for 'Isolation of Genomic DNA from Small Volumes of Blood', with samples being eluted in 50µL of sterile H_2O, which was run twice over the column to maximise DNA yield. A 1:10 dilution was prepared from each sample, and qPCR was carried out using the mtDNA primers as stated in Table 2.1, with the final dilution factor being 250X (i.e. copy number equation was: total mtDNA copy number = (10^x)*250, where x=(y-intercept of standard curve – Ct value of sample)/slope of standard curve).

2.2.5 Agarose Gel

To confirm amplification of the expected products, blastocyst qPCR products were run on a 4% agarose (Promega, #V3125) gel containing 0.01% gel red (Fisher). 5µL of 5X loading dye was added per 20µL qPCR plate well and 8µL of sample loaded per lane. The gel was run at 100V for 2 hours in 0.5X TBE buffer (Biorad, #161-0770), and imaged using Image Lab software.

2.2.6 Sample lysis and preparation for qPCR

Nuclear genomic DNA (nDNA) and mtDNA were extracted by adding 9µL of lysis buffer (50mM Tris-HCl pH 8.0, 1mM EDTA, 200µg/mL Proteinase K, 0.5% Tween-20) to each sample with a volume of 1µL (final volume of 10µL) following brief centrifugation, and heated to 55°C for 2 hours, followed by 95°C for 10 minutes to inactivate Proteinase K activity. This lysis method is referred to as the PK (Proteinase K) method in 2.3.3, and Fig. 2.5. Samples were then allowed to cool to 4°C and briefly centrifuged. Following this, 1µL of lysis product was removed and added to 9µL of sterile H_2O for mtDNA analysis, and the rest kept for telomere and *Rn18S* analysis.

2.2.7 Triple test qPCR assay

To generate 'calibrator' DNA for use as a standard within every assay, a whole ovary from a 6 week old PMSG and hCG stimulated CBA female mouse was collected and total DNA extracted (as described previously, 2.2.2 and 2.2.3). DNA concentration and purity were quantified by NanoDrop One Microvolume UV-Vis Spectrophotometer and diluted to 2.5ng/µL.

qPCR was performed using Power SYBR Green PCR Master Mix (Applied Biosystems, #4367659), standard MicroAmp Optical 96-well Reaction Plates (Life Technologies, #4306737), and custom made primers (Sigma, forward and reverse primer sequences outlined in Table 2.1), using an Applied Biosystems 7900HT Fast Real-Time PCR system. Cycling conditions for all primers were set at 95°C for 10 minutes, followed by 40 cycles of 95°C for 10s, 60°C annealing for 30s and extension at 72°C for 30s, followed by standard melt curve cycling. Two repeat reactions were performed for each sample and each primer pair, using 2µL of sample per reaction.

For *Rn18S* and telomere analysis, the final reaction for each well was 10µL Power SYBR Green PCR Master Mix, 0.5µL each of forward and reverse primer (*Rn18S* or telomere, stock at 10µM), 2µL of sample, and sterile H_2O to a final volume of 20µL. To minimise any plate-to-plate variations, *Rn18S* and telomere reactions for each sample were run on the same plate, and calibrator DNA assays included on every plate.

For mtDNA analysis, the final reaction for each well consisted of 10µL Power SYBR Green PCR Master Mix, 0.2µL each of forward and reverse primer (stock at 10µM), 2µL of sample or standard, and sterile H_2O to a final volume of 20µL. Total mtDNA copy number was quantified using the standard curve method as previously described (Kameyama et al., 2010). Briefly, quantification standards were prepared by PCR amplifying a 1186bp fragment in the *12S rRNA* region of mtDNA from mouse liver using the primer pair 5'-ACA CCT TGC CTA GCC A-3' and 5'-TTT GCC ACA TAG ACG AGT T-3'. The PCR product was extracted from the gel using QIAquick Gel Extraction Kit (Qiagen) and cloned using the Qiagen PCR Cloning Kit. Plasmid DNA was purified using QIAprep Spin Miniprep Kit (Qiagen), quantified by spectrophotometry, and diluted to 10^7 copies per 2µL. To create a standard curve, 10µL of standard stock was removed and serially diluted (1:10) from 10^7 to 10^1 copies. qPCR assay of the standard curve produced correlation coefficients consistently greater than 0.98. Serial dilutions were made fresh on the day. Total mtDNA copy number per sample was calculated according to the generated equation for Ct value against copy number for the corresponding standard curve (excluding 10^1 copies), and multiplied by the dilution factor of the sample (final dilution factor of 50) i.e. total mtDNA copy number = (10^x)*50, where x=(y-intercept of standard curve – Ct value of sample)/slope of standard curve.

When the calibrator sample was not used, telomere and mtDNA relative to total cell number were calculated using the $2^{-\Delta Ct}$ method, where the ΔCt of the sample was calculated as telomere or mtDNA Ct – *Rn18S* Ct. When the calibrator was used, telomere and mtDNA relative to total cell number were calculated using the $2^{-\Delta\Delta Ct}$ method, where the ΔCt of the calibrator (telomere or mtDNA Ct – *Rn18S* Ct) was subtracted from the ΔCt of the sample (telomere or mtDNA Ct – *Rn18S* Ct) to give the ΔΔCt.

Table 2.1 PCR and qPCR primers

Primer target	Forward primer sequence	Reverse primer sequence	Source
Telomere	5'-CGG TTT GTT TGG GTT TGG GTT TGG GTT TGG GTT-3'	5'-GGC TTG CCT TAC CCT TAC CCT TAC CCT TAC CCT TAC CCT-3'	de Frutos et al., 2016 Cawthon, 2002
mtDNA	5'-CGT TAG GTC AAG GTG TAG CC-3'	5'-CCA GAC ACA CTT TCC AGT ATG-3'	Kameyama et al., 2010
Rn18S	5'-AGA AAC GGC TAC CAC ATC CAA-3'	5'-CCT GTA TTG TTA TTT TTC GTC ACT ACC T-3'	de Frutos et al., 2016
18S rRNA	5'-CCA GAG CGA AAG CAT TTG CCA AGA-3'	5'-GCA TTG CCA GTC GGC ATC GTT TAT-3'	Wang et al., 2013
36B4	5'-ACT GGT CTA GGA CCC GAG AAG-3'	5'- TCA ATG GTG CCT CTG GAG ATT-3'	Wang et al., 2013

2.2.8 Statistical analysis

Results are presented as mean +/- SEM. Statistical analysis was performed using Graph Pad Prism 7 version for Windows (GraphPad Software Inc., La Jolla, CA). Unpaired t-test, and one way analysis of variance (ANOVA, comparison of means) were used as indicated and statistical significance was considered at p-value <0.05.

2.3 Results

2.3.1 Validation of primer efficiencies and reference selection

Establishment of a highly quantitative multiplex assay requires validation of primer efficiency and linearity. In typical telomere length qPCR assays on tissues or populations of cells, a single copy reference gene is used, most commonly *36B4*. However, due to single cells containing very small amounts of genomic DNA (~6-7pg) (Dolezel et al., 2003), a single copy gene has been shown to be unreliable for analysis of individual cells (Wang et al., 2013) and instead, a multi-copy gene is more suitable for accurate detection in a single cell. To evaluate and compare the efficiency of each PCR assay, primers were used with decreasing DNA concentrations at identical conditions, and linearity and Pearson's Correlation Coefficients of the relationship between cycle threshold (Ct) and input DNA concentration was examined. Ovary tissue was selected as a relevant tissue type to test primer efficiency on known amounts of DNA and was diluted to 6ng/µL, 3ng/µL, 1.5ng/µL, 0.75ng/µL, and 0.375ng/µL. The ovary DNA serial doubling dilutions (1:2) then underwent qPCR with 5 primer pairs: mtDNA, telomere, *36B4*, and two primer pairs targeting different regions of the same gene (18S ribosomal RNA), referred to as *18S rRNA* (Wang et al., 2013) and *Rn18S* (de Frutos et al., 2016) (Fig. 2.1). To visualise linearity, input DNA concentration was log transformed and graphed with Ct values. mtDNA, Telomere, *36B4*, and the two candidate reference genes (*18S rRNA* and *Rn18S*) all showed very strong correlations between DNA concentration and the Ct values, with correlation coefficients consistently above 0.99 (Fig. 2.1 A, B, C).

To determine whether normalisation of telomeric DNA to each of the possible reference genes would give identical results, thus indicating equivalent efficiency, the telomere Ct to reference Ct ratio (telomere:ref) and mtDNA Ct to reference Ct ratio (mtDNA:ref) was then calculated for each DNA dilution and reference. The ratio was graphed for *36B4* (as the gold standard) against the two potential multi-copy reference genes (Fig. 2.1). For telomere, the ratio with both *18S rRNA* and *Rn18S* showed strong correlations with the telomere to *36B4* ratio of above 0.98 (Fig 2.1 D, E), and when the ratios for the two potential reference genes were graphed together, their correlation was equally as strong (r^2=0.9973, Fig 2.1 F). Similarly, the mtDNA ratio with both multi-copy reference genes also showed very strong correlations with the *36B4* ratio, of 0.99

(Fig 2.1 G, H), with an equally as strong correlation when the two multi-copy gene ratios were graphed together (Fig. 2.1). Although both primer sets for *18S ribosomal RNA* were validated, *18S rRNA* was selected to act as the multi-copy gene for ongoing optimisation as it had the strongest correlation with DNA concentration (Fig 2.1 C), the telomere:*36B4* ratio (Fig 2.1 D), and the mtDNA:*36B4* ratio (r^2=0.999, Fig. 2.1 G).

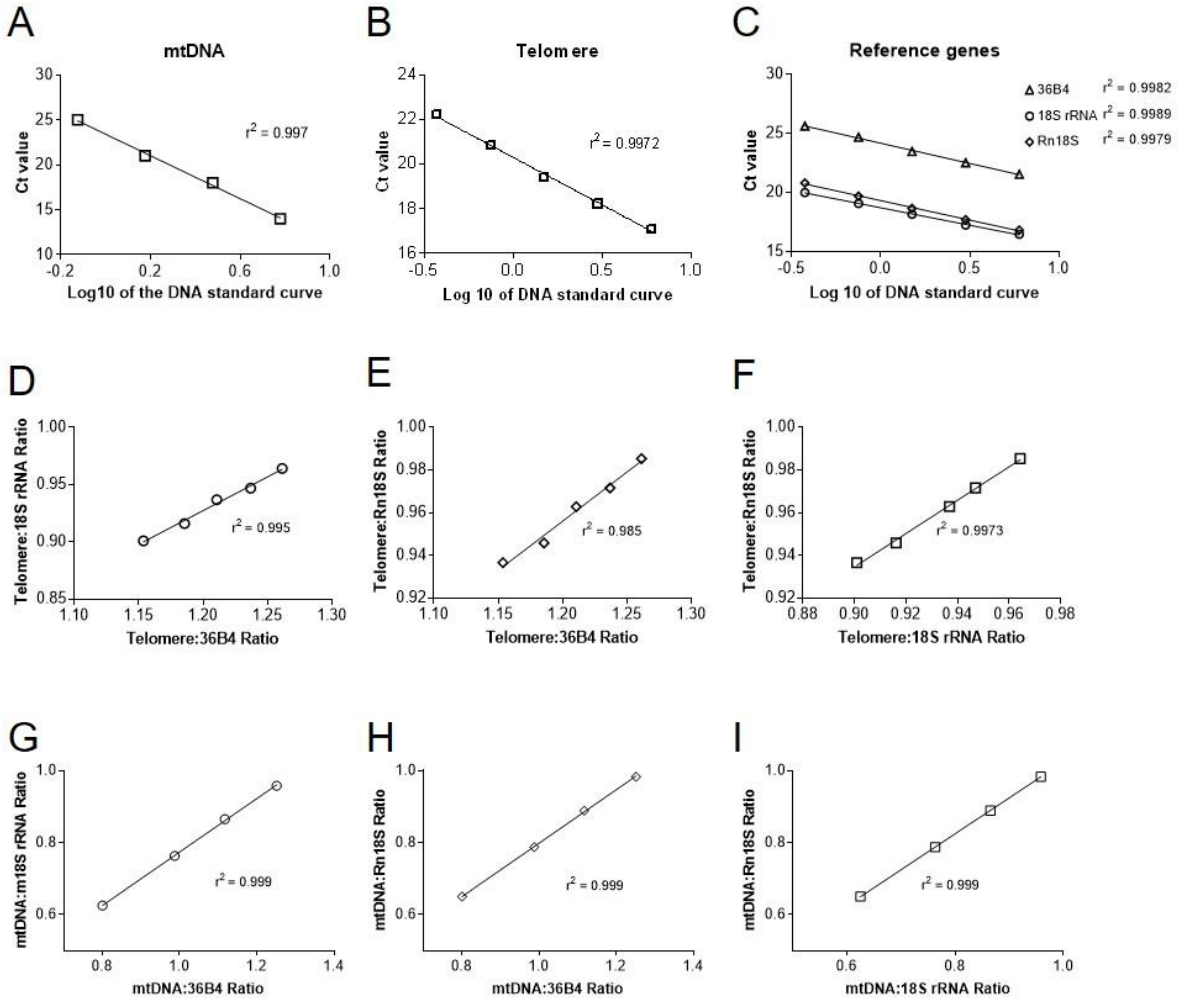


Figure 2.1. Linear correlations of primer efficiency and normalisation telomere length and mtDNA content using candidate reference genes

DNA was extracted from one whole ovary and serially diluted (1:2) to produce 5 dilutions at concentrations of 6ng/µL, 3ng/µL, 1.5ng/µL, 0.75ng/µL, and 0.375ng/µL which were used to test the efficiency of the mtDNA primers (A), telomere primers (B), and the two potential reference gene primers: *18S rRNA* and *Rn18S*, with *36B4* as a comparator (C), under the same cycling conditions. To test for linearity, DNA concentration was log10 transformed for data plotting with Ct values and r^2 values shown. Each data point is derived from triplicate PCR reactions. The telomere:ref ratio (D, E, F), and the mtDNA:ref ratio with each potential reference (G, H, I) was calculated and linear correlation analysis performed.

2.3.2 Optimising established method

The Triple Test assay was developed for assessment of single oocytes and embryos from the zygote to blastocyst stage. The most challenging aspect was to design assay conditions which are able to measure relatively scarce nDNA targets in the same sample as the more abundant mtDNA. Being just single cells, immature (GV) oocytes and mature (MII) oocytes with the attached polar body will have the lowest amount of nDNA out of all the intended samples, therefore initial optimisations were performed on individual MII oocytes. To increase the amount of target nDNA available for qPCR detection, pre amplification was performed as in previous published methods (Wang et al., 2013), with 8, 10, 12, and 14 cycles using telomere and *18S rRNA* primers followed by standard PCR of 40 cycles using each primer pair individually. As expected, with increasing pre-amp cycles, target DNA Ct decreased in the qPCR assay step (Fig. 2.2 A, B). Further, target DNA was detected at much lower Ct in all samples that underwent pre-amp compared to samples that did not undergo pre-amp ("No Pre-amp Oocytes", Fig, 2.2 A, B). Importantly, the number of pre-amp cycles did not change the telomere:reference ratio (Fig. 2.2 C). A protocol using 12 pre-amp cycles was selected for ongoing assays because these reactions were the lowest pre-amp cycles that yielded mean Ct values less than 30 in the telomere assays, indicating the assay has dynamic range to detect either higher or lower amounts of telomeric DNA.

Negative controls were used to detect any contamination or artefactual amplification. A pre-amp control, with oocyte DNA replaced by an equivalent volume of H_2O, was used to detect non-specific primer interactions in the pre-amp reaction. Surprisingly, at 14 pre-amp cycles, Ct values for both telomere and *18S rRNA* were detected in this negative control (Fig. 2.2 A, B – "Pre-amp H_2O"). For telomere primers, a Ct of 37 was obtained which, although 9.9 cycles higher than identical reactions containing oocyte DNA (Fig 2.2 A), is considered a valid reading that could interfere with assay precision. Similarly, *18S rRNA* primers used on samples containing only H_2O, produced a Ct of 24, just 4.4 cycles greater than samples containing oocyte DNA (Fig. 2.2 B), and is indicative of artefactual amplification. A second type of negative control, which did not involve pre-amp but where oocyte DNA was replaced with water (qPCR H_2O, Fig. 2.2 A, B), showed that there was a very minor interaction of the telomere primers (Ct=39), and none between the *18S rRNA* primers. Checking the frequency of

this occurrence, across ten independent pre-amp and subsequent qPCR runs of individual oocytes, Ct values were detected intermittently in the telomere qPCR results (Fig 2.2 D, 5/10 runs), but consistently in the *18S rRNA* reactions (Fig. 2.2 E, 10/10 runs).

To determine if the detected product in the pre-amp H_2O negative controls was a result of excessive primer, pre-amp primer concentrations for *18S rRNA* forward and reverse primers were decreased from 250nm to 75nm and 25nm (Fig 2.2 F), while other qPCR assay reagent concentrations were unchanged. Four oocytes and four parallel pre-amp water controls were assayed at each of the three primer concentrations, yet an artefact product was still detected in the pre-amp water controls at all concentrations. Decreasing pre-amp primer concentration from 75nm to 25nm did not even markedly decrease the Ct difference between the oocytes and water control, with the Ct differences at: 250nm = 0.87, 75nm = 4.19, 25nm = 3.46.

An artefact product was being generated during the pre-amp step of the assay. Most likely, this product is the result of secondary structures being formed when the telomere and *18S rRNA* primers are combined in the pre-amp reaction, because when these same primers are used in the negative control for qPCR only (Fig. 2.2 A, B) there is no product generation (with *18S rRNA* primers) or low levels (telomere primers). This artefact product could possibly influence the accuracy of the assay in oocyte samples and needed to be resolved.

To verify that the *18S rRNA* primers were suitable for use as the reference gene in the redesign of this assay, they and the *Rn18S* primer sequences underwent NCBI primer BLAST to determine the amplicon (product) sequence (Sup Fig. 2.1). Interestingly the 18S rRNA primers gave products of different sizes, ranging from 116 to 108bp (Sup Fig 2.1 A). The Rn18S primers gave products of a consistent size of 91pb (Sup Fig. 2.1 C). The resulting amplicon sequence from the first product generated with 100% primer identity (Sup Fig 2.1 A and C, red box) was aligned to the mouse genome via NCBI nucleotide BLAST (Sup Fig. 2.1 B and D). The 18S rRNA amplicon sequence returned 30 significant alignments, however only 23 of these had 100% query coverage, and only four had 100% identity match between the target and query sequence, while only three alignments had 100% for both query coverage and identity match (Sup Fig. 2.1 B). This suggests a high degree of sequence variability for the genomic region that the 18S rRNA primers are targeting. The Rn18S amplicon

sequence returned 27 significant alignments, all of which had 100% query coverage, and 24 had 100% identity match, meaning 24 out of 27 total matches were a complete match for query coverage and sequence identity (Sup Fig. 2.1 D). Taken together, these results stipulate that the Rn18S primers target a region of the genome that shows a lower degree of sequence variability than the 18S rRNA primers. Given these results, the Rn18S primers are likely to give more reliable detection than the 18S rRNA primers going forward.

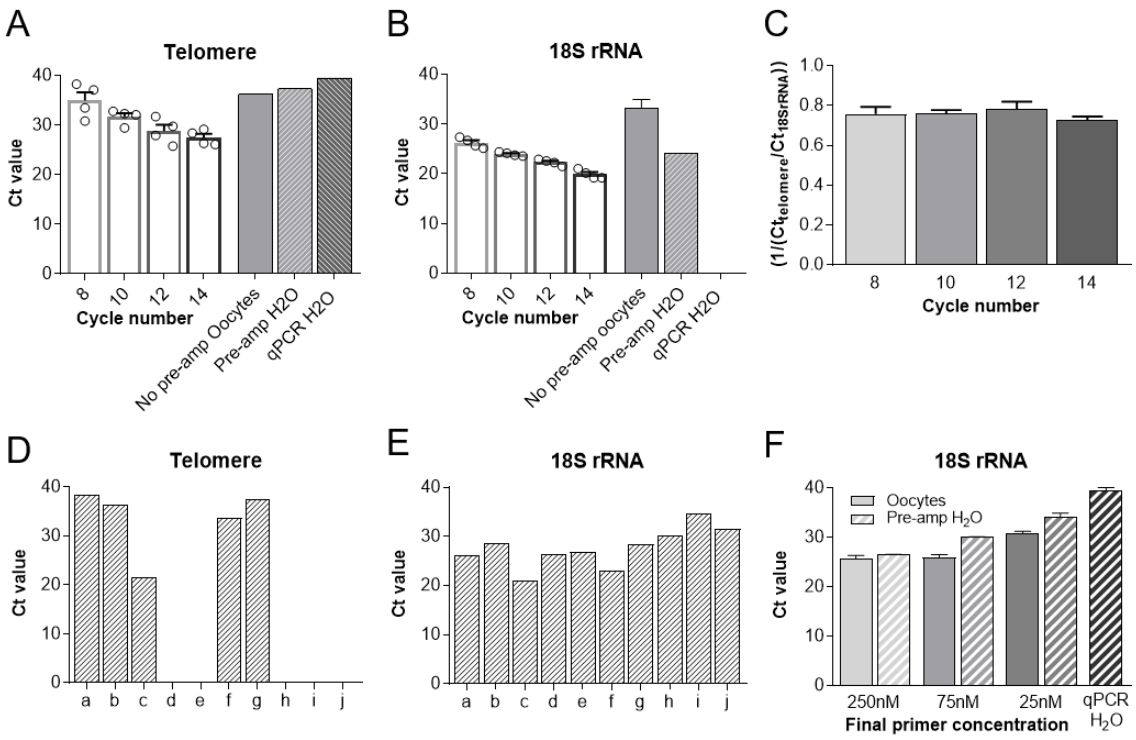


Figure 2.2. Pre-amp optimisation in single MII oocytes

Four individual oocytes per group underwent pre-amp for the indicated number of cycles, followed by identical qPCR for both telomere and *18S rRNA* (A, B). Oocytes that did not receive pre-amp, along with pre-amp and qPCR negative controls - where the volume of oocyte per reaction was replaced with water and underwent the highest indicated number of cycles - were also used (A, B). The telomere to *18S rRNA* ratio was not altered by the pre-amp cycle number increase (C). To assess artefactual product generation, water (10 independent replicates) was used instead of DNA for 12 cycles of pre-amp followed by PCR for either telomere (D) or *18S rRNA* (E); and artefacts were detected. *18S rRNA* primer concentration was reduced and oocytes or water (negative control) were assayed generating detectable product in both (F, n=4 oocytes 3 water controls per primer concentration).

One possible reason for the generation of PCR products in the negative controls to the same extent as the oocyte samples was that primer-primer interactions were occurring because there was no target DNA available for primers to interact with. To determine if low DNA content in the sample contributes to artefact product, the assay was conducted using blastocysts (as they contain approximately 100 cells (Chen et al., 2019)) and thus considerably more DNA) eliminating the need for two rounds of PCR. Six individual blastocysts had DNA extracted and underwent qPCR, along with 6 water negative controls (equivalent volume of H_2O replaced blastocyst DNA), with all four primers included in the same reaction (Fig 2.3) to mimic the pre-amp reaction. The average Ct for the blastocysts was 26.51, and the water controls was 26.98 (Fig. 2.3 A). The qPCR reaction was separated on a 4% agarose gel and one low molecular weight band was visible in the water controls, while the same band and one larger product were present in the blastocyst samples (Fig. 2.3 B). An exception, blastocyst 'e' had a slightly higher Ct value than the others (26.86) and only the smaller band was detected on the agarose gel (Fig 2.3 A and B, respectively). This suggests this blastocyst sample was lost prior to being placed in the collection tube (i.e. likely stuck to the pipette tip and was not expelled), meaning no nDNA was extracted, essentially making this sample equivalent to a water control. When comparing the melt curve plots generated following qPCR, two distinct peaks are seen for the blastocyst samples (Fig 2.3 C), with the exception of blastocyst 'e' (arrowhead), while only one peak is seen in the water controls (Fig. 2.3 D). The water control peak occurs at the same point in the plot as the highest peak for the blastocyst samples, indicating that this reaction generates artificial signal in the qPCR reaction. These results show that an artefact signal is generated by combining the telomere and *18S rRNA* primers into one reaction, even in the presence of abundant DNA template, likely due to the repetitive nature of the telomere primers or potential primer dimer formation, and therefore pre-amp cannot be used to enhance sensitivity in this assay.

The presented results (Fig. 2.2 and 2.3) clearly demonstrate that the use of multiplex pre-amp simply cannot be utilised for quantification of telomeric and genomic DNA as it results in artefact product formation, even in the presence of sufficient DNA (Fig. 2.3). Due to this substantial flaw, this published method (Wang et al., 2013) very likely gives highly inaccurate results due to the production of artefact product that contributes to generated Ct values in the reference gene. Further, due to the peculiar

alignment of the *18S rRNA* primers within the mouse genome, and varying predicted product sizes, these primers are also not suitable for detection of the reference gene. Overall, this published method (Wang et al., 2013) contains undeniable flaws that invalidate the use of any components for detection and quantification of telomeric and reference DNA. As such, a new assay that uses a more sophisticated lysis method (involving proteinase K), does not utilise a pre-amp step, or use *18S rRNA* primers for the reference must be developed if quantification of telomere length in individual oocytes and embryos is to be possible.

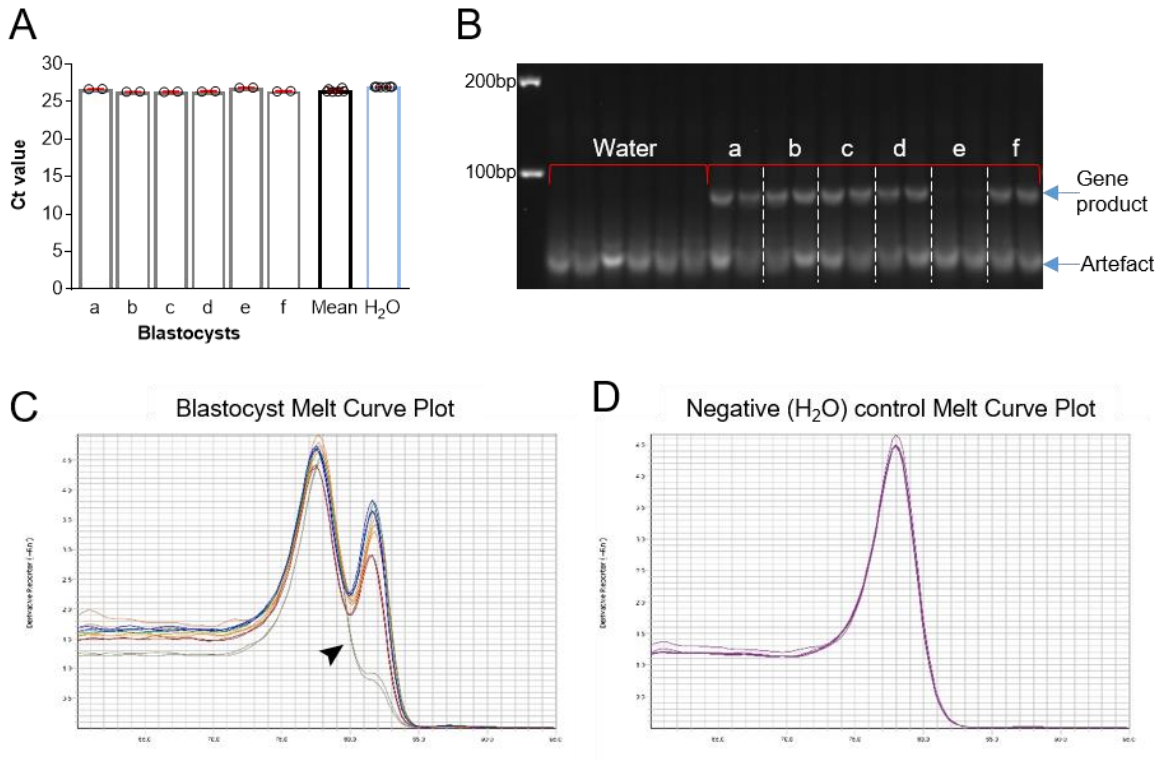


Figure 2.3. Products generated using telomere primers and *18S rRNA* primers together in qPCR

DNA was extracted from 6 blastocysts (A, a-f) and qPCR performed with the telomere and *18S rRNA* primers together, as in pre-amp, along with 6 water controls (H_2O). The mean Ct (bar) from 2 technical replicates for all blastocysts is plotted (A). The total qPCR reaction was run on a 4% agarose gel (B). Melt curve plots for the 6 blastocysts (C) and water controls (D). Arrow head (C) corresponds to blastocyst 'e' which had same pattern of bands as water controls (B).

2.3.3 Optimisation of mtDNA extraction efficiency

The assay for mtDNA copy number uses a standard curve method for copy number calculation in order to provide absolute (instead of relative) number of copies of the target DNA. Due to the sensitivity of PCR, standard curves must be validated as highly reproducible. Replicate experiments producing independent standard curves indicated that the point representing the lowest copy number (10^1), which has been used in previous studies, was not entirely reproducible (two example standard curves shown in Sup Fig. 2.2 A, B). This level of inaccuracy greatly affects the correlation coefficient of the entire curve, as demonstrated by calculating the coefficient with or without the 10^1 copies standard (Sup Fig. 2.2 A, B). When this data point is excluded, the independently generated curves overlap demonstrating excellent reproducibility (Sup Fig. 2.2 C). As no samples used for this assay are expected to have copy numbers in the 10^1 to 10^2 range, this dilution was not used to calculate the correlation coefficients or equations generated for mtDNA copy number calculations.

Assessment of total mtDNA copy number in individual oocytes and embryos is routinely performed using the Qiagen method of DNA isolation (Wu et al., 2015). However, a comparison of mtDNA extraction methods was undertaken to determine if efficiency of mtDNA isolation could be improved. To do this, DNA (nDNA and mtDNA) was purified from individual oocytes via two different published methods: the lysis, pre-amp and Zymo column purification method as previously described by Wang et al. (2013), or the Qiagen column kit which is conventionally used for mtDNA extraction for standard curve quantification (Kameyama et al., 2010; Wu et al., 2015). mtDNA qPCR was then performed under identical conditions and mtDNA copy number calculated for oocytes (Fig. 2.4). Comparison of oocyte DNA from the lysis/pre-amp/column method and the Qiagen kit extraction method showed no differences in Ct values (Fig. 2.4 A), however calculation of the mtDNA copy number revealed samples generated by lysis/pre-amp/column detected a meaningfully lower mtDNA copy number (Fig 2.4 B, $p<0.0001$). Product specifications for the column used for pre-amp product purification state that it has a recovery rate of 50-70% for DNA fragments ranging from 11kb to 23kb (Zymo, DNA Clean & Concentrator-5 product specifications). The mitochondrial genome is ~16.5kb, meaning that potentially half of the oocyte mtDNA can be lost due to the low efficiency of recovery in this size range. Oocytes from the Qiagen method yielded an average copy number of 73,750.5, while

oocytes that had been purified through the Zymo column yielded average copy numbers of 36,413.5, which is a difference of 37,337 copies, or a 50.6% reduction compared to the Qiagen extracted oocytes, indicating large mtDNA loss from the Zymo column (Fig 2.4 B), and is much lower than the numbers in the literature. To avoid this column-related mtDNA loss, a small volume of the pre-amp product (where the telomere and reference gene DNA had been amplified) was removed prior to Zymo column purification and diluted as it would have been if column-purified. The Ct values for the DNA removed prior to the column were lower than that removed after the column, indicating more product and hence decreased recovery efficiency by the column (Fig. 2.4 C, $p<0.0001$). This was further reflected in the calculated mtDNA per oocyte (Fig. 2.4 D, $p<0.0001$), where the average copy number before the column was 737,326 compared to 40,458.6 after the column. Importantly, the average copy number generated by measuring the DNA sample before column processing was ~10X higher than that generated by the Qiagen purification method (Fig 2.4 B and D, respectively), indicating a marked loss of mtDNA on the Qiagen kit column as well.

Next, three DNA extraction methods were compared for mtDNA recovery in oocytes: the Qiagen column (referred to as “column”), the lysis method (now referred to as no enzyme method, or NE), and a lysis buffer that uses a larger volume and contains Proteinase K (referred to as the Proteinase K method, or PK). mtDNA copy number calculations revealed that the two lysis methods had much higher mtDNA yields than the Qiagen column method (Fig. 2.5 A, $p<0.0001$), while not being different from each other. Due to this finding, the Qiagen column method was no longer used. As an MII oocyte is a single cell, lysis methods are likely to be equally as efficient as long as no DNA degradation is occurring. Therefore, the two lysis methods were tested on blastocysts for nDNA and mtDNA extraction as blastocysts are the intended sample type that have the highest cell number and would be the most challenging to efficiently lyse all cells. Individual blastocysts were lysed in 1µL of NE buffer or 9µL of PK buffer and then diluted in H_2O to a total volume of 100µL before undergoing qPCR for telomere, *Rn18S* and mtDNA (Fig. 2.5 B). Ct values were lower for blastocysts lysed using the PK method than the NE method for telomere and *Rn18S* ($p<0.0001$) and mtDNA ($p=0.0089$), and therefore calculated mtDNA copy number was higher for the PK extracted blastocysts (Fig. 2.5 C, $p<0.0001$). These findings indicate that while either lysis method could be used for oocytes, the lysis method using a buffer

containing Proteinase K was the most efficient for extraction of nDNA and mtDNA from blastocysts and thus was selected as the optimal extraction method for further developing the assay.

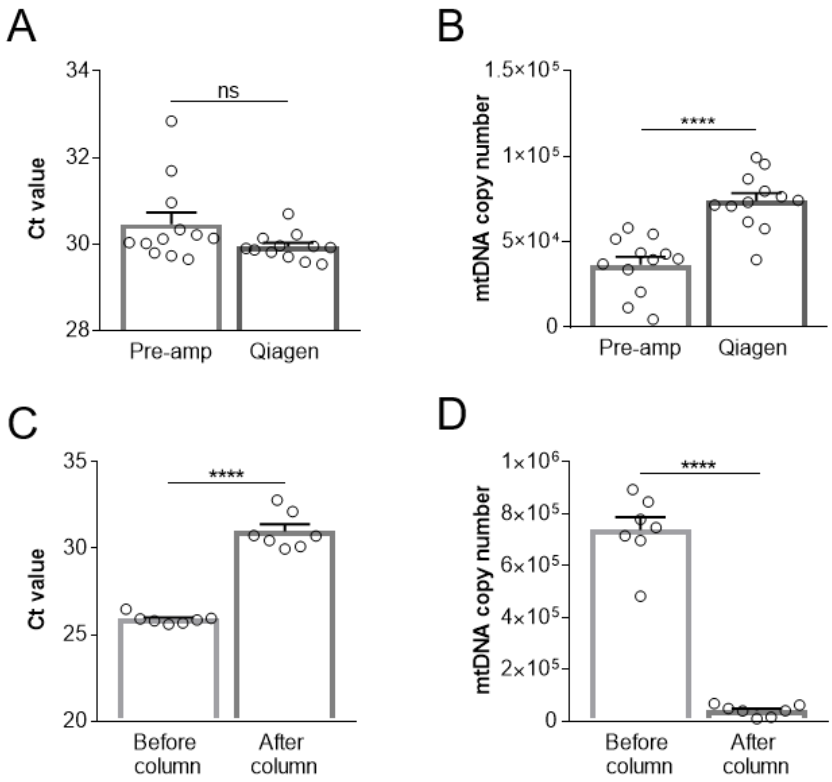


Figure 2.4. mtDNA extraction optimisation in oocytes

MII oocytes had mtDNA extracted using either the lysis/pre-amp/column clean up method, or the Qiagen protocol (n=12 per group); and qPCR for mtDNA was run to compare mtDNA extraction efficiencies (A, B). Raw Ct values (A) and mtDNA copy number per oocyte calculated from the standard curve (B). mtDNA Ct values were determined for oocytes that were undergoing the lysis/pre-amp/column clean up method where an aliquot of DNA for analysis was removed either before or after the Zymo column clean up (C) and mtDNA copy numbers calculated (D). Data analysed using unpaired t-test, **** $p<0.0001$.

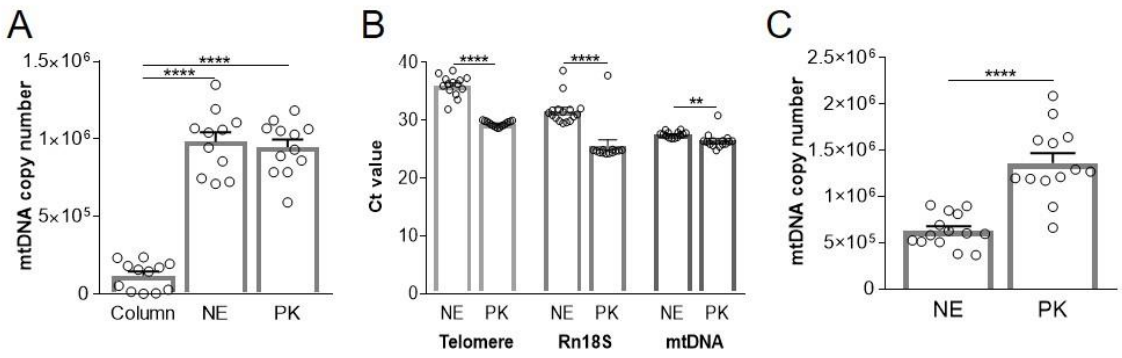


Figure 2.5. Lysis optimisation in oocytes and blastocysts for mtDNA and nDNA

Oocytes had mtDNA extracted using the Qiagen protocol (column), a lysis buffer with no active enzyme (NE), or a lysis buffer containing Proteinase K (PK) (n=12 per group), and underwent qPCR to calculate their total mtDNA copy number (A). Blastocysts (n=14 per group) had DNA extracted using either the no enzyme, or proteinase K lysis methods and qPCR performed for telomere, *Rn18S*, and mtDNA (B), and mtDNA copy number calculated (C). Data analysed using unpaired t-test, ** p=0.0089, **** p<0.0001.

2.3.4 Re-design and validation of the Triple Test qPCR

Optimisations of the previously described individual assays revealed critical flaws in published methods and resulted in the requirement for a complete redesign of this assay. The exclusion of the pre-amp step due to unavoidable artefact product generation means that sample preparation must be in the smallest volume possible for qPCR assays. The most efficient lysis method requires cells to be frozen in 1µL and then 9µL of buffer added to give a total volume of 10µL, therefore it is ideal to not increase this volume. For a reference gene, *18S rRNA* still remains a suitable candidate, however primers from the previously published single-cell assay (Wang et al., 2013) were demonstrated to be unsuitable. The primers termed '*Rn18S*' (de Frutos et al., 2016) gave more consistent genome alignments and predicted product sizes (Sup. Fig. 2.1), and were carried through for re-design. mtDNA is highly abundant in oocytes and embryos (starting in the ~10^4 copies range (Pikó and Taylor, 1987; Santos et al., 2006; Wu et al., 2015)) and therefore can be made more dilute than nDNA as ample target remains in the diluted samples and the dilution factors are accounted for in the copy number calculation equation. Blastocysts contain ~100 cells, therefore much more nDNA than oocytes, and can be diluted further than oocyte DNA. Therefore the following method was designed: following lysis, when the sample was in a total volume of 10µL, all oocyte and embryos prior to the blastocyst stage had 1µL removed and added to 9µL of H_2O for mtDNA analysis, the remaining 9µL of sample underwent telomere and *Rn18S* qPCR each in two technical replicates using 2µL sample per replicate, leaving 1µL of the sample left over. As blastocysts contain more DNA than oocytes and other pre-implantation embryos, following lysis, 90µL of H_2O was added to bring the total volume to 100µL for qPCR analysis for mtDNA, telomere and *Rn18S* (see Sup Fig. 2.3 A for workflow). The revised protocol was first verified on individual oocytes with raw Ct values for all primer pairs compared (Sup Fig. 2.3 B) and mtDNA copy number calculated (Sup Fig. 2.3 C). The full work flow was tested on MII oocytes, 2C embryos and blastocysts for telomere, *Rn18*S and mtDNA (Sup Fig. 2.3 D, E, F, respectively). Decreases in Ct value were seen with increases in cell number for telomere and *Rn18S* satisfying the expectation that increases in nDNA copy number should be detectable as cell number increased. Calculation of mtDNA copy number confirmed an increase in mtDNA copy number from the MII and 2C stage

to the blastocyst stage, consistent with the literature (Ebert et al., 1988; Pikó and Taylor, 1987) (Sup Fig. 2.3 G, $p<0.0001$).

The relevant dilutions of the nDNA need to be taken into account for comparisons of calculations across developmental stages. While all samples destined for mtDNA assays ended up at a final dilution of 1/100, the samples for nDNA assays were differentially diluted, i.e. blastocysts were diluted 1/100 whereas oocyte nDNA was at a dilution of 1/10 (Sup Table 2.1). This means that it is not possible to compare mtDNA relative to nuclear genome content across all developmental stages. Therefore the protocol was further revised so that blastocysts were processed in the same manner as oocytes and other cleavage stage embryos so that dilutions for mtDNA and nDNA were identical (see Sup Table 2.1, see Fig. 2.6 for revised workflow). The revised protocol was tested on a developmental time course (MII oocyte, 2C embryo, and blastocyst) for telomere, *Rn18S* and mtDNA qPCR (Fig. 2.6 B, C, D). Decreases in Ct for nDNA markers was seen at each stage, again consistent with increasing cell number (Fig. 2.6 B, C, $p<0.0003$). A decrease in mtDNA Ct was only seen at the blastocyst stage (Fig. 2.6 D, $p=0.0184$). This assay was then validated in cases where mtDNA and telomere length are known to be decreased compared to controls. The sensitivity of the mtDNA copy number assay was tested in oocytes and blastocysts from wild-type and oocyte-specific TFAM knock out (KO) mice, where mtDNA is reduced in oocytes from KO mice by using GDF9-Cre (Larsson et al., 1998). As expected reduced mtDNA was observed (Fig. 2.6 E, $p<0.0001$) due to a lack of replication from the absence of TFAM (Wai et al., 2010). As oocytes from older females are known to have shorter telomeres (Yamada-Fukunaga et al., 2013) and decreased mtDNA copy number (Simsek-Duran et al., 2013), these assays were further validated by assessing telomere and mtDNA relative to nuclear DNA content, and mtDNA copy number in oocytes from old mice compared to young (Fig. 2.6 F, G, H). Consistent with the literature, telomere, mtDNA and mtDNA copy number were each reduced in oocytes from old females, compared to controls (Fig. 2.6: (F) $p=0.0011$; (G) $p=0.0014$; (H) $p=0.0003$).

Exclusion criteria were established to account for samples where DNA degradation or loss of the very small sample volumes may have occurred during processing. A sample was excluded from the analysis if the Ct for the *Rn18S* reference technical replicates was more than ~1-1.5Ct outside of the mean for all samples of the same

type on the same plate. This threshold was selected as each unit of Ct increase in qPCR represents an approximate halving of DNA, therefore an increase in the magnitude of greater than 1.5 Ct suggest a substantial loss of DNA which can only be explained by loss or degradation of the sample, since the sample represents a single input oocyte or embryo.

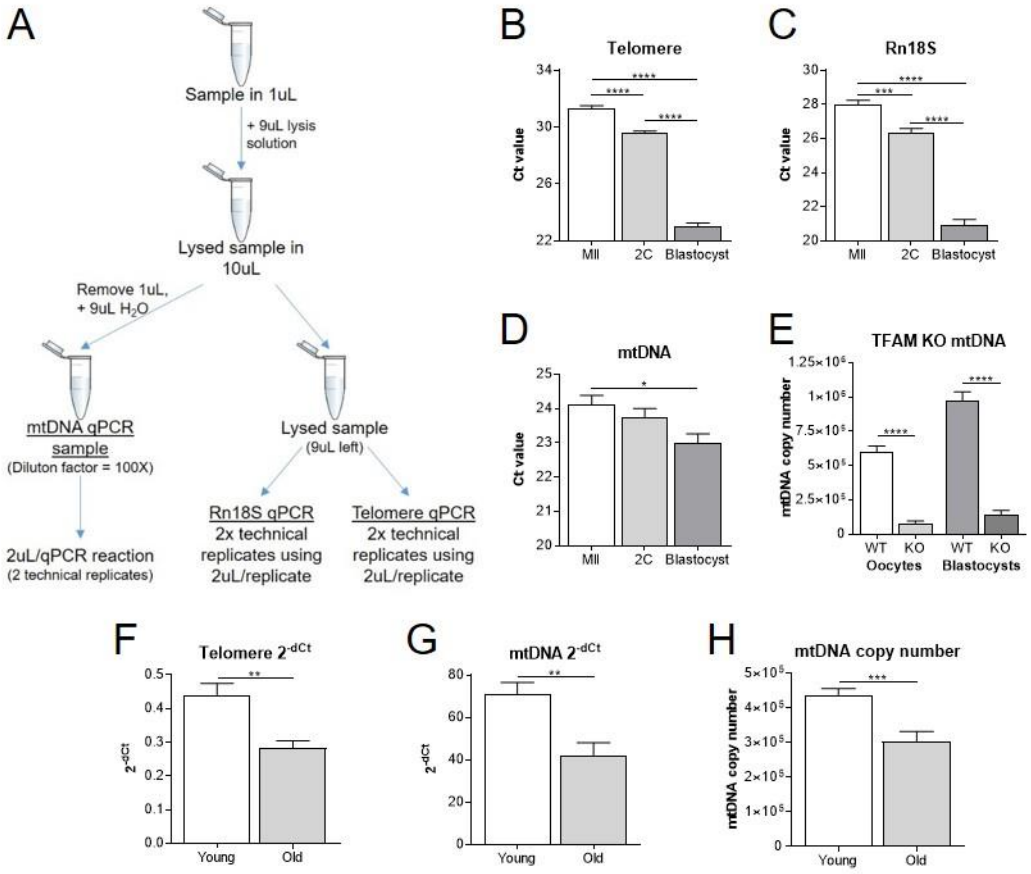


Figure 2.6. Triple test qPCR work flow and validation using oocytes and embryos

Final optimised protocol work flow for triple test qPCR on oocyte and embryo samples (A). The sensitivity of the protocol was validated by using oocytes and embryos (generated by IVF with CBA mice) and observing expected decreases in Ct values for telomere (B), *Rn18S* (C), and mtDNA (D) with increasing cell number. mtDNA copy number assay was validated by analysing mtDNA copy number (E) in TFAM wild type and knock out oocytes and blastocysts. Assay sensitivity for telomere, mtDNA and mtDNA copy number was validated by analysing MII oocytes from hormonally primed young and old (≥12 months) female mice (F-H). Data analysed using ordinary one-way ANOVA (comparison of means) (B-D), and unpaired t-test (E-H), * p=0.0184, ** p=0.001, *** p=0.0003, **** p<0.0001.

One final refinement made to this assay was the addition of a DNA calibrator control, which due to the sensitivity of this assay, improves precision by accounting for any minor plate to plate variations. Therefore the relative telomere and mtDNA per cell were calculated using the $2^{-\Delta\Delta Ct}$ method, where the ΔCt of the calibrator (telomere or mtDNA Ct – *Rn18S* Ct) was subtracted from the ΔCt of the sample (telomere or mtDNA Ct – *Rn18S* Ct) to give the ΔΔCt. Throughout the remainder of this thesis, results are shown with this methodological modification.

2.4 Discussion

Here I have developed and validated a qPCR assay designed for use with single oocytes and embryos that gives three quantitative measurements for 1) telomere content relative to nuclear DNA (representing cell number), 2) mtDNA content relative to nuclear DNA, and 3) total mtDNA copy number for the individual sample using qPCR, named the 'Triple Test'.

Previously, analysis of telomere length required pools of cells or embryos, meaning that potential heterogeneity within the population was masked. To overcome this, a previous method to analyse telomere length in single cells had been developed (Wang et al., 2013), which utilised a pre-amp step followed by a clean-up step. Here I found that this published and highly cited protocol introduces artefact amplification during pre-amplification, and major mtDNA loss during the column clean up. Thus this assay is not suitable for reliable detection of nDNA and mtDNA, and also throws into question the conclusions of this well-known paper. These issues have now been overcome through the redesign and refinement of the protocol to preserve the nDNA in the absolute minimal volume, and exploit the abundance of mtDNA in oocytes and embryos to eliminate these areas of inadequacy in previous methods.

Due to its individual approach, this assay will vastly improve the ability to study telomere length and mtDNA copy numbers in oocytes and embryos by allowing these measurements to be linked to other factors such as cleavage timing in pre-implantation embryos, where such correlations would not be possible when analysing pooled samples. This assay also allows the number of oocytes and embryos required for analysis to be minimised, as each sample contributes an individual data point, rather than requiring a pool of oocytes/embryos to generate one data point. Another important application for this assay is in the study of the quality of oocytes and embryos derived from sub-fertile females, with underlying contributing factors such as advanced reproductive age or obesity. In cases such as these, the quantity of material available for analysis may be reduced, for example, ovulation rates in old mice (>12 months old) are markedly decreased compared to young controls (3-4 months old) (see Fig. 5.8 A for instance). The Triple Test enables telomeres and mtDNA to be assayed for each individual oocyte or embryo and correlational analyses with physiological measures such as female age and body weight can be directly addressed. It is hypothesised that

there will be greater heterogeneity in these biomarkers in oocytes and embryos from females with obesity or advanced age, which can now be thoroughly investigated.

The results also demonstrate that different methods of sample preparation dramatically affect measurements of DNA. For instance, analysis of mtDNA copy number in individual oocytes and embryos has previously been established (Kameyama et al., 2010) and is widely used. Yet here we have found that methods such as these that rely on a silica-based membrane utilising column for DNA extraction and purification lose a substantial amount of mtDNA (Fig 2.5 A). This means that mtDNA copy numbers reported in the scientific literature may be greatly under-estimated and that comparisons between studies should carefully consider the purification methods utilised.

The Triple Test is a robust, novel methodological pipeline that allows three qPCR measurements to be reliably obtained from single oocytes or embryos. It will be extensively used throughout the remainder of this thesis, to investigate changes in telomeres and mtDNA during preimplantation development and in contexts of compromised mitochondrial function and/or physiological subfertility.

2.5 References

Cawthon, R.M., 2002. Telomere measurement by quantitative PCR. Nucleic Acids Res. 30, 47e – 47. https://doi.org/10.1093/nar/30.10.e47

Chen, M., Wong, S.L., Wu, L.L., Gordon, Y.E., Heilbronn, L.K., Robker, R.L., 2019. Differential impacts of gonadotrophins, IVF and embryo culture on mouse blastocyst development. Reprod. Biomed. Online 39, 372–382. https://doi.org/10.1016/j.rbmo.2019.02.007

de Frutos, C., López-Cardona, A.P., Fonseca Balvís, N., Laguna-Barraza, R., Rizos, D., Gutierrez-Adán, A., Bermejo-Álvarez, P., 2016. Spermatozoa telomeres determine telomere length in early embryos and offspring. Reprod. Camb. Engl. 151, 1–7. https://doi.org/10.1530/REP-15-0375

Dolezel, J., Bartos, J., Voglmayr, H., Greilhuber, J., 2003. Nuclear DNA content and genome size of trout and human. Cytom. Part J. Int. Soc. Anal. Cytol. 51, 127–128; author reply 129. https://doi.org/10.1002/cyto.a.10013

Ebert, K.M., Liem, H., Hecht, N.B., 1988. Mitochondrial DNA in the mouse preimplantation embryo. J. Reprod. Fertil. 82, 145–149.

Hayflick, L., Moorhead, P.S., 1961. The serial cultivation of human diploid cell strains. Exp. Cell Res. 25, 585–621.

Kameyama, Y., Filion, F., Yoo, J.G., Smith, L.C., 2007. Characterization of mitochondrial replication and transcription control during rat early development in vivo and in vitro. Reproduction 133, 423–432. https://doi.org/10.1530/REP-06-0263

Kameyama, Y., Ohnishi, H., Shimoi, G., Hashizume, R., Ito, M., Smith, L.C., 2010. Asymmetrical allocation of mitochondrial DNA to blastomeres during the first two cleavages in mouse embryos. Reprod. Fertil. Dev. 22, 1247. https://doi.org/10.1071/RD10076

Larsson, N.-G., Wang, J., Wilhelmsson, H., Oldfors, A., Rustin, P., Lewandoski, M., Barsh, G.S., Clayton, D.A., 1998. Mitochondrial transcription factor A is necessary for mtDNA maintance and embryogenesis in mice. Nat. Genet. 18, 231–236. https://doi.org/10.1038/ng0398-231

Lee, M., Napier, C.E., Yang, S.F., Arthur, J.W., Reddel, R.R., Pickett, H.A., 2017. Comparative analysis of whole genome sequencing-based telomere length measurement techniques. Methods 114, 4–15. https://doi.org/10.1016/j.ymeth.2016.08.008

Memon, A.A., Zöller, B., Hedelius, A., Wang, X., Stenman, E., Sundquist, J., Sundquist, K., 2017. Quantification of mitochondrial DNA copy number in suspected cancer patients by a well optimized ddPCR method. Biomol. Detect. Quantif. 13, 32–39. https://doi.org/10.1016/j.bdq.2017.08.001

Mengel-From, J., Thinggaard, M., Dalgård, C., Kyvik, K.O., Christensen, K., Christiansen, L., 2014. Mitochondrial DNA copy number in peripheral blood cells declines with age and is associated with general health among elderly. Hum. Genet. 133, 1149–1159. https://doi.org/10.1007/s00439-014-1458-9

Olovnikov, A.M., 1973. A theory of marginotomy. J. Theor. Biol. 41, 181–190. https://doi.org/10.1016/0022-5193(73)90198-7

Ozturk, S., Sozen, B., Demir, N., 2014. Telomere length and telomerase activity during oocyte maturation and early embryo development in mammalian species. Mol. Hum. Reprod. 20, 15–30. https://doi.org/10.1093/molehr/gat055

Pasquariello, R., Ermisch, A.F., Silva, E., McCormick, S., Logsdon, D., Barfield, J.P., Schoolcraft, W.B., Krisher, R.L., 2019. Alterations in oocyte mitochondrial number and function are related to spindle defects and occur with maternal aging in mice and humans†. Biol. Reprod. 100, 971–981. https://doi.org/10.1093/biolre/ioy248

Pikó, L., Taylor, K.D., 1987. Amounts of mitochondrial DNA and abundance of some mitochondrial gene transcripts in early mouse embryos. Dev. Biol. 123, 364–374.

Pyle, A., Anugrha, H., Kurzawa-Akanbi, M., Yarnall, A., Burn, D., Hudson, G., 2016. Reduced mitochondrial DNA copy number is a biomarker of Parkinson's disease. Neurobiol. Aging 38, 216.e7-216.e10. https://doi.org/10.1016/j.neurobiolaging.2015.10.033

Rudolph, K.L., Chang, S., Lee, H.W., Blasco, M., Gottlieb, G.J., Greider, C., DePinho, R.A., 1999. Longevity, stress response, and cancer in aging telomerase-deficient mice. Cell 96, 701–712.

Santos, T.A., El Shourbagy, S., St John, J.C., 2006. Mitochondrial content reflects oocyte variability and fertilization outcome. Fertil. Steril. 85, 584–591. https://doi.org/10.1016/j.fertnstert.2005.09.017

Schaetzlein, S., Lucas-Hahn, A., Lemme, E., Kues, W.A., Dorsch, M., Manns, M.P., Niemann, H., Rudolph, K.L., 2004. Telomere length is reset during early mammalian embryogenesis. Proc. Natl. Acad. Sci. 101, 8034–8038. https://doi.org/10.1073/pnas.0402400101

Thundathil, J., Filion, F., Smith, L.C., 2005. Molecular control of mitochondrial function in preimplantation mouse embryos. Mol. Reprod. Dev. 71, 405–413. https://doi.org/10.1002/mrd.20260

Umylny, B., Presting, G., Efird, J.T., Klimovitsky, B.I., Ward, W.S., 2007. Most human Alu and Murine B1 repeats are unique. J. Cell. Biochem. 102, 110–121. https://doi.org/10.1002/jcb.21278

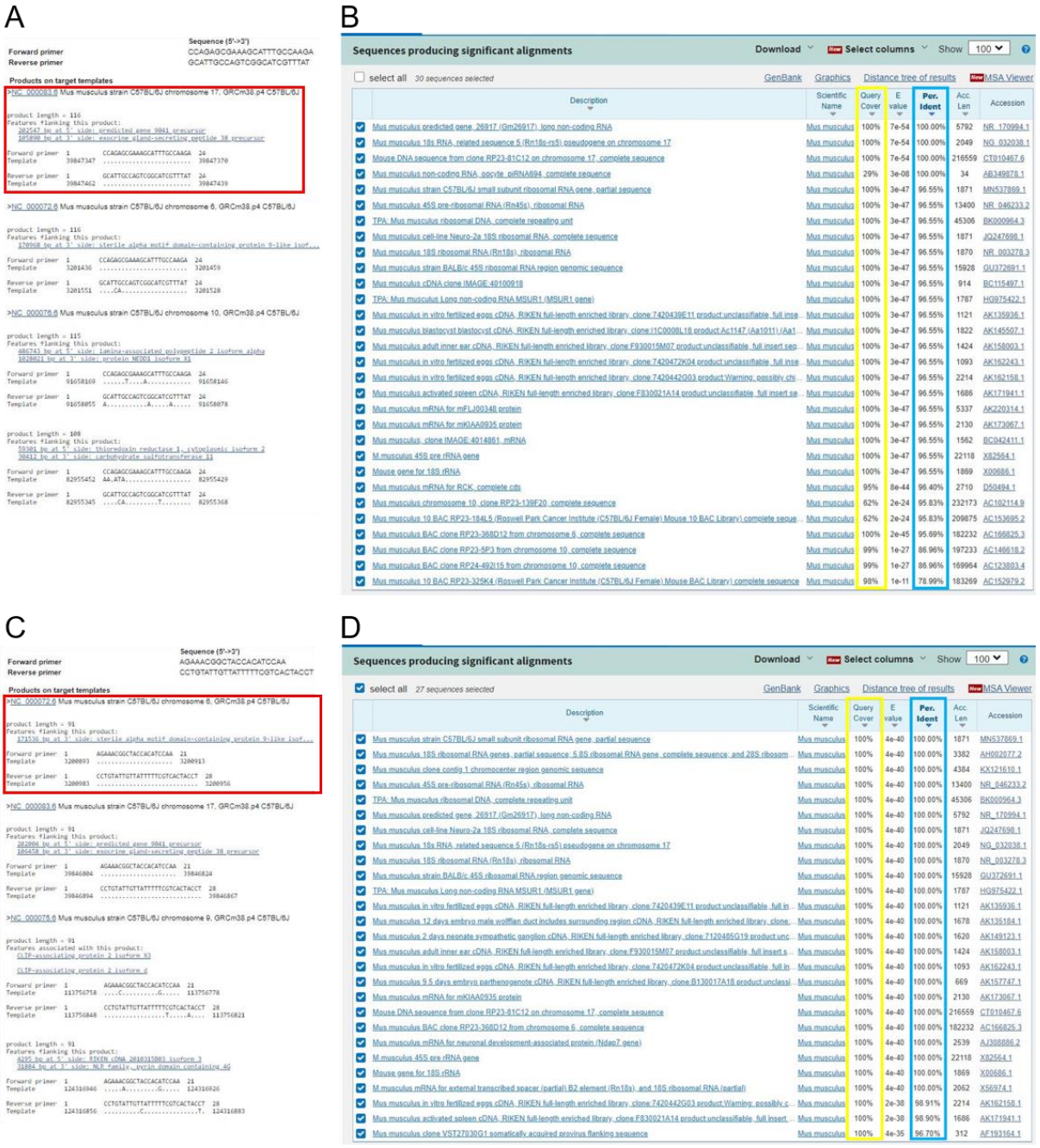
Wai, T., Ao, A., Zhang, X., Cyr, D., Dufort, D., Shoubridge, E.A., 2010. The role of mitochondrial DNA copy number in mammalian fertility. Biol. Reprod. 83, 52–62. https://doi.org/10.1095/biolreprod.109.080887

Wang, F., Pan, X., Kalmbach, K., Seth-Smith, M.L., Ye, X., Antumes, D.M.F., Yin, Y., Liu, L., Keefe, D.L., Weissman, S.M., 2013. Robust measurement of telomere length in single cells. Proc. Natl. Acad. Sci. U. S. A. 110, E1906-1912. https://doi.org/10.1073/pnas.1306639110

Wu, L.L., Russell, D.L., Wong, S.L., Chen, M., Tsai, T.-S., St John, J.C., Norman, R.J., Febbraio, M.A., Carroll, J., Robker, R.L., 2015. Mitochondrial dysfunction in oocytes of obese mothers: transmission to offspring and reversal by pharmacological endoplasmic reticulum stress inhibitors. Dev. Camb. Engl. 142, 681–691. https://doi.org/10.1242/dev.114850

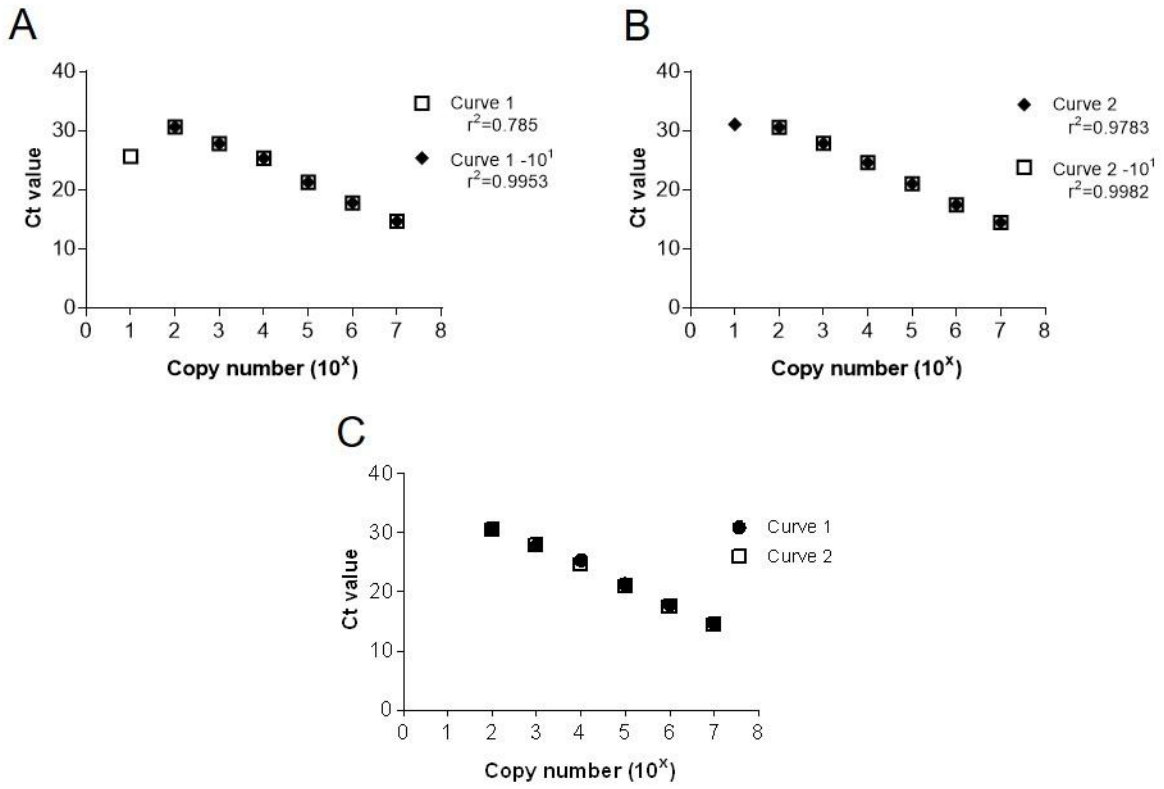
Yoon, C.-Y., Park, J.T., Kee, Y.K., Han, S.G., Han, I.M., Kwon, Y.E., Park, K.S., Lee, M.J., Han, S.H., Kang, S.-W., Yoo, T.-H., 2016. Low Mitochondrial DNA Copy Number is Associated With Adverse Clinical Outcomes in Peritoneal Dialysis Patients: Medicine (Baltimore) 95, e2717. https://doi.org/10.1097/MD.0000000000002717

2.6 Supplementary information



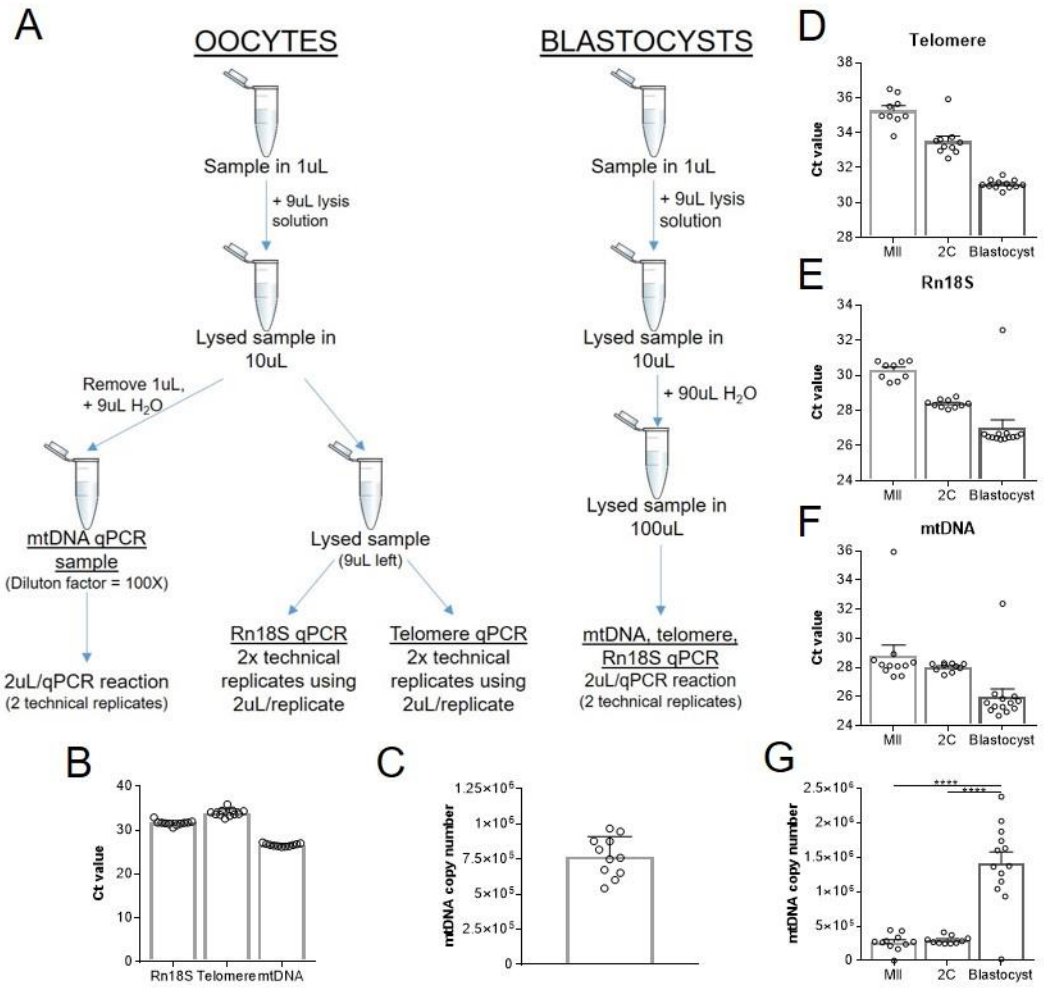
Supplementary figure 2.1. Primer BLAST and product alignment

NCBI Primer BLAST was used for primer pairs for 18S rRNA (A) and Rn18S (C), and the generated amplicon sequence from the top result (red box) was aligned to the mouse genome via NCBI nucleotide BLAST (B and D, respectively). The yellow box in B and D indicates the query coverage (i.e. how much of the query sequence is covered by the target sequence) and the blue box indicates the percent identity of the alignment (i.e. how similar the query sequence is to the target sequence, where a higher percentage indicates a more significant match).



Supplementary figure 2.2. Reproducibility of mtDNA standard curve

mtDNA standard used to calculate copy number underwent serial dilution and qPCR on two separate occasions (A, B). These curves were then superimposed to test reproducibility (C). The Ct value of the lowest concentration of standard (copy number 10^1) varied between the two curves (Ct = 25.6 curve 1 (A), Ct = 31.1 curve 2 (B)), suggesting that it is not reliably detected at this low concentration.



Supplementary figure 2.3. Design of triple test qPCR and use on oocytes and embryos

Revised protocol for triple test qPCR of oocyte and blastocyst samples (A). Revised protocol was carried out on individual C57BL/6 MII oocytes (B) and mtDNA copy number calculated (C). MII, 2C, and blastocysts (derived from CBAxCBA IVF) were analysed using the revised protocol (D-G), with 2C samples processed using 'oocytes' work flow as in (A). Data analysed using unpaired t-test, *** p=0.0004, **** p<0.0001.

Supplementary table 2.1. Dilutions of relevant DNA regions of interest in each sample type

Blastocysts in 100uL

	DNA dilution		
	Rn18S	**Telomere**	**mtDNA**
Oocyte	10	10	100
2C embryo	10	10	100
Blastocyst	100	100	100

Blastocysts in 10uL

	DNA dilution		
	Rn18S	**Telomere**	**mtDNA**
Oocyte	10	10	100
2C embryo	10	10	100
Blastocyst	10	10	100

CHAPTER 3

TELOMERE ELONGATION AND mtDNA REGULATION DURING MOUSE PRE-IMPLANTATION EMBRYOGENESIS

3.1 Introduction

Mitochondria are cellular organelles with primary roles in energy metabolism, homeostasis, and apoptosis. A feature of mitochondria that is unique from other organelles is that they possess their own genome, distinct from the nuclear genome. The mitochondrial genome is multi-copy and maternally transmitted, therefore the integrity of the mitochondria and their DNA (mtDNA) in the oocyte is crucial for oocyte quality, fertilisation and subsequent embryo development, and offspring health. Mitochondrial dynamics have been thoroughly documented during pre-implantation development, including localisation, metabolism, and mtDNA copy number (reviewed in St. John et al., 2010). Mitochondrial DNA copy numbers show defined patterns during this time. As the embryo undergoes cleavage, its mitochondria, and thus mtDNA, are segregated into the blastomeres, meaning that the mtDNA copy number per cell decreases with each cell division during preimplantation development. The total mtDNA copy number in an embryo is known to fluctuate, in some cases decreasing slightly during the early cleavage stages after fertilisation, before increasing at the blastocyst stage (Thundathil et al., 2005). While mitochondrial function and dynamics are well characterised during pre-implantation embryogenesis, there is another profound DNA change during this time that is less understood, telomere elongation.

Telomeres are repetitive TTAGGG duplex DNA sequences found at the ends of eukaryotic linear chromosomes that function as essential protectors of genome stability and integrity. Telomeres are bound by the shelterin complex, which is a highly specific set of proteins including TRF-1 and -2 (Telomeric Repeat binding Factor, Xin et al., 2008) which protect the chromosome ends from degradation and from being recognised by the DNA double stranded break repair mechanism. Due to limitations in linear DNA replication at the end of chromosomes, telomeres progressively shorten with each round of cell division (Blackburn, 1984; Olovnikov, 1973) until a critical length is reached (known as the Hayflick limit), where the cell ceases dividing and enters senescence (Hayflick and Moorhead, 1961). As cells continuously divide over a person's lifespan, telomere lengths decrease correspondingly, thus telomeres serve as a marker of cellular lifespan and ageing, with short telomeres linked to ageing phenotypes and chronic diseases (Rudolph et al., 1999). Thus it is vital that telomeres

are elongated during embryogenesis to ensure that health span and longevity do not progressively decline with each generation.

Telomere elongation occurs via two well characterised mechanisms; the ribonucleoprotein Telomerase, and Alternative Lengthening of Telomeres. The enzyme telomerase is perhaps the most well-known mechanism, which has the capacity to add approximately 50-100 base pairs of telomeric DNA in one cell cycle (Cristofari and Lingner, 2006), allowing it to efficiently maintain telomere lengths over time, but unable to produce rapid, large scale extension. Telomerase access to telomeres is regulated by many protein factors, such as CTC1 and TEN1, which form the CST complex which directly binds to the telomere ends. Alternative Lengthening of Telomeres (commonly referred to as ALT), does not rely on enzymatic function and instead utilises recombination (Pickett and Reddel, 2015), providing the ability to add up to 1kb of telomeric DNA in one cell cycle. ALT requires the co-operation of many proteins, with some of the most well characterised including PML as a major component of ALT-associated Promyelocytic Leukaemia Bodies (APBs, Yeager et al., 1999), and BLM (Yankiwski et al., 2000), which is a RecQ helicase involved in recombination and repair as well as G4-quadruplex DNA unwinding (Ellis et al., 1995; Sun et al., 1998). Telomere-associated protein RIF1 is involved in the DNA damage response, replication timing regulation, and chromatin structure organisation (Kumar and Cheok, 2014). In human cells RIF1 has been shown to localise at dysfunctional telomeres, and at telomere clusters in cells utilising ALT (Silverman, 2004; Xu and Blackburn, 2004). Another protein known to be heavily involved in telomere length regulation is Regulator of Telomere Elongation helicase 1 (RTEL1), which also has additional roles in DNA replication, stability, and repair (Uringa et al., 2012). Interestingly, RTEL1 is known to counteract G4-quadruplex structures, similar to the ALT-involved protein BLM (Lansdorp and van Wietmarschen, 2019). Further to this, RTEL1 has significant roles in homologous recombination (Uringa et al., 2011). The maintenance of telomere length homeostasis is also regulated by telomere trimming in order to prevent the accumulation of aberrantly long telomeres, involving length based targeting by specific proteins such as ZBTB48 (TZAP, Li et al., 2017), which facilitate trimming processes.

Due to the vital function telomeres serve in every cell, it is essential that their length is regenerated at the outset of each generation. It has been established that blastocyst

telomere lengths are the set point for telomere length during development (Schaetzlein et al., 2004), however there is still much work to be done to characterise telomere elongation dynamics and regulatory mechanisms prior to this set point. In mice, one study showed consistent telomere elongation by the 2C embryo stage, and sometimes in zygotes (strain dependent), when compared to MII oocytes (Liu et al., 2007), however whether telomere lengths were different between zygotes and 2C embryos was not noted. Another study identified quantifiable increases in telomere length at each successive stage between zygotes, 2C, and 4C embryos (Wang et al., 2013). Importantly, the findings of this study (Wang et al., 2013) are not considered robust since the PCR assay used is flawed (refer to Chapter 2). Telomere elongation has also been observed at the morula to blastocyst transition (Varela et al., 2011), however preceding stages of development were not analysed. There is yet to be a study that documents telomere lengths throughout a comprehensive pre-implantation embryogenesis time course that uses a consistent approach to measure telomere lengths. Therefore much work is needed to elucidate the patterns of telomere elongation, which is a vital process occurring during embryogenesis to enable a long health- and life-span for offspring. In addition, it is essential to have telomere elongation patterns in normal embryo development fully documented to allow for further research into how elongation is disrupted in situations such as maternal obesity, where offspring are known to have shorter telomeres (Martens et al., 2016; McAninch et al., 2020).

This study characterised telomere length dynamics throughout pre-implantation embryo development alongside the well characterised mitochondrial DNA. Expression of telomere regulatory genes was characterised throughout oocyte maturation and pre-implantation embryogenesis using RT-PCR. Telomere length and mtDNA copy number was analysed in embryos derived from four different mouse strain combinations to determine the consistency in trends over pre-implantation development. To determine the role of oocyte factors, telomere length was analysed in parthenogenetically activated embryos. Male and female blastocysts were compared for sex-related differences in telomere length. Finally, susceptibility of telomere length to environmental stress was analysed by subjecting embryos to high O_2 culture. Overall this study has provided a comprehensive insight into telomere

elongation events during early embryogenesis and shown that these can be modulated under the stress condition of high oxygen culture.

3.2 Materials and Methods

3.2.1 Mice

Female C57/BL6Arc (referred to as C57/BL6), CBA/CaH (referred to as CBA), and CBA F1 mice at 6-7 weeks of age, and males at 6-8 weeks of age were obtained from the Western Australian Animal Resources Centre (ARC, C57/BL6Arc mice) or the University of Adelaide's Laboratory Animal Services (LAS, CBA/CaH and CBA F1 mice). Mice were maintained in 12h/12h light/dark conditions and given water and 10% fat rodent chow *ad libitum*. All animal experiments were approved by the University of Adelaide's Animal Ethics Committee and conducted in accordance with the Australian Code of Practice for the Care and Use of Animals for Scientific Purposes.

3.2.2 Derivation of oocytes, early embryos, and blastocysts

3.2.2.1 Hormone stimulation

Female mice were given 7.5IU pregnant mare's serum gonadotropin (PMSG, National Hormone and Pituitary Program), followed by the equivalent dose of human chorionic gonadotropin (hCG, Pregnyl) 47.5 hours later, each via intraperitoneal (ip) injection.

3.2.2.2 Oocyte collection

For GV oocyte collection, mice were culled via cervical dislocation 45 hours after PMSG administration. Ovaries were placed in pre-warmed αMEM-HEPES handling media (Life Technologies, #12000-014) supplemented with 1% FCS. Germinal vesicle (GV) oocytes were isolated by puncturing large antral ovarian follicles using a 30G needle, and attached cumulus cells removed by aspiration using a glass pipette (VWR, #612-4897) pulled to an appropriate diameter.

For MII oocyte collection, mice were culled via cervical dislocation 14.5h post-hCG administration, and ovaries and oviducts collected and placed in pre-warmed (37°C) αMEM-HEPES handling media, supplemented with 1% FCS. Meiosis II (MII) oocytes were isolated by puncturing the oviducts using a 30G needle. Complete cumulus cell removal was achieved via treatment with hyaluronidase (Seikagaku, #100741) for 5-10 minutes at 37°C, followed by aspiration using a glass pipette pulled to an appropriate diameter.

3.2.2.3 Oocyte *in vivo* maturation time course

C57/BL6 mice (21 days old or 6 weeks old) were culled via cervical dislocation either without hormonal stimulation, at 24 or 48 hours post-PMSG stimulation, or at 16 hours post-hCG stimulation. Oocytes were fully denuded as previously described (see section 3.2.2.2, GV protocol followed for all stages except 16 hours post-hCG, which were denuded according to MII protocol).

3.2.2.4 *In vitro* fertilisation (IVF)

To generate embryos via *in vitro* fertilisation, MII COCs were collected as previously described (section 3.2.2.2). Following oviduct puncturing, whole cumulus-oocyte complex (COC) clusters were gently washed twice in pre-warmed (37°C) fertilisation media (Vitro Fertilisation; Cook Australia, Brisbane, Australia), before being placed in a 100µL fertilisation drop containing the equivalent of 10µL of capacitated sperm from a male of proven fertility (referred to as 'fertilisation time'), before being returned to the incubator (37°C, 5% O_2, 6% CO_2) for 4 hours. Following this, fertilised oocytes were cleaned of all excess sperm and cumulus cells via gentle aspiration and transferred to a culture dish containing cleave media (Vitro Cleave; Cook Australia, Brisbane, Australia, 10 embryos per 20µL cleave media drop) and returned to the incubator until 24 hours post fertilisation time. At this time, the number of embryos that successfully reached the 2C stage were scored and a proportion collected for qPCR analysis, or at 36 hours post-fertilisation for mRNA analysis or Zscan4 staining. The remaining embryos were returned to the incubator until 39 hours post-fertilisation time for 4C collection, then until 55 hours post fertilisation time for 8C collection, then until 96 hours post fertilisation time, where the remaining embryos that had successfully reached the blastocyst stage were scored and all were collected for analysis.

3.2.2.5 Strontium chloride parthenogenetic activation

Isolated MII oocytes were collected at 15.5 hours post hCG administration and fully denuded of cumulus cells as previously described (section 3.2.2.2). Denuded oocytes were washed three times in αMEM-HEPES handling media (Life Technologies, #12000-014), supplemented with 1% FCS, then washed three times in calcium-free CZB media (81.62mM NaCl, 4.83mM KCl, 1.18mM $MgSO_4$, 0.11mM EDTA, 5.6mM glucose, 37mM sodium lactate, 1.2mM KH_2PO_4, 25.1mM $NaHCO_3$, 0.27mM pyruvate, 5mg/mL BSA at pH 7.4, 0.0001g/L phenol red, with 1mM L-glutamine added the day

of use). Oocytes were briefly washed twice in calcium-free CZB media containing 10µM Cytochalasin D and 10mM $SrCl_2$, followed by a two hour culture in this media at a density of 20-30 oocytes per 30µL culture drop in an incubator (37°C, 5% O_2, 6% CO_2) (referred to as activation time). Oocytes were then washed in standard αMEM culture medium (Life Technologies, #1200-014) containing 10µM Cytochalasin D, and cultured in this media for three hours. Activated oocytes were washed 5 times in cleave media (Vitro Cleave; Cook Australia, Brisbane, Australia) and cultured in this media (10 embryos per 20µL cleave media drop) until 24 hours post-activation time. At this time, the number of embryos that successfully reached the 2C stage were scored and a proportion collected for analysis. The remaining embryos were returned to the incubator until 37 hours post-activation time for 4C collection, then until 53 hours post-activation time for 8C collection, then at 96 hours post-activation time the remaining embryos that had successfully reached the blastocyst stage were scored and collected for analysis.

3.2.2.6 *In vivo* 2C embryo collection

Following hCG administration (see section 3.2.2.1), female mice were mated (1:1) with male mice of proven fertility and separated after 16 hours. Females were culled via cervical dislocation 24 hours later (40h post-hCG) and 2C embryos collected via oviduct puncture in pre-warmed αMEM-HEPES handling media (Life Technologies, #12000-014) supplemented with 1% FCS.

3.2.3 Blastocyst dissections

3.2.3.1 Manual dissections for Inner Cell Mass and Trophectoderm populations

IVF or parthenogenetically activated embryos that had successfully reached the blastocyst stage had their zona pellucida dissolved using Acid Tyrode's Embryomax solution (Millipore, #MR-004D). Blastocysts were transferred to individual 5µL pre-warmed (37°C) drops of αMEM handling media, supplemented with 1% FCS in a 50 x 9mm petri dish (Falcon, #351006). Blastocysts were manually separated into their two cell populations (inner cell mass, ICM, and trophectoderm, TE) using the Eppendorf TransferMan 4r system, and a standard holding pipette with a 15µM inner diameter and 120µM outer diameter (The Pipette Company, #LHC-ID15) and biopsy pipette with a 30µM tip (OD) and 90° bevel (The Pipette Company, #LBC-OD30-BA90). Cell

populations were separated and frozen individually per blastocyst (see 2.2.4), but kept paired for analysis.

3.2.3.2 Immunosurgery to isolate the Inner Cell Mass

Blastocysts first had their zona pellucida removed via treatment with Acidic Tyrode's Embryomax solution, washed twice in cleave media and transferred to a 200µL drop of cleave media containing 20% heat inactivated rabbit anti-mouse serum (Sigma, #M5774). Following a one hour incubation period (37°C, 5% O_2, 6% CO_2), blastocysts were washed three times in cleave media and transferred to a 200µL cleave media drop containing 20% guinea pig serum (Sigma, #G9774) and incubated for 15 minutes. Blastocysts were washed three times in cleave media and incubated for a further 30 minutes in this media. Lysed TE cells were removed by gently aspirating ICMs in a finely drawn glass pipette. For validation, see Sup Fig. 3.2 B-F.

3.2.4 Sample collection

3.2.4.1 Oocytes, embryos, and blastocyst cell populations

Individual GV and MII oocytes, IVF or parthenogenetically activated embryos at the various stages, or blastocyst cell populations were first washed three times in 1x phosphate buffered saline (PBS) containing 1mg/mL polyvinylpyrrolidone (PVP, Sigma), and transferred in 1µL to a 0.5mL PCR tube (Axygen, #PCR-05-C) for qPCR analysis. Pools of 40 oocytes or embryos for mRNA analysis were transferred in a minimal volume to a 1.7mL microcentrifuge tube (Axygen, #MCT-175-C-S), centrifuged at 1,200 rpm for three minutes, and supernatant carefully removed using aspiration without disrupting samples under microscope magnification. All samples were snap frozen in liquid nitrogen (LN_2), and stored at -80°C until use.

3.2.4.2 Sperm

Following one hour of capacitation, 50µL of sperm was collected in a 0.5mL PCR tube (Axygen, #PCR-05-C) and centrifuged at 2,000 rpm for 3 minutes before supernatant removal, snap freezing in LN_2 and storage at -80°C until use.

3.2.5 Sample lysis and preparation for qPCR

3.2.5.1 Oocytes and embryos

Individual oocytes and embryos had their nuclear genomic DNA (nDNA) and mitochondrial DNA (mtDNA) extracted by adding 9µL of lysis buffer (50mM Tris-HCl pH 8.0, 1mM EDTA, 200µg/mL Proteinase K, 0.5% Tween-20) to each sample with a volume of 1µL (final volume of 10µL) following brief centrifugation, and heated to 55°C for 2 hours, followed by 95°C for 10 minutes to inactivate Proteinase K activity. Samples were allowed to cool to 4°C and briefly centrifuged. Following this, 1µL of lysis product was removed and added to 9µL of sterile H_2O for mtDNA analysis and the rest kept for telomere and Rn18S analysis. For blastocysts that were also undergoing sex determination, an additional 10µL of sterile H_2O was added after lysis to give a total volume of 20µL which was used for the Triple Test and sex determination PCR without further dilution.

3.2.5.2 Sperm

Sperm nDNA and mtDNA was extracted by adding 50µL of lysis buffer (as described previously) to each sample followed by vortex mixing and brief centrifugation. Samples were then heated to 55°C for 2 hours, followed by 95°C for 10 minutes to inactivate Proteinase K activity. Once cooled, samples were centrifuged at 10,000 rpm for 5 minutes to pellet cellular debris and supernatant was moved to a clean 0.5mL tube (Axygen, #PCR-05-C). Samples were quantified using a NanoDrop One Microvolume UV-Vis Spectrophotometer and diluted to 20ng/µL for use.

3.2.6 Triple test qPCR assay

To generate ‘calibrator’ DNA for use as a standard within every assay, a whole ovary from a 6 week old PMSG and hCG stimulated CBA female mouse was collected and had total DNA extracted (as described previously, see sections 2.2.2). DNA concentration and purity were quantified by NanoDrop One Microvolume UV-Vis Spectrophotometer and diluted to 2.5ng/µL.

qPCR was performed using Power SYBR Green PCR Master Mix (Applied Biosystems, #4367659), standard MicroAmp Optical 96-well Reaction Plates (Life Technologies, #4306737), and custom made primers (Sigma, forward and reverse

primer sequences outlined in Table 3.1), using an Applied Biosystems 7900HT Fast Real-Time PCR system. Cycling conditions for all primers were set at 95°C for 10 minutes, followed by 40 cycles of 95°C for 10s, 60°C annealing for 30s and extension at 72°C for 30s, followed by standard melt curve cycling. Two repeat reactions were performed for each sample and each primer pair, using 2µL of sample per reaction.

For Rn18S and telomere analysis, the final reaction for each well was 10µL Power SYBR Green PCR Master Mix, 0.5µL each of forward and reverse primer (stock at 10µM), 2µL of sample, and sterile H_2O to a final volume of 20µL. To minimise any plate-to-plate variations, Rn18S and telomere reactions for each sample were run on the same plate, and calibrator DNA assays included on every plate.

For mtDNA analysis, the final reaction for each well consisted of 10µL Power SYBR Green PCR Master Mix, 0.2µL each of forward and reverse primer (stock at 10µM), 2µL of sample or standard, and sterile H_2O to a final volume of 20µL. Total mtDNA copy number was quantified using the standard curve method as previously described (Kameyama et al., 2010). Briefly, quantification standards were prepared by PCR amplifying a 1186bp fragment in the 12S rRNA region of mtDNA from mouse liver using the primer pair 5'-ACA CCT TGC CTA GCC A-3' and 5'-TTT GCC ACA TAG ACG AGT T-3'. The PCR product was extracted from the gel using QIAquick Gel Extraction Kit (Qiagen) and cloned using the Qiagen PCR Cloning Kit. Plasmid DNA was purified using QIAprep Spin Miniprep Kit (Qiagen), quantified by spectrophotometry, and diluted to 10^7 copies per 2µL. To create a standard curve, 10µL of standard stock was removed and serially diluted (1:10) from 10^7 to 10^1 copies, and standard curve correlation coefficients were consistently greater than 0.98. Serial dilutions were made fresh on the day. Total mtDNA copy number per sample was calculated according to the generated equation for Ct value against copy number for the corresponding standard curve (excluding 10^1 copies), and multiplied by the dilution factor of the sample i.e. total mtDNA copy number = (10^x) * [dilution factor], where x=(y-intercept of standard curve – Ct value of sample)/slope of standard curve.

Telomere and mtDNA relative to total cell number were calculated using the $2^{-\Delta\Delta Ct}$ method, where the ΔCt of the calibrator (telomere or mtDNA Ct – Rn18S Ct) was subtracted from the ΔCt of the sample (telomere or mtDNA Ct – Rn18S Ct) to give the ΔΔCt.

3.2.7 Embryo sex determination

Embryos that underwent sex determination first underwent the Triple Test qPCR assay (section 3.2.6).

qPCR was performed using Power SYBR Green PCR Master Mix (Applied Biosystems, #4367659), standard MicroAmp Optical 96-well Reaction Plates (Life Technologies, #4306737), and custom made primers (Sigma, forward and reverse primer sequences outlined in Table 3.1), using an Applied Biosystems 7900HT Fast Real-Time PCR system, using the same cycling conditions as in section 3.2.6. One reaction was performed for each sample, using a 4µL of sample. The final reaction for each sample consisted of 10µL Power SYBR Green PCR Master Mix, 0.5µL each of forward and reverse primer (stock at 10µM), 4µL of sample, and sterile H_2O to a final volume of 20µL.

To confirm qPCR product size, reactions were run on a 4% agarose (Promega, #V3125t) gel with gel red (Biotium, #41003). Each sample had 2.5µL of 6x loading dye (New England Bio Labs, #B70245) added and 10µL run per lane using a 100bp ladder (ThermoFisher Scientific, #SM0243) for reference. Gels were run at 100V for 1 hour and imaged using a Biorad Gel Doc EZ Imager with Image Lab software. Male embryos have a distinct band at 105bp (Sup Fig. 3.2 A).

Table 3.1 qPCR primers

Primer target	Forward primer sequence	Reverse primer sequence
Telomere	5'-CGG TTT GTT TGG GTT TGG GTT TGG GTT TGG GTT TGG GTT-3'	5'-GGC TTG CCT TAC CCT TAC CCT TAC CCT TAC CCT TAC CCT-3'
mtDNA	5'-CGT TAG GTC AAG GTG TAG CC-3'	5'-CCA GAC ACA CTT TCC AGT ATG-3'
Rn18S	5'-AGA AAC GGC TAC CAC ATC CAA-3'	5'-CCT GTA TTG TTA TTT TTC GTC ACT ACC T-3'
SRY	5'-AAG CGC CCC ATG AAT GCA TT-3'	5'-TCC CAG CTG CTT GCT GAT CT-3'

3.2.8 RT-PCR for mRNA expression of telomere elongation and stability associated genes

Pools of 40 fully denuded oocytes or IVF derived embryos were collected and stored as previously described (see section 3.2.4.1). RNA was extracted using the RNEasy kit (Qiagen) according to manufacturer's instructions for "Purification of Total RNA from Animal Cells Using Spin Technology", with final products eluted in 10µL. RNA concentration and purity were quantified using a NanoDrop One Microvolume UV-Vis Spectrophotometer (ThermoFisher). cDNA synthesis was carried out using the SuperScript III First-Strand Synthesis System for RT-PCR (Invitrogen, #18080-051) according to manufacturer's instructions. RT-PCR was performed using Taqman Probes (ThermoFisher, see Table 3.2 for assay IDs) and Master Mix (ThermoFisher, #4369016), and MicroAmp Fast Optical 96 well reaction plates (Applied Biosystems, #4346906), using Quantstudio 12K Flex (ThermoFisher) and standard cycling conditions. Reactions were made to a final volume of 10µL, consisting of 5µL of Taqman Master Mix, 0.5µL of Taqman assay, 2.5µL of MilliQ H_2O, and 2µL of sample. mRNA expression was first normalised to the house keeper (β-actin), then calculated

for oocyte maturation relative to the 21 day old unstimulated mice, and relative to MII oocytes for embryo development.

Table 3.2 Taqman assays

Gene target	Gene name	Assay ID
β-actin	Beta actin	Mm01205647_g1
BLM	Bloom Syndrome RecQ Like Helicase	Mm00476150_m1
CTC1	CST Telomere Maintenance Complex Component 1	Mm00660668_m1
PML	Promyelocytic Leukaemia Protein	Mm00476969_m1
RIF1	Rap1 Interacting Factor 1	Mm00613842_m1
RTEL1	Regulator of Telomere Elongation Helicase 1	Mm01220420_m1
TEN1	TEN1 Telomerase Capping Complex Subunit	Mm01252631_m1
Terf1	Telomeric Repeat Binding Factor 1	Mm00436928_m1
Terf2	Telomeric Repeat Binding Factor 2	Mm01253555_m1
TERT	Telomerase Reverse Transcriptase	Mm00436931_m1
Zbtb48 (TZAP)	Zinc Finger and BTB domain containing 48	Mm00505672_m1
ZSCAN4	Zinc Finger and SCAN domain containing 4	Mm01234988_g1

3.2.9 Immunofluorescence

3.2.9.1 Zscan4 immunofluorescence

To be able to visualise Zscan4 expression, 2C embryos must be collected late in development, at 36 hours post fertilisation. Embryos were fixed and permeabilised in 4% PFA with 0.5% Triton X-100 in PBS for 30 minutes at RT, with shaking, followed by three ten-minute washes in PBS-PVP. Embryos were blocked overnight at 4°C in blocking solution (10% filtered normal goat serum, Sigma, #G9023), then incubated overnight at 4°C with rabbit anti-Zscan4 polyclonal antibody (1:500, Abnova, #000-

18886) in blocking solution. Following three ten-minute washes with PBS-PVP, embryos were incubated for one hour at RT, while protected from light, with Alexa Fluor 488-conjugated goat anti-rabbit secondary antibody (1:500, Invitrogen). For the final 30 minutes of secondary antibody incubation, Hoechst-33342 (1:250) was added. Samples were briefly washed three times and mounted on slides with 1.5µL Prolong™ Diamond Antifade Mountant (Invitrogen, #P36965) and imaged using a confocal microscope (Olympus FV3000).

3.2.9.2 Pronuclear cytosine methylation immunofluorescence

A broad epigenetic analysis on generated embryos was desired to be included in this study, and so a literature search was undertaken to determine the most appropriate methodology as there is controversy in the field about the accuracy of the most commonly used assay (Li and O'Neill, 2012). Specifically, an important discrepancy between this study (Li and O'Neill, 2012) and others, is that this study found that 5mC is undetectable in the maternal pronucleus by PN5, whereas other studies showed a persistence of 5mC in the maternal pronucleus in the PN5 stage, and even just prior to syngamy (Amouroux et al., 2016; Gu et al., 2011; Han et al., 2018; Iqbal et al., 2011; Santos et al., 2002). This difference is likely due to differences in antigen unmasking; as the Li and O'Neill study used an additional 0.25% trypsin treatment after the standard HCl antigen retrieval used in all other studies. Other differences may be due to authors (Li and O'Neill, 2012) using a primary antibody from a source different to other studies that only use HCl unmasking (Amouroux et al., 2016; Gu et al., 2011; Han et al., 2018; Iqbal et al., 2011; Wossidlo et al., 2010). Following consideration of the different methodologies, a protocol using DNA denaturing and antigen unmasking with HCl only was used as this method is more extensively used in the literature, thus allowing comparison of results to other published observations (Amouroux et al., 2016; Han et al., 2018; Liu et al., 2014; Shen et al., 2014; Tsukada et al., 2015). Further, this method has been demonstrated to be sensitive enough to detect differences between zygotes of lean and obese mothers (Han et al., 2018), which is also a feature of the current study.

Fertilized zygotes (stage PN3 to PN4) were collected 6 hours after fertilisation, and successfully parthenogenetically activated 1C embryos were collected 6 hours after activation time (see section 3.2.2.4). The zona pellucida was dissolved using Acid Tyrode's Embryomax solution (Millipore, #MR-004D), followed by a brief wash in

phosphate buffered saline (PBS) containing 1mg/ml polyvinylpyrrolidone (PVP, Sigma) (PBS-PVP). Samples were fixed in 3.7% PFA-PBS for 20 minutes at room temperature (RT), followed by two five-minute washes in PBS-PVP, then permeabilised in 0.2% Triton X-100 (in PBS) for 10 minutes at room temperature, followed by three five-minute washes in PBS-PVP. Samples were incubated in 4N HCl solution for 10 minutes at RT, and washed thoroughly in 0.05% Tween-20 in PBS (PBS-T). Samples were blocked overnight at 4°C in blocking solution (1% BSA, 0.02% Triton X-100 in PBS), then incubated overnight at 4°C with mouse anti-5mC (1:200, Biorad, #ab10805), and rabbit anti-5hmC (1:600, Active Motif, #39769), diluted in blocking solution. Following three ten-minute washes in PBS-T, samples were incubated for one hour at RT, while protected from light, with Alexa Fluor 594-conjugated goat anti-mouse (1:500, Invitrogen) and Alexa Fluor 488-conjugated goat anti-rabbit secondary antibodies (1:1000, Invitrogen). Samples were mounted on slides with 1.5µL Prolong™ Diamond Antifade Mountant (Invitrogen, #P36965) and examined using a confocal microscope (Olympus FV3000). Images were acquired using the same image acquisition settings. Pronuclear size and staining intensity was calculated using ImageJ software. Mean signal intensity was calculated first by subtracting the signal from the cytoplasmic area (representing background staining), then dividing by the area of the pronuclei.

3.2.9.3 Blastocyst differential stain

Blastocysts were fixed late on day 5 in 4% PFA-PBS overnight at 4°C. Samples were washed once in PBS-PVP and incubated for 5 min at RT in 0.1M glycine, followed by 3x 5 min washes in PBS-PVP. Samples were permeabilised in 0.5% Triton X-100 for 30 min at RT, washed 3x in PBS-PVP and blocked for 1 hour at RT in 10% donkey serum (Sigma). Primary antibodies were diluted 1:500 (Oct 3/4 Santa Cruz #sc-8626, CDX2 Abcam #ab76541) in 10% donkey serum and samples incubated overnight at 4°C. Following 3x 5 min washes in PBS-PVP, samples were incubated in secondary antibodies at a dilution of 1:1000 for 1 hour (Life technologies, Alexa Fluor 594 donkey anti-rabbit and Alexa Fluor 488 donkey anti-goat), with 1:250 Hoescht-3342 added for the final 10 minutes of the incubation. Samples were mounted using Prolong™ Diamond Antifade Mountant (Invitrogen, #P36965) and imaged using a Cell Voyager CV1000 spinning disc confocal (Yokogawa) with a 40x objective and z-stacked with a

0.8µM step height. Z-stacks were imported to Image J and a maximum intensity z-project was created to enable counting of individual cells.

3.2.10 Statistical analysis

Results are presented as mean ± SEM. Telomere, mtDNA per cell, and total mtDNA copy number displayed as mean ± SEM overlayed on a violin plot to illustrate the distribution of data points. Analysis of normality showed that telomere and mtDNA data required log transformation for statistical analysis. Statistical analysis was performed using Graph Pad Prism version 8 for Windows (GraphPad Software Inc., La Jolla, CA) and SPSS Statistics 26 (IBM, Armonk, NY). Paired t-test, unpaired t-test, one-way analysis of variance (ANOVA, comparison of means), and linear-mixed effects models were used as indicated and statistical significance was considered at P-value <0.05.

3.3 Results

3.3.1 Telomere length and mtDNA copy number remain stable throughout oocyte maturation

Expression of telomere associated genes was measured throughout the oocyte maturation process. Oocytes from unstimulated 21 day old mice were collected as a baseline since they are immature (GV) oocytes in prophase I within secondary to small antral follicles. In parallel, oocytes were collected from large antral follicles of 6 week old females to represent GV oocytes from the final stage of follicle growth prior to ovulation and in the absence of exogenous gonadotropin stimulation. In order to analyse oocytes at specific subsequent stages of maturation, oocytes were isolated 24h and 48h after PMSG stimulation to represent immature oocytes at different stages of growth and address the potential impact of gonadotropin stimulation. Finally, oocytes were isolated from the oviduct at 16h post-hCG after ovulation has occurred and the oocytes have completed maturation and are at MII (Fig. 3.1). TRF1 and TRF2 (Fig. 3.1 A and B, respectively) had relatively stable expression throughout, with a possible upregulation between the 48 hours post-PMSG (GV oocyte) and 16 hours post-hCG (MII oocyte) stages, although this was inconsistent between samples. PML showed a substantial upregulation between oocytes collected from 21-day old and 6-week old unstimulated mice which did not appear to occur with PMSG stimulation (Fig. 3.1 C). Similar to TRF1 and TRF2, PML showed an indication of upregulation between the PMSG-stimulated GV and MII oocyte stages. Consistent with PML, BLM expression also appeared to be upregulated in oocytes from 6-week old unstimulated mice when compared to 21-day old mice (Fig. 3.1 D). This upregulation was once again not apparent following PMSG stimulation, but was markedly upregulated between GV and MII oocytes. Contrasting to the two genes encoding ALT-related proteins, expression of the TERT gene was reduced in 6-week old unstimulated mice compared to 21-day old mice, and this lower level of expression remained stable throughout PMSG stimulation (Fig. 3.1 E). However, in a similar fashion to BLM, TERT expression was upregulated following hCG stimulation. Due to the interesting potential upregulation in each of these telomere associated genes between the GV and MII stages of oocyte maturation, we next investigated whether the telomere lengths of oocytes change during this time.

Individual GV and MII oocytes were analysed for relative telomere content and total mtDNA copy number using the Triple Test (Fig. 3.2). Oocytes were analysed from both CBA inbred mice and CBA.F1 hybrid mice to account for possible strain-related differences as hybrid mice are known to have greater developmental competence following IVF than inbred mice. Telomere lengths were not different between GV and MII oocytes in either strain of mouse (Fig. 3.2 A), which was not unexpected due to the absence of DNA replication between meiosis I and meiosis II. mtDNA copy number did not increase during oocyte maturation (Fig. 3.2 B) consistent with previous reports (Mahrous et al., 2012).

This study is the first to analyse these telomere-associated genes in an oocyte maturation time course. The age of the mice that oocytes were collected from in the absence of gonadotropin stimulation was a factor in the level of expression for PML, BLM and TERT, but not TRF1 and TRF2. PMSG stimulation (24h) was seen to downregulate the expression of PML and BLM when compared to oocytes from 6-week old unstimulated mice, but not the other genes analysed. Expression of PML was higher, and TERT lower, in oocytes collected 48 hours after PMSG stimulation than those collected 24 hours after stimulation, suggesting that PMSG and/or follicle growth may play a role in the regulation of these genes. Finally, for all genes analysed, although one of the two pools of oocytes collected after hCG stimulation showed higher levels of expression than the other, expression of BLM and TERT was consistently higher in both pools than 48h post-PMSG stimulation, suggesting that the completion of follicle growth, ovulation and meiosis I may play a role in the regulation of these genes. While GV and MII oocytes differed in expression of analysed genes, telomere lengths were not detectably different between these two oocyte stages.

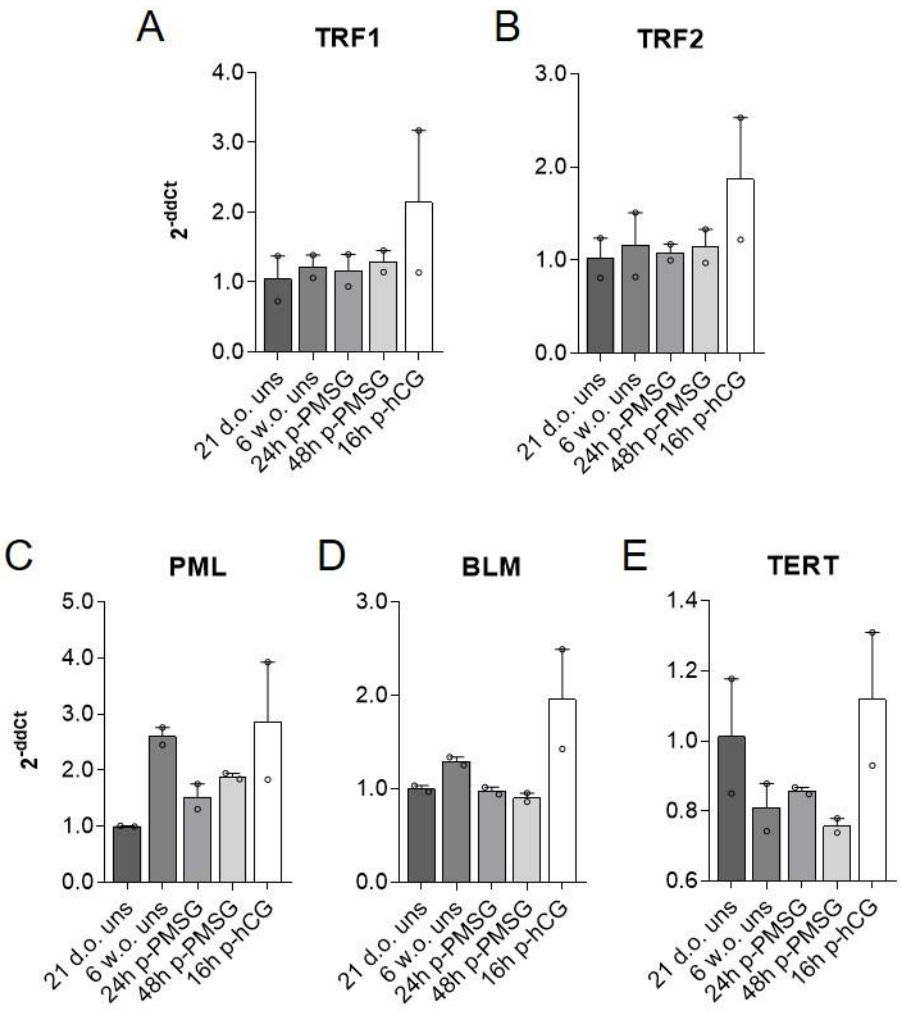


Figure 3.1. Expression of telomere binding and extension-associated proteins throughout oocyte maturation

mRNA expression of gene products with roles in telomere binding (A, B), ALT mediated- (C, D) or telomerase-mediated telomere elongation (E) were analysed throughout oocyte maturation. Oocytes were collected from female C57/BL6 mice (21 days old or 6 weeks old) either without hormonal stimulation, at 24 or 48 hours post-PMSG stimulation, or at 16 hours post-hCG stimulation and fully denuded oocytes were frozen in groups of 40 for cDNA synthesis and RT-PCR. mRNA expression was first normalised to β-actin expression and then calculated relative to 21 day old unstimulated mice to give 2^{-ddCt}. n=2 pools of 40 oocytes collected from two independent experiments.

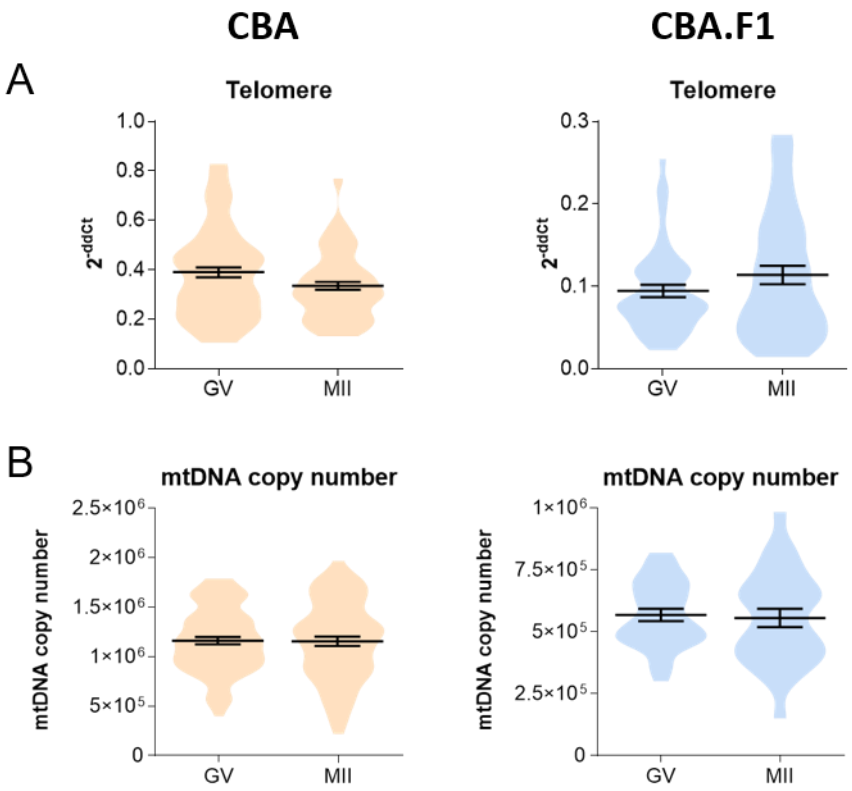


Figure 3.2. Telomere length and mtDNA copy number in GV and MII oocytes

Female CBA or CBA.F1 mice (6 weeks old) were stimulated with PMSG and oocytes collected either 45 hours later (GV oocytes) or underwent hCG stimulation 47 hours later and collected at 14.5 hours post-hCG (MII oocytes). Oocytes were denuded, individually frozen and underwent Triple Test qPCR for telomere, Rn18S, and mtDNA. Relative telomere length was calculated relative to a calibrator sample (A) and total mtDNA copy number (B) was calculated from the standard curve. For CBA, n=80 GV and n=75 MII oocytes, and for CBA.F1 telomere n=42 GV and MII oocytes. Log transformed data analysed using unpaired t-test. No significant differences in telomere length or mtDNA copy number were detected. Shaded areas represent the population distributions, while horizontal lines represent mean ± SEM.

3.3.2 Telomere elongation occurs throughout pre-implantation embryogenesis

Gene expression patterns of multiple telomere associated genes were examined throughout pre-implantation embryogenesis to look for identifying trends in elongation mechanisms (Fig. 3.3). TRF1 and TRF2 were both decreased in expression by the 2C stage compared to MII oocytes and remained lower through the blastocyst stage (Fig. 3.3 A and B, respectively). Other telomere binding proteins, RIF1, CTC1, and TEN1, also showed dynamic regulation however no distinct patterns were evident (Fig. 3.3, C, D and E, respectively). RIF1 mRNA remained at relatively similar levels throughout the stages analysed. CTC1 was highest at 2C and lowest at 8C. TEN1 mRNA was lower at each of the embryonic stages compared to MII oocytes. Interestingly, RTEL1 expression increased around the time of embryonic genome activation (late 2C stage), and progressively decreased from there (Fig. 3.3 F). Both PML and BLM showed decreased expression in embryos compared to MII oocytes (Fig. 3.3 G and H), however PML mRNA was often elevated in 8C embryos. Surprisingly, TERT showed very low levels of expression throughout all cleavage stages, including at the blastocyst stage although one of three samples was dramatically higher (Fig. 3.3 I). TZAP mRNA levels were investigated to indicate whether telomere trimming processes may be occurring during this period and showed a very distinct pattern, with MII oocytes and 2C embryos exhibiting the highest expression, which progressively decreased with each subsequent cleavage (Fig. 3.3 J). ZSCAN4 was used to validate the mRNA time course as the regulation pattern of this gene has been well characterised and is known to be selectively expressed in late 2C embryos (Falco et al., 2007). Its involvement in telomere maintenance has been characterised, and it also plays a key role in mouse embryonic stem cells, where transient expression is associated with elongation of telomeres and these cells are referred to as being in a 2-cell like state during this period (Zalzman et al., 2010). As expected, high expression of ZSCAN4 was specific to the 2C stage in the mRNA time course (Fig. 3.3 K) and this was further validated with immunofluorescence (Fig. 3.3 L).

Next, telomere elongation patterns were analysed at the same developmental stages (Fig. 3.4). Both hybrid and inbred embryos were examined as previous studies suggested that telomere elongation between MII oocytes and zygotes was strain dependent (Liu et al., 2007). Embryos were derived from four different strain

combinations: CBA.F1 hybrid mice, CBA ♀ with C57/BL6 ♂ - to generate hybrid F1 embryos, CBA inbred mice, and C57/BL6 inbred mice. To ensure analysis of representative development, multiple rounds of IVF were performed with subsets of embryos collected for measurement at each stage. Embryos of each type exhibited marked telomere elongation at the blastocyst stage when compared to MII oocytes (Fig. 3.4 A). Interestingly both hybrid embryo types showed incremental increases in telomere length at successive analysed stages, with increases in telomere length seen from MII to 2C, and from 2C to 8C, whereas inbred embryos only saw substantial elongation by the blastocyst stage (Fig. 3.4 A). To further clarify the scale of telomere elongation occurring with each cell cycle, mean relative telomere length (from Fig. 3.4 A) was converted to a percentage of final length reached (Fig. 3.4 B, Supp. Table 3.2). As blastocyst telomere length is considered the "set point" for the offspring (Schaetzlein et al., 2004), this was converted to 100%, i.e. the "final" telomere length. As the MII oocyte is the initial length measured for this time course, this was set at 0%, with the intervening stages calculated as a percentage of the final telomere length (blastocyst). In hybrid embryos, up to 45% of the final telomere length was reached in three cell cycles (8C stage), whereas the two inbred crosses observed less than one fifth of their final length reached by the same point (Fig. 3.4 B). All embryo derivations appeared to show the most substantial gain in telomere length between the 8C and blastocyst stage.

The onset of compaction begins at the late 8C stage of development and signifies the onset of polarisation (Johnson and Ziomek, 1981). As this is a major event during pre-implantation embryo development, the relative change in telomere length prior to, and after compaction was analysed (Fig. 3.4 C). As the scale for relative telomere length varies greatly between strains (Fig. 3.4 A, y-axis), the fold change in relative telomere length was calculated for the pre-compaction (from MII oocytes to 8C embryos) and post-compaction (from 8C embryos to blastocysts) stages of development (Fig. 3.4 C), to further gauge the extent to which telomere elongation was occurring in these distinct stages of development.

Interestingly, despite pre-compaction elongation only accounting for 45% of the final telomere length in CBA.F1 hybrid embryos (Fig. 4.3 B), the fold change difference in telomere length was greater in pre-compaction than post-compaction development (Fig. 4.3 C, 2.4-fold compared to 1.7-fold, respectively). In CBAxC57/BL6 hybrid

embryos, the fold change in telomere length was relatively consistent between the pre- and post-compaction stages (Fig. 3.4 C, 1.56-fold and 1.65-fold, respectively). For inbred embryos, while the fold change was different between strains (CBA and C57/BL6), the overall trend in telomere length fold change was consistent, with double the elongation occurring after compaction than prior to (Fig. 3.4 C, CBA 0.9-fold and 2-fold, and C57/BL6 1.6-fold and 3.2-fold, for the pre- and post-compaction stages, respectively). This indicates that, consistent with the proportion of lengthening analysis (Fig. 3.4 B), inbred embryos appear to undergo the most substantial telomere elongation after compaction has been initiated.

In vitro culture is known to impact embryo developmental competence, as such telomere length was assessed in embryos from different derivation methods. Telomere length in 2C embryos derived either through *in vitro* fertilisation (IVF) or fertilised *in vivo* (via mating) and flushed from the tract at the 2C stage were assessed to determine if the telomere elongation seen at this pre-compaction phase is an artefact of the IVF process or conversely if IVF negatively impacts telomere length (Fig. 3.4 D). CBA.F1 embryos were generated as these displayed elongation between the MII and 2C stages of development (Fig. 3.4 A, B). Embryos were collected from three independent experiments and 2C development rates did not differ between the groups (mean ± SD: *in vitro* 72.67 ± 9.29%, *in vivo* 75.64 ± 3.03%). Telomere lengths did not differ (Fig. 3.4 D, p=0.473), indicating that the mode of conception did not impact telomere elongation events within the first cell cycle.

To determine if telomere elongation continues in the ICM (inner cell mass) after day 5 of development, ICMs were immunosurgically isolated from day 5 and day 6 blastocysts (Fig. 3.4 E). Telomere length did not change with an additional day of development (Fig. 3.4 E, p=0.3). Thus, although this culture system may not faithfully recapitulate all aspects of in vivo development, these results indicate that further ICM telomere lengthening does not occur beyond day 5.

As telomere elongation events showed strain specific differences, both total mtDNA copy number and relative mtDNA per cell were also analysed (Fig. 3.5). Total copy number patterns maintained a degree of consistency between strains, with relatively small to no change in copy number throughout the cleavage stages (Fig. 3.5 A). In particular, the CBAxC57/BL6 and C57/BL6xC57/BL6 embryos exhibited no detectable changes following fertilisation through to blastocyst development, and CBA.F1 and

C57/BL6 blastocysts contained more mtDNA in blastocysts than MII oocytes (Fig. 3.5 A). The relative mtDNA per cell showed the expected trend that was consistent between all strains of embryos, with the relative mtDNA content decreasing with each successive cell division as the mitochondria, and thus mtDNA are segregated into each new blastomere (Fig. 3.5 B). As expected, MII oocytes contained the highest quantity of mtDNA per cell in all strains, and blastocyst contained the least. Therefore, unlike telomeres, mtDNA copy number and mtDNA segregation do not show differential characteristics based on the strain of the embryo.

Mitochondrial DNA content was analysed comparing *in vitro* and *in vivo* derived 2C embryos to determine if the mode of conception impacted mtDNA copy number (Fig. 3.5 C, D). In line with telomere elongation, total mtDNA copy number was not different between the two different types of 2C embryos, and therefore the relative mtDNA per cell was also unchanged (Fig. 3.5 C $p=0.142$ and D $p=0.908$, respectively).

Mitochondrial DNA per cell was also compared in day 5 and 6 ICMs (Fig. 3.5 E) which, consistent with observations of telomere length, were not different ($p=0.731$).

Cumulatively, these experiments demonstrate that telomere elongation during pre-implantation embryogenesis showed strain-specific patterns in the pre- and post-compaction stages of development (MII to 8C and 8C to blastocyst), with hybrid embryos exhibiting elongation during both stages and inbred embryos predominantly displaying elongation during the post-compaction stage (8C to blastocyst). Further, identification of specific telomere regulatory proteins exhibiting regulated expression during these same stages sheds light on the mechanisms by which the dynamic changes in telomere length occur.

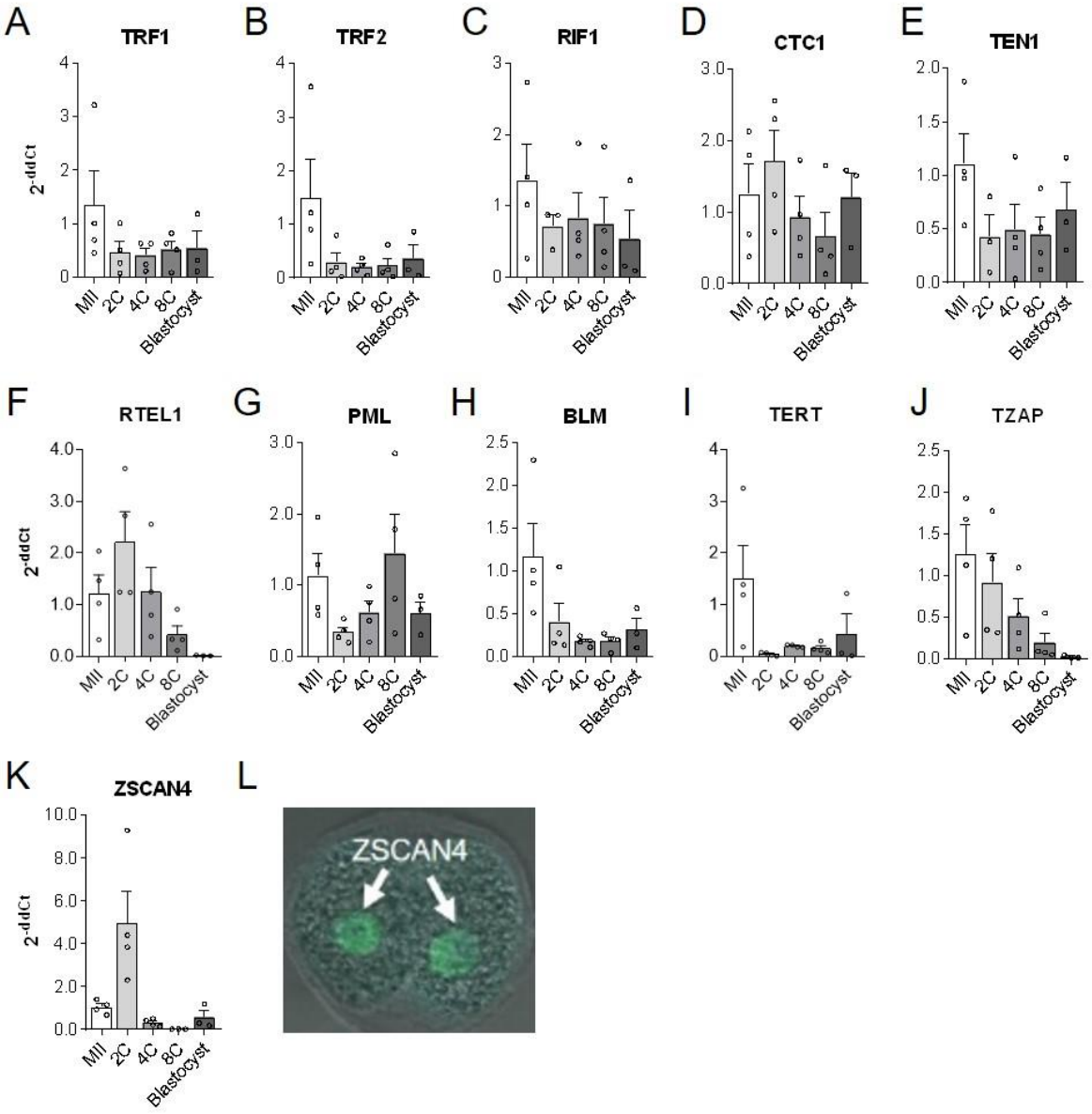


Figure 3.3. Expression of telomere binding and extension associated proteins throughout pre-implantation embryogenesis

mRNA expression of gene products with roles in telomere binding (A-F), ALT mediated- (G & H) or telomerase mediated-telomere elongation (I), and telomere trimming (J) were analysed throughout pre-implantation embryo development. Oocytes were collected from female CBA.F1 mice at 14.5 hours post-hCG stimulation, fertilised via IVF and cultured to the indicated stages. mRNA expression was normalised to β-actin expression and then calculated relative to MII oocytes to give 2^{-ddCt}. Zscan4 expression (K) was further validated by immunofluorescence in 2C embryos (L). n=3-4 pools of 40 oocytes or embryos collected from independent experiments.

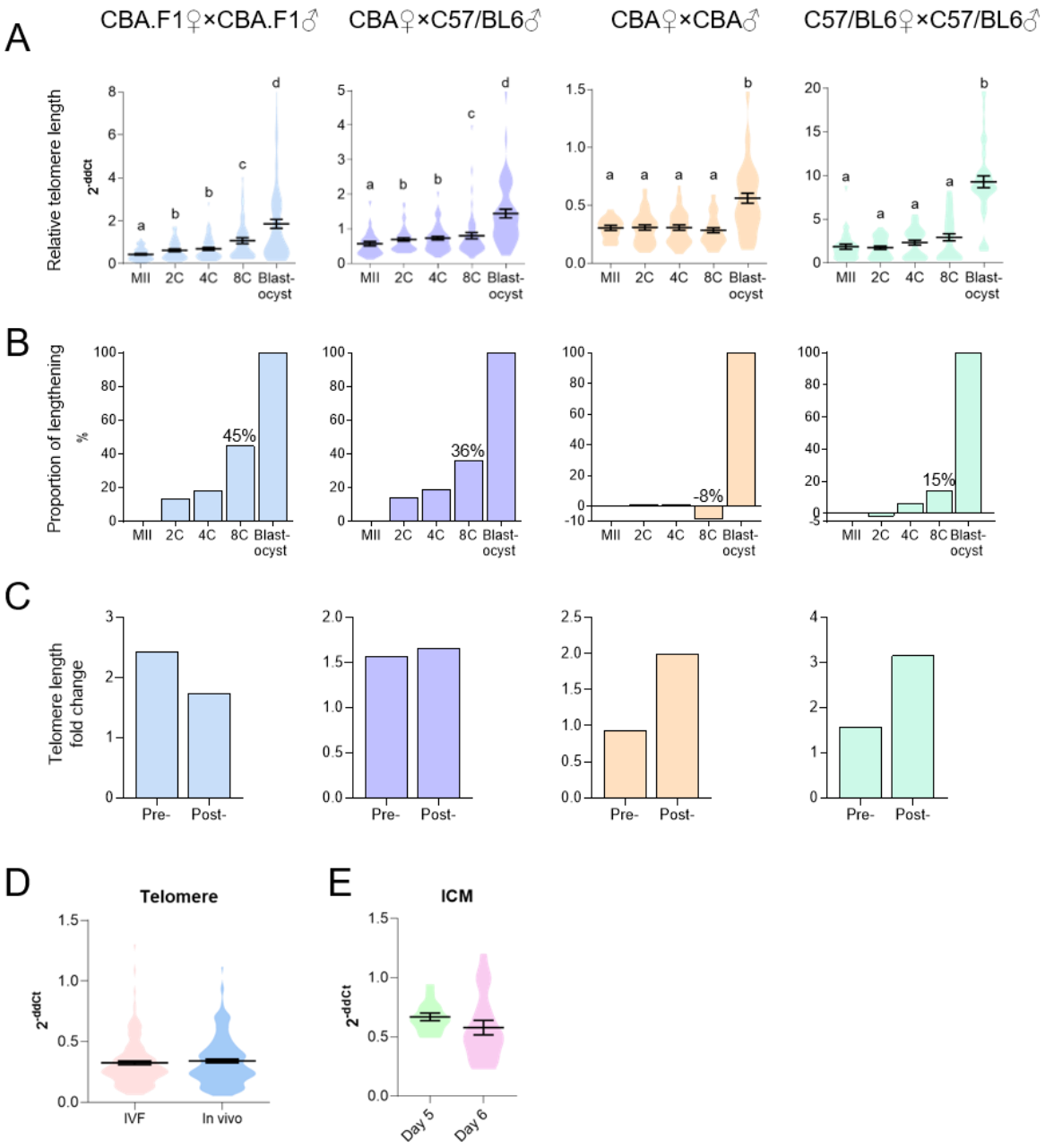

A
CBA.F1♀×CBA.F1♂
CBA♀×C57/BL6♂
CBA♀×CBA♂
C57/BL6♀×C57/BL6♂
Relative telomere length
2-ddct
MII 2C 4C 8C Blast-ocyst
B
Proportion of lengthening
%
45%
36%
-8%
15%
C
Telomere length fold change
Pre- Post-
D
Telomere
IVF
In vivo
E
ICM
Day 5
Day 6

Figure 3.4. Telomere elongation dynamics throughout pre-implantation embryogenesis

Oocytes were collected from female CBA, C57/BL6 or CBA.F1 mice and fertilised with sperm from a male of the indicated strain via *in vitro* fertilisation (IVF) and cultured. Individual denuded oocytes or embryos were frozen for Triple Test qPCR analysis. Relative telomere length was calculated relative to a calibrator sample (A) and then converted to a proportion of lengthening with MII set as 0% of the final length, and blastocyst set as 100% of the final length (B), with proportion of lengthening to the 8C stage indicated. Further, the fold change in relative telomere length was calculated (C) from MII oocytes to 8C embryos (pre-compaction), and from 8C embryos to blastocysts (post-compaction). Minimum number of oocytes or embryos analysed was MII n=17, 2C and 4C n=37, 8C n=39, blastocyst n=41. For exact n-values, refer to Supplementary Table 3.1. 2C embryos were generated by IVF or flushed from the oviduct following mating (in vivo) and relative telomere length compared (D). n= 157 IVF and n=176 *in vivo* derived 2C embryos. Isolated ICM populations from day 5 and day 6 blastocysts were compared for relative telomere length (E). n=16 day 5 and n=21 day 6 ICMs. Data was log transformed for statistical analysis using a linear mixed-effects model (A) where different lowercase letters indicate statistical significance between groups of at least $p<0.05$, or unpaired t-test (D, E). Statistical analysis was not conducted on data in B or C. For A, D, and E, shaded areas represent the population distributions, while horizontal lines represent mean ± SEM.

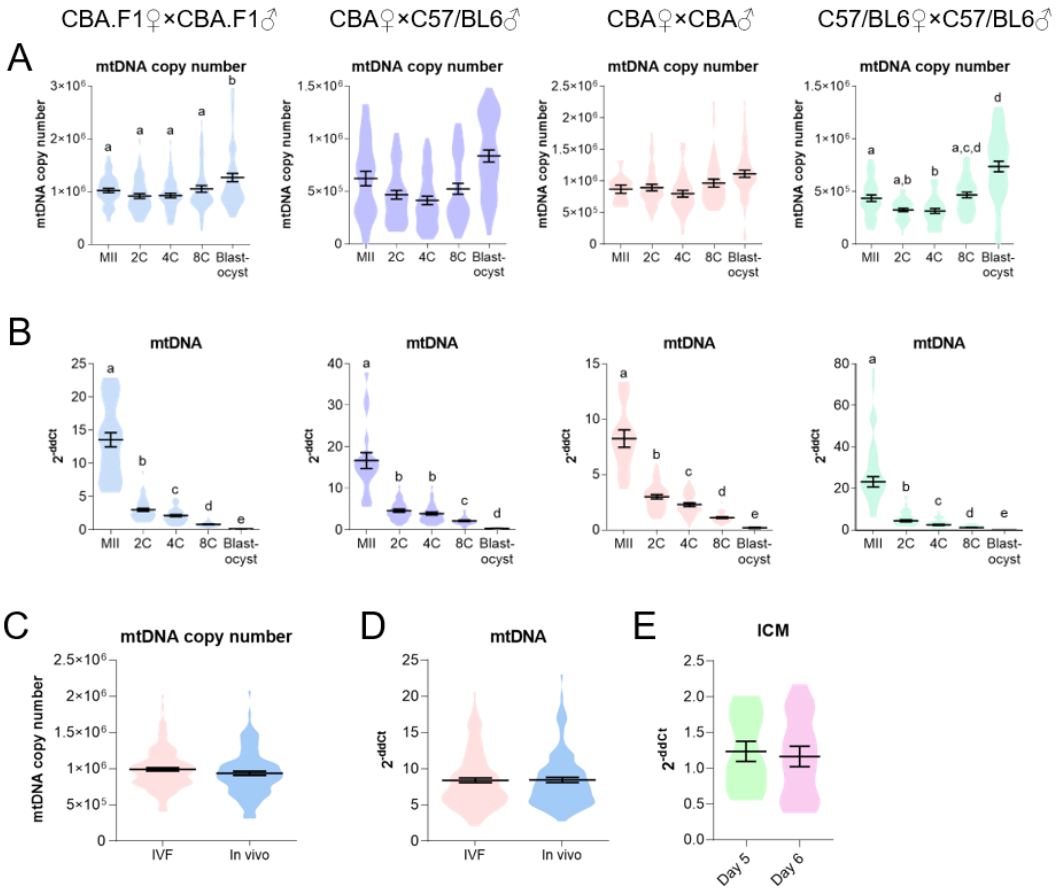


Figure 3.5. Mitochondrial DNA dynamics throughout pre-implantation embryogenesis

Oocytes were collected from female CBA, C57/BL6 or CBA.F1 mice and fertilised with sperm from a male of the indicated strain via *in vitro* fertilisation (IVF) and cultured to the indicated stages. Total mtDNA copy number per embryo was calculated using the standard curve method (A) and as mtDNA per Rn18S copy (i.e. relative to cell number) (B). Minimum number of oocytes or embryos analysed was MII n=17, 2C and 4C n=37, 8C n=39, blastocyst n=41. For n-values, refer to Supplementary Table 3.1. IVF derived 2C embryos were compared to *in vivo* derived 2Cs to determine if the mode of derivation influences mtDNA total copy number (C) and relative mtDNA per cell (D). n= 157 IVF and n=176 *in vivo* derived 2C embryos. Isolated ICM populations from day 5 and day 6 blastocysts were analysed to compare mtDNA content per cell (E). n=16 day 5 and n=21 day 6 ICMs. Data was log transformed for statistical analysis using a linear mixed-effects model (A, B) where different lowercase letters indicate statistical significance between groups of at least $p<0.05$, or unpaired t-test (C-E). Shaded areas represent the population distributions, while horizontal lines represent mean ± SEM.

3.3.3 Telomere length is reset following fertilisation, prior to the first mitosis

A critical time for embryo development is fertilisation, the event that triggers the completion of meiosis and results in the formation of the embryonic genome. To characterise changes in telomeres and mtDNA following fertilisation, telomere length and mtDNA were examined at 6 hours after fertilisation in comparison to sperm and individual MII oocytes (Fig. 3.6). This post-fertilisation time point was selected because at this time the paternal genome has been remodelled by undergoing extensive demethylation and protamine to histone transfer. The Triple Test was used to analyse sperm, oocytes, and zygotes from CBA.F1 mice (Fig. 3.6), due to their consistent incremental pre-implantation elongation pattern (Fig. 3.4 A, B).

Proliferating spermatogonia are known to have high telomerase activity levels and as a consequence, sperm have considerably lengthened telomeres (Ozturk, 2015). Oocytes were found to have shorter telomeres than sperm (Fig. 3.6 A), and more mtDNA per Rn18S copy (Fig. 3.6 B). Previous assays demonstrated that telomeric DNA in 2C embryos was relatively similar to that in MII oocytes (Fig. 3.4 A, B), suggesting that sperm telomeres are not maintained into the 2C embryo stage. To examine post-fertilisation modifications to telomeric DNA content, fertilised zygotes (confirmed by presence of two pronuclei, Sup. Fig. 3.1 A) were analysed. Within six hours of fertilisation, telomere length in the zygotes was not only shorter than in sperm, but also shorter than the starting oocytes (Fig. 3.6 A), suggesting that telomere trimming pathways may be activated upon the presence of disproportionately long telomeres from the sperm-derived paternal genome. Relative mtDNA showed a reduction after fertilisation due to the increase in genomic DNA (Fig. 3.6 B), however the total mtDNA copy number was not affected by fertilisation (Fig. 3.6 C, $p=0.638$).

These findings demonstrate that telomere length regulation during pre-implantation embryogenesis is a highly dynamic process, beginning with telomere trimming immediately after fertilisation (Fig. 3.6), prior to the first mitosis, and then exhibiting elongation until the set point is reached at the blastocyst stage (Fig. 3.4).

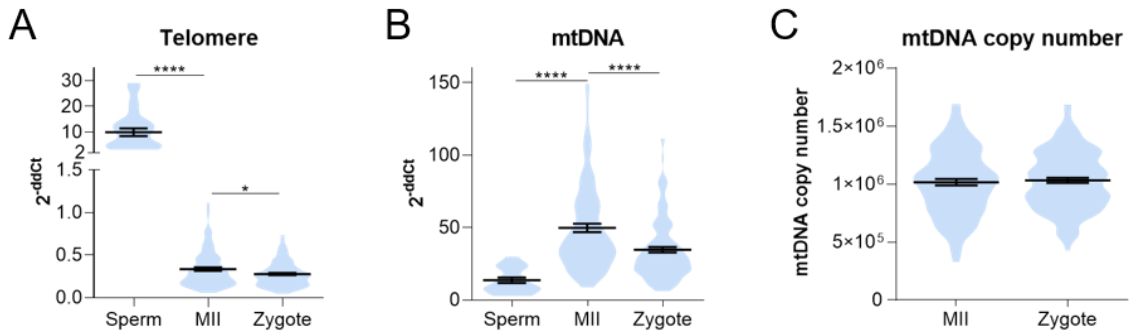


Figure 3.6. Telomere length and mtDNA copy number following fertilisation

Oocytes were collected from CBA.F1 mice, denuded of cumulus cells and individually frozen or fertilised via IVF. Fertilised zygotes were confirmed by the presence of two visible pronuclei and individually frozen. Sperm samples were acquired at the time of IVF from different males. All samples underwent the Triple Test to analyse relative telomere length (A), mtDNA relative to Rn18S (B), and total mtDNA copy number (C). n=20 pools of sperm from individual males, n=113 MII oocytes and n=133 zygotes. Data was log transformed for statistical analysis using one-way ANOVA (A, B) or unpaired t-test (C), * $p<0.03$, **** $p<0.0001$. Shaded areas represent the population distributions, while horizontal lines represent mean ± SEM.

3.3.4 Parthenogenetically activated embryos display similar telomere dynamics to IVF embryos

To determine the extent to which oocyte factors regulate telomere elongation, this process was examined in parthenogenetic embryos. Parthenogenetically activated embryos are generated by exposing unfertilised oocytes to medium containing strontium which triggers calcium release from the endoplasmic reticulum and exit from meiosis, and induces embryo formation. IVF fertilised zygotes contain distinguishing features of two polar bodies and two pronuclei (one maternal and one paternal pronucleus, Sup Fig. 3.1 A). In parthenogenetic embryo studies, it is important to determine which type of embryos develop out of the three possible types: haploid parthenotes, homozygous parthenotes (which become diploid through auto-diploidization), or heterozygous diploid parthenotes (Bos-Mikich et al., 2016). Heterozygous diploid parthenotes are easily distinguishable from the other two types as use of an inhibitor of actin filament polymerisation (cytochalasin D) means the second polar body is not extruded, indicating that all the genomic material within the MII oocyte is retained. The parthenogenetically activated embryos used in this study are heterozygous diploid, meaning they contain the two sister chromatids of each maternal chromosome, as successfully activated one cell embryos retain the second polar body and display two pronuclei (Sup Fig. 3.1 B). Heterozygous diploid embryos were used as their diploid status means that they retain the same number of chromosomes as are found in a fertilised zygote, and their heterozygosity indicates that a small degree of genetic variation (formed from the crossovers in prophase I) is present between homologous chromosomes.

Firstly, to further characterise these embryos, epigenetic reprogramming between parthenotes and IVF embryos was examined (Fig. 3.7). The global methylation landscapes of the pronuclei were analysed by comparing fluorescence intensities of 5mC and 5hmC (Fig. 3.7 A). IVF-derived zygotes exhibited the expected characteristics indicating that these embryos are undergoing normal reprogramming processes. Specifically, the paternal pronuclei was larger in area than the maternal pronuclei (Fig. 3.7 B). The maternal pronuclei had higher levels of 5mC fluorescence intensity than the paternal pronuclei (Fig. 3.7 C), and on the other hand, the paternal pronuclei had higher levels of 5hmC fluorescence intensity (Fig. 3.8 D). Unexpectedly, in parthenogenetic embryos (i.e. activated 1C embryos) the size of the pronuclei was

not similar to that of the maternal pronuclei in IVF zygotes despite consisting only of maternally derived chromosomes (Fig. 3.7 B). Instead, the size was different to both the maternal and paternal IVF pronuclei, being intermediate to the size of each, and both of the parthenogenetic pronuclei were similar in size to each other (paired t-test, p=0.9741). Unlike the IVF pronuclei, the parthenogenetic pronuclei did not exhibit differential methylation, i.e. the 5mC and 5hmC mean fluorescence intensity levels were similar (Fig. 3.7 C and D, respectively). The fluorescence intensities of the pronuclei from IVF or parthenogenetically derived embryos was converted to a ratio of paternal to maternal fluorescence for IVF embryos, and pronuclei 1 to pronuclei 2 for parthenogenetic embryos (Fig. 3.7 C and D, right y-axis). The ratio of 5mC from IVF zygotes was below one, indicating that the maternal pronuclei has a higher level of fluorescence than the paternal pronuclei, which was lower than the ratio for parthenotes, with the mean ratio at 1.07, meaning the pronuclear 5mC fluorescence was close to identical (Fig. 3.7 C). The mean ratio of 5hmC in IVF zygotes was 3.22 which is consistent with the paternal pronuclei having higher 5hmC abundance than the maternal pronuclei (Fig. 3.7 D). This ratio was higher than the ratio in parthenotes which, similarly to 5mC, had a mean ratio of 1.06 as the fluorescence between the pronuclei was once again close to identical (Fig. 3.7 D). Together these results indicate that parthenogenetically activated embryos have dysregulated epigenetic programming, specifically they remain at a midpoint six hours after activation, and lack the differential characteristics of normal maternal or paternal pronuclei.

Following the demonstration that epigenetic reprogramming is greatly dysregulated in parthenogenetically activated embryos, telomere length reprogramming was investigated (Fig. 3.8). Firstly, parthenotes were examined to determine whether activation resulted in a similar overall telomere length decrease that was seen in IVF zygotes six hours after fertilisation (Fig. 3.6 A). Fully denuded MII oocytes and successfully activated parthenogenetic 1C embryos were individually frozen and analysed using the Triple Test (Fig. 3.8 A-C). Activated 1C embryos had shorter telomeres than MII oocytes (Fig. 3.8 A) and total mtDNA copy number was not changed (Fig. 3.8 B), consistent with what was seen in IVF zygotes (Fig 3.6). The relative mtDNA per cell remained unchanged between MII oocytes and activated 1Cs (Fig. 3.8 C), as there was no change to the total quantity of genomic DNA. Due to the consistency in telomere shortening events following fertilisation (Fig. 3.6 A) and

strontium-induced activation (Fig. 3.8 A), telomere elongation throughout pre-implantation embryogenesis was investigated in parthenogenetically activated embryos (Fig. 3.8 D-F). Telomere elongation occurred in a step-wise manner in parthenogenetic embryos (Fig. 3.8 D), with 4C embryos having longer telomeres than MII oocytes, and the most pronounced increase occurring between the 8C and blastocyst stage. When converting telomere elongation with each cell cycle to a proportion of lengthening, it is clear that pre-compaction elongation in parthenogenetic embryos contributes to the final telomere length to a much lesser extent than in IVF embryos, as only 14% of the final telomere length was achieved during pre-compaction development (Fig. 3.8 E) compared to 45% in IVF embryos (Fig 3.4). The fold change difference in telomere length prior to and after the onset of compaction was examined (Fig. 3.8 F). While the fold change difference during pre-compaction development was only slightly lower to that in IVF embryos (Fig. 3.8 F at 1.9 fold, and Fig. 3.4 C at 2.4 fold, respectively), parthenogenetic embryos displayed excessive telomere elongation post-compaction when compared to IVF embryos (Fig. 3.8 F at 4.1 fold, and Fig. 3.4 C at 1.7 fold, respectively). This indicates that despite epigenetic reprogramming dysregulation in parthenogenetic zygotes, embryos still exhibit telomere reprogramming, albeit exacerbated post-compaction in comparison to IVF embryos.

Mitochondrial DNA trends were also analysed and these were consistent with the overall trend of IVF embryos, with total mtDNA copy number remaining relatively stable until mtDNA replication at the blastocyst stage where there was an increase (Fig. 3.8 G), and relative mtDNA per cell decreasing with each successive cleavage (Fig. 3.8 H).

Embryo quality, reflected by blastocyst cell numbers, was compared between day five IVF and parthenogenetically derived blastocysts (Fig. 3.9). Blastocysts were co-stained with Oct 3/4 antibody to specifically label the nucleus of inner cell mass (ICM) cells, and CDX2 to label the nucleus of trophectoderm (TE) cells, with all cell nuclei labelled with the DNA stain Hoechst, to allow counting of cells in each category (Fig. 3.9 A). No difference was observed in the number of cells within the ICM of each blastocyst type (Fig. 3.9 B, $p=0.459$), however parthenotes had more TE cells than IVF blastocysts (Fig. 3.9 C) and this lead to an increase in the total cell number (Fig. 3.9 D). Despite the increase in TE and therefore total cell number, the overall

percentage of total cells comprising the ICM was not different between the groups (Fig. 3.9 E, p=0.826). TE proliferation is known to coincide with an upregulation of mtDNA replication (St. John et al., 2010), so total mtDNA copy numbers were compared in whole blastocysts (Fig. 3.9 F), and increased TE proliferation was associated with a higher total mtDNA copy number in the parthenogenetic blastocysts.

Taken together, these results indicate that while parthenogenetic embryos have aberrant epigenetic reprogramming, they are still able to undergo telomere length reprogramming, indicating that this is likely controlled (at least pre-compaction) by maternal factors inherited by the MII oocyte (mRNA and proteins). The observation that telomeres shorten following activation (Fig. 3.8 A), even though there is no addition of disproportionately long telomeres from sperm, indicates that this is also likely a maternally pre-programmed mechanism. At day 5, parthenogenetic blastocysts have a higher total cell number due to increased TE proliferation, and therefore higher mtDNA copy number (Fig 3.9 D, C, F, respectively). This suggests that the parthenogenetic embryos are developing at a faster rate than IVF blastocysts, and their dysregulated epigenetic reprogramming may mean that elongation events post-compaction are exacerbated or persist longer than in IVF embryos, leading to a greater fold increase post-compaction in parthenogenetic embryos than IVF (Fig. 3.8 F and Fig. 3.4 C, respectively).

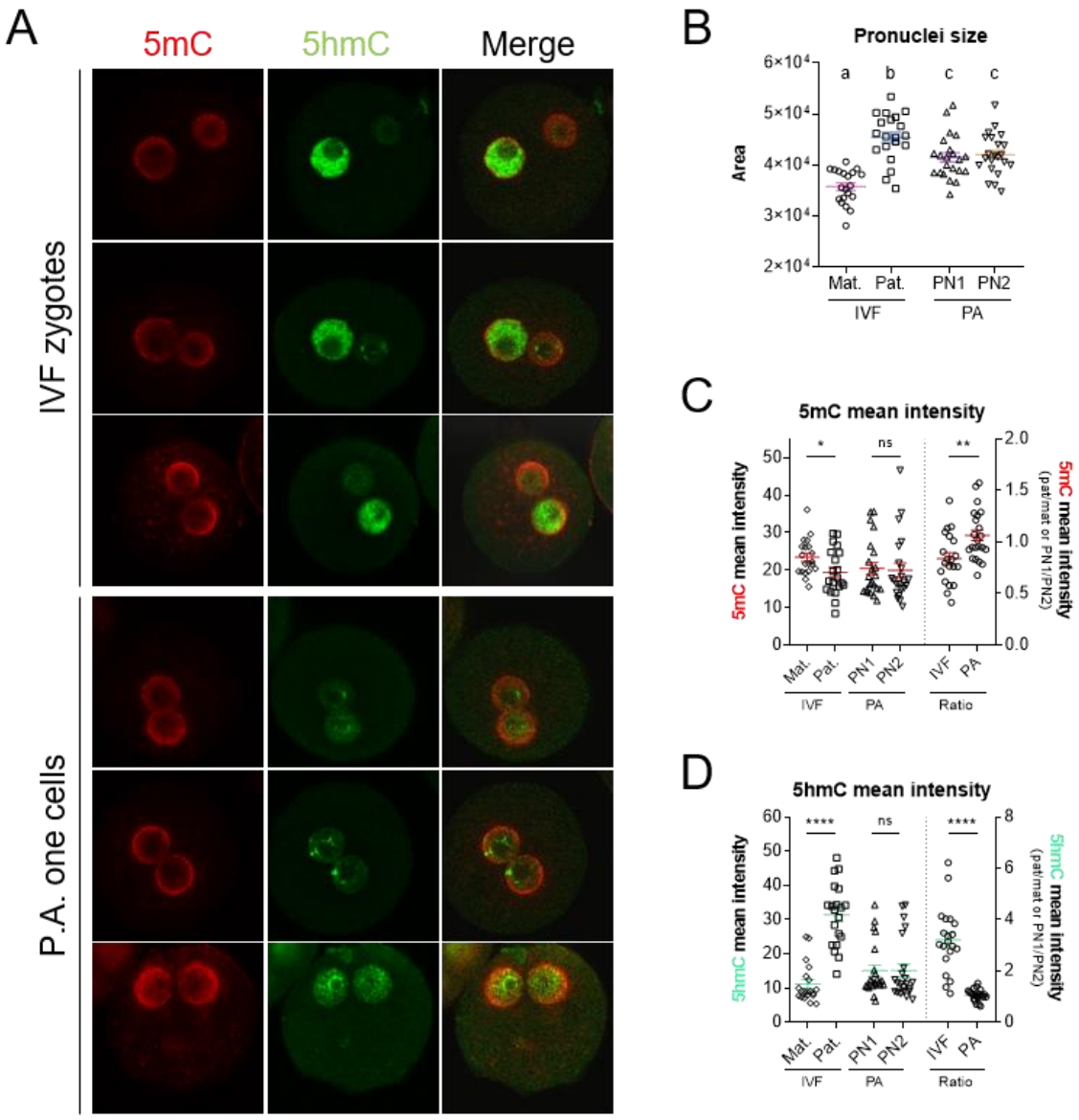


Figure 3.7. Methylation patterns in fertilised zygotes and parthenogenetically activated once-cell embryos

IVF derived zygotes or parthenogenetically activated 1C embryos were collected 6 hours after fertilisation or activation, respectively, and co-stained with anti-5mC (red) and anti-5hmC (green) antibodies (A). Pronuclei size was measured (B) and signal intensity fluorescence levels were quantified for 5mC (C) and 5hmC (D) in zygote and 1C pronuclei. Data presented as signal intensity for maternal (Mat.), paternal (Pat.), or either parthenogenetic pronuclei (PN) on the left axis, and the ratio of the signal for the paternal and maternal, or PN1 and PN2 on the right axis. Data analysed using one-way ANOVA (B) or unpaired t-test (C, D). For (B), statistical significance determined as $p<0.05$, for (C) and (D), * $p<0.05$, ** <0.005, **** $p<0.0001$, ns = not significant.

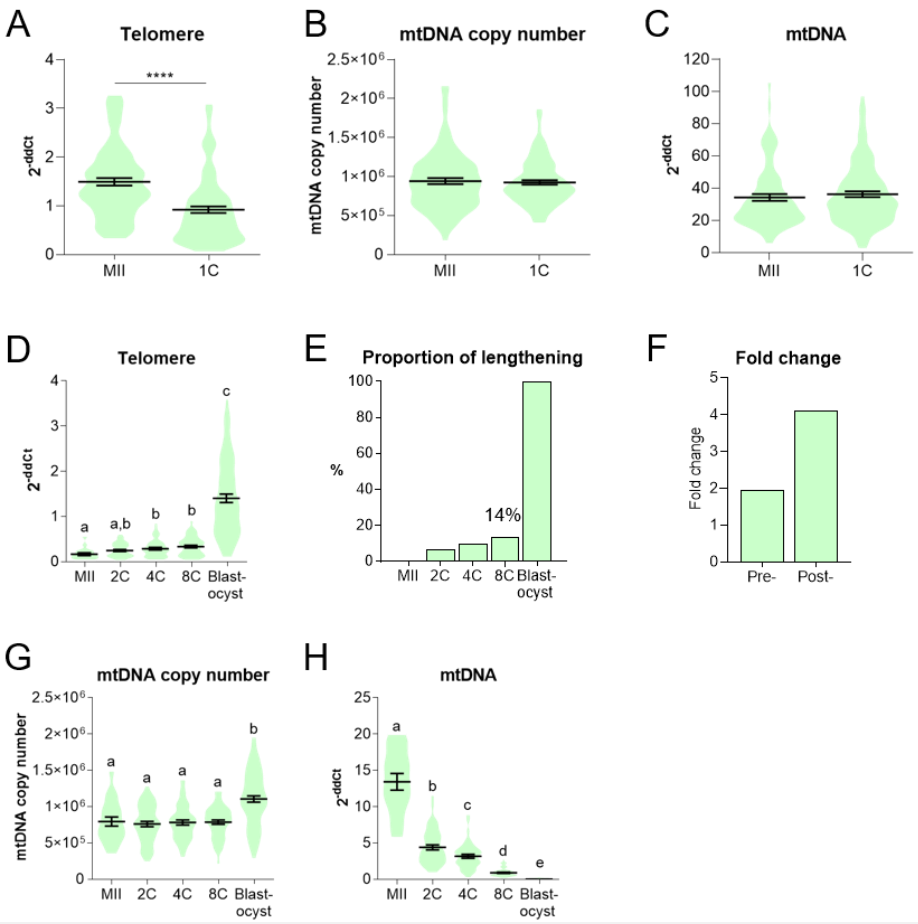


Figure 3.8. Telomere length regulation characteristics in parthenogenetic embryos

CBA.F1 MII oocytes were parthenogenetically activated using strontium chloride and cultured to the indicated stages. Individual denuded oocytes, activated one cells, and embryos were frozen for Triple Test qPCR analysis. Relative telomere length was calculated (A, D). Total mtDNA copy number was calculated using the standard curve method (B, G) and mtDNA per Rn18S copy (i.e. relative to cell number) was calculated (C, H). Telomere length was converted to a proportion of lengthening with MII set as 0% of the final length, and blastocyst set as 100% of the final length (E), with proportion of lengthening to the 8C stage indicated. Further, the fold change in relative telomere length was calculated (F) from MII oocytes to 8C embryos (pre-compaction), and from 8C embryos to blastocysts (post-compaction). For A-C n=92 MII oocytes and n=111 activated 1Cs, for embryogenesis time course, MII oocytes n=17, 2C n=50, 4C n=49, 8C n=51, blastocyst n=79. Data was log transformed for statistical analysis using an unpaired t-test (A-C), **** $p<0.0001$, or linear mixed-effects model (D, G, H), $p<0.05$. For A-D, G, H, shaded areas represent the population distributions, while horizontal lines represent mean ± SEM.

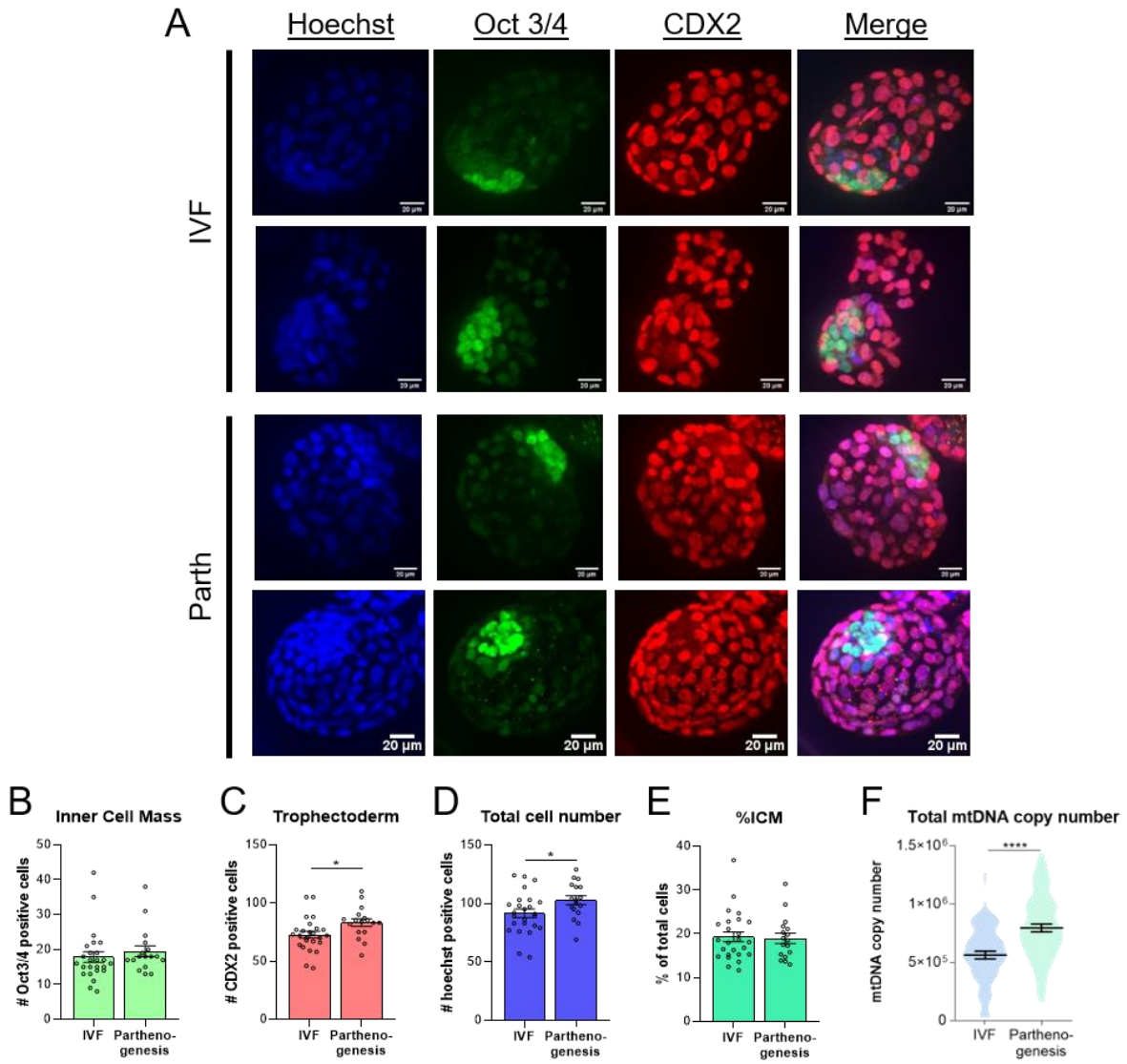


Figure 3.9. Day 5 blastocyst development in IVF and parthenogenetic blastocysts

CBA.F1 IVF or parthenogenetic derived blastocysts were collected late on day five and underwent immunocytochemistry to identify and count specific cell populations (A). Blastocysts were labelled with Oct3/4 (green) to define the ICM (B), CDX2 (red) to define the TE (C), and Hoechst (blue) to identify all cells (D). The percentage of inner cell mass cells from the total cell number was calculated (E). n=25 IVF and n=17 parthenogenetic blastocysts. Total mtDNA copy number was analysed in individual blastocysts (F) and log transformed for statistical analysis. n=62 IVF and n=63 parthenogenetic blastocysts. Data analysed using unpaired t-test, * $p<0.05$, **** $p<0.0001$. For F, shaded areas represent the population distributions, while horizontal lines represent mean ± SEM.

3.3.5 Male and female embryos do not differ in telomere length or mtDNA content at the blastocyst stage

Male and female embryos are known to show several sex differences, such as male mouse embryos forming blastocysts faster than female embryos (Tsunoda et al., 1985), proteomic (Epstein et al., 1978) and metabolic differences (Gardner and Leese, 1987) due to female embryos having two active copies of the X-chromosome prior to X-inactivation, and female mouse embryos having higher glucose uptake than male embryos (Lane and Gardner, 1996). While adult females are known to have longer telomeres than males, there is no difference in telomere length in male and female newborns (Okuda et al., 2002). To determine if the sex of the embryo influenced telomere elongation kinetics and therefore telomere length or mtDNA proliferation by the blastocyst stage, male and female embryos were compared. To do this, a PCR assay specific to the SRY gene, which is found on the Y chromosome and therefore specific to male embryos, was used to determine the sex of the embryo following the Triple Test (Fig. 3.10). Whole blastocysts were analysed and had their sex confirmed by visualising SRY PCR products on an agarose gel (Sup Fig. 3.2 A). Male and female embryos did not exhibit any differences in telomere length, mtDNA per cell, or total mtDNA copy number (Fig. 3.10 A-C, respectively).

To more precisely rule out sex differences specifically in the embryonic lineage, telomere length and mtDNA were measured in the ICM cells. Immunosurgery was used to remove a substantial proportion of trophectoderm and enrich the relative proportion of ICM (Sup Fig. 3.2 B-F). Once again, embryo sex did not have an effect on telomere length or mtDNA content per cell (Fig. 3.10 D $p=0.40$ & E $p=0.376$, respectively). Total mtDNA copy number was not analysed in ICM fractions due to potential differences in cell numbers between samples. These results indicate that the telomere length and mtDNA content of an embryo are regulated independent of embryo sex or sex-specific gene regulation.

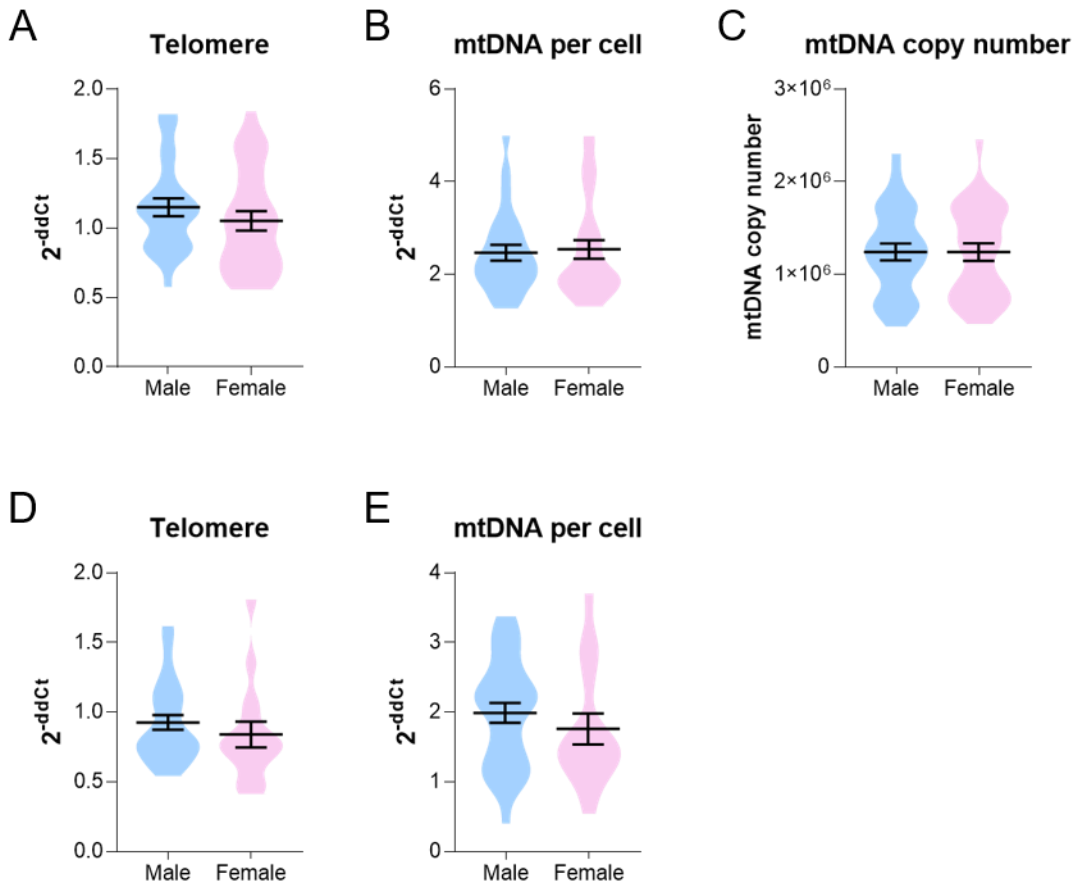


Figure 3.10. Telomere and mtDNA content in male and female embryos

IVF derived blastocysts from CBA.F1 mice were either left whole (A-C) or underwent immunosurgery to obtain an enriched ICM component (D, E). Following Triple Test analysis for relative telomere length (A & D), mtDNA per cell (B & E), and total mtDNA copy number (C), embryos were assayed for the SRY gene to allow grouping by sex. n=26 male and n=28 female whole blastocysts. n=30 male ICM and n=15 female ICM fractions. Log transformed data analysed using unpaired t-test, no significant differences were detected. Shaded areas represent the population distributions, while horizontal lines represent mean ± SEM.

3.3.6 IVF and parthenogenetically derived blastocysts display differences in cell-specific telomere elongation

Both IVF and parthenogenetic embryos exhibit telomere elongation pre- and post-compaction to achieve their blastocyst telomere length (Fig. 3.4 A-C, Fig. 3.8 D-F, respectively) with parthenotes exhibiting a greater fold change in telomere length post-compaction. To directly compare the two types of embryos, telomere length was compared between whole blastocysts derived via IVF or parthenogenesis. The results revealed that at the blastocyst stage, parthenotes had longer telomeres than IVF embryos (Fig. 3.11 A). When relative mtDNA per cell was compared between whole blastocysts no difference was observed (Fig. 3.11 B). Of note, parthenogenetic blastocysts were shown to have a higher total cell number (Fig. 3.9 D) and higher total mtDNA copy number (Fig. 3.9 F) than IVF blastocysts. Together these results suggest that the parthenogenesis-derived blastocysts were at a slightly more advanced stage of development than the IVF-conceived embryos.

To investigate whether there are any differences in telomere length or mtDNA in the portion of the embryo that will form the foetus, these were analysed in the ICM and TE cell populations of IVF and parthenogenetic blastocysts via manual dissection and the Triple Test (Fig. 3.11 C-F). No differences were found in telomere length between the two cell populations in parthenogenetic blastocysts (Fig. 3.11 C), however mtDNA per cell was higher in the TE cells than the ICM (Fig. 3.11D). This observation is consistent with the previous findings of increased TE proliferation in parthenogenetic blastocysts leading to increased mtDNA copy number (Fig. 3.9 C, F). In IVF derived blastocysts, telomeres in the ICM were longer than those in the TE (Fig. 3.11 E). mtDNA per cell was not different in IVF blastocysts cell populations (Fig. 3.11 F), consistent with upregulation of TE proliferation having not occurred yet in these embryos (Fig. 3.9 C).

Together these results indicate that telomere length regulation and mtDNA replication are differentially regulated in the distinct cell types of blastocysts. In IVF blastocysts, cells of the ICM undergo more extensive telomere elongation than the TE, likely as the cells of the ICM enter a pluripotent stem cell fate which includes the use of telomerase to maintain telomere length (Hiyama and Hiyama, 2007). These cells will go on to form the foetus and as such required a lifetime of genome integrity. TE cells increase proliferation prior to the ICM, and this corresponds with mitochondrial DNA replication

occurring. Comparison of telomere lengths in ICMs and TE in parthenogenetic and IVF blastocysts indicates that fertilised embryos exhibit greater telomere elongation in ICMs than parthenotes. This suggests that even though parthenotes exhibit slightly accelerated embryo development to the blastocyst stage, their ICM and TE telomere lengthening is dysregulated. This further suggests that events activated by either fertilization, or introduced by sperm play a role in programming ES cell telomere elongation capacity.

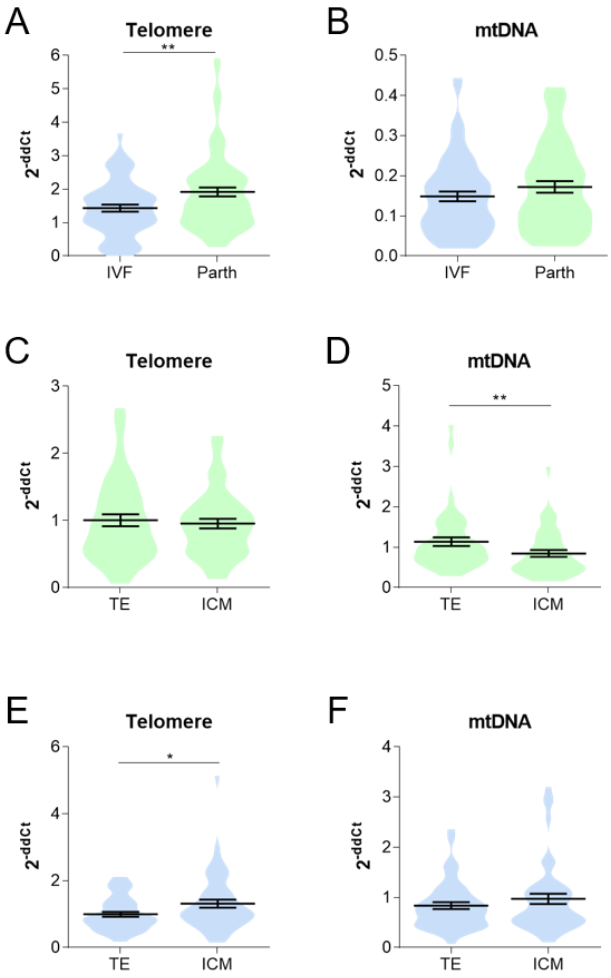


Figure 3.11. Telomere and mtDNA content in blastocyst ICM and TE cell populations

Oocytes from female CBA.F1 mice were fertilised via IVF or parthenogenetically activated using strontium chloride and cultured to the blastocyst stage. Whole blastocysts were individually frozen (A, B), or fully hatched through dissolving the zona pellucida using Acidic Tyrode's Solution, and manually dissected into the trophectoderm (TE) and inner cell mass (ICM) populations which were frozen separately for each blastocyst (C-F). Relative telomere length (A- whole blastocysts, C- parthenogenetic cell populations, E- IVF cell populations) and mtDNA per cell (B- whole blastocysts, D- parthenogenetic cell populations, F- IVF cell populations) were calculated. For whole blastocysts IVF n=62 and parthenogenesis n=63. For blastocyst cell populations IVF n=51, parthenogenesis n=48. Data was log transformed for statistical analysis. Whole blastocysts were analysed using an unpaired t-test, and blastocyst cell populations of the same embryo type were analysed using a paired t-test, * $p<0.02$, ** $p<0.007$. Shaded areas represent population distributions, while horizontal lines represent mean ± SEM.

3.3.7 Telomere elongation mechanisms are sensitive to culture conditions

Historically, *in vitro* embryo culture was carried out in environments with similar gas concentrations to atmospheric conditions, namely 20% oxygen (O_2); however studies revealed that the physiological concentrations of oxygen within the female reproductive tract are around 5% (Fischer and Bavister, 1993). Culture of embryos in atmospheric oxygen conditions (20%) has been widely associated with negative impacts on pre-implantation embryos, including alterations to both the transcriptome (Gardner and Lane, 2005; Rinaudo et al., 2006) and proteome (Katz-Jaffe et al., 2005), compromised carbohydrate and amino acid metabolism (Wale and Gardner, 2012), and poorer blastocyst and pregnancy outcomes (Ciray et al., 2009; Kovačič et al., 2010; Kovačič and Vlaisavljević, 2008; Waldenström et al., 2009) than those cultured in low oxygen (5%). As oxygen culture conditions affect many aspects of pre-implantation embryo development and viability, the effect of high (20%) and low (5%) oxygen conditions on telomere elongation and mtDNA per cell was investigated (Fig. 3.12). This analysis was conducted in hybrid embryos as these have been used for other published analyses of telomere dynamics and display a distinct lengthening pattern across development. Of note, all of the embryo cultures presented in this thesis were conducted at 5% O_2, with the exception of this experiment.

First, embryo development rates were evaluated. High oxygen culture did not alter the proportion of embryos that successfully cleaved to the 2C stage (96.77% low and 92% high O_2), however, there were fewer embryos that reached the 8C stage on time (91.11% low and 63.04% high O_2). Similarly, fewer blastocysts formed (92.22% low and 70.65% high O_2), and further to this, fewer of the blastocysts that were cultured in 20% O_2 had begun hatching on day 5 compared to those cultured in 5% O_2 (95.18% and 35.38%, respectively). These results are consistent with previous studies that found delays in overall blastocyst development rates at 96 hours post-hCG, which was normalised by 116 hours, however at this time the proportion of hatching blastocysts was reduced in embryos cultured in 20% O_2 compared to those cultured in 5% O_2 regardless of culture media used (Jin and O'Neill, 2014).

ICMs from day 5 blastocysts that were cultured in either high or low oxygen conditions were isolated using immunosurgery techniques and individually analysed for relative

telomere length and mtDNA per cell using the Triple Test (Fig. 3.12). High oxygen culture (20%) resulted in ICMs with shorter telomeres than those from embryos cultured in low oxygen (5%, Fig. 3.12 A). Conversely, mtDNA per cell was higher in the ICMs that had been in high oxygen culture than those in low oxygen (Fig. 3.12 B). These results demonstrate that telomere elongation events are adversely impacted by physiological stress conditions resulting from alterations to ideal culture conditions.

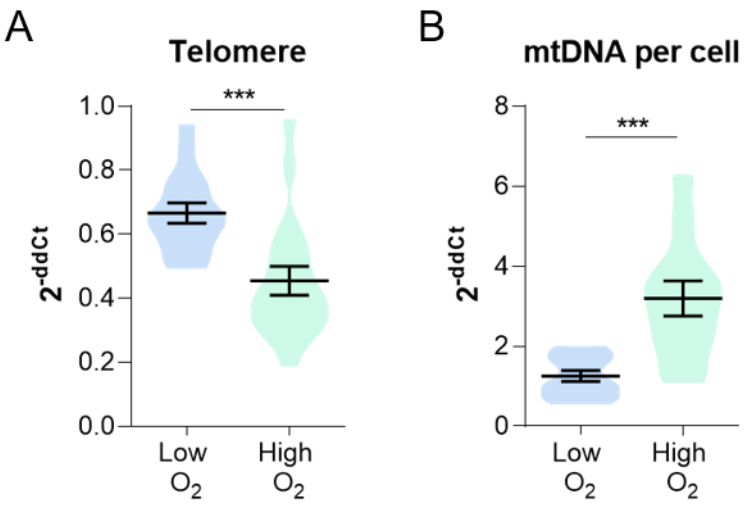


Figure 3.12. Telomere elongation and mtDNA per cell in adverse high oxygen culture conditions

Hybrid IVF embryos were cultured from fertilisation (day 1) to the blastocyst stage of development (day 5) in identical culture conditions except for oxygen concentration, which was at typical culture and physiologically relevant levels (low O_2 at 5%), or atmospheric levels (high O_2 at 20%). Immunosurgery was used to isolate the ICM population for Triple Test analysis of relative telomere length (A) and mtDNA per cell (B). n=16 low O_2 ICMs and n=18 high O_2 ICMs. Log transformed data analysed using unpaired t-test, *** $p<0.0008$. Shaded areas represent the population distributions, while horizontal lines represent mean ± SEM.

3.4 Discussion

Cumulatively, this work has provided a more comprehensive overview of the dynamic state of telomeres during pre-implantation embryogenesis. Telomeres are widely known to be important regulators of cell cycle and life span, with short telomeres associated with early onset of ageing characteristics and adverse health outcomes. Defects in genes associated with telomere length homeostasis or telomere regulation are also known to lead to a wide variety of diseases. Despite the extensive knowledge of the roles and importance of telomeres and their length, there is relatively little understanding of how telomeres are modified during the pre-implantation phase of embryogenesis, a developmental window which is known to establish many life-long trajectories for the offspring.

Telomere regulatory genes display dynamic expression

This study conducted the first characterisation of telomere associated protein gene expression throughout oocyte growth and maturation (Fig 3.1). The journey to form a fertilisable oocyte requires recruitment of follicles to the growing follicle pool and culminates in ovulation, oocyte completion of meiosis I and arrest in meiosis II. Interestingly, in the absence of exogenous gonadotropin stimulation, age was a modulating factor for oocyte expression of several telomere genes. This observation is consistent with the knowledge that transcription is actively occurring throughout oocyte growth (reviewed in Christou-Kent et al., 2020), and that oocytes from 6-week old mice are likely to have more follicles containing larger, more mature oocytes than those from 21-day old mice, therefore allowing time for further accumulation of transcribed mRNAs. The differences in oocyte gene expression between 6-week old unstimulated mice and those that had undergone PMSG stimulation is likely due to PMSG-induced synchronisation of follicle growth and thus oocytes collected following PMSG stimulation are more homogeneous. The latest time point analysed, 16h post-hCG stimulation, was highly variable in contrast to the other time points, suggesting that there are dynamic changes in expression between GV and MII oocytes. Analysis of telomeres between GV and MII oocytes showed no detectable difference in length, which was anticipated as no DNA replication occurs after the initiation of meiosis. Telomere elongation is known to occur during the S-phase of the cell cycle, however the chromatin remains extremely condensed during meiosis, making it nearly

impossible for proteins required for elongation to gain access to the telomeres during this time. No changes in the total mtDNA copy number of the oocyte were observed over this period either, which was expected, as mtDNA copy numbers have previously been shown to increase during oocyte growth but not during meiotic maturation (Mahrous et al., 2012).

This study was also the first to characterise a broad range of telomere associated genes in a detailed pre-implantation embryogenesis time course, as there has been little to no prior characterisation of many of the analysed genes. Of interest, TERT mRNA levels were highest in MII oocytes and substantially lower at the other analysed stages. Telomerase activity has been characterised as being low to undetectable in oocytes through to at least 4-cell embryos but greatly increased from the morula-blastocyst transition (Liu et al., 2007, 2002; Turner et al., 2010; Wright, 2001), observations which the mRNA expression data does not necessarily agree with. Therefore, the mRNA levels may not necessarily reflect protein levels, and as such, further characterisation of these proteins through assays such as Western blot analysis to confirm the presence of protein and immunocytochemistry to look at cellular localisation, are vital to progressing the understanding the mechanisms responsible for telomere elongation during pre-implantation embryogenesis. In addition, use of publically available RNA-seq databases will broaden the panel of telomere elongation and maintenance genes able to be analysed, and also allow for expression patterns between different mammalian species, such as human, mouse, bovine, and non-human primates, to be compared.

Telomeres undergo trimming and elongation

Telomere length reprogramming during pre-implantation embryogenesis appears to be a highly dynamic process including both telomere trimming and elongation mechanisms. Work in hybrid embryos confirmed that sperm have longer telomeres than MII oocytes (Fig. 3.6 A), likely due to proliferating spermatogonia possessing high levels of telomerase activity (Kalmbach et al., 2013). Interestingly though, zygote telomeres were shortened 6 hours after fertilisation when compared to MII oocyte telomeres (Fig. 3.6 A). A likely explanation for this marked decrease in telomere length is that regulatory mechanisms exist in oocytes to account for the major discrepancy in sperm and oocyte telomere lengths. Telomere shortening to equalise lengths between

the maternal and paternal telomeres could also play a functional role to allow for proper pairing and segregation of homologous chromosomes after pronuclei fusion in the first mitosis. Expression data for the telomere trimming-associated protein TZAP (J. S. Z. Li et al., 2017) supports this notion of telomere trimming occurring following fertilisation as the highest mRNA abundance is in MII oocytes and 2C embryos, and progressively decreases with each subsequent cleavage (Fig. 3.3 A). Activated one-cell parthenogenetic embryos also had reduced telomere length when compared to MII oocytes (Fig. 3.8 A), suggesting that regulatory mechanisms for telomere lengths in oocytes are automatic and function independent of input telomere lengths (i.e. whether telomere lengths are disproportionate as between oocytes and sperm, or telomeres are similar from chromosomes within the same oocyte). Curiously, these results disagree with previous work which showed an increase in telomere length in fertilised zygotes in two hybrid IVF embryo types, and parthenogenetically activated 1C embryos derived from CD1 mice, but no decreases in embryos derived from other mouse strains (Liu et al., 2007). This discrepancy could likely be influenced by the timing of the analysis, as sperm telomere length remodelling is unlikely to begin immediately following fertilisation due to the highly dense nature of sperm chromatin, therefore an increase in overall telomere length is likely to be seen. However 6 hours after fertilisation, extensive remodelling of the pronuclei has taken place, allowing access to the chromatin by many proteins.

Telomere length analysis of subsequent pre-implantation embryo development stages revealed potentially informative differences in elongation patterns between hybrid and inbred embryos. Hybrid embryos displayed increases in telomere length at each successive stage, thus exhibiting relatively similar levels of elongation during both pre- and post-compaction development. Inbred embryos did not display changes in telomere length by the two cell, and only minor increases were seen in C57/BL6 embryos at the 4C and 8C stage, and overall, inbred embryos demonstrated greater telomere elongation in post-compaction than pre-compaction development (Fig. 3.4 A-C). These differences perhaps suggest that embryos possess the ability to sense telomere elongation progress and control elongation rate to enable a certain degree of elongation to be achieved by the time of implantation. While it is well established that cells are able to sense when their telomeres reach a critical shortness, it is unknown if cells possess the ability to sense the progression of elongation, and this

poses an interesting line of further enquiry for telomere elongation biology. Further, one possible explanation for the difference observed in pre- and post-compaction elongation may simply lie in the genetic diversity introduced when producing hybrid embryos. Further, a requirement of genetic diversity, or chromosomal heterogeneity, for the early-stage ALT-based telomere elongation to occur appears rational as ALT is recombination based. Therefore, ALT during this early stage of development could serve as a mechanism to homogenize telomere composition between chromosomes derived from maternal and paternal lineages. Another conceivable explanation for this difference could reside in the reduced capacity of inbred embryos to thrive, particularly *in vitro*. Previous studies have established that hybrid mice typically have higher 2C and blastocyst IVF rates than inbred embryos, and hybrid sperm tend to be more resilient, of better quality and higher fertilisation capability than inbred sperm (Szczygiel et al., 2002; Sztein et al., 2000). Thus reduced telomere elongation in inbred embryos may be one expression of the diminished capacity to complete multiple vital cellular processes compared to hybrid embryos. Further, inbred blastocysts have been reported to have a lower total cell number 96 hours after the beginning of culture than hybrid embryos (Khan et al., 2013). This indicates less completed cell cycles by inbred embryos at the same time in development. It is entirely possible that inbred embryos have longer cell cycles after the onset blastulation to allow for recovery of any developmental checkpoints, including telomere elongation, which did not occur in the earlier cell cycle. This work highlights the importance for consideration of embryo type (inbred or hybrid) when conducting any studies of pre-implantation embryogenesis.

Parthenogenetic embryos exhibit altered telomere elongation patterns

Analysis of parthenogenetically activated hybrid embryos demonstrated that telomere elongation still occurs in the absence of a paternal contribution, and therefore the capacity for telomere elongation is inherit within the oocyte itself, consistent with previous reports (Liu et al., 2007). Remarkably, parthenogenetic embryos exhibited relatively greater telomere elongation in post-compaction development than the IVF embryos even if inbred (evidenced by a four-fold increase in length post-compaction which accounted for 85% of the final relative telomere length, Fig. 3.8 F and E), indicating greater telomere lengthening during post-compaction development in these embryos. Another curiosity of parthenogenetic embryos is that while they exhibit

slightly accelerated embryo development to blastocyst, as evidenced by cell counts, they appear to be deficient in ICM telomere lengths, as there was no difference in telomere length between the ICM and TE populations (Fig. 3.11 C), which was seen in IVF embryos in this study and previous studies (Fig. 3.11 E, Iqbal et al., 2011; Varela et al., 2011).

Accelerated development, divergent telomere elongation patterns, and loss of known telomere length characteristics in specific cell populations may be a consequence of the dysregulated epigenetic reprogramming seen in the activated parthenogenetic 1C embryos in this study (Fig. 3.7). While this is a simplistic analysis that does not allow for definitive conclusions to be drawn, disordered methylation patterns across the genome could likely culminate in alterations to gene expression, as such this could be consequential for expression of key genes involved in telomere regulation and elongation. These findings warrant further investigation using more quantitative measures such as amplicon bisulfite sequencing using next-generation sequencing (NGS) (The BLUEPRINT consortium, 2016). Further, telomeres form heterochromatin and as such are highly methylated sequences (Blasco, 2007). Alterations to genomic methylation levels may decrease the amount of methyl marks on telomeric DNA and histones, which leads to aberrant telomere elongation and acts as a signal for telomerase to elongate telomeres (Blasco, 2007). As telomerase is known to be active in morula and blastocyst embryos, these altered methylation patterns could certainly result in excessive telomere elongation in blastocysts and a loss of controlled length regulation in specific cell populations.

Blastocyst cell populations exhibit distinct telomere length differences

Telomere lengths are longer in the ICM population than the TE in blastocysts (Fig. 3.11 E, Iqbal et al., 2011; Varela et al., 2011). It is likely that cells in the TE are endowed with shorter telomeres as these cells will have a limited lifespan and are only required for a relatively limited time, i.e. ~40 weeks in women. In contrast, telomeres in the cells of the ICM are required for the lifetime of the offspring, thus perhaps undergoing more extensive elongation as these first two distinct cell populations are established. These observations highlight that telomere length in the ICM is of utmost importance for the established telomere length of the foetus. Further, these differences between ICM and TE telomere length are lost in parthenogenetic embryos (Fig. 3.11

C), signifying dysregulated elongation in comparison to fertilised embryos. Comparison of telomere length maintenance in embryonic stem (ES) cells derived from fertilised embryos (fES) or parthenogenetic embryos (pES) revealed that pES cells exhibited longer telomeres and greater elongation throughout passages than fES cells (Yin et al., 2014). While Zscan4 is transiently expressed in small populations of ES cells undergoing recombination based telomere elongation (Zalzman et al., 2010), pES cells display greater Zscan4 gene expression and protein levels than fES cells, and Zscan4 was shown to be required for telomere length maintenance and elongation in these pES cells (Yin et al., 2014). These results indicate the pES cells more extensively utilise recombination based mechanisms for telomere elongation than fES cells. Given that the elongation mechanisms in the ES cells, which are derived from the ICM, differ between fertilised and parthenogenetic embryos, this also suggests that elongation mechanisms throughout early embryogenesis are differentially utilised in the two types of embryos, which may well lead to divergences in telomere length characteristics of the blastocyst cell populations, as seen in this study.

Telomere elongation is sensitive to culture conditions

Culture of embryos in atmospheric oxygen conditions (20%) markedly reduced ICM telomere length compared to those cultured in physiologic conditions (5%, Fig. 3.12 A), suggesting that telomere elongation mechanism are susceptible to stress conditions. High oxygen culture is known to result in several perturbations in embryo function and development (Ciray et al., 2009; Gardner and Lane, 2005; Katz-Jaffe et al., 2005; Kovačič et al., 2010; Kovačič and Vlaisavljević, 2008; Rinaudo et al., 2006; Waldenström et al., 2009). An overarching effector of this perturbed developmental is likely to be mitochondrial function, which is also altered with high oxygen culture (Belli et al., 2019). Interestingly, mtDNA copy number per cell was higher in high oxygen ICMs than low oxygen ICMs, while previous studies found embryos cultured in high oxygen contained fewer mitochondria than those in low oxygen (Belli et al., 2019). These observations suggest that the mitochondria may contain more mtDNA as a result of less mitochondrial fission, or that perhaps mtDNA replication was upregulated in these embryos to deal with cellular stress.

Summary and Outstanding Questions

This study is the most thorough investigation to date of telomere dynamics during pre-implantation embryogenesis, and has provided a detailed time course of expression of telomere regulatory genes during oocyte maturation and pre-implantation embryogenesis. We have shown that telomere elongation occurs from fertilisation to the 8C embryo with strain differences that align with inbred vs hybrid categories. Subsequently all embryos underwent elongation from the 8C to blastocyst stage, regardless of strain. Consistent with previous studies, I have demonstrated that the capacity for telomere elongation resides within the oocyte as parthenogenetically activated embryos still exhibit telomere elongation. Telomeres are trimmed following fertilisation by a mechanism that appears pre-set in the oocyte, likely involving TZAP. This occurrence in parthenogenetically activated embryos, independent of the addition of extremely long telomeres from sperm, further implicates maternally derived oocyte factors as major regulators of early telomere elongation events. Although I confirmed the presence of mRNAs for many telomere binding, associated, and elongation proteins, more detailed protein analysis and localisation is required to determine their role during early embryogenesis. Finally, culture in high oxygen conditions resulted in decreased ICM telomere lengths, signifying that mitochondria may be a key mediator of telomere elongation events in pre-implantation embryogenesis. This finding warrants further investigation, particularly in physiological scenarios of mitochondrial dysfunction in oocytes, as seen in maternal aging and obesity.

3.5 References

Amouroux, R., Nashun, B., Shirane, K., Nakagawa, S., Hill, P.W.S., D'Souza, Z., Nakayama, M., Matsuda, M., Turp, A., Ndjetehe, E., Encheva, V., Kudo, N.R., Koseki, H., Sasaki, H., Hajkova, P., 2016. De novo DNA methylation drives 5hmC accumulation in mouse zygotes. Nature Cell Biology 18, 225–233. https://doi.org/10.1038/ncb3296

Belli, M., Zhang, L., Liu, X., Donjacour, A., Ruggeri, E., Palmerini, M.G., Nottola, S.A., Macchiarelli, G., Rinaudo, P., 2019. Oxygen concentration alters mitochondrial structure and function in *in vitro* fertilized preimplantation mouse embryos. Human Reproduction 34, 601–611. https://doi.org/10.1093/humrep/dez011

Blackburn, E.H., 1984. Telomeres: Do the ends justify the means? Cell 37, 7–8. https://doi.org/10.1016/0092-8674(84)90295-2

Blasco, M.A., 2007. The epigenetic regulation of mammalian telomeres. Nature Reviews Genetics 8, 299–309. https://doi.org/10.1038/nrg2047

Bos-Mikich, A., Bressan, F.F., Ruggeri, R.R., Watanabe, Y., Meirelles, F.V., 2016. Parthenogenesis and Human Assisted Reproduction. Stem Cells International 2016, 1–8. https://doi.org/10.1155/2016/1970843

Christou-Kent, M., Dhellemmes, M., Lambert, E., Ray, P.F., Arnoult, C., 2020. Diversity of RNA-Binding Proteins Modulating Post-Transcriptional Regulation of Protein Expression in the Maturing Mammalian Oocyte. Cells 9, 662. https://doi.org/10.3390/cells9030662

Ciray, H.N., Aksoy, T., Yaramanci, K., Karayaka, I., Bahceci, M., 2009. In vitro culture under physiologic oxygen concentration improves blastocyst yield and quality: a prospective randomized survey on sibling oocytes. Fertility and Sterility 91, 1459–1461. https://doi.org/10.1016/j.fertnstert.2008.07.1707

Cristofari, G., Lingner, J., 2006. Telomere length homeostasis requires that telomerase levels are limiting. The EMBO Journal 25, 565–574. https://doi.org/10.1038/sj.emboj.7600952

Ellis, N.A., Groden, J., Ye, T.-Z., Straughen, J., Lennon, D.J., Ciocci, S., Proytcheva, M., German, J., 1995. The Bloom's syndrome gene product is homologous to RecQ helicases. Cell 83, 655–666. https://doi.org/10.1016/0092-8674(95)90105-1

Epstein, C.J., Smith, S., Travis, B., Tucker, G., 1978. Both X chromosomes function before visible X-chromosome inactivation in female mouse embryos. Nature 274, 500–503. https://doi.org/10.1038/274500a0

Falco, G., Lee, S.-L., Stanghellini, I., Bassey, U.C., Hamatani, T., Ko, M.S.H., 2007. Zscan4: A novel gene expressed exclusively in late 2-cell embryos and embryonic stem cells. Developmental Biology 307, 539–550. https://doi.org/10.1016/j.ydbio.2007.05.003

Fischer, B., Bavister, B.D., 1993. Oxygen tension in the oviduct and uterus of rhesus monkeys, hamsters and rabbits. Reproduction 99, 673–679. https://doi.org/10.1530/jrf.0.0990673

Gardner, D.K., Lane, M., 2005. Ex vivo early embryo development and effects on gene expression and imprinting. Reproduction, Fertility and Development 17, 361. https://doi.org/10.1071/RD04103

Gardner, D.K., Leese, H.J., 1987. Assessment of embryo viability prior to transfer by the noninvasive measurement of glucose uptake. Journal of Experimental Zoology 242, 103–105. https://doi.org/10.1002/jez.1402420115

Gu, T.-P., Guo, F., Yang, H., Wu, H.-P., Xu, G.-F., Liu, W., Xie, Z.-G., Shi, L., He, X., Jin, S., Iqbal, K., Shi, Y.G., Deng, Z., Szabó, P.E., Pfeifer, G.P., Li, J., Xu, G.-L., 2011. The role of Tet3 DNA dioxygenase in epigenetic reprogramming by oocytes. Nature 477, 606–610. https://doi.org/10.1038/nature10443

Han, L., Ren, C., Li, L., Li, X., Ge, J., Wang, H., Miao, Y.-L., Guo, X., Moley, K.H., Shu, W., Wang, Q., 2018. Embryonic defects induced by maternal obesity in mice derive from Stella insufficiency in oocytes. Nature Genetics 50, 432–442. https://doi.org/10.1038/s41588-018-0055-6

Hayflick, L., Moorhead, P.S., 1961. The serial cultivation of human diploid cell strains. Exp. Cell Res. 25, 585–621.

Hiyama, E., Hiyama, K., 2007. Telomere and telomerase in stem cells. British Journal of Cancer 96, 1020–1024. https://doi.org/10.1038/sj.bjc.6603671

Iqbal, K., Jin, S.-G., Pfeifer, G.P., Szabó, P.E., 2011. Reprogramming of the paternal genome upon fertilization involves genome-wide oxidation of 5-methylcytosine.

Proceedings of the National Academy of Sciences 108, 3642–3647. https://doi.org/10.1073/pnas.1014033108

Iqbal, K., Kues, W.A., Baulain, U., Garrels, W., Herrmann, D., Niemann, H., 2011. Species-Specific Telomere Length Differences Between Blastocyst Cell Compartments and Ectopic Telomere Extension in Early Bovine Embryos by Human Telomerase Reverse Transcriptase. Biology of Reproduction 84, 723–733. https://doi.org/10.1095/biolreprod.110.087205

Jin, X.L., O'Neill, C., 2014. Systematic analysis of the factors that adversely affect the rate of cell accumulation in mouse embryos during their culture in vitro. Reproductive Biology and Endocrinology 12, 35. https://doi.org/10.1186/1477-7827-12-35

Johnson, M.H., Ziomek, C.A., 1981. Induction of polarity in mouse 8-cell blastomeres: specificity, geometry, and stability. The Journal of Cell Biology 91, 303–308. https://doi.org/10.1083/jcb.91.1.303

Kalmbach, K.H., Fontes Antunes, D.M., Dracxler, R.C., Knier, T.W., Seth-Smith, M.L., Wang, F., Liu, L., Keefe, D.L., 2013. Telomeres and human reproduction. Fertility and Sterility 99, 23–29. https://doi.org/10.1016/j.fertnstert.2012.11.039

Kameyama, Y., Ohnishi, H., Shimoi, G., Hashizume, R., Ito, M., Smith, L.C., 2010. Asymmetrical allocation of mitochondrial DNA to blastomeres during the first two cleavages in mouse embryos. Reproduction, Fertility and Development 22, 1247. https://doi.org/10.1071/RD10076

Katz-Jaffe, M.G., Linck, D.W., Schoolcraft, W.B., Gardner, D.K., 2005. A proteomic analysis of mammalian preimplantation embryonic development. Reproduction 130, 899–905. https://doi.org/10.1530/rep.1.00854

Khan, Z., Wolff, H.S., Fredrickson, J.R., Walker, D.L., Daftary, G.S., Morbeck, D.E., 2013. Mouse strain and quality control testing: improved sensitivity of the mouse embryo assay with embryos from outbred mice. Fertility and Sterility 99, 847-854.e2. https://doi.org/10.1016/j.fertnstert.2012.10.046

Kovačič, B., Sajko, M.Č., Vlaisavljević, V., 2010. A prospective, randomized trial on the effect of atmospheric versus reduced oxygen concentration on the outcome of intracytoplasmic sperm injection cycles. Fertility and Sterility 94, 511–519. https://doi.org/10.1016/j.fertnstert.2009.03.077

Kovačič, B., Vlaisavljević, V., 2008. Influence of atmospheric versus reduced oxygen concentration on development of human blastocysts in vitro: a prospective study on sibling oocytes. Reproductive BioMedicine Online 17, 229–236. https://doi.org/10.1016/S1472-6483(10)60199-X

Kumar, R., Cheok, C.F., 2014. RIF1: A novel regulatory factor for DNA replication and DNA damage response signaling. DNA Repair 15, 54–59. https://doi.org/10.1016/j.dnarep.2013.12.004

Lane, M., Gardner, D.K., 1996. Fertilization and early embryology: Selection of viable mouse blastocysts prior to transfer using a metabolic criterion. Human Reproduction 11, 1975–1978. https://doi.org/10.1093/oxfordjournals.humrep.a019527

Lansdorp, P., van Wietmarschen, N., 2019. Helicases FANCJ, RTEL1 and BLM Act on Guanine Quadruplex DNA in Vivo. Genes 10, 870. https://doi.org/10.3390/genes10110870

Li, J.S.Z., Miralles Fusté, J., Simavorian, T., Bartocci, C., Tsai, J., Karlseder, J., Lazzerini Denchi, E., 2017. TZAP: A telomere-associated protein involved in telomere length control. Science 355, 638–641. https://doi.org/10.1126/science.aah6752

Li, Y., O'Neill, C., 2012. Persistence of cytosine methylation of DNA following fertilisation in the mouse. PLoS One 7, e30687. https://doi.org/10.1371/journal.pone.0030687

Liu, W., Yin, J., Kou, X., Jiang, Y., Gao, H., Zhao, Y., Huang, B., He, W., Wang, H., Han, Z., Gao, S., 2014. Asymmetric Reprogramming Capacity of Parental Pronuclei in Mouse Zygotes. Cell Reports 6, 1008–1016. https://doi.org/10.1016/j.celrep.2014.02.018

Liu, L., Bailey, S.M., Okuka, M., Muñoz, P., Li, C., Zhou, L., Wu, C., Czerwiec, E., Sandler, L., Seyfang, A., Blasco, M.A., Keefe, D.L., 2007. Telomere lengthening early in development. Nature Cell Biology 9, 1436–1441. https://doi.org/10.1038/ncb1664

Liu, L., Blasco, M.A., Trimarchi, J.R., Keefe, D.L., 2002. An Essential Role for Functional Telomeres in Mouse Germ Cells during Fertilization and Early Development. Developmental Biology 249, 74–84. https://doi.org/10.1006/dbio.2002.0735

Mahrous, E., Yang, Q., Clarke, H.J., 2012. Regulation of mitochondrial DNA accumulation during oocyte growth and meiotic maturation in the mouse. REPRODUCTION 144, 177–185. https://doi.org/10.1530/REP-12-0113

Martens, D.S., Plusquin, M., Gyselaers, W., De Vivo, I., Nawrot, T.S., 2016. Maternal pre-pregnancy body mass index and newborn telomere length. BMC Med 14, 148. https://doi.org/10.1186/s12916-016-0689-0

McAninch, D., Bianco-Miotto, T., Gatford, K.L., Leemaqz, S.Y., Andraweera, P.H., Garrett, A., Plummer, M.D., Dekker, G.A., Roberts, C.T., Smithers, L.G., Grieger, J.A., 2020. The metabolic syndrome in pregnancy and its association with child telomere length. Diabetologia 63, 2140–2149. https://doi.org/10.1007/s00125-020-05242-0

Okuda, K., Bardeguez, A., Gardner, J.P., Rodriguez, P., Ganesh, V., Kimura, M., Skurnick, J., Awad, G., Aviv, A., 2002. Telomere Length in the Newborn. Pediatric Research 52, 377–381. https://doi.org/10.1203/00006450-200209000-00012

Olovnikov, A.M., 1973. A theory of marginotomy. Journal of Theoretical Biology 41, 181–190. https://doi.org/10.1016/0022-5193(73)90198-7

Ozturk, S., 2015. Telomerase Activity and Telomere Length in Male Germ Cells. Biology of Reproduction 92. https://doi.org/10.1095/biolreprod.114.124008

Pickett, H.A., Reddel, R.R., 2015. Molecular mechanisms of activity and derepression of alternative lengthening of telomeres. Nat. Struct. Mol. Biol. 22, 875–880. https://doi.org/10.1038/nsmb.3106

Rinaudo, P., Giritharan, G., Talbi, S., Dobson, A., Schultz, R., 2006. Effects of oxygen tension on gene expression in preimplantation mouse embryos. Fertility and Sterility 86, 1265.e1-1265.e36. https://doi.org/10.1016/j.fertnstert.2006.05.017

Rudolph, K.L., Chang, S., Lee, H.W., Blasco, M., Gottlieb, G.J., Greider, C., DePinho, R.A., 1999. Longevity, stress response, and cancer in aging telomerase-deficient mice. Cell 96, 701–712.

Santos, F., Hendrich, B., Reik, W., Dean, W., 2002. Dynamic Reprogramming of DNA Methylation in the Early Mouse Embryo. Developmental Biology 241, 172–182. https://doi.org/10.1006/dbio.2001.0501

Schaetzlein, S., Lucas-Hahn, A., Lemme, E., Kues, W.A., Dorsch, M., Manns, M.P., Niemann, H., Rudolph, K.L., 2004. Telomere length is reset during early mammalian

embryogenesis. Proceedings of the National Academy of Sciences 101, 8034–8038. https://doi.org/10.1073/pnas.0402400101

Shen, L., Inoue, A., He, J., Liu, Y., Lu, F., Zhang, Y., 2014. Tet3 and DNA Replication Mediate Demethylation of Both the Maternal and Paternal Genomes in Mouse Zygotes. Cell Stem Cell 15, 459–471. https://doi.org/10.1016/j.stem.2014.09.002

Silverman, J., 2004. Human Rif1, ortholog of a yeast telomeric protein, is regulated by ATM and 53BP1 and functions in the S-phase checkpoint. Genes & Development 18, 2108–2119. https://doi.org/10.1101/gad.1216004

St. John, J.C., Facucho-Oliveira, J., Jiang, Y., Kelly, R., Salah, R., 2010. Mitochondrial DNA transmission, replication and inheritance: a journey from the gamete through the embryo and into offspring and embryonic stem cells. Human Reproduction Update 16, 488–509. https://doi.org/10.1093/humupd/dmq002

Sun, H., Karow, J.K., Hickson, I.D., Maizels, N., 1998. The Bloom's Syndrome Helicase Unwinds G4 DNA. Journal of Biological Chemistry 273, 27587–27592. https://doi.org/10.1074/jbc.273.42.27587

Szczygiel, M.A., Kusakabe, H., Yanagimachi, R., Whittingham, D.G., 2002. Separation of Motile Populations of Spermatozoa Prior to Freezing Is Beneficial for Subsequent Fertilization In Vitro: A Study with Various Mouse Strains1. Biology of Reproduction 67, 287–292. https://doi.org/10.1095/biolreprod67.1.287

Sztein, J.M., Farley, J.S., Mobraaten, L.E., 2000. In Vitro Fertilization with Cryopreserved Inbred Mouse Sperm1. Biology of Reproduction 63, 1774–1780. https://doi.org/10.1095/biolreprod63.6.1774

The BLUEPRINT consortium, 2016. Quantitative comparison of DNA methylation assays for biomarker development and clinical applications. Nature Biotechnology 34, 726–737. https://doi.org/10.1038/nbt.3605

Thundathil, J., Filion, F., Smith, L.C., 2005. Molecular control of mitochondrial function in preimplantation mouse embryos. Molecular Reproduction and Development 71, 405–413. https://doi.org/10.1002/mrd.20260

Tsukada, Y., Akiyama, T., Nakayama, K.I., 2015. Maternal TET3 is dispensable for embryonic development but is required for neonatal growth. Scientific Reports 5. https://doi.org/10.1038/srep15876

Tsunoda, Y., Tokunaga, T., Sugie, T., 1985. Altered sex ratio of live young after transfer of fast- and slow-developing mouse embryos. Gamete Research 12, 301–304. https://doi.org/10.1002/mrd.1120120308

Turner, S., Wong, H.P., Rai, J., Hartshorne, G.M., 2010. Telomere lengths in human oocytes, cleavage stage embryos and blastocysts. Mol. Hum. Reprod. 16, 685–694. https://doi.org/10.1093/molehr/gaq048

Uringa, E.-J., Lisaingo, K., Pickett, H.A., Brind'Amour, J., Rohde, J.-H., Zelensky, A., Essers, J., Lansdorp, P.M., 2012. RTEL1 contributes to DNA replication and repair and telomere maintenance. Molecular Biology of the Cell 23, 2782–2792. https://doi.org/10.1091/mbc.e12-03-0179

Uringa, E.-J., Youds, J.L., Lisaingo, K., Lansdorp, P.M., Boulton, S.J., 2011. RTEL1: an essential helicase for telomere maintenance and the regulation of homologous recombination. Nucleic Acids Research 39, 1647–1655. https://doi.org/10.1093/nar/gkq1045

Varela, E., Schneider, R.P., Ortega, S., Blasco, M.A., 2011. Different telomere-length dynamics at the inner cell mass versus established embryonic stem (ES) cells. Proceedings of the National Academy of Sciences 108, 15207–15212. https://doi.org/10.1073/pnas.1105414108

Waldenström, U., Engström, A.-B., Hellberg, D., Nilsson, S., 2009. Low-oxygen compared with high-oxygen atmosphere in blastocyst culture, a prospective randomized study. Fertility and Sterility 91, 2461–2465. https://doi.org/10.1016/j.fertnstert.2008.03.051

Wale, P.L., Gardner, D.K., 2012. Oxygen Regulates Amino Acid Turnover and Carbohydrate Uptake During the Preimplantation Period of Mouse Embryo Development1. Biology of Reproduction 87. https://doi.org/10.1095/biolreprod.112.100552

Wang, F., Pan, X., Kalmbach, K., Seth-Smith, M.L., Ye, X., Antumes, D.M.F., Yin, Y., Liu, L., Keefe, D.L., Weissman, S.M., 2013. Robust measurement of telomere length in single cells. Proc. Natl. Acad. Sci. U.S.A. 110, E1906-1912. https://doi.org/10.1073/pnas.1306639110

Wossidlo, M., Arand, J., Sebastiano, V., Lepikhov, K., Boiani, M., Reinhardt, R., Schöler, H., Walter, J., 2010. Dynamic link of DNA demethylation, DNA strand breaks and repair in mouse zygotes. The EMBO Journal 29, 1877–1888. https://doi.org/10.1038/emboj.2010.80

Wright, D.L., 2001. Characterization of telomerase activity in the human oocyte and preimplantation embryo. Molecular Human Reproduction 7, 947–955. https://doi.org/10.1093/molehr/7.10.947

Xin, H., Liu, D., Songyang, Z., 2008. The telosome/shelterin complex and its functions. Genome Biology 9, 232. https://doi.org/10.1186/gb-2008-9-9-232

Xu, L., Blackburn, E.H., 2004. Human Rif1 protein binds aberrant telomeres and aligns along anaphase midzone microtubules. Journal of Cell Biology 167, 819–830. https://doi.org/10.1083/jcb.200408181

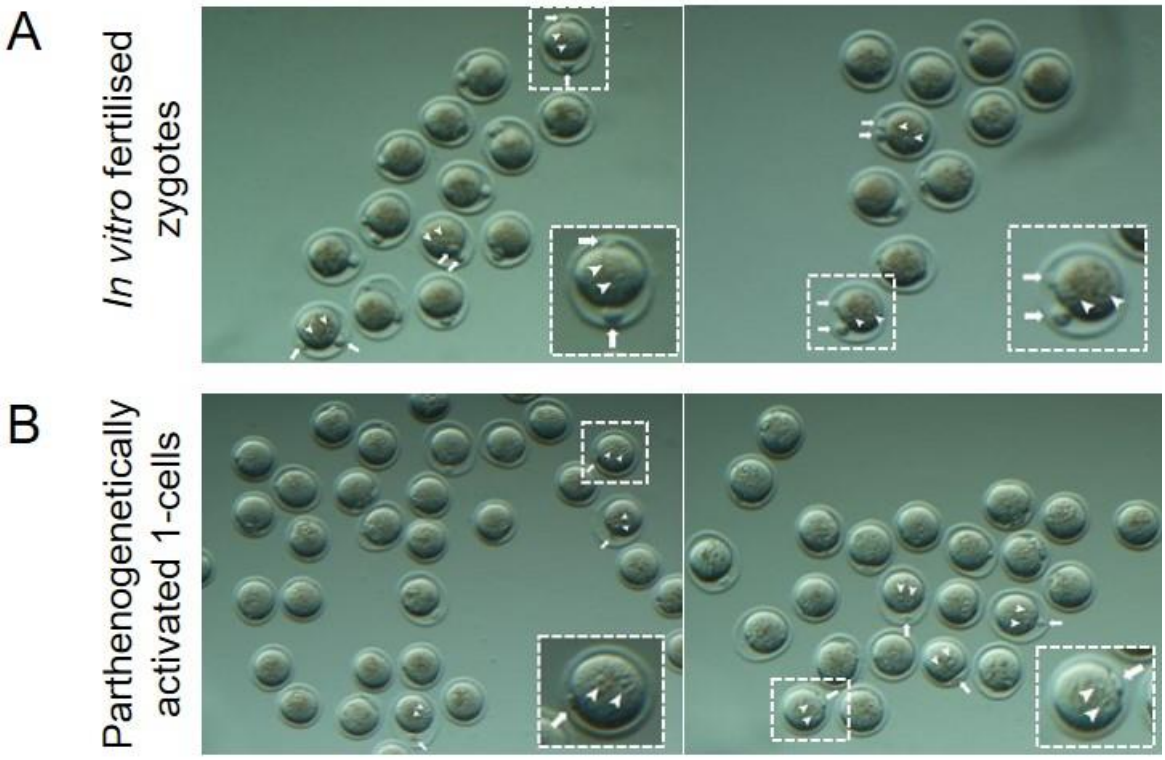
Yankiwski, V., Marciniak, R.A., Guarente, L., Neff, N.F., 2000. Nuclear structure in normal and Bloom syndrome cells. Proc. Natl. Acad. Sci. U.S.A. 97, 5214–5219. https://doi.org/10.1073/pnas.090525897

Yeager, T.R., Neumann, A.A., Englezou, A., Huschtscha, L.I., Noble, J.R., Reddel, R.R., 1999. Telomerase-negative immortalized human cells contain a novel type of promyelocytic leukemia (PML) body. Cancer Res. 59, 4175–4179.

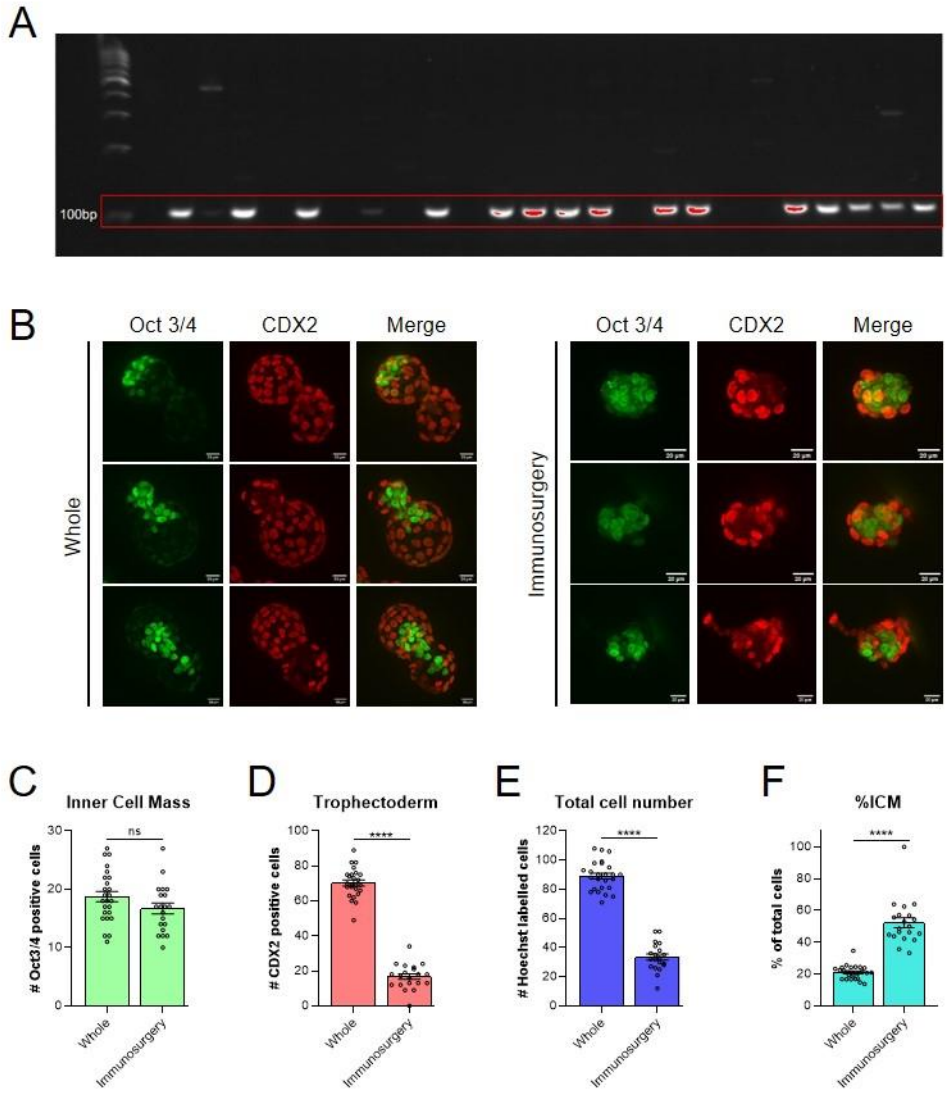
Yin, Y., Liu, N., Ye, X., Guo, R., Hao, J., Wang, F., Liu, L., 2014. Telomere elongation in parthenogenetic stem cells. Protein & Cell 5, 8–11. https://doi.org/10.1007/s13238-013-0006-z

Zalzman, M., Falco, G., Sharova, L.V., Nishiyama, A., Thomas, M., Lee, S.-L., Stagg, C.A., Hoang, H.G., Yang, H.-T., Indig, F.E., Wersto, R.P., Ko, M.S.H., 2010. Zscan4 regulates telomere elongation and genomic stability in ES cells. Nature 464, 858–863. https://doi.org/10.1038/nature08882

3.6 Supplementary information



Supplementary Figure 3.1. Parthenogenetically activated embryos are diploid
CBA.F1 MII oocytes were either fertilised with CBA.F1 sperm via IVF or parthenogenetically activated using strontium chloride in the absence of sperm. A) IVF zygotes were confirmed as fertilised by the presence of two polar bodies (arrows) and two pronuclei (arrow heads). B) Parthenogenetically activated 1C embryos were identified by the presence of two pronuclei (arrow heads) and only one polar body (arrow), indicating that the second set of chromosomes had not been extruded as a second polar body but instead were retained to form a diploid embryo (B).



Supplementary Figure 3.2. Confirmation of embryo sex and immunosurgery validation

Products from SRY qPCR on CBA.F1 blastocysts were visualised on a 4% agarose gel to confirm male embryos by presence of a band at 105bp (A). Blastocysts were left whole (left panels), or underwent immunosurgery to remove a substantial portion of the TE cells (right panels) followed by immunocytochemistry to identify the two unique cell populations and allow for individual cells to be counted (B). Oct3/4 (green) defined the ICM (C), and CDX2 (red) defined the TE (D), and the sum of which gave total number of cells present (E). The percentage of inner cell mass cells from the total cell number was calculated (F). n=25 whole and n=20 immunosurgery blastocysts. Data analysed using unpaired t-test, **** $p<0.0001$.

Supplementary table 3.1. n-values for telomere elongation and mtDNA copy number time course

♀	♂	MII	2C	4C	8C	Blastocyst
CBA.F1	CBA.F1	58	51	57	44	77
CBA	C57	31	51	50	52	51
CBA	CBA	32	39	37	42	41
C57	C57	17	37	38	39	52
CBA.F1	NA	17	50	49	51	79

Supplementary table 3.2. Proportion of telomere elongation with each cell division

♀	♂	MII	2C	4C	8C	Blast-ocyst
CBA.F1	CBA.F1	0	13.12 (+13.12%)	18.04 (+4.91%)	44.7 (+26.67%)	100 (+55.3%)
CBA	C57	0	14.25 (+14.25%)	18.7 (+4.45%)	35.69 (+16.99%)	100 (+64.31%)
CBA	CBA	0	1.17 (+1.17%)	1.17 (0%)	-8.2 (-9.38%)	100 (+108.2%)
C57	C57	0	-1.64 (-1.64%)	6.29 (+7.93%)	14.49 (+8.21%)	100 (+85.51%)
CBA.F1	NA	0	6.63 (+6.63%)	9.86 (+3.23%)	13.58 (+3.7%)	100 (+86.42%)

Number contained in parentheses indicates gain or loss in telomere length proportion from previous developmental stage

CHAPTER 4

ROTENONE-INDUCED MITOCHONDRIAL DYSFUNCTION DISRUPTS PRE-IMPLANTATION EMBRYO DEVELOPMENT AND TELOMERE LENGTH

4.1 Introduction

There are many scenarios where both mitochondrial and telomeric dysfunction coincide, suggesting that the two are functionally linked (Sahin et al., 2011; Sohal et al., 1994). For instance, telomeres and mitochondria both have critical roles in cellular lifespan and decline with age. This link is supported by extensive data, including induced telomere dysfunction resulting in decreased mitochondrial biogenesis, and increased mitochondrial dysfunction and therefore reactive oxygen species (ROS) production (Sahin et al., 2011). Perhaps the most well established mechanism in this link between mitochondria and telomeres is mitochondrial dysfunction inducing telomere damage and shortening via ROS generation. Generation of ROS through normal mitochondrial metabolism is typically well tolerated by the cell due to sequestering mechanisms, however in circumstances of aberrant mitochondrial function, ROS production can greatly exceed the anti-oxidant capacities of the cell, leading to oxidative damage to the mitochondria, mtDNA, and nuclear DNA (Cottrell and Turnbull, 2000; Edgar et al., 2009; Hiona et al., 2010). Of note, telomeres are particularly susceptible to oxidative damage as their TTAGGG sequence is rich in guanine residues (Oikawa and Kawanishi, 1999; von Zglinicki et al., 1995). Oxidative stress and subsequent damage to telomeres induces double stranded DNA breaks, increases base alteration rate in telomeric DNA, and greatly increases the rate of telomeric DNA shortening with each population doubling and inhibits proliferation, which leads to premature cellular senescence (Kawanishi and Oikawa, 2004; Oikawa and Kawanishi, 1999; von Zglinicki et al., 1995). To date, the majority of the literature surrounding a functional link between telomeres and mitochondria has focussed on situations of stress and mitochondrial or telomeric DNA damage and exacerbation of these phenotypes. Little is known about whether there are positive relationships occurring between telomeres and mitochondria and regulation of functions, particularly during early development.

Culturing embryos in high oxygen (20%) is known to disrupt embryo mitochondria, resulting in fewer mitochondria, and increased morphological abnormalities, decreased mtDNA copy number, and decreased mitochondrial membrane potential; this also leads to reduced blastocyst development rates and cell numbers, and even reduces implantation, pregnancy, and birth rates in humans (Belli et al., 2019; Ciray et al., 2009; Preis et al., 2007; Waldenström et al., 2009). Analysis of ICMs from

blastocysts that had been cultured in high oxygen following IVF revealed shorter telomeres than those cultured in low oxygen (5%, Fig. 3.12 A). This provocative data implicates mitochondrial function as an important factor in telomere elongation during pre-implantation embryogenesis. To further investigate the role of mitochondrial function in telomere elongation, the potent mitochondrial inhibitor rotenone was used to induce systemic mitochondrial dysfunction, including oocyte and embryo mitochondria. Rotenone is a naturally occurring compound that is found in the roots of several plant species and has been used as an insecticide and pesticide. Rotenone is a strong, reversible, specific inhibitor of the site of NADH oxidation on complex I of the mitochondrial respiratory chain (Fig. 4.1) by impeding electron transfer from complex I to coenzyme Q (CoQ), overall leading to a block in oxidative phosphorylation and reduced ATP synthesis (Palmer et al., 1968). Moreover, rotenone exposure has been associated with increased ROS production (Fato et al., 2009; Li et al., 2003).

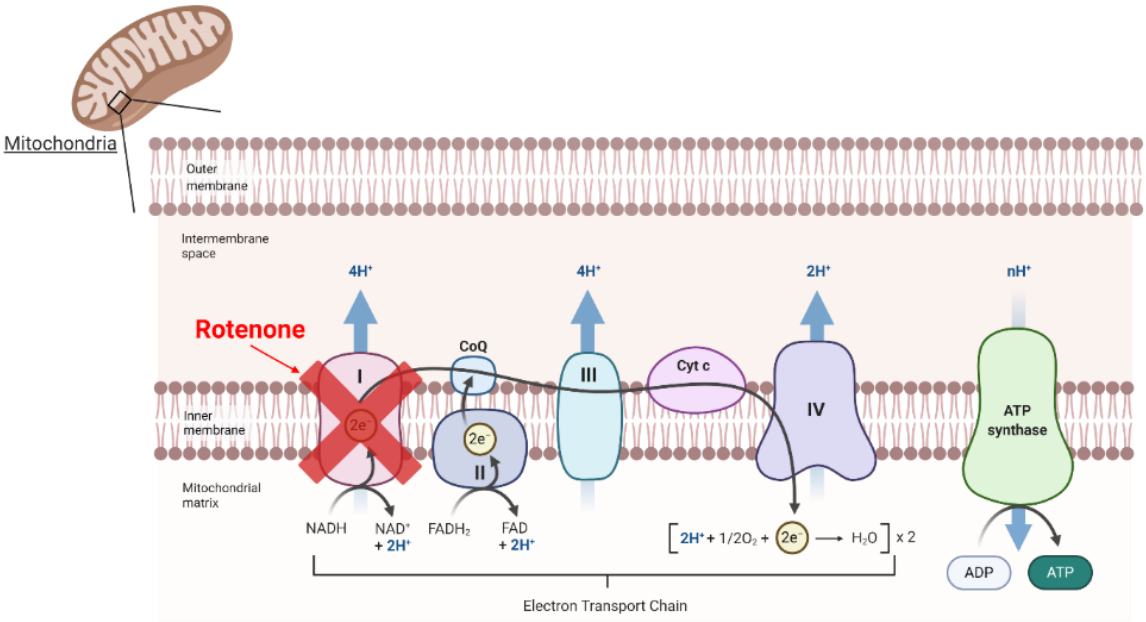


Figure 4.1. Rotenone inhibits the mitochondrial electron transport chain
Rotenone selectively inhibits Complex I of the respiratory chain, thereby preventing electron transfer and resulting in decreased ATP production via oxidative phosphorylation.

Lozoya et al. (2020) studied the impact of maternal exposure to rotenone through the diet prior to- and for the duration of pregnancy as well as lactation on the methylome

of offspring and found alterations, included advanced aging-related epigenetic patterns. Mitochondrial function of the offspring was also perturbed at 12 months of age in the rotenone exposed mice compared to controls, indicated by decreased mitochondrial complex I and coupled complex II activity, and decreased manganese superoxide dismutase (MnSOD) activity (Lozoya et al., 2020). Mothers exposed to rotenone diet also had a lower pregnancy rate, decreased litter size, and lower pup survival rate than controls (Lozoya et al., 2020), and these phenotypes are similar to what is seen in cases of maternal age and obesity. This work provides insight into how mitochondrial dysfunction during fetal development impacts fetal development as well aging phenotypes in adult offspring.

This study hypothesised that the advanced aging phenotype seen in offspring exposed to rotenone in utero (Lozoya et al., 2020) is due to decreased telomere lengths, thereby indicating advanced molecular aging in offspring. Further, this model of systemic mitochondrial inhibition is ideal to test the hypothesis that mitochondria are involved in telomere elongation events during preimplantation development. For this study, mice were treated with rotenone for three weeks as previously described prior to oocyte collection and *in vitro* fertilisation (IVF). Embryo development was closely monitored. Telomere length in mature oocytes, 8C embryos, blastocysts and the blastocyst inner cell mass (ICM) were assessed to determine if mitochondrial dysfunction perturbed elongation events (see Fig. 4.2, 'Experimental Design').

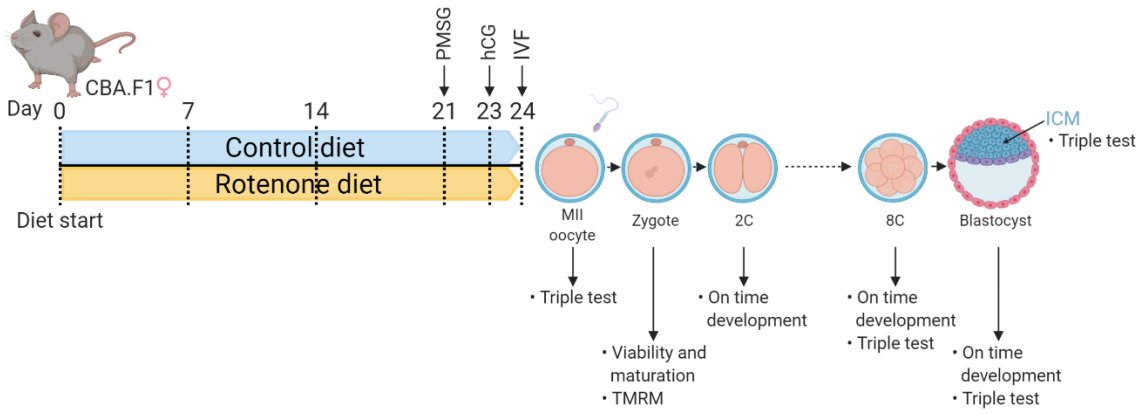


Figure 4.2. Experimental design

Mice were exposed to 150ppm of rotenone via their diet for three weeks before superovulation and IVF. Key developmental time points were analysed for successful development, morphology, and telomere length and mtDNA copy number via the Triple Test, as indicated.

4.2 Materials and Methods

4.2.1 Mice

Male CBA F1 mice at 8 weeks of age, and cohorts of 12 female mice at 7 weeks of age were obtained from the University of Adelaide's Laboratory Animal Services (LAS). Mice were maintained in 12h/12h light/dark conditions and given water *ad libitum*. Mice were allowed to acclimatise for five days with 10% fat rodent chow *ad libitum* prior to commencing the diet study. All animal experiments were approved by the University of Adelaide's Animal Ethics Committee and conducted in accordance with the Australian Code of Practice for the Care and Use of Animals for Scientific Purposes.

4.2.2 Rotenone diet

Rotenone diet was prepared and used as in Lozoya et al. (2020). Rotenone was sourced from Sigma. Control diet was a modified diet of AIN-93G that was suitable for irradiation (TD.97184), and Rotenone was formulated at 150ppm in TD.97184 meal diet by Teklad/Envigo exactly as for Lozoya et al. (2020). Both Control and Rotenone diets were irradiated and stored at 4°C. Mice were provided the diet for a period of three weeks. Food was available to mice *ad libitum* and was refreshed every two days. Mice were monitored daily for potential adverse health effects and none were observed.

4.2.3 Derivation of oocytes, early embryos, and blastocysts

Female mice were given 7.5IU pregnant mare's serum gonadotropin (PMSG, National Hormone and Pituitary Program) on day 21, followed by the equivalent dose of human chorionic gonadotropin (hCG, Pregnyl) 47.5 hours later (on day 23), each via intraperitoneal (ip) injection. Mice were culled at 15h post-hCG via cervical dislocation. Whole ovaries and oviducts were dissected from females and placed in pre-warmed (37°C) αMEM-HEPES handling media, supplemented with 1% FCS. Cumulus-oocyte complex (COC) clusters were isolated by puncturing oviducts using a 30G needle. For individual MII oocyte collection, complete cumulus cell removal was achieved via treatment with hyaluronidase (Seikagaku, #100741) for 5-10 minutes at 37°C, followed

by aspiration using a glass pipette pulled to an appropriate diameter. To generate embryos via IVF, whole COC clusters were gently washed twice in pre-warmed (37°C) fertilisation media (Vitro Fertilisation; Cook Australia, Brisbane, Australia), before being placed in a 100µL fertilisation drop containing the equivalent of 10µL of capacitated sperm from a male of proven fertility (referred to as 'fertilisation time'), before being returned to the incubator (37°C, 5% O_2, 6% CO_2) for 4 hours. Following this, fertilised oocytes were cleaned of all excess sperm and cumulus cells via gentle aspiration and transferred to a culture dish containing cleave media (Vitro Cleave; Cook Australia, Brisbane, Australia, 10 embryos per 20µL cleave media drop) and returned to the incubator until 24 hours post fertilisation time. At this time, the number of embryos that successfully reached the 2C state were scored. The remaining embryos were returned to the incubator until 55 hours post fertilisation time where a proportion of successful 8C embryos were collected for analysis. At 96 hours post fertilisation time the remaining embryos that had successfully reached the blastocyst stage were scored and all were collected for analysis. Collection times were kept constant across cohorts.

4.2.4 Blastocyst immunosurgery

Blastocysts first had their zona pellucida removed via treatment with Acidic Tyrode's Embryomax solution (Millipore, #MR-004D), washed twice in cleave media and transferred to a 200µL drop of cleave media containing 20% heat inactivated rabbit anti-mouse serum (Sigma, #M5774). Following a one hour incubation period (37°C, 6% CO_2, 5% O_2), blastocysts were washed three times in cleave media and transferred to a 200µL cleave media drop containing 20% guinea pig serum (Sigma, #G9774) and incubated for 15 minutes. Blastocysts were washed three times in cleave media and incubated for a further 30 minutes in cleave media. Dead TE cells were removed by gently aspirating ICMs in a finely drawn glass pipette.

4.2.5 Sample preparation for qPCR

Individual MII oocytes, 8C embryos, whole blastocysts, or ICMs were first washed three times in 1x phosphate buffered saline (PBS) containing 1mg/mL polyvinylpyrrolidone (PVP, Sigma), and transferred in 1µL to a 0.5mL PCR tube (Axygen, #PCR-05-C) for qPCR analysis. All samples were snap frozen in liquid nitrogen (LN_2), and stored at -80°C until use.

Samples had their nuclear genomic DNA (nDNA) and mitochondrial DNA (mtDNA) extracted by adding 9µL of lysis buffer (50mM Tris-HCl pH 8.0, 1mM EDTA, 200µg/mL Proteinase K, 0.5% Tween-20) to each sample with a volume of 1µL (final volume of 10µL) following brief centrifugation, and heated to 55°C for 2 hours, followed by 95°C for 10 minutes to inactivate Proteinase K activity. Samples were allowed to cool to 4°C and briefly centrifuged. Following this, 1µL of lysis product was removed and added to 9µL of sterile H_2O for mtDNA analysis and the rest kept for telomere and Rn18S analysis. For ICMs, an additional 10µL of pure, sterile water was added to give a final volume of 20µL, and this was used for mtDNA, telomere, and Rn18S analysis.

4.2.6 Triple test qPCR assay

To generate ‘calibrator’ DNA for use as a standard within every assay, a whole ovary from a 6 week old PMSG and hCG stimulated CBA female mouse was collected and had total DNA extracted (as described previously, see sections 2.2.2). DNA concentration and purity were quantified by NanoDrop One Microvolume UV-Vis Spectrophotometer and diluted to 2.5ng/µL.

qPCR was performed using Power SYBR Green PCR Master Mix (Applied Biosystems, #4367659), standard MicroAmp Optical 96-well Reaction Plates (Life Technologies, #4306737), and custom made primers (Sigma, forward and reverse primer sequences outlined in Table 3.1), using an Applied Biosystems 7900HT Fast Real-Time PCR system. Cycling conditions for all primers were set at 95°C for 10 minutes, followed by 40 cycles of 95°C for 10s, 60°C annealing for 30s and extension at 72°C for 30s, followed by standard melt curve cycling. Two repeat reactions were performed for each sample and each primer pair, using 2µL of sample per reaction.

For Rn18S and telomere analysis, the final reaction for each well was 10µL Power SYBR Green PCR Master Mix, 0.5µL each of forward and reverse primer (stock at 10µM), 2µL of sample, and sterile H_2O to a final volume of 20µL. To minimise any plate-to-plate variations, Rn18S and telomere reactions for each sample were run on the same plate, and calibrator DNA assays included on every plate.

For mtDNA analysis, the final reaction for each well consisted of 10µL Power SYBR Green PCR Master Mix, 0.2µL each of forward and reverse primer (stock at 10µM), 2µL of sample or standard, and sterile H_2O to a final volume of 20µL. Total mtDNA copy number was quantified using the standard curve method as previously described (Kameyama et al., 2010). Briefly, quantification standards were prepared by PCR amplifying a 1186bp fragment in the 12S rRNA region of mtDNA from mouse liver using the primer pair 5'-ACA CCT TGC CTA GCC A-3' and 5'-TTT GCC ACA TAG ACG AGT T-3'. The PCR product was extracted from the gel using QIAquick Gel Extraction Kit (Qiagen) and cloned using the Qiagen PCR Cloning Kit. Plasmid DNA was purified using QIAprep Spin Miniprep Kit (Qiagen), quantified by spectrophotometry, and diluted to 10^7 copies per 2µL. To create a standard curve, 10µL of standard stock was removed and serially diluted (1:10) from 10^7 to 10^1 copies, and standard curve correlation coefficients were consistently greater than 0.98. Serial dilutions were made fresh on the day. Total mtDNA copy number per sample was calculated according to the generated equation for Ct value against copy number for the corresponding standard curve (excluding 10^1 copies), and multiplied by the dilution factor of the sample i.e. total mtDNA copy number = (10^x) * [dilution factor], where x=(y-intercept of standard curve – Ct value of sample)/slope of standard curve.

Telomere and mtDNA relative to total cell number were calculated using the $2^{-\Delta\Delta Ct}$ method, where the ΔCt of the calibrator (telomere or mtDNA Ct – Rn18S Ct) was subtracted from the ΔCt of the sample (telomere or mtDNA Ct – Rn18S Ct) to give the ΔΔCt.

Table 4.1 qPCR primers

Primer target	Forward primer sequence	Reverse primer sequence
Telomere	5'-CGG TTT GTT TGG GTT TGG GTT TGG GTT TGG GTT TGG GTT-3'	5'-GGC TTG CCT TAC CCT TAC CCT TAC CCT TAC CCT TAC CCT-3'
mtDNA	5'-CGT TAG GTC AAG GTG TAG CC-3'	5'-CCA GAC ACA CTT TCC AGT ATG-3'
Rn18S	5'-AGA AAC GGC TAC CAC ATC CAA-3'	5'-CCT GTA TTG TTA TTT TTC GTC ACT ACC T-3'

4.2.7 TMRM

Fully denuded fertilised zygotes (confirmed by presence of 2 pronuclei) were washed twice in pre-warmed (37°C) cleave media and incubated for 30 minutes at 37°C in cleave media containing 25µM TMRM (Sigma, #T5428) with 1:250 Hoescht-3342 added for the final 15 minutes of the incubation. Samples were washed briefly in cleave media before being mounted in pre-warmed cleave media and imaged using a Cell Voyager CV1000 spinning disc confocal (Yokogawa) with a 40x objective.

4.2.8 Pronuclear cytosine methylation immunofluorescence

Fertilized zygotes (stage PN3 to PN4) were collected 6 hours after fertilisation. The zona pellucida was dissolved using Acid Tyrode's Embryomax solution (Millipore, #MR-004D), followed by a brief wash in phosphate buffered saline (PBS) containing 1mg/ml polyvinylpyrrolidone (PVP, Sigma) (PBS-PVP). Zygotes were fixed in 3.7% PFA-PBS for 20 minutes at room temperature (RT), followed by two five-minute washes in PBS-PVP, then permeabilised in 0.2% Triton X-100 (in PBS) for 10 minutes at room temperature, followed by three five-minute washes in PBS-PVP. Zygotes were incubated in 4N HCl solution for 10 minutes at RT, and washed thoroughly in 0.05% Tween-20 in PBS (PBS-T). Zygotes were blocked overnight at 4°C in blocking solution (1% BSA, 0.02% Triton X-100 in PBS), then incubated overnight at 4°C with mouse anti-5mC (1:200, Biorad, #ab10805), and rabbit anti-5hmC (1:600, Active Motif, #39769), diluted in blocking solution. Following three ten-minute washes in PBS-T,

samples were incubated for one hour at RT, while protected from light, with Alexa Fluor 594-conjugated goat anti-mouse (1:500, Invitrogen) and Alexa Fluor 488-conjugated goat anti-rabbit secondary antibodies (1:1000, Invitrogen). Samples were mounted on slides with 1.5µL Prolong™ Diamond Antifade Mountant (Invitrogen, #P36965) and examined using a Cell Voyager CV1000 spinning disc confocal (Yokogawa) with a 40x objective. Images were acquired using the same confocal microscope settings. Pronuclear size and staining intensity was calculated using ImageJ software. Mean signal intensity was calculated first by subtracting the signal from the cytoplasmic area (representing background staining), then dividing by the area of the pronuclei.

4.2.9 Blastocyst differential stain

Blastocysts were fixed late on day 5 in 4% PFA-PBS overnight at 4°C. Samples were washed once in PBS-PVP and incubated for 5 min at RT in 0.1M glycine, followed by 3x 5 min washes in PBS-PVP. Samples were permeabilised in 0.5% Triton X-100 for 30 min at RT, washed 3x in PBS-PVP and blocked for 1 hour at RT in 10% donkey serum (Sigma). Primary antibodies were diluted 1:500 (Oct 3/4 Santa Cruz #sc-8626, CDX2 Abcam #ab76541) in 10% donkey serum and samples incubated overnight at 4°C. Following 3x 5 min washes in PBS-PVP, samples were incubated in secondary antibodies at a dilution of 1:1000 for 1 hour (Life technologies, Alexa Fluor 594 donkey anti-rabbit and Alexa Fluor 488 donkey anti-goat), with 1:250 Hoescht-3342 added for the final 10 minutes of the incubation. Samples were mounted using Prolong™ Diamond Antifade Mountant (Invitrogen, #P36965) and imaged using a Cell Voyager CV1000 spinning disc confocal (Yokogawa) with a 40x objective and z-stacked with a 0.8µM step height. Z-stacks were imported to Image J and a maximum intensity z-project was created to enable counting of individual cells.

4.2.10 Statistical analysis

Results are presented as mean ± SEM. Telomere, mtDNA per cell, and total mtDNA copy number displayed as mean ± SEM overlayed on a violin plot to illustrate the distribution of data points. Analysis of normality showed that telomere and mtDNA data

required log transformation for statistical analysis. Statistical analysis was performed using Graph Pad Prism version 8 for Windows (GraphPad Software Inc., La Jolla, CA). Paired t-test, unpaired t-test, and one-way analysis of variance (ANOVA, comparison of means) were used as indicated and statistical significance was considered at P-value <0.05.

4.3 Results

4.3.1 *In vivo* rotenone exposure compromises oocyte quality and telomere length

Mice were monitored daily for adverse health issues and changes in behaviour, none of which presented and similar to (Lozoya et al., 2020), signifying that any effects seen on fertility are caused by rotenone-induced mitochondrial dysfunction and not due to systemic toxicity or poor overall health. Consumption of the rotenone diet did result in a minor weight change, with mice consuming rotenone lighter than those on the control diet at the time of tissue collection (control 20.64g ± 0.2816g, rotenone 19.4g ± 0.2582g, n=24 mice per group, analysed using unpaired t-test, p=0.0021). This small decrease in weight (~1g) is not expected to alter responses to hormones.

Mice began hormone stimulation after three weeks on their assigned diets and tissues were collected 15 hours after hCG administration. COCs underwent *in vitro* fertilisation (IVF) and oocyte quality was assessed four hours later (Fig. 4.3). The total number of oocytes ovulated were counted and surprisingly mice on the rotenone diet ovulated more oocytes than those on the control diet (control mice 30.17 ± 2.78 oocytes, rotenone mice 39.88 ± 2.62 oocytes, n=24 mice per group, analysed using an unpaired t-test, $p<0.02$). Oocytes were assessed for their quality and separated into three classifications based on their visual morphology (Fig. 4.3 A). Oocytes that were fragmented (Fig. 4.3 B, arrows) or otherwise degenerated (Fig. 4.3 B, arrow heads) were discarded and live oocytes were cultured further. Mice that had been exposed to rotenone had a higher proportion of degenerated oocytes than those on the control diet ($p<0.0001$, unpaired t-test) and as a result the proportion of live ovulated oocytes was reduced (Fig. 4.3 A). The number of live oocytes was not different between groups (control mice 26.96 ± 2.2 oocytes, rotenone mice 28.5 ± 2.23 oocytes, n=24 mice per group, unpaired t-test, p=0.533), indicating that rotenone exposure caused an increase in ovulation of non-viable oocytes. Live oocytes were further assessed for their maturation status (Fig. 4.3 C), identified as having a sizeable MII polar body and therefore deemed normal (Fig. 4.3 D, arrow heads), or having a very small polar body or no polar body at all, indicating abnormal maturation and likely meiotic arrest (Fig. 4.3 D, arrows). Mice that had been exposed to rotenone had higher proportions of abnormal maturation than those on the control diet (Fig. 4.3 C), signifying that

mitochondrial dysfunction induced by rotenone exposure was disrupting normal meiotic maturation processes in oocytes.

Next it was investigated whether this mitochondrial dysfunction was also affecting mitochondrial DNA copy number and telomere length in MII oocytes. Fully denuded morphologically normal MII oocytes were individually frozen and analysed using the Triple Test (Fig. 4.4). Rotenone diet resulted in shorter telomeres in MII oocytes compared to controls (Fig. 4.4 A), yet the total mtDNA copy number was unchanged in these oocytes (Fig. 4.4 B).

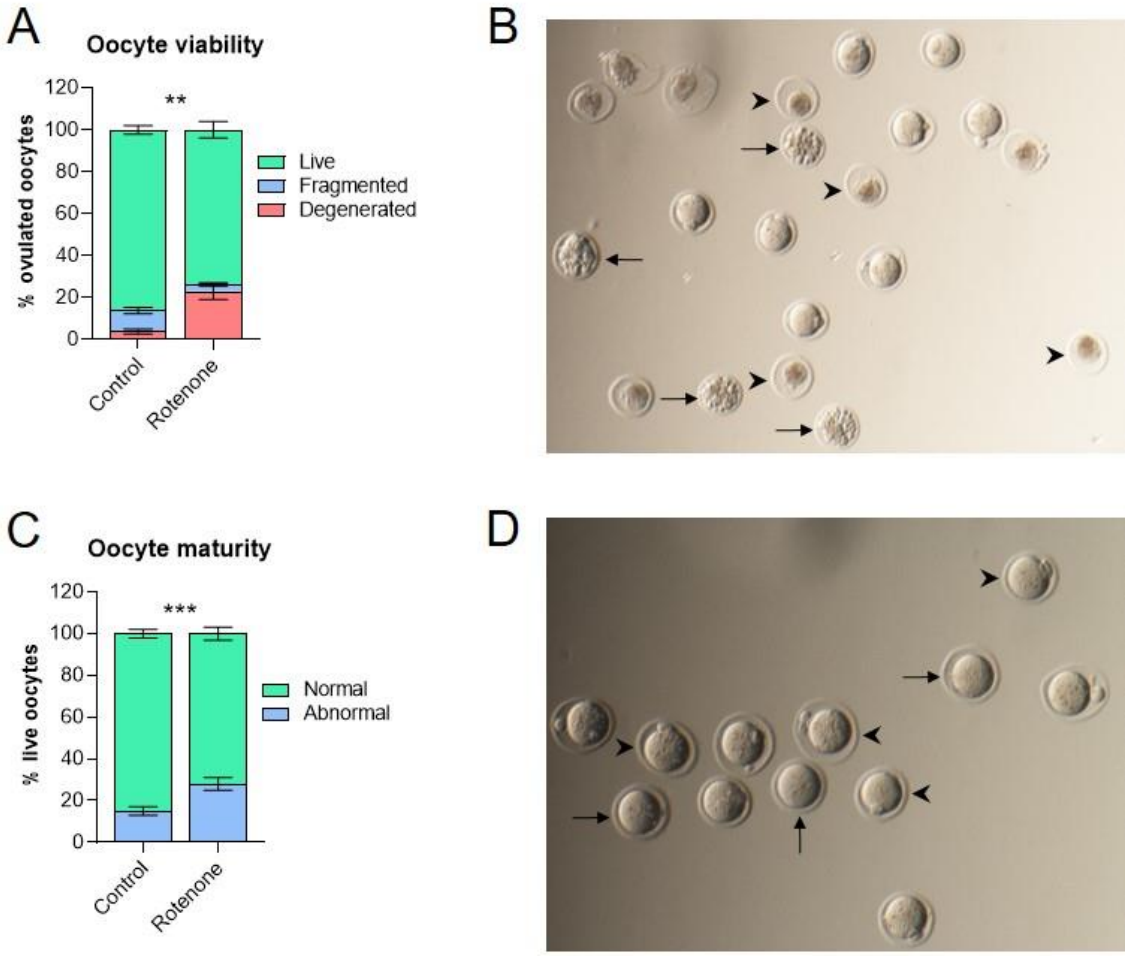


Figure 4.3. Oocyte quality following *in vivo* rotenone exposure

COCs were collected 15 hours after hCG administration and fertilised via IVF. Four hours after fertilisation, oocytes and presumptive zygotes were scored for viability (live, fragmented or degenerated, A & B where arrow heads indicate degenerated oocytes and arrows indicate fragmented oocytes) and maturity (presence of at least one polar body, C & D, where arrow heads indicate normally matured oocytes and arrows indicate abnormal maturation). n=24 mice per group, data analysed using unpaired t-test for the proportion of live (A) and normally matured (C) oocytes, ** p=0.0086, *** p=0.0006.

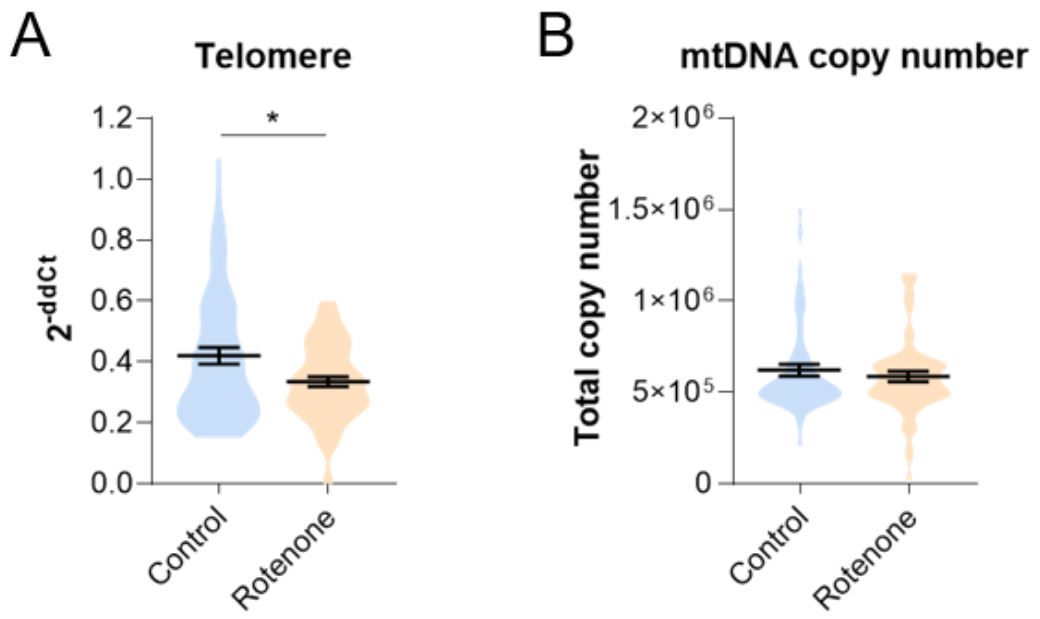


Figure 4.4. Telomere length in MII oocytes following *in vivo* rotenone exposure

Oocytes were collected 15 hours after hCG administration and a subset of fully denuded oocytes were individually frozen for Triple Test analysis. Relative telomere length (A) and total mtDNA copy number (B) were compared between control and rotenone-exposed oocytes. n=65 control and n=66 rotenone MII oocytes, log transformed data analysed using an unpaired t-test, * $p<0.02$. Shaded areas represent the population distributions, while horizontal lines represent mean ± SEM.

4.3.2 Rotenone induced mitochondrial dysfunction is present in zygotes and disrupts epigenetic reprogramming

To examine the extent of rotenone-induced mitochondrial dysfunction at the time of epigenetic reprogramming, zygotes were analysed six hours after fertilisation for disruptions in mitochondrial membrane potential using the fluorescent dye TMRM (Fig. 4.5 A). Quantification of fluorescence levels to give the Corrected Total Cell Fluorescence (CTCF) revealed that mitochondrial function was markedly inhibited in zygotes that had been exposed to rotenone as oocytes *in vivo*, as these zygotes had lower TMRM fluorescence than controls (Fig. 4.5 B).

To investigate whether the chronic mitochondrial dysfunction induced by rotenone exposure affects the dynamic epigenetic reprogramming of pronuclei, zygotes were collected 6 hours after fertilisation for global methylation pattern assessment of the maternal and paternal pronuclei (Fig. 4.6 A). In both experimental groups, the paternal pronucleus was larger in size than the maternal pronucleus, and the size of the respective pronuclei was not different between treatment groups (Fig. 4.6 B). Consistent with previous results (see Fig. 3.7), the level of 5mC fluorescence was higher in the maternal pronucleus than in the paternal for both groups, however the difference between pronuclei in zygotes from the rotenone group was less pronounced than in control zygotes, although absolute fluorescence levels were not different between groups (Fig. 4.6 C). Comparison of the 5mC fluorescence ratio between the paternal and maternal pronuclei, showed the ratio was higher, and closer to 1, in the rotenone zygotes when compared to controls (Fig. 4.6 C, right y-axis). The closer the fluorescence ratio is to 1, the more similar are the maternal and paternal pronuclei. Thus rotenone-exposed zygotes exhibit a marked reduction in maternal-specific 5mC.

When comparing 5hmC in pronuclei, both groups displayed higher levels of 5hmC fluorescence in the paternal pronucleus than the maternal. However, similar to 5mC, the difference between the pronuclei was not as prominent in zygotes from the rotenone group (Fig. 4.6 D). Interestingly, rotenone exposure was associated with a higher 5hmC intensity in the maternal pronuclei than in control embryos, but no differences were seen between paternal pronuclei (Fig. 4.6 D). When assessing the fluorescence ratio between pronuclei of a zygote, the 5hmC ratio should be much higher than 1, as the paternal pronuclei have much greater 5hmC levels than the

maternal. The paternal/maternal 5hmC ratio was reduced in the rotenone group compared to the control zygotes, demonstrating that, as with 5mC, the levels of 5hmC fluorescence are more similar between the pronuclei of rotenone exposed zygotes than controls (Fig. 4.6 D, y-axis). This indicates that increased 5hmC on maternal pronuclei is leading to a loss of the normal paternal-biased pattern.

Taken together, these results indicate that rotenone exposure caused lasting mitochondrial dysfunction which dysregulated the epigenetic reprogramming that takes place following fertilisation. In particular, the levels of 5mC in the maternal and paternal pronuclei are more similar to one another than in the control zygotes, and the maternal pronuclei contained higher 5hmC levels in rotenone treated zygotes than controls. This alteration in epigenetic reprogramming could have implications for gene expression in the developing embryo, however further in-depth characterisation of epigenetic changes is required.

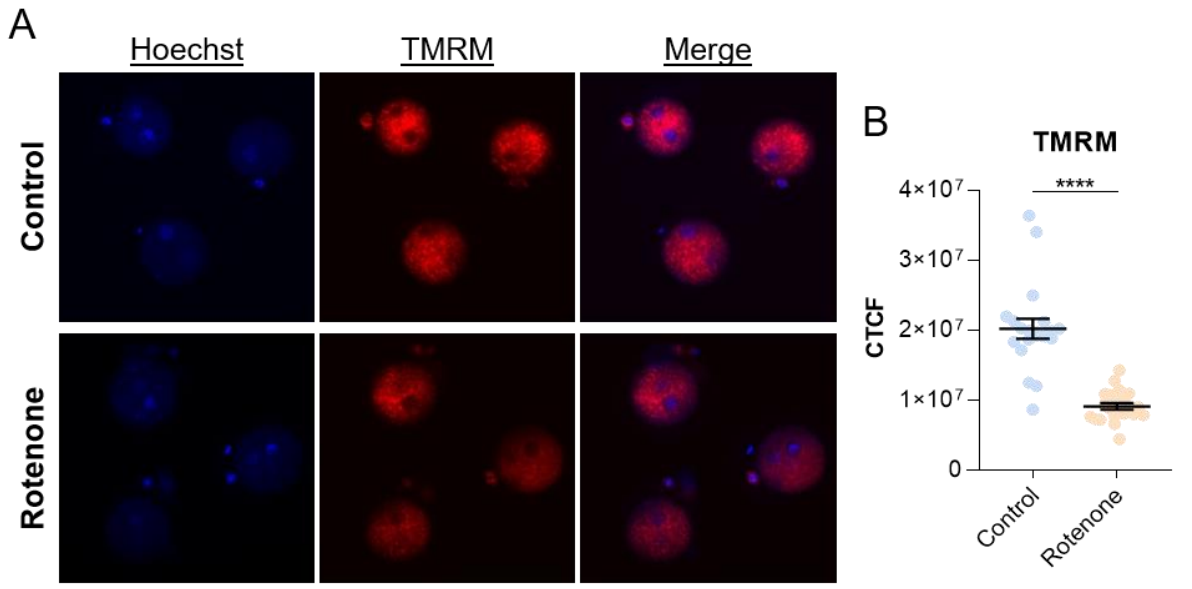


Figure 4.5. Zygote mitochondrial membrane potential

Zygotes were collected six hours after fertilisation and co-stained with mitochondrial membrane potential indicator TMRM, and Hoechst-3342 to identify pronuclei (A). Total cell fluorescence was calculated and adjusted for background fluorescence using Image J to give the corrected total cell fluorescence (CTCF, B). Data analysed using an unpaired t-test, **** $p<0.0001$.

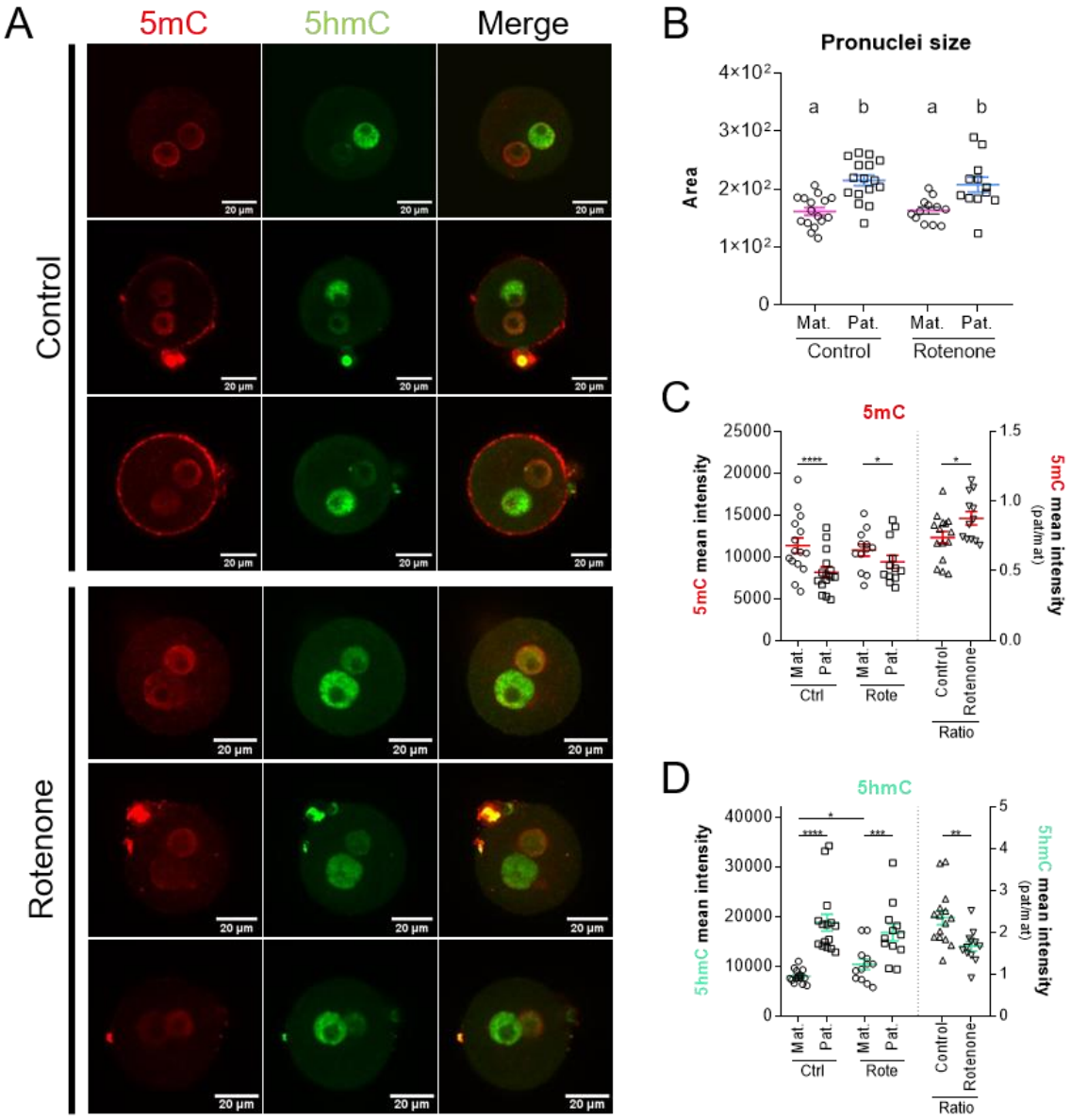


Figure 4.6. Methylation patterns in fertilised zygotes

Zygotes were collected 6 hours after fertilisation and co-stained with anti-5mC (red) and anti-5hmC (green) antibodies (A). Pronuclei size was measured (B) and signal intensity fluorescence levels were quantified for 5mC (C) and 5hmC (D) in maternal and paternal pronuclei. Data presented as signal intensity for maternal (Mat.) and paternal (Pat.) pronuclei on the left axis, and the ratio of the signal for paternal to maternal fluorescence on the right axis. Data analysed using paired t-test for comparisons between maternal and paternal pronuclei of the same oocytes, and unpaired t-test for pronuclei comparisons and ratio comparisons between groups. For B, $p<0.02$, for C & D * $p<0.05$, ** $p=0.0038$, *** $p=0.0003$, **** $p<0.0001$.

4.3.3 Rotenone exposure impairs early embryogenesis and alters telomere elongation dynamics

Morphologically normal MII oocytes were fertilised via IVF and capacity for successful fertilisation was identified by the percentage that successfully developed to 2C embryos 24 hours after fertilisation (Fig. 4.7 A). Rotenone treatment impacted the oocyte competence to fertilise and cleave as on-time 2C embryo development was reduced compared to controls (mean 2C development was 80% in controls and 47% in the rotenone treated group, Fig. 4.7 A). The 2C embryos continued in culture and were assessed for on-time 8C development (Fig. 4.7 B). Rotenone treatment caused a decrease in the number of 2C embryos that reached 8C at the expected time (mean on time development was 93% for controls and 77% for rotenone embryos, Fig. 4.7 B). At this time, a proportion of on-time 8C embryos were individually frozen and analysed for telomere length and total mtDNA copy number using the Triple Test (Fig. 4.7 C & D). Interestingly, the opposite trend in telomere length was seen in 8C embryos compared to MII oocytes, with rotenone embryos having slightly longer telomeres than control embryos (Fig. 4.7 C), indicating the initial deficit in telomere length seen in oocytes was not detectable, and that elongation exceeded that in control embryos. Total mtDNA copy number was not different in 8C embryos derived from control or rotenone exposed oocytes (Fig. 4.7 D).

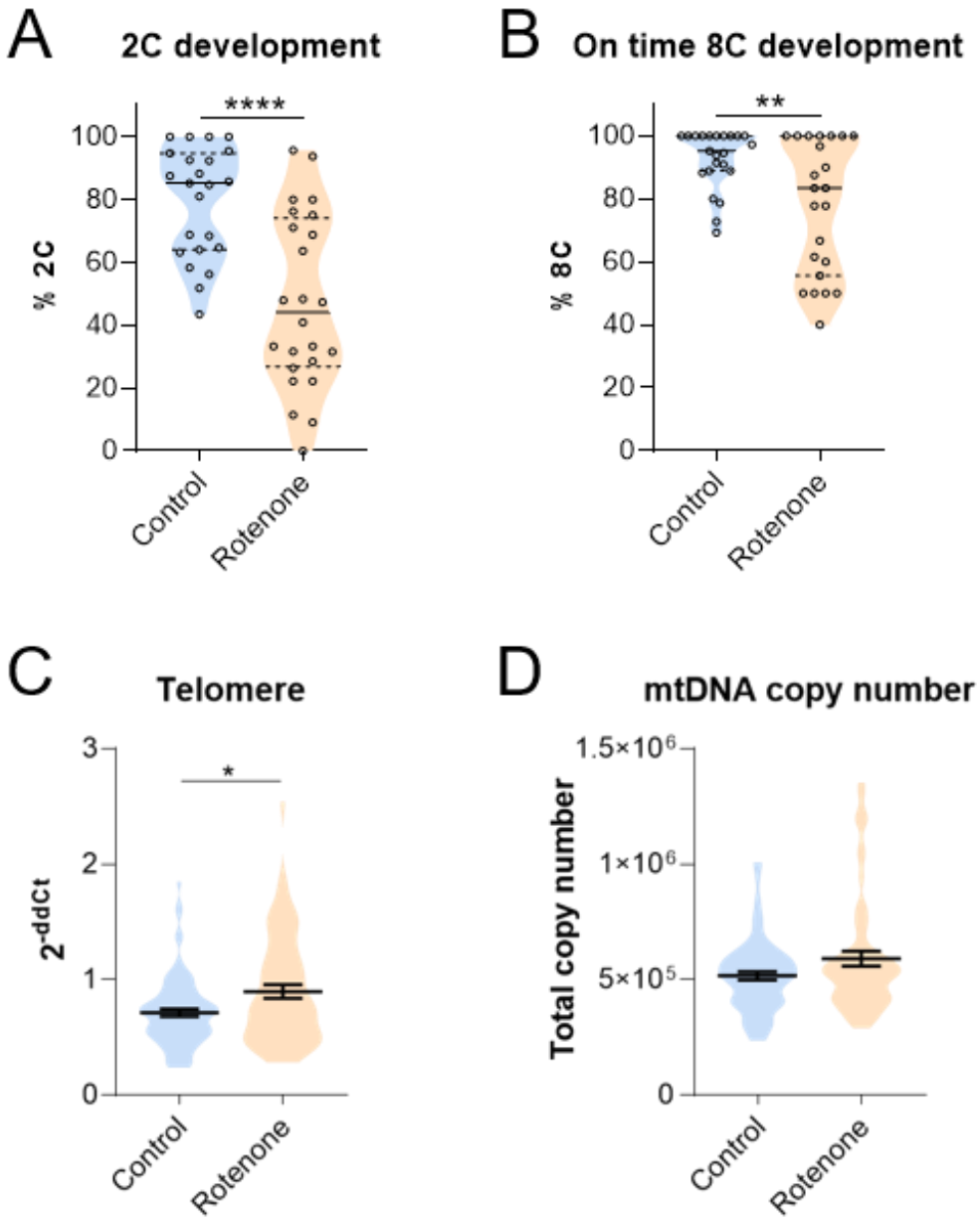


Figure 4.7. Two-cell and eight-cell embryo development rates and eight-cell telomere length and mtDNA copy number

Oocytes were fertilised via IVF and scored 24 hours later for successful development to the 2C stage (A) and 56 hours later for on time development to the 8C stage (B). A proportion of 8C embryos were collected and individually analysed for telomere length (C) and total mtDNA copy number (D) using the Triple Test and data log transformed for analysis. n=24 females per group for embryo development, n=86 for control and n=61 for rotenone 8C embryos for Triple Test analysis. Data analysed using unpaired t-test, * $p<0.02$, ** $p<0.005$, **** $p<0.0001$. Shaded areas represent the population distributions, while horizontal lines represent mean ± SEM.

4.3.4 Rotenone exposure decreases blastocyst cell numbers

On-time development was reduced at both the 2C and 8C stage in embryos that were derived from oocytes that had been exposed to rotenone (Fig. 4.7 A and B, respectively). Despite this, rotenone exposure did not impact the proportion of 2C embryos that successfully developed to blastocysts on-time (Fig. 4.8 A); however the proportion of blastocysts that had begun hatching at 96-hours after fertilisation was reduced (Fig. 4.8 B). To determine if rotenone exposure delayed the number of cell divisions that had occurred since blastulation, the inner cell mass (ICM), trophectoderm (TE), and nuclei were labelled in day five blastocysts and quantified (Fig. 4.8 C). A decrease was seen in the number of inner cell mass (Fig. 4.8 D) and trophectoderm (Fig. 4.8 E) cells in the rotenone group when compared to control blastocysts, in line with a reduced total cell number compared to controls (Fig. 4.7 F). The percentage of total cells in the blastocyst that were identified as ICM was not different between the two groups (Fig. 4.7 G), suggesting that the proliferation of both cell types in the rotenone blastocysts was slowed, leading to proportional decreases in both the ICM and TE cell types.

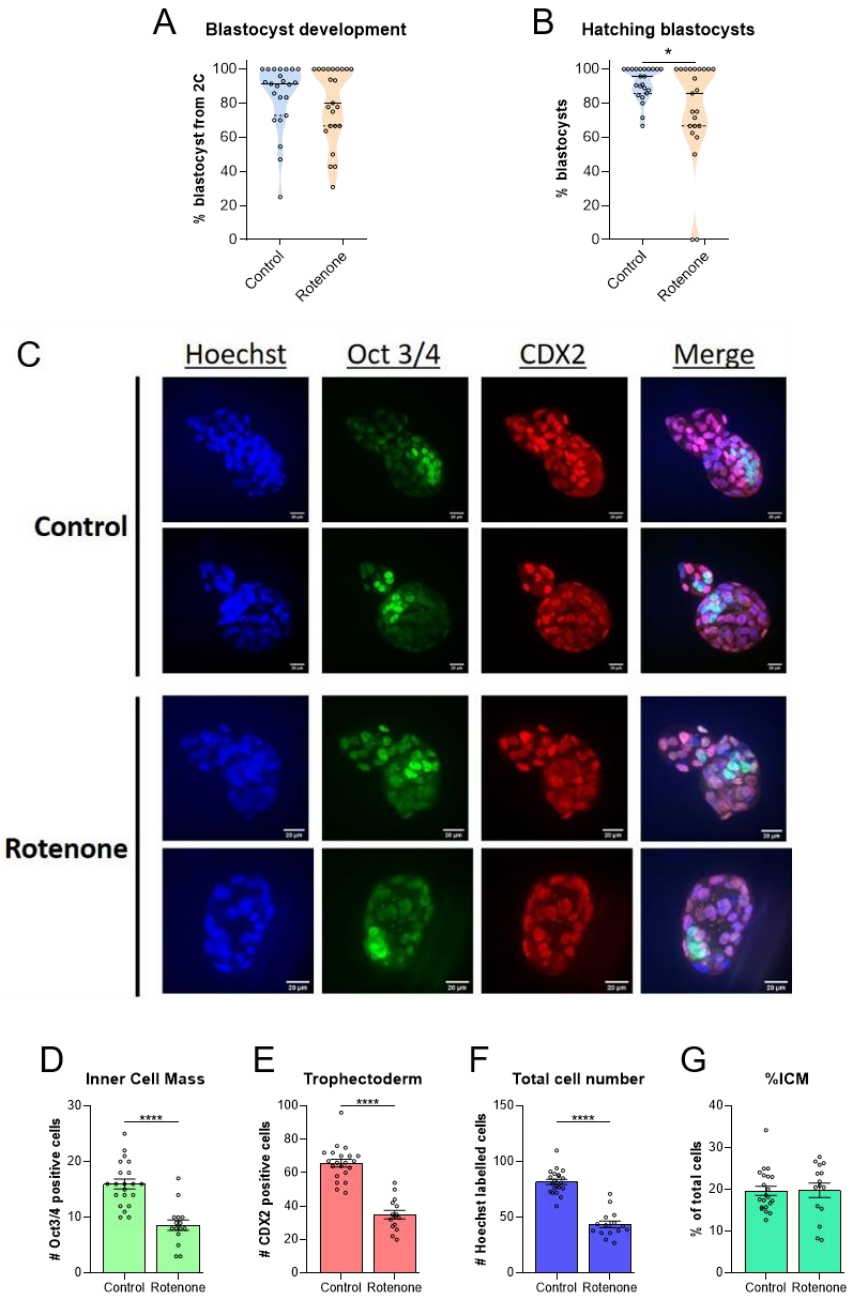


Figure 4.8. Day 5 blastocyst development

Blastocyst development was scored 96 hours post-fertilisation (A), and the proportion of successful blastocysts that had begun hatching was assessed (B). Blastocysts were collected 6 hours later and underwent immunocytochemistry to identify the two specified cell populations and allow individual cells to be counted (A). Oct3/4 (green) defines the ICM (B), CDX2 (red) defines the TE (C), and Hoechst (blue) marks all cells (D). The percentage of inner cell mass cells from the total cell number was calculated for each embryo (E). n=24 females for blastocyst development, n=21 control and n=15 rotenone for cell counts. Data analysed using unpaired t-test, * p=0.022, **** p<0.0001.

4.3.5 Oocyte rotenone exposure correlates with decreased blastocyst telomere lengths

To determine how rotenone inhibition of mitochondrial activity in oocytes influenced telomere elongation at the blastocyst stage, whole blastocysts underwent the Triple Test to analyse telomere length and mtDNA content (Fig. 4.9). Blastocysts derived from oocytes that were exposed to rotenone exhibited shorter telomeres than controls (Fig. 4.9 A). This result, combined with the observations of telomere lengths in 8C embryos, which were not reduced in rotenone embryos, indicates that mechanisms utilised for telomere elongation prior to-8C and post-8C embryo development are differentially impacted by mitochondrial dysfunction. Remarkably, mtDNA per cell and total mtDNA copy number were not negatively impacted by rotenone-induced mitochondrial dysfunction (Fig. 4.9 B, C).

Telomere elongation was directly compared across the three analysed developmental stages (MII, 8C, blastocyst) for both treatment groups to determine if normal telomere elongation patterns were occurring (Fig. 4.9 D, E). In both the control and rotenone groups, 8C embryos exhibited longer telomeres than MII oocytes, and likewise blastocysts displayed longer telomeres than the 8Cs, thus telomere elongation was occurring in both the pre-compaction and post-compaction phases of development.

To determine if the telomere length defects detected in whole blastocysts were present in the cells that form the foetus (ICM), ICMs were immunosurgically isolated from blastocysts and analysed via the Triple Test (Fig. 4.9 F & G). Telomere lengths were decreased in ICMs from rotenone-exposed oocytes (Fig. 4.9 F), and consistent with other stages of development, the mtDNA per cell not affected (Fig. 4.9 G).

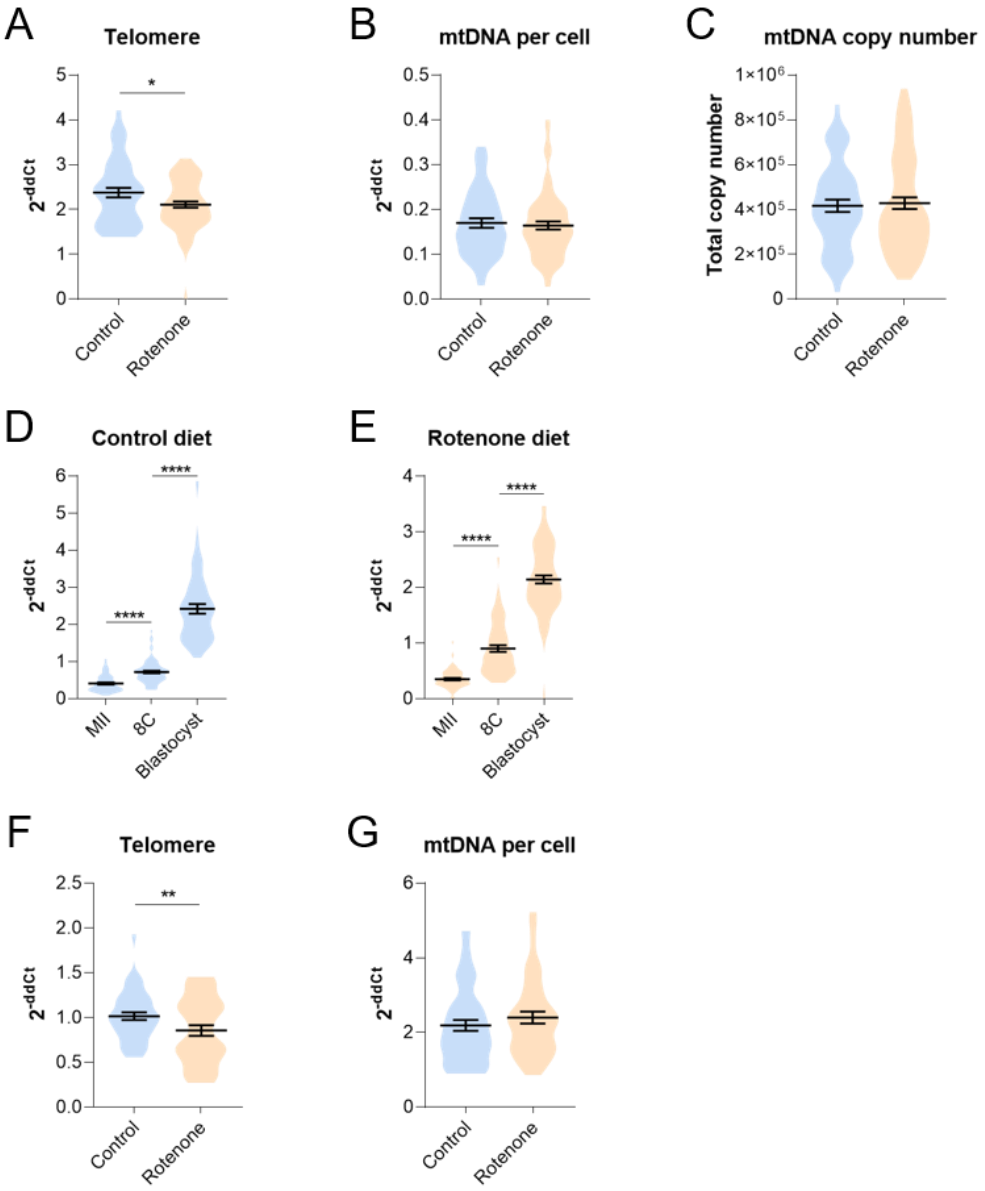


Figure 4.9. Telomere elongation during embryogenesis and telomere length in blastocysts and ICM populations

Individual whole blastocysts and immunosurgery purified ICMs were analysed using the Triple Test for telomere content (A & F), mtDNA per cell (B & G), and total mtDNA copy number (C), respectively. Telomere elongation between each developmental stage was compared for control embryos (D) and rotenone embryos (E) by combining with the data from MII oocytes (Fig 4.4) and 8C embryos (Fig 4.9). For telomere length analysis, n=45 control and n=69 rotenone blastocysts, and n=42 control and n=38 rotenone ICMs for the Triple Test. Log transformed data analysed using unpaired t-test (A-C, F, G), or one-way ANOVA (D, E), * $p<0.03$, ** $p=0.0075$, **** $p<0.0001$. Shaded areas represent the population distributions, while horizontal lines represent mean ± SEM.

4.4 Discussion

Rotenone exposure resulted in many ovulated oocytes being unviable or improperly matured with perturbed embryo development in all analysed measures, with the exception of on-time blastocyst development from 2C. While mtDNA copy number was not adversely impacted, telomere length was reduced in MII oocytes, blastocysts, and the inner cell mass. Interestingly, global zygote methylation patterns were altered, with less 5mC and more 5hmC seen in the maternal pronuclei of rotenone exposed zygotes compared to controls. The results of this study implicate oocyte mitochondrial function as a key regulatory mechanism in embryo telomere elongation and zygote epigenetic reprogramming.

Rotenone exposure results in shorter oocyte and blastocyst telomeres

Telomere length reprogramming is a critical process that occurs during pre-implantation embryogenesis. It has previously been demonstrated that oocyte telomere lengths do not change during meiosis (Fig. 3.2 A), therefore the observation that MII oocytes that have been exposed to rotenone have shorter telomeres (Fig. 4.4 A) alludes to the notion that this has resulted from telomere shortening, rather than deficiencies in elongation. During meiosis, up to 40% of oocyte mitochondria localise around the developing MI spindle and remain associated without the spindle during its migration to the cortex, before dispersing by MII arrest (Dalton and Carroll, 2013). This localisation brings a significant proportion of mitochondria into very close proximity with the nuclear DNA, and is considered likely to increase exposure of DNA to ROS produced by dysfunctional mitochondria (resulting from rotenone treatment). As telomeres are known to be highly sensitive to ROS-induced damage and oxidation (Kawanishi and Oikawa, 2004; Oikawa and Kawanishi, 1999; von Zglinicki et al., 1995), this provides a rational mechanism by which rotenone-induced mitochondrial dysfunction can result in MII oocytes with shorter telomeres than controls.

Curiously, despite rotenone-exposed oocytes exhibiting shorter telomeres than control oocytes, the 8C embryos resulting from these oocytes had longer telomeres than controls (Fig. 4.7 C). By the blastocyst stage however, telomeres in embryos derived from rotenone-exposed oocytes were once again shorter than controls (Fig. 4.9 A). It has been proposed that telomere elongation during pre-implantation embryogenesis occurs via two distinct mechanisms, with Alternative Lengthening of Telomeres (ALT)

occurring in the early stages, and the later stages (morula-blastocyst) being mediated by telomerase (Liu et al., 2007). Telomere length analysis in this study may add further support to this theory as telomere elongation was not inhibited as a result of alterations in mitochondrial function by the 8C stage. Another explanation for this observation could be that, like several processes, early telomere elongation is coordinated by maternally derived mRNAs and proteins already present in the mature oocyte, therefore their expression and/or function may not be impeded by mitochondrial dysfunction.

The observation of shorter telomeres in whole blastocysts, and ICMs, suggests that a second mechanism is responsible for elongation during this time that is susceptible to perturbations in mitochondrial function. Telomerase activity has been well characterised in blastocysts, and studies inducing oxidative stress in cancer cells have shown that ROS supresses telomerase activity (Ahmed and Lingner, 2018); thus suggesting ROS-mediated telomerase activity suppression, rather than telomere attrition, as a mechanism by which blastocysts and ICMs derived from rotenone-exposed oocytes end up with shorter telomeres. Further, TERT, the catalytic component of the telomerase enzyme, is known to be redistributed under circumstances of cellular stress is exported from the nucleus and accumulates in the mitochondria. Here, TERT binds to and protects mtDNA, which is hypothesised to help maintain proper electron transport chain function, and in parallel, ROS levels decrease (Rosen et al., 2020). The embryos in this study are expected to be experiencing oxidative stress as a result of oocyte rotenone exposure. Therefore TERT may be preferentially localising in the mitochondria at this time to try to stabilise function, leading to a decrease in the rate of telomere elongation, thus resulting in shorter telomeres. As telomere elongation still occurred between each analysed developmental stage (Fig. 4.9 D, E), mitochondrial function is not a sole regulator of pre-implantation telomere elongation, but must still play a critical role in this process.

Shorter telomeres in the ICM lineage of the rotenone group (Fig. 4.9 F) indicate that mitochondrial dysfunction originating in the oocyte may result in offspring born with shorter telomeres that may have implications for their life- and health-span. Therefore future work should build on these results and those from the previous study (Lozoya et al., 2020) by analysing offspring for telomere length, mtDNA content, and mtDNA mutation load in various tissues, as well as premature onset of aging phenotypes and disease characteristics.

Mitochondrial dysfunction does not affect mtDNA copy number

Despite rotenone being a potent inhibitor of mitochondrial function, no decreases in mtDNA copy number were observed in the analysed oocyte and embryo stages. This observation is likely explained due to suppression of mtDNA replication until after the blastocyst stage in mice (Pikó and Taylor, 1987). While mtDNA copy number was not altered, mtDNA damage and mutation load were not assessed in this study. A study exposing rats to rotenone found no alterations to mtDNA copy number in muscle or blood even after exposure to 3mg/kg of rotenone per day for 5 days (Sanders et al., 2014). However, the amount of mtDNA damage per 10kb greatly increased following even one day of treatment (Sanders et al., 2014). mtDNA damage and mutations are known to contribute to mitochondrial dysfunction (reviewed in Boczonadi and Horvath, 2014; Greaves et al., 2012) and may theoretically be a mechanism by which this dysfunction could persist after mitochondrial biogenesis is resumed in late blastocysts.

Mitochondrial dysfunction induced epigenetic alterations begin at fertilisation

Epigenetic reprogramming begins to take place in the zygote prior to the first cleavage and is characterised by rapid demethylation of the paternal pronucleus (with the exception of paternally imprinted genes) and protection of the methylation landscape in the maternal pronucleus. It is thought that these changes allow the zygote to erase the inherited epigenetic profile and regain developmental totipotency (Seisenberger et al., 2013). Rotenone exposure resulted in alterations to epigenetic reprogramming in zygotes (Fig. 4.6). While typical differences in pronuclei size were observed, the relative fluorescence of 5mC and 5hmC between the maternal and paternal pronuclei appeared more similar to one another than in control zygotes; signifying sensitivity to perturbations in mitochondrial function. The previous study using rotenone to investigate the effects of mitochondrial toxicant exposure during gestation utilised the viable yellow agouti mouse (A^{vy}) strain, as the coat colour of these mice reflects the epigenetic status of a locus which is established before the differentiation of the three germ cell layers at gastrulation. Authors saw a shift in offspring coat colour towards the hypomethylated state of this locus when mothers had been exposed to rotenone (Lozoya et al., 2020). The current study further supports the role for rotenone exposure in altered epigenetic reprogramming and reveals that this may occur from fertilisation. The fact that both 5mC and 5hmC levels are perturbed in zygotes indicates that mitochondrial dysfunction may be affecting the enzymes responsible for maintenance

or establishment of 5mC marks, and those responsible for catalysing the conversion of 5mC to 5hmC (active demethylation). The mechanism for this action likely lies in the reliance of these epigenetic regulatory enzymes on metabolites for their function (Reid et al., 2017). Therefore, mitochondrial dysfunction leading to a deficiency or accumulation of these metabolites has the potential to alter the epigenetic landscape of the genome and thereby dictate cellular phenotype (reviewed in Frezza, 2017). Future work to further interrogate this concept may include addition of metabolites to IVF media during the fertilisation period up to the end of the first cell cycle (2-cell stage) to identify if restoration of pronuclear reprogramming characteristics occurs. In addition, this work could be coupled with more quantitative measures for changes in methylation levels and also analysis of alterations to histone modifications (such as H3K9me3 levels).

Mitochondrial function influences oocyte quality

Ovulation is a tightly regulated process encompassing multiple physiological systems that culminates in the on-time release of high-quality oocytes from the ovary and requires coordination of multiple factors ((Robker et al., 2018). The observation that mice exposed to rotenone ovulated more oocytes than controls, as well as a higher incidence of degenerated oocytes being ovulated (Fig 4.3 A), suggests that metabolism may be a key regulator of follicle selection and ovulation. The higher proportion of degenerated oocytes indicates that metabolic dysfunction during key times of follicle growth and ovulation allows for unhealthy and potentially apoptotic oocytes to be ovulated from follicles that are likely atretic.

A higher proportion of the live oocytes ovulated from mice exposed to rotenone had failed to successfully complete polar body extrusion than from controls (Fig 4.3 C). Studies have demonstrated that rotenone inhibits microtubule assembly through tubulin binding (Brinkley et al., 1974; Marshall and Himes, 1978; Srivastava and Panda, 2007). These studies were conducted in mitotic cells and found rotenone-dependent inhibition of microtubule assembly resulted in mitotic arrest. It is entirely plausible that the defects seen in oocyte maturation are also due to rotenone's effect on microtubule assembly, as microtubule formation is required for the separation of homologous chromosomes in meiosis I, and attachment to sister chromatids in pro-metaphase of meiosis II. Not only could improper microtubule formation account for

abnormal oocyte maturation, resulting in a lack of polar body extrusion, it could also account for the decrease seen in 2C development rates from oocytes that were exposed to rotenone (Fig. 4.7 A). From control mice, 85% of live oocytes ovulated were properly matured, and 80% of total live oocytes progressed to 2C, suggesting that a small proportion of mature oocytes were not able to fertilise or cleave. In rotenone-exposed live oocytes, 72% were properly matured, however only 47% of total live oocytes successfully progressed to 2C, suggesting that a much higher proportion of mature oocytes were unable to fertilise or cleave. While these oocytes may have been able to progress through meiosis I, improper microtubule assembly may have inhibited the completion of meiosis II, thereby rendering the oocyte incapable of cleaving into a 2C embryo. Given that issues in microtubule formation or attachment are also linked to ploidy status (reviewed in Kitajima, 2018), an important consideration that was not addressed in this study is the ploidy of those embryos that did develop through to blastocysts, as this may affect gene dosage, and warrants further investigation.

Summary and outstanding questions

This study has provided the first insight into mitochondria as a mechanism for the regulation of telomere elongation during pre-implantation embryogenesis and is critically relevant to physiological scenarios where oocyte metabolism is known to be compromised. This work also sheds further light on the mechanisms by which this telomere elongation occurs, as early elongation occurred independently of normal mitochondrial function, while elongation after the 8C stage was impaired when mitochondrial dysfunction was induced. Future work should aim to quantify the levels of mtDNA and nuclear DNA damage occurring as a result of rotenone exposure, and whether addition of mitochondrial activators or metabolites to IVF media can restore the defects in epigenetic and telomere length reprogramming observed here.

Perturbations to oocyte mitochondrial function are observed and associated with the decline in fertility and ART success outcomes in advanced maternal aging (Eichenlaub-Ritter et al., 2011) and maternal obesity (Grindler and Moley, 2013; Wu et al., 2015). This work provides a simple and efficient model to examine the impacts of mitochondrial dysfunction on oocyte quality and embryo development induced by the maternal environment without other complications associated with models of advanced maternal age and obesity, such as greatly reduced ovulation rates.

4.5 References

Ahmed, W., Lingner, J., 2018. PRDX1 and MTH1 cooperate to prevent ROS-mediated inhibition of telomerase. Genes & Development 32, 658–669. https://doi.org/10.1101/gad.313460.118

Belli, M., Zhang, L., Liu, X., Donjacour, A., Ruggeri, E., Palmerini, M.G., Nottola, S.A., Macchiarelli, G., Rinaudo, P., 2019. Oxygen concentration alters mitochondrial structure and function in *in vitro* fertilized preimplantation mouse embryos. Human Reproduction 34, 601–611. https://doi.org/10.1093/humrep/dez011

Boczonadi, V., Horvath, R., 2014. Mitochondria: Impaired mitochondrial translation in human disease. The International Journal of Biochemistry & Cell Biology 48, 77–84. https://doi.org/10.1016/j.biocel.2013.12.011

Brinkley, B.R., Barham, S.S., Barranco, S.C., Fuller, G.M., 1974. Rotenone inhibition of spindle microtubule assembly in mammalian cells. Experimental Cell Research 85, 41–46. https://doi.org/10.1016/0014-4827(74)90210-9

Ciray, H.N., Aksoy, T., Yaramanci, K., Karayaka, I., Bahceci, M., 2009. In vitro culture under physiologic oxygen concentration improves blastocyst yield and quality: a prospective randomized survey on sibling oocytes. Fertility and Sterility 91, 1459–1461. https://doi.org/10.1016/j.fertnstert.2008.07.1707

Cottrell, D.A., Turnbull, D.M., 2000. Mitochondria and ageing: Current Opinion in Clinical Nutrition and Metabolic Care 3, 473–478. https://doi.org/10.1097/00075197-200011000-00009

Dalton, C.M., Carroll, J., 2013. Biased inheritance of mitochondria during asymmetric cell division in the mouse oocyte. Journal of Cell Science 126, 2955–2964. https://doi.org/10.1242/jcs.128744

Edgar, D., Shabalina, I., Camara, Y., Wredenberg, A., Calvaruso, M.A., Nijtmans, L., Nedergaard, J., Cannon, B., Larsson, N.-G., Trifunovic, A., 2009. Random Point Mutations with Major Effects on Protein-Coding Genes Are the Driving Force behind Premature Aging in mtDNA Mutator Mice. Cell Metabolism 10, 131–138. https://doi.org/10.1016/j.cmet.2009.06.010

Eichenlaub-Ritter, U., Wieczorek, M., Lüke, S., Seidel, T., 2011. Age related changes in mitochondrial function and new approaches to study redox regulation in mammalian

oocytes in response to age or maturation conditions. Mitochondrion 11, 783–796. https://doi.org/10.1016/j.mito.2010.08.011

Fato, R., Bergamini, C., Bortolus, M., Maniero, A.L., Leoni, S., Ohnishi, T., Lenaz, G., 2009. Differential effects of mitochondrial Complex I inhibitors on production of reactive oxygen species. Biochimica et Biophysica Acta (BBA) - Bioenergetics 1787, 384–392. https://doi.org/10.1016/j.bbabio.2008.11.003

Frezza, C., 2017. Mitochondrial metabolites: undercover signalling molecules. Interface Focus 7, 20160100. https://doi.org/10.1098/rsfs.2016.0100

Greaves, L.C., Reeve, A.K., Taylor, R.W., Turnbull, D.M., 2012. Mitochondrial DNA and disease. The Journal of Pathology 226, 274–286. https://doi.org/10.1002/path.3028

Grindler, N.M., Moley, K.H., 2013. Maternal obesity, infertility and mitochondrial dysfunction: potential mechanisms emerging from mouse model systems. Molecular Human Reproduction 19, 486–494. https://doi.org/10.1093/molehr/gat026

Hiona, A., Sanz, A., Kujoth, G.C., Pamplona, R., Seo, A.Y., Hofer, T., Someya, S., Miyakawa, T., Nakayama, C., Samhan-Arias, A.K., Servais, S., Barger, J.L., Portero-Otín, M., Tanokura, M., Prolla, T.A., Leeuwenburgh, C., 2010. Mitochondrial DNA Mutations Induce Mitochondrial Dysfunction, Apoptosis and Sarcopenia in Skeletal Muscle of Mitochondrial DNA Mutator Mice. PLoS ONE 5, e11468. https://doi.org/10.1371/journal.pone.0011468

Kameyama, Y., Ohnishi, H., Shimoi, G., Hashizume, R., Ito, M., Smith, L.C., 2010. Asymmetrical allocation of mitochondrial DNA to blastomeres during the first two cleavages in mouse embryos. Reproduction, Fertility and Development 22, 1247. https://doi.org/10.1071/RD10076

Kawanishi, S., Oikawa, S., 2004. Mechanism of Telomere Shortening by Oxidative Stress. Annals of the New York Academy of Sciences 1019, 278–284. https://doi.org/10.1196/annals.1297.047

Kitajima, T.S., 2018. Mechanisms of kinetochore-microtubule attachment errors in mammalian oocytes. Development, Growth & Differentiation 60, 33–43. https://doi.org/10.1111/dgd.12410

Li, N., Ragheb, K., Lawler, G., Sturgis, J., Rajwa, B., Melendez, J.A., Robinson, J.P., 2003. Mitochondrial Complex I Inhibitor Rotenone Induces Apoptosis through Enhancing Mitochondrial Reactive Oxygen Species Production. Journal of Biological Chemistry 278, 8516–8525. https://doi.org/10.1074/jbc.M210432200

Liu, L., Bailey, S.M., Okuka, M., Muñoz, P., Li, C., Zhou, L., Wu, C., Czerwiec, E., Sandler, L., Seyfang, A., Blasco, M.A., Keefe, D.L., 2007. Telomere lengthening early in development. Nature Cell Biology 9, 1436–1441. https://doi.org/10.1038/ncb1664

Lozoya, O.A., Xu, F., Grenet, D., Wang, T., Grimm, S.A., Godfrey, V., Waidyanatha, S., Woychik, R.P., Santos, J.H., 2020. Single Nucleotide Resolution Analysis Reveals Pervasive, Long-Lasting DNA Methylation Changes by Developmental Exposure to a Mitochondrial Toxicant. Cell Reports 32, 108131. https://doi.org/10.1016/j.celrep.2020.108131

Marshall, L.E., Himes, R.H., 1978. Rotenone inhibition of tubulin self-assembly. Biochimica et Biophysica Acta (BBA) - General Subjects 543, 590–594. https://doi.org/10.1016/0304-4165(78)90315-X

Oikawa, S., Kawanishi, S., 1999. Site-specific DNA damage at GGG sequence by oxidative stress may accelerate telomere shortening. FEBS Letters 453, 365–368. https://doi.org/10.1016/S0014-5793(99)00748-6

Palmer, G., Horgan, D.J., Tisdale, H., Singer, T.P., Beinert, H., 1968. Studies on the respiratory chain-linked reduced nicotinamide adenine dinucleotide dehydrogenase. XIV. Location of the sites of inhibition of rotenone, barbiturates, and piericidin by means of electron paramagnetic resonance spectroscopy. J. Biol. Chem. 243, 844–847.

Pikó, L., Taylor, K.D., 1987. Amounts of mitochondrial DNA and abundance of some mitochondrial gene transcripts in early mouse embryos. Dev. Biol. 123, 364–374.

Preis, K.A., Seidel, G.E., Gardner, D.K., 2007. Reduced oxygen concentration improves the developmental competence of mouse oocytes following in vitro maturation. Molecular Reproduction and Development 74, 893–903. https://doi.org/10.1002/mrd.20655

Reid, M.A., Dai, Z., Locasale, J.W., 2017. The impact of cellular metabolism on chromatin dynamics and epigenetics. Nature Cell Biology 19, 1298–1306. https://doi.org/10.1038/ncb3629

Robker, R.L., Hennebold, J.D., Russell, D.L., 2018. Coordination of Ovulation and Oocyte Maturation: A Good Egg at the Right Time. Endocrinology 159, 3209–3218. https://doi.org/10.1210/en.2018-00485

Rosen, J., Jakobs, P., Ale-Agha, N., Altschmied, J., Haendeler, J., 2020. Non-canonical functions of Telomerase Reverse Transcriptase – Impact on redox homeostasis. Redox Biology 34, 101543. https://doi.org/10.1016/j.redox.2020.101543

Sahin, E., Colla, S., Liesa, M., Moslehi, J., Müller, F.L., Guo, M., Cooper, M., Kotton, D., Fabian, A.J., Walkey, C., Maser, R.S., Tonon, G., Foerster, F., Xiong, R., Wang, Y.A., Shukla, S.A., Jaskelioff, M., Martin, E.S., Heffernan, T.P., Protopopov, A., Ivanova, E., Mahoney, J.E., Kost-Alimova, M., Perry, S.R., Bronson, R., Liao, R., Mulligan, R., Shirihai, O.S., Chin, L., DePinho, R.A., 2011. Telomere dysfunction induces metabolic and mitochondrial compromise. Nature 470, 359–365. https://doi.org/10.1038/nature09787

Sanders, L.H., Howlett, E.H., McCoy, J., Greenamyre, J.T., 2014. Mitochondrial DNA Damage as a Peripheral Biomarker for Mitochondrial Toxin Exposure in Rats. Toxicological Sciences 142, 395–402. https://doi.org/10.1093/toxsci/kfu185

Seisenberger, S., Peat, J.R., Hore, T.A., Santos, F., Dean, W., Reik, W., 2013. Reprogramming DNA methylation in the mammalian life cycle: building and breaking epigenetic barriers. Philosophical Transactions of the Royal Society B: Biological Sciences 368, 20110330. https://doi.org/10.1098/rstb.2011.0330

Sohal, R.S., Ku, H.-H., Agarwal, S., Forster, M.J., Lal, H., 1994. Oxidative damage, mitochondrial oxidant generation and antioxidant defenses during aging and in response to food restriction in the mouse. Mechanisms of Ageing and Development 74, 121–133. https://doi.org/10.1016/0047-6374(94)90104-X

Srivastava, P., Panda, D., 2007. Rotenone inhibits mammalian cell proliferation by inhibiting microtubule assembly through tubulin binding: Antiproliferative mechanism of action of rotenone. FEBS Journal 274, 4788–4801. https://doi.org/10.1111/j.1742-4658.2007.06004.x

von Zglinicki, T., Saretzki, G., Döcke, W., Lotze, C., 1995. Mild Hyperoxia Shortens Telomeres and Inhibits Proliferation of Fibroblasts: A Model for Senescence? Experimental Cell Research 220, 186–193. https://doi.org/10.1006/excr.1995.1305

Waldenström, U., Engström, A.-B., Hellberg, D., Nilsson, S., 2009. Low-oxygen compared with high-oxygen atmosphere in blastocyst culture, a prospective randomized study. Fertility and Sterility 91, 2461–2465. https://doi.org/10.1016/j.fertnstert.2008.03.051

Wu, L.L., Russell, D.L., Wong, S.L., Chen, M., Tsai, T.-S., St John, J.C., Norman, R.J., Febbraio, M.A., Carroll, J., Robker, R.L., 2015. Mitochondrial dysfunction in oocytes of obese mothers: transmission to offspring and reversal by pharmacological endoplasmic reticulum stress inhibitors. Development 142, 681–691. https://doi.org/10.1242/dev.114850

CHAPTER 5

MATERNAL OBESITY OR ADVANCED MATERNAL AGE ALTERS TELOMERE LENGTH IN EMBRYOS

5.1 Introduction

Females are born with a fixed quantity of oocytes for their entire reproductive span. Female fertility is known to decline with aging, beginning around 30 years of age, with a more rapid decline from 35 (Menken et al., 1986). As every oocyte a female will ever ovulate is present within her ovaries from birth, they are exposed to a range of external and internal stressors. Aside from age, other factors that can influence female fertility include psychological stress, drug and alcohol use, and exposure to pollutants, chemicals, heavy metals and endocrine disruptors (Sharma et al., 2013). Perhaps one of the most thoroughly addressed, and most prominent influences on female fertility is inappropriate diet and insufficient exercise, leading to obesity. Obese women experience higher rates of ovulatory infertility (Grodstein et al., 1994), longer time to pregnancy, higher rates of miscarriage (including recurrent, early miscarriage), and decreased successful implantation rates when compared to healthy-weight women (Sharma et al., 2013). Both maternal obesity and advanced maternal reproductive age are prominent factors resulting in subfertility and infertility, and a dominating issue in both of these scenarios is an overarching general decline in oocyte quality.

Shifts in societal trends are seeing women waiting until later in life than ever before to try to conceive. Not only do oocyte reserves decrease with age, but oocyte quality has been shown to decline too. Changes to oocyte quality with aging include epigenetic alterations, and mitochondrial decline, encompassing abnormal energy metabolism, increased dysfunction, and increased mtDNA mutation load, among many others as shown by studies in both mice and humans (Cimadomo et al., 2018; Krisher, 2019; Tarín et al., 2002; Zhang et al., 2020). Telomeres are shorter in oocytes from older women (Henderson and Edwards, 1968), and this observation persisted through to blastocysts of advanced maternal reproductive age patients, where telomere length in whole blastocysts was analysed using quantitative fluorescence *in situ* hybridisation (qFISH) (Mania et al., 2014). Advanced maternal reproductive age is also associated with increased incidence of aneuploidy (such as trisomy 21), and a direct relationship between aneuploidy and telomere length in advanced maternal reproductive age has been observed (Ghosh et al., 2010; Ray et al., 2015; Treff et al., 2011). Further, epidemiological studies show that maternal age at conception is inversely related to offspring lifespan (Gavrilov and Gavrilova, 2012).

The incidence of obesity in today's society is rising at a worrying rate and obese women often require ART due to alterations in cyclicity as well as oocyte and subsequent embryo quality (Robker, 2008). Analysis of oocytes from obese mice have revealed altered oocyte quality, identified by increased spindle abnormalities, lipid content, endoplasmic reticulum stress, and autophagy levels, along with decreased mitochondrial activity (Han et al., 2018; Wu et al., 2015, 2010). Foetuses generated from obese mice also had decreased mtDNA copy number in liver and kidney tissue, combined with increased mtDNA variant numbers in liver tissues (Wu et al., 2015), indicating a predisposition of these offspring to metabolic issues, as seen in children of obese women (Catalano and deMouzon, 2015; Glastras et al., 2018; Ma et al., 2020; Morea et al., 2013; Page et al., 2019). In humans, maternal obesity has been directly linked to decreased telomere lengths in offspring cord blood and placenta (Martens et al., 2016), while children of women who had metabolic syndrome during pregnancy (mean BMI was 31.4) had shorter telomeres than those born to mothers that did not have metabolic syndrome during pregnancy (McAninch et al., 2020). This indicates that obese women are giving birth to chronologically older babies (indicated by telomere length), however it is not known how and when in development this telomere deficiency is established and whether there is any link between maternal obesity and oocyte or embryo telomere lengths.

Using a model of rotenone-induced oocyte mitochondrial dysfunction, it was found that mitochondrial function is a key regulator of telomere elongation during pre-implantation embryogenesis, particularly during the post-compaction development phase (8C – blastocyst, see Chapter 4). Maternal obesity and advanced maternal reproductive age are two physiological scenarios which are known to result in perturbations to embryo development, which originate from abnormalities in the oocyte; at least in part due to compromised oocyte mitochondrial function. Therefore, this study (see Fig. 5.1., 'Experimental design') set out to characterise telomere length in oocytes, 8C embryos, blastocysts, and ICMs in mouse models of obesity and advanced maternal reproductive age. Zygotic epigenetic reprogramming, was also investigated in these contexts, as it was disrupted by rotenone-induced mitochondrial dysfunction and could represent a link with telomere elongation mechanisms.

The hypothesis that mitochondrial function is a key regulator of pre-implantation telomere elongation events was further addressed by treating obese or aging mothers

with the mitochondrial activator compound BGP-15 (see Fig. 5.1.), to determine if improving oocyte mitochondrial function can restore telomere length deficits. BGP-15 has previously been shown to improve the quality of oocytes from obese females by normalising spindle abnormalities, reducing autophagy levels, increasing mtDNA copy number, and increasing TFAM and Drp1 protein abundance (Wu et al., 2015).

Analysis of oocytes and embryos from obese and aging mice revealed many parallels, and further, treatment with BGP-15 was able to rectify many of the deficiencies seen. The results of this study further support the hypothesis of oocyte mitochondrial function being a key regulator of telomere elongation during pre-implantation embryo development.

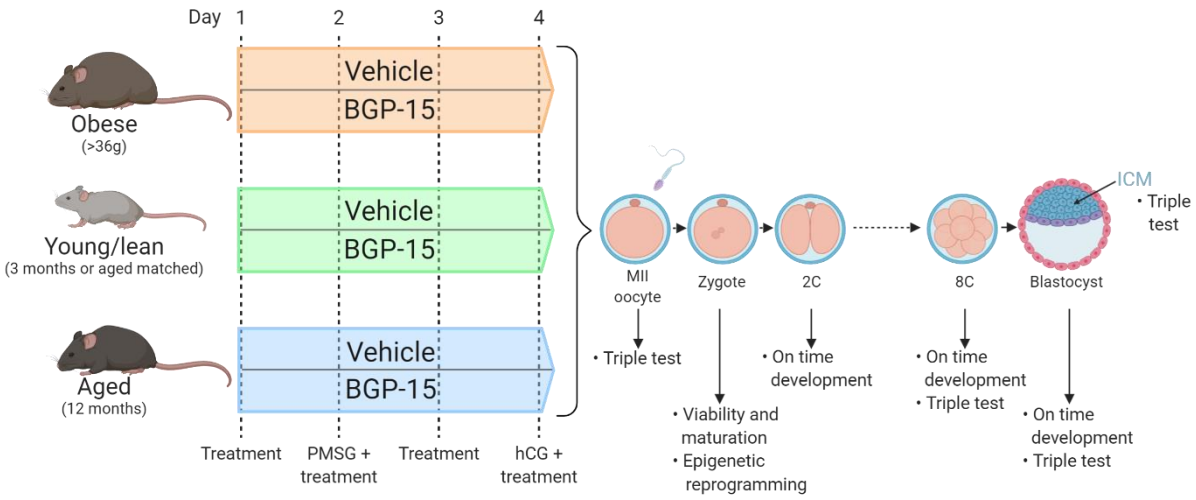


Figure 5.1. Experimental design

Young/lean, obese, and reproductively aged females were treated with vehicle or BGP-15 via i.p. injection for 4 days, starting the day prior to PMSG stimulation. Oocytes and embryos were assessed for morphology, epigenetic reprogramming and developmental timing as well as telomere length and mtDNA copy number analysis using the Triple Test, as indicated.

5.2 Materials and Methods

5.2.1 Mice

Mice with obesity or reproductive aging, as well as lean and young controls were generated from the same colony (C57BL/6JSfdAnu-Alms1bbb/Apb mouse strain maintained as heterozygous breeding pairs), termed “Blobby” mice, and fed an identical standard chow diet as in (Wu et al., 2015). Obese mice were homozygous (bbb/bbb) for the ‘Blobby’ mutation of the Alms1 gene which results in hyperphagia and profound obesity even when maintained on a standard mouse chow diet (Wu et al., 2015). Females were deemed obese when they weighed at least 36g, which occurred at around 5 months of age, and wild-type littermates were used in parallel as lean controls. ‘Old’ females were wild-type or heterozygous (+/+ or bbb/+) at 12 months of age and young females (3-4 months old) were used in parallel as controls.

Mice were maintained in 12h/12h light/dark conditions and given water and standard rodent chow *ad libitum*. All animal experiments were approved by the University of Adelaide’s Animal Ethics Committee and conducted in accordance with the Australian Code of Practice for the Care and Use of Animals for Scientific Purposes.

5.2.2 Derivation of oocytes, early embryos, and blastocysts

5.2.2.1 Hormone stimulation and BGP-15 treatment

Female mice were given 5IU/12g bodyweight pregnant mare’s serum gonadotropin (PMSG, National Hormone and Pituitary Program), followed by the equivalent dose of human chorionic gonadotropin (hCG, Pregnyl) 47.5 hours later, each via intraperitoneal (ip) injection. BGP-15 ([(O-[3-piperidino-2-hydroxy-1-propyl]-nicotinic amidoxime)], CAS 66611-37-8; Hangzhou Molcore Biopharmatech Co Ltd, and N-Gene Research Laboratories Ltd) was injected at 100mg/kg of bodyweight in saline for 4 days, starting the day before PMSG injection (as in Wu et al. 2015, refer to Figure 5.1). Controls were injected with saline vehicle.

5.2.2.2 MII oocyte retrieval

Mice were culled via cervical dislocation 15h post-hCG administration, and ovaries and oviducts collected and placed in pre-warmed (37°C) αMEM-HEPES handling

media, supplemented with 1% FCS. Meiosis II (MII) oocytes were isolated by puncturing the oviducts using a 30G needle. Complete cumulus cell removal was achieved via treatment with hyaluronidase (Seikagaku, #100741) for 5-10 minutes at 37°C, followed by aspiration using a glass pipette pulled to an appropriate diameter.

5.2.2.3 *In vitro* fertilisation (IVF)

To generate embryos via *in vitro* fertilisation, MII COCs were collected as previously described (section 3.2.2.2). Following oviduct puncture, whole cumulus-oocyte complex (COC) clusters were gently washed twice in pre-warmed (37°C) fertilisation media (Vitro Fertilisation; Cook Australia, Brisbane, Australia), before being placed in a 100µL fertilisation drop containing the equivalent of 10µL of capacitated sperm from a male of proven fertility (this is deemed 'fertilisation time'), before being returned to the incubator (37°C, 5% O_2, 6% CO_2) for 4 hours. Following this, fertilised oocytes were cleaned of all excess sperm and cumulus cells via gentle aspiration and transferred to a culture dish containing cleave media (Vitro Cleave; Cook Australia, Brisbane, Australia, 10 embryos per 20µL cleave media drop) and returned to the incubator until 24 hours post fertilisation time. At this time, the number of embryos that successfully reached the 2C stage were scored. The remaining embryos were returned to the incubator until 55 hours post fertilisation time for 8C collection, then until 96 hours post fertilisation time, where the remaining embryos that had successfully reached the blastocyst stage were scored and collected for analysis.

5.2.3 Blastocyst Immunosurgery

Blastocysts first had their zona pellucida removed via treatment with Acidic Tyrode's Embryomax solution, washed twice in cleave media and transferred to a 200µL drop of cleave media containing 20% heat inactivated rabbit anti-mouse serum (Sigma, #M5774). Following a one hour incubation period (37°C, 5% O_2, 6% CO_2), blastocysts were washed three times in cleave media and transferred to a 200µL cleave media drop containing 20% guinea pig serum (Sigma, #G9774) and incubated for 15 minutes. Blastocysts were washed three times in cleave media and incubated for a further 30 minutes in this media. Lysed TE cells were removed by gently aspirating ICMs in a finely drawn glass pipette.

5.2.4 Sample collection, lysis and preparation for qPCR

MII oocytes or embryos at the various stages, or ICM populations were first washed three times in 1x phosphate buffered saline (PBS) containing 1mg/mL polyvinylpyrrolidone (PVP, Sigma), and transferred in 1µL to a 0.5mL PCR tube (Axygen, #PCR-05-C) for qPCR analysis. All samples were snap frozen in liquid nitrogen (LN_2), and stored at -80°C until use.

Individual oocytes, embryos, and ICM populations had their nuclear genomic DNA (nDNA) and mitochondrial DNA (mtDNA) extracted by adding 9µL of lysis buffer (50mM Tris-HCl pH 8.0, 1mM EDTA, 200µg/mL Proteinase K, 0.5% Tween-20) to each sample with a volume of 1µL (final volume of 10µL) following brief centrifugation, and heated to 55°C for 2 hours, followed by 95°C for 10 minutes to inactivate Proteinase K activity. Samples were allowed to cool to 4°C and briefly centrifuged. Following this, 1µL of lysis product was removed and added to 9µL of sterile H_2O for mtDNA analysis and the rest kept for telomere and *Rn18S* analysis. For ICMs, an additional 10µL of sterile H_2O was added after lysis to give a total volume of 20µL which was used for the Triple Test without further dilution.

5.2.5 Triple test qPCR assay

To generate 'calibrator' DNA for use as a standard within every assay, a whole ovary from a 6 week old PMSG and hCG stimulated CBA female mouse was collected and had total DNA extracted (as described previously, see sections 2.2.2). DNA concentration and purity were quantified by NanoDrop One Microvolume UV-Vis Spectrophotometer and diluted to 2.5ng/µL.

qPCR was performed using Power SYBR Green PCR Master Mix (Applied Biosystems, #4367659), standard MicroAmp Optical 96-well Reaction Plates (Life Technologies, #4306737), and custom made primers (Sigma, forward and reverse primer sequences shown in Table 5.1), using an Applied Biosystems 7900HT Fast Real-Time PCR system. Cycling conditions for all primers were set at 95°C for 10 minutes, followed by 40 cycles of 95°C for 10s, 60°C annealing for 30s and extension at 72°C for 30s, followed by standard melt curve cycling. Two repeat reactions were performed for each sample and each primer pair, using 2µL of sample per reaction.

For *Rn18S* and telomere analysis, the final reaction for each well was 10µL Power SYBR Green PCR Master Mix, 0.5µL each of forward and reverse primer (stock at 10µM), 2µL of sample, and sterile H_2O to a final volume of 20µL. To minimise any plate-to-plate variations, *Rn18S* and telomere reactions for each sample were run on the same plate, and calibrator DNA assays included on every plate.

For mtDNA analysis, the final reaction for each well consisted of 10µL Power SYBR Green PCR Master Mix, 0.2µL each of forward and reverse primer (stock at 10µM), 2µL of sample or standard, and sterile H_2O to a final volume of 20µL. Total mtDNA copy number was quantified using the standard curve method as previously described (Kameyama et al., 2010). Briefly, quantification standards were prepared by PCR amplifying a 1186bp fragment in the 12S rRNA region of mtDNA from mouse liver using the primer pair 5'-ACA CCT TGC CTA GCC A-3' and 5'-TTT GCC ACA TAG ACG AGT T-3'. The PCR product was extracted from the gel using QIAquick Gel Extraction Kit (Qiagen) and cloned using the Qiagen PCR Cloning Kit. Plasmid DNA was purified using QIAprep Spin Miniprep Kit (Qiagen), quantified by spectrophotometry, and diluted to 10^7 copies per 2µL. To create a standard curve, 10µL of standard stock was removed and serially diluted (1:10) from 10^7 to 10^1 copies, and standard curve correlation coefficients were consistently greater than 0.98. Serial dilutions were made fresh on the day. Total mtDNA copy number per sample was calculated according to the generated equation for Ct value against copy number for the corresponding standard curve (excluding 10^1 copies), and multiplied by the dilution factor of the sample i.e. total mtDNA copy number = (10^x) * [dilution factor], where x=(y-intercept of standard curve – Ct value of sample)/slope of standard curve.

Telomere and mtDNA relative to total cell number were calculated using the $2^{-\Delta\Delta Ct}$ method, where the ΔCt of the calibrator (telomere or mtDNA Ct – *Rn18S* Ct) was subtracted from the ΔCt of the sample (telomere or mtDNA Ct – *Rn18S* Ct) to give the ΔΔCt.

Table 5.1 qPCR primers

Primer target	Forward primer sequence	Reverse primer sequence
Telomere	5'-CGG TTT GTT TGG GTT TGG GTT TGG GTT TGG GTT TGG GTT-3'	5'-GGC TTG CCT TAC CCT TAC CCT TAC CCT TAC CCT TAC CCT-3'
mtDNA	5'-CGT TAG GTC AAG GTG TAG CC-3'	5'-CCA GAC ACA CTT TCC AGT ATG-3'
Rn18S	5'-AGA AAC GGC TAC CAC ATC CAA-3'	5'-CCT GTA TTG TTA TTT TTC GTC ACT ACC T-3'

5.2.6 Pronuclear cytosine methylation immunofluorescence

Fertilized zygotes (stage PN3 to PN4) were collected 6 hours after fertilisation, and successfully parthenogenetically activated 1C embryos were collected 6 hours after activation time (see section 3.2.2.4). The zona pellucida was dissolved using Acid Tyrode's Embryomax solution (Millipore, #MR-004D), followed by a brief wash in phosphate buffered saline (PBS) containing 1mg/ml polyvinylpyrrolidone (PVP, Sigma) (PBS-PVP). Samples were fixed in 3.7% PFA-PBS for 20 minutes at room temperature (RT), followed by two five-minute washes in PBS-PVP, then permeabilised in 0.2% Triton X-100 (in PBS) for 10 minutes at room temperature, followed by three five-minute washes in PBS-PVP. Samples were incubated in 4N HCl solution for 10 minutes at RT, and washed thoroughly in 0.05% Tween-20 in PBS (PBS-T). Samples were blocked overnight at 4°C in blocking solution (1% BSA, 0.02% Triton X-100 in PBS), then incubated overnight at 4°C with mouse anti-5mC (1:200, Biorad, #ab10805), and rabbit anti-5hmC (1:600, Active Motif, #39769), diluted in blocking solution. Following three ten-minute washes in PBS-T, samples were incubated for one hour at RT, while protected from light, with Alexa Fluor 594-conjugated goat anti-mouse (1:500, Invitrogen) and Alexa Fluor 488-conjugated goat anti-rabbit secondary antibodies (1:1000, Invitrogen). Samples were mounted on slides with 1.5µL Prolong™ Diamond Antifade Mountant (Invitrogen, #P36965) and examined using a confocal microscope (Olympus FV3000). Images were acquired using the same image acquisition settings. Pronuclear size and staining intensity was

calculated using ImageJ software. Mean signal intensity was calculated first by subtracting the signal from the cytoplasmic area (representing background staining), then dividing by the area of the pronuclei.

5.2.7 Statistical analysis

Results are presented as mean ± SEM. Telomere, mtDNA per cell, and total mtDNA copy number displayed as mean ± SEM overlayed on a violin plot to illustrate the distribution of data points. Analysis of normality showed that telomere and mtDNA data required log transformation for statistical analysis. Statistical analysis was performed using Graph Pad Prism version 8 for Windows (GraphPad Software Inc., La Jolla, CA) and SPSS Statistics 26 (IBM, Armonk, NY). Paired t-test, unpaired t-test, one-way analysis of variance (ANOVA, comparison of means), and linear-mixed effects models were used as indicated and statistical significance was considered at P-value <0.05.

5.3 Results

5.3.1 C57BL/6JSfdAnu-Alms1 embryos exhibit telomere elongation and typical mtDNA characteristics

To enable the study of maternal obesity and advanced maternal aging characteristics for this chapter, the “blobby” strain of mouse (C57BL/6JSfdAnu-Alms1) was utilised (for details see section 5.2.1). First, telomere elongation and mitochondrial DNA kinetics throughout pre-implantation embryogenesis were characterised in young lean control mice (Fig. 5.2). C57BL/6JSfdAnu-Alms1 mouse embryos exhibited a degree of telomere elongation at each analysed stage (Fig. 5.2 A), which equated to 13% of their final length by the 8C stage (Fig. 5.2 B). Thus C57BL/6JSfdAnu-Alms1 embryos primarily exhibit telomere elongation in the second phase (from 8C to blastocyst), and this is confirmed by calculation of the relative fold change in telomere length (Fig. 5.2 C) after the first phase (MII oocyte to 8C) and the second phase (8C to blastocyst). Total mitochondrial DNA copy number and relative mtDNA (Fig. 5.2 D and E) was consistent with observations in other strains (Fig. 3.5 A and B, respectively).

As telomere elongation and mtDNA dynamics were successfully characterised in young lean mice from the blobby colony, the effect of maternal obesity and advanced maternal age on these was investigated.

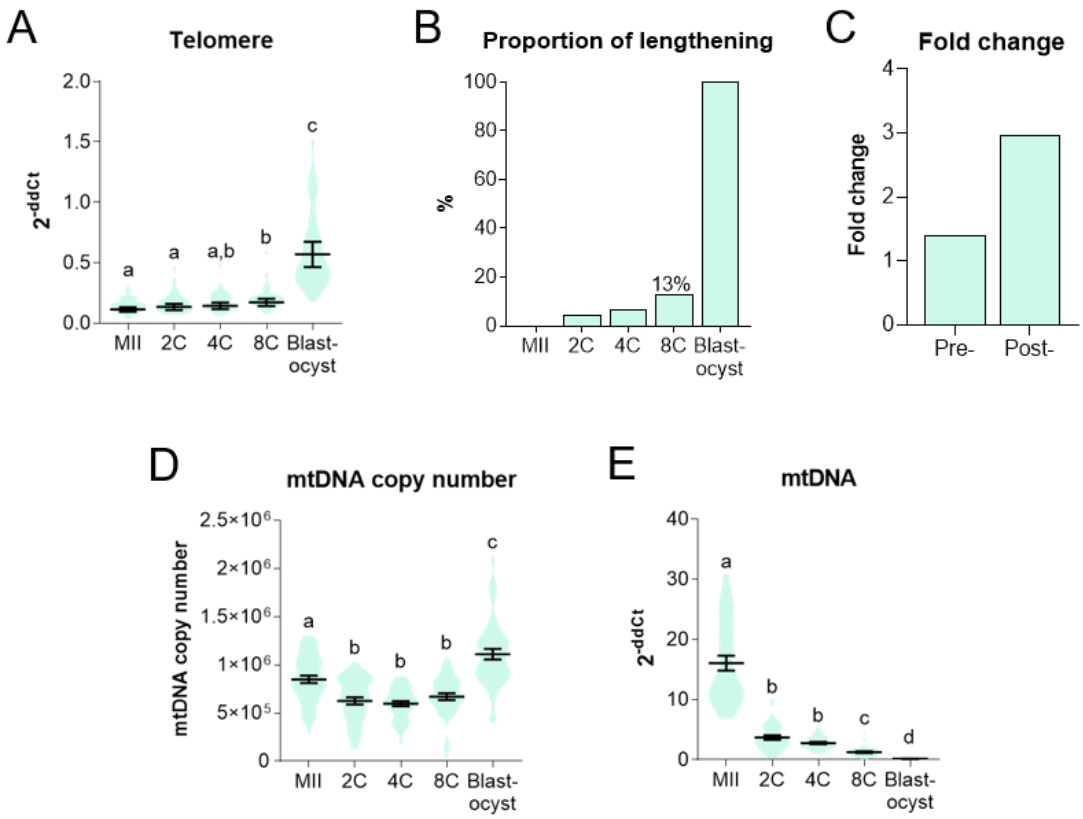


Figure 5.2. C57BL/6JSfdAnu-Alms1 embryos display typical telomere elongation and mtDNA characteristics

Oocytes were collected from young, lean female mice, fertilised via *in vitro* fertilisation (IVF) and cultured to the indicated stages. Individual denuded oocytes and embryos were frozen for Triple Test qPCR analysis. Total telomere content was calculated relative to a calibrator sample (A) and then converted to a proportion of lengthening with MII set as 0% of the final length, and blastocyst set as 100% of the final length (B), with proportion of lengthening to the 8C stage indicated. Further, the fold change in relative telomere length was calculated (C) from MII oocytes to 8C embryos (pre-compaction), and from 8C embryos to blastocysts (post-compaction). Total mtDNA copy number was calculated using the standard curve method (D) and mtDNA per nuclear gene (*Rn18S*) copy was calculated relative to a calibrator sample (E). n=42 MII oocytes and 2C embryos, and n=40 embryos from each of the 4C, 8C, and blastocyst stages. Data was log transformed for statistical analysis using a linear mixed-effects model (A, D, E) where different lowercase letters indicate statistical significance between groups of at least $p<0.05$. Statistical analysis was not conducted on data in B or C. Shaded areas represent the population distributions, while horizontal lines represent mean ± SEM.

5.3.2 Maternal obesity reduces oocyte telomere lengths

To examine the effects of maternal obesity on telomere and mtDNA dynamics in oocytes and throughout embryo development, obese (≥36g) and lean (wild-type) aged-matched females underwent four daily injections of 100mg/kg BGP-15 or the equivalent volume of saline, with PMSG and hCG stimulation according to body weight (5IU/12g) as depicted in the experimental design schematic (Fig 5.1). COCs were collected 15 hours after hCG administration for *in vitro* fertilisation (IVF), and oocyte quality was assessed four hours after fertilisation (Fig. 5.3). The total number of oocytes at this time was counted and established that obese females ovulate fewer oocytes than lean females, and this was not altered by BGP-15 treatment (Fig. 5.3 A). These results differ from previous studies using the Blobby strain of mouse as an obesity model, where treatment of either lean or obese females with BGP-15 increased ovulation (Wu et al., 2015). A potential reason for this discrepancy may lie in differences in ovulation numbers for controls mice. In this study, lean control mice ovulated an average of 27 oocytes, compared to just below 20 in the previous study, while control obese mice ovulated an average of 13 oocytes in this study, in comparison to the previously reported average of 7.5 (Wu et al., 2015), suggesting a better response overall to hyperstimulation techniques. This could derive from differences between the mice in the two studies, their housing conditions, or the use of different hormones, thus leaving less opportunity for enhancement from BGP-15 treatment. The proportion of females that ovulated was not different between groups, with 98% of lean mice ovulating (vehicle and BGP-15 treatment groups) and 96% of obese vehicle and 93% of obese BGP-15 treated mice ovulating (analysed using Chi-square test, p=0.22). Oocytes were assessed for their viability and separated into three classifications (live, fragmented, degenerated) based on their morphology (Fig. 5.3 B). Obesity was not associated with increased oocyte fragmentation or degeneration compared to controls, and BGP-15 did not alter these proportions (Fig. 5.3 B). Unexpectedly, BGP-15 treatment of lean mice reduced the quantity of degenerated oocytes, thereby increasing the proportion of live oocytes, with fragmented oocytes remaining unchanged. No other differences were found in oocyte proportions between other groups. Live oocytes were further assessed for maturation status, with those exhibiting a sizeable MII polar body categorised as “normal” maturation, and those with a very small or complete lack of a polar body as having undergone “abnormal”

maturation (Fig. 5.3 C). Maternal obesity did not influence the proportion of live oocytes that had matured abnormally, and BGP-15 treatment did not modulate these proportions.

Ovulated oocytes were fully denuded and individually frozen for Triple Test analysis (Fig. 5.4). Maternal obesity was associated with reduced telomere lengths in MII oocytes compared to controls (Fig. 5.4 A), and no differences were found between oocytes from mice that received BGP-15 treatment when compared to vehicle controls. While maternal obesity did not alter the total mtDNA copy number of oocytes, treating obese females with BGP-15 resulted in an increase in mtDNA in comparison to oocytes from lean or obese vehicle groups (Fig. 5.4 B), consistent with previous results (Wu et al., 2015).

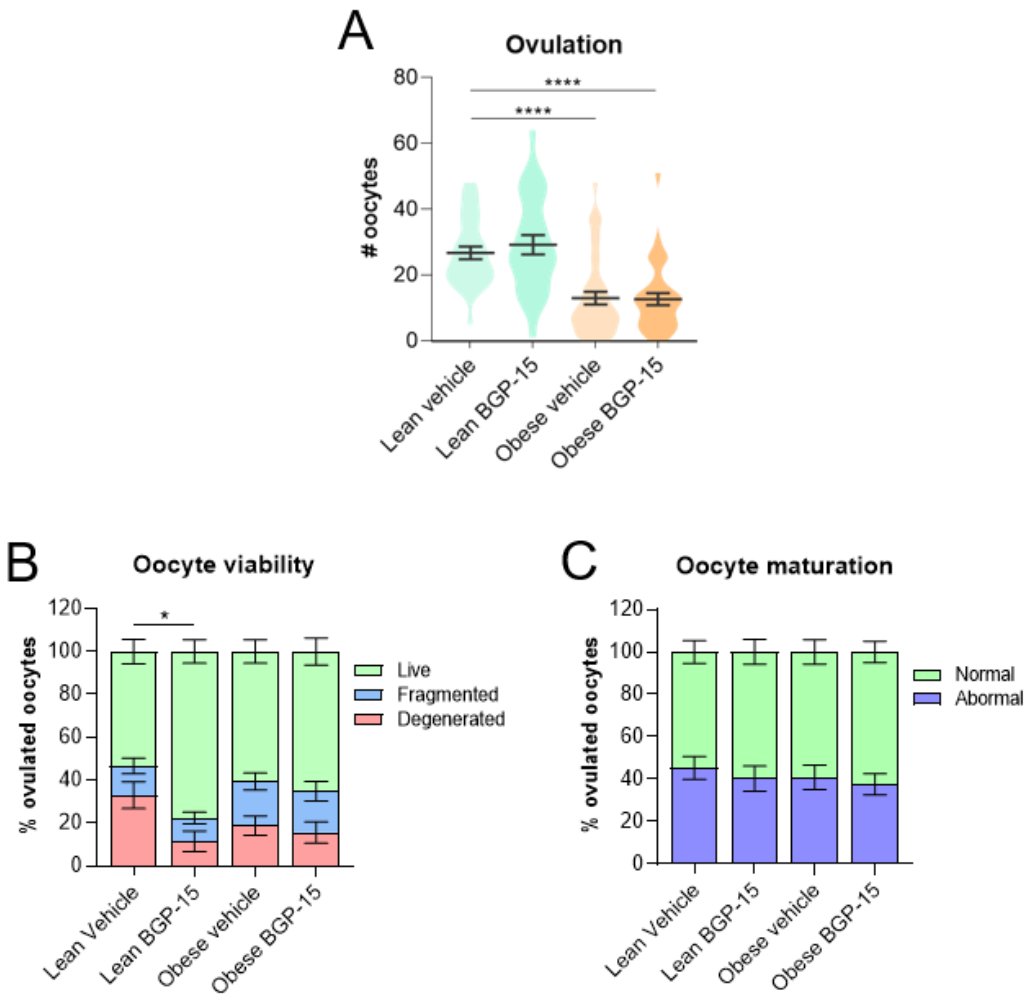


Figure 5.3. Obesity reduces ovulation numbers but does not impact oocyte viability or maturation

COCs were collected 15 hours after hCG administration and fertilised via IVF. Four hours after fertilisation, the total oocytes ovulated were counted (A), oocytes and presumptive zygotes were scored for viability (live, fragmented or degenerated, B) and maturity (presence of at least one polar body, C). For ovulation counts n=29 lean vehicle, n= 26 lean BGP-15, n=39 obese vehicle, and n=32 obese BGP-15 mice. For viability and maturation n=20 lean vehicle, n=19 lean BGP-15, n=30 obese vehicle, and n=24 obese BGP-15 mice. Data analysed using one-way ANOVA, % live oocytes analysed for (B), and % normal oocytes analysed for (C) where no difference was observed, * $p<0.05$, **** $p<0.0001$. For A, shaded areas represent the population distributions, while horizontal lines represent mean ± SEM.

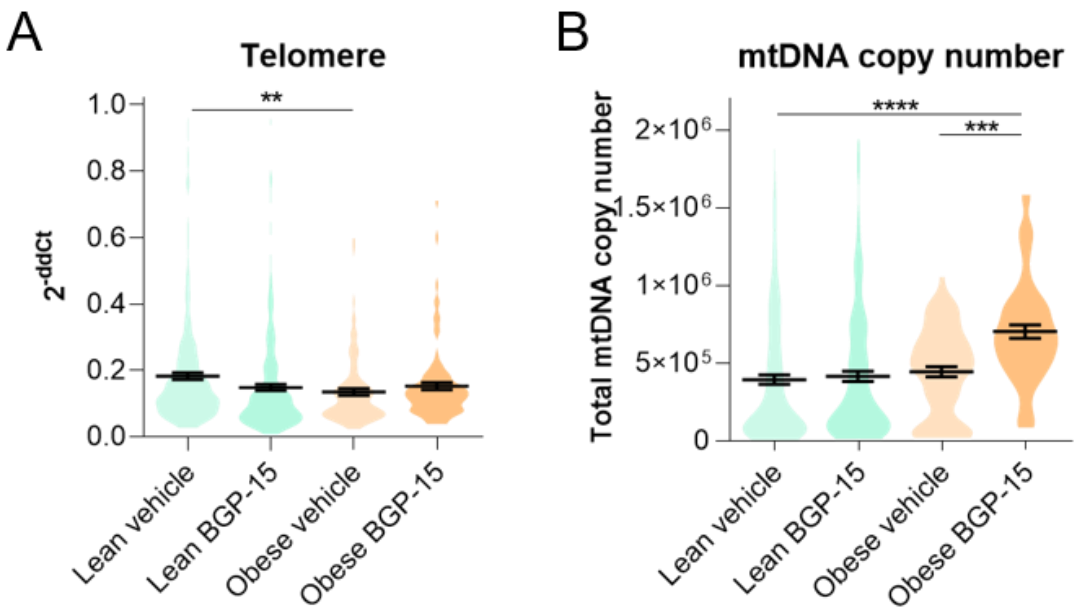


Figure 5.4. Obesity reduces MII oocyte telomere length

Fully denuded MII oocytes were individually frozen for Triple Test analysis. Relative telomere length (A) and total mtDNA copy number (B) were compared between lean and obese oocytes with or without *in vivo* BGP-15 exposure. n=220 lean vehicle, n=191 lean BGP-15, n=93 obese vehicle, and n=87 obese BGP-15 MII oocytes, log transformed data analysed using one-way ANOVA, ** p=0.0022, *** p=0.0008, **** p<0.0001. Shaded areas represent the population distributions, while horizontal lines represent mean ± SEM.

5.3.3 Maternal obesity alters zygote pronuclear epigenetic reprogramming events

To determine if maternal obesity affects zygote pronuclei epigenetic reprogramming, zygotes were collected 6 hours after fertilisation for methylation pattern assessment of the maternal and paternal pronuclei (Fig. 5.5 A). Analysis of pronuclear size showed the expected difference, with the paternal pronuclei being larger in size than the maternal pronuclei for all groups, however the difference in pronuclear size was diminished in zygotes from obese females (Fig. 5.5 B). Further, the paternal pronucleus was smaller in zygotes derived from obese females than those from lean females, and were also smaller than the paternal pronucleus of zygotes from obese females that were treated with BGP-15 (Fig. 5.5 B).

5mC fluorescence levels showed established patterns in zygotes from lean females, with the maternal pronucleus exhibiting higher levels of 5mC fluorescence than the paternal pronucleus (Fig. 5.5 C). This difference in pronuclear fluorescence was not observed in zygotes derived from obese females, and mean fluorescence intensity was higher in both pronuclei in zygotes from obese females than those from lean (Fig. 5.5 C). Further, treatment of obese females with BGP-15 saw a restoration of this difference between the maternal and paternal pronuclei, and 5mC fluorescence intensity was not different from the other groups (Fig. 5.5 C). This indicates that treating obese females with BGP-15 may rectify defects in 5mC reprogramming in obese females, to similar levels seen in zygotes from lean females. When comparing the ratio for fluorescence between the paternal and maternal pronuclei, the levels were more similar (indicated by a ratio closer to 1) between zygote pronuclei from obese females than those from lean. There was a difference in the ratio when comparing obese females that had undergone BGP-15 treatment compared to vehicle treated (Fig. 5.5 C, right y-axis), indicating that BGP-15 treatment restored the expected differential in 5mC between parental pronuclei.

Quantification of 5hmC fluorescence in pronuclei displayed established differences, with the paternal pronucleus having higher levels of fluorescence than the maternal across all groups, however this difference was reduced in zygotes from obese females (Fig. 5.5 D). Further, no differences in fluorescence intensity between either the maternal or paternal pronucleus across groups were observed. The ratio of

fluorescence between the paternal and maternal pronuclei was reduced in zygotes from obese females than those from lean, indicating a loss of differential 5hmC modifications between the pronuclei (Fig. 5.5 D). Treatment of obese females with BGP-15 did not alter this ratio, however the ratio was no longer statistically different to that from lean mice.

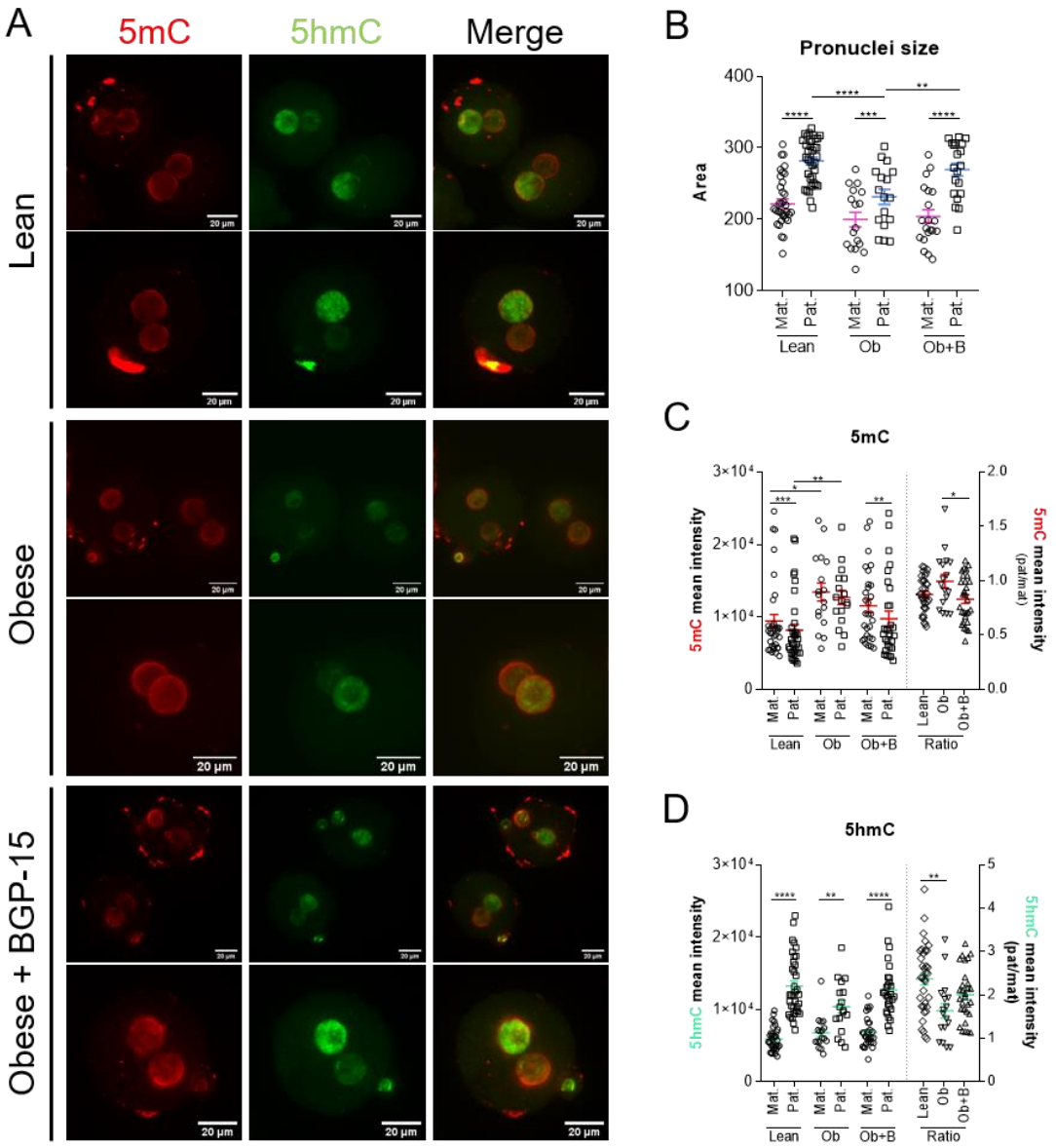


Figure 5.5. Maternal obesity results in alterations to zygotic epigenetic reprogramming events that are reversed by BGP-15 treatment

Zygotes from lean, obese (Ob) and obese females treated with BGP-15 (Ob+B) were collected 6 hours after *in vitro* fertilisation and co-stained with anti-5mC (red) and anti-5hmC (green) antibodies (A). Pronuclei size was measured (B) and signal intensity fluorescence levels were quantified for 5mC (C) and 5hmC (D) in maternal and paternal pronuclei. Data presented as signal intensity for maternal (Mat.) and paternal (Pat.) pronuclei on the left axis, and the ratio of the signal for paternal to maternal fluorescence on the right axis. Data analysed using paired t-test for comparisons between maternal and paternal pronuclei of the same zygote, and one-way ANOVA for pronuclei comparisons and ratio comparisons between groups, * $p<0.034$, ** $p<0.008$, *** $p<0.0002$, **** $p<0.0001$.

5.3.4 Maternal obesity does not impact on-time embryo development but results in shorter blastocyst telomeres

Embryo development from oocytes of lean or obese mothers was assessed 24 hours after fertilisation for successful 2C development (Fig. 5.6 A). While the impact of maternal obesity on 2C development rates was not apparent when compared to lean controls, the treatment of obese females with BGP-15 resulted in an improvement in successful 2C development in this group compared to vehicle treated obese mice (Fig 5.6 A). Embryos were allowed to develop for an additional 32 hours before on-time 8C development was assessed, which showed no differences between any groups (Fig. 5.6 B).

A proportion of on-time 8Cs were individually frozen for Triple Test analysis (Fig. 5.6 C & D). Surprisingly, the deficit in telomere length in obese oocytes was not detectable in embryos at the 8C stage and no differences were found between groups (Fig. 5.6 C). Total mtDNA copy number was not reduced in 8Cs from obese females compared to those from lean, and BGP-15 treatment of obese females did not alter 8C total mtDNA copy number (Fig. 5.6 D).

Successful blastocyst development was scored after five days of culture and similar to 2C and 8C, maternal obesity did not impact on-time development to the blastocyst stage (Fig. 5.7 A). A previous study using this mouse model of obesity indicated large decreases in on-time 2C and blastocyst development that were improved with maternal BGP-15 treatment (Wu et al., 2015). Aside from higher rates of 2C development from obese females that had undergone treatment with BGP-15 when compared to those who had not received treatment, no embryo development differences were observed in the current study. This may stem from continuous improvements to IVF procedures and culture conditions to better support the *in vitro* development of all embryos, and particularly those with compromised developmental potential. A critical difference in culture conditions between the two studies was the oxygen concentration used for culture, with the previous study using 20% O_2, and the current study using 5% O_2, where previous work has highlighted perturbed embryo development in 20% O_2 culture (see section 3.3.7).

Triple Test analysis of individual blastocysts revealed that those derived from obese females had measurably shorter telomeres than those from lean females (Fig. 5.7 B).

BGP-15 treatment of obese females resulted in blastocysts with longer telomeres than those from vehicle treated mice, and also were not different to those from lean mice (Fig. 5.7 B). Interestingly, blastocysts from obese females had more mtDNA per cell, which correlated with a higher total mtDNA copy number than those from lean mice (Fig. 5.7 C & D, respectively). Unlike telomere length, mtDNA copy numbers were not altered between embryos from obese females that were given BGP-15 compared to vehicle treated (Fig. 5.7 C & D). The inner cell mass (ICM) cell population of blastocysts was immunosurgically isolated for triple test analysis to determine if telomere length defects associated with maternal obesity carried through to the lineage that gives rise to the foetus. Similar to whole blastocysts, maternal obesity was associated with shorter telomeres than those derived from lean females, and treatment of obese females with BGP-15 restored this deficit such that telomere lengths were not different to those in ICMs derived from lean mice (Fig. 5.7 E). Unlike in whole blastocysts, the mtDNA per cell was not different in the ICMs from either group (Fig. 5.7 F), suggesting the differences seen in mtDNA per cell in whole blastocysts may be due to differences specifically in the trophectoderm.

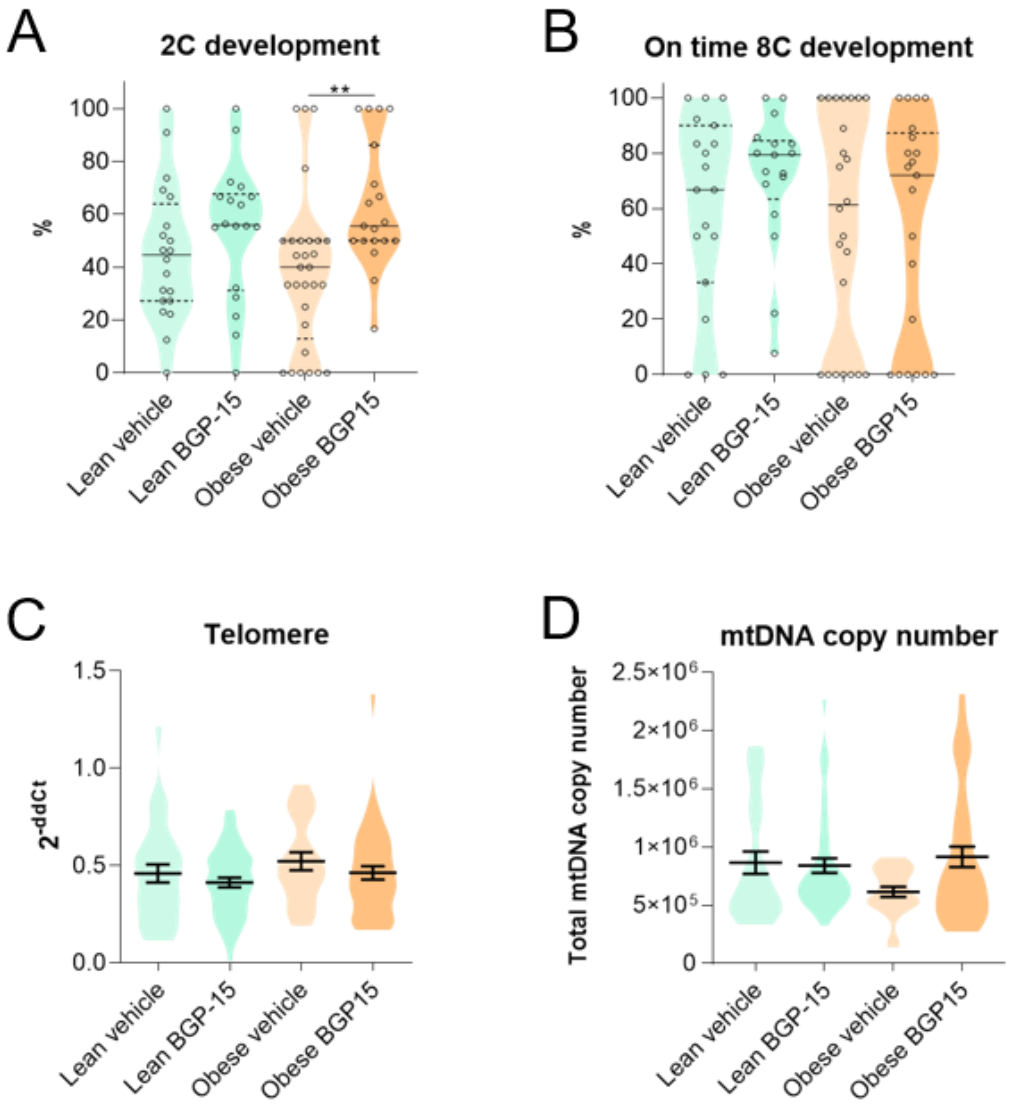


Figure 5.6. Obesity does not impact embryo development or 8C telomere lengths

Oocytes were fertilised via IVF and scored 24 hours later for successful development to the 2C stage (A) and a further 32 hours later for on time development to the 8C stage (B). A proportion of 8C embryos were collected and individually analysed for telomere length (C) and total mtDNA copy number (D) using the Triple Test. For embryo development n=20 lean vehicle, n=18 lean BGP-15 treated, n=27 obese vehicle, and n=20 obese BGP-15 treated mice. For Triple Test n=30 lean vehicle, n=50 lean BGP-15 treated, n=22 obese vehicle, and n=45 obese BGP-15 treated 8C embryos. Development data (A, B) and log transformed telomere (C) and mtDNA copy number (D) data analysed using one-way ANOVA, ** p=0.0061. Shaded areas represent the population distributions, while horizontal lines represent mean ± SEM.

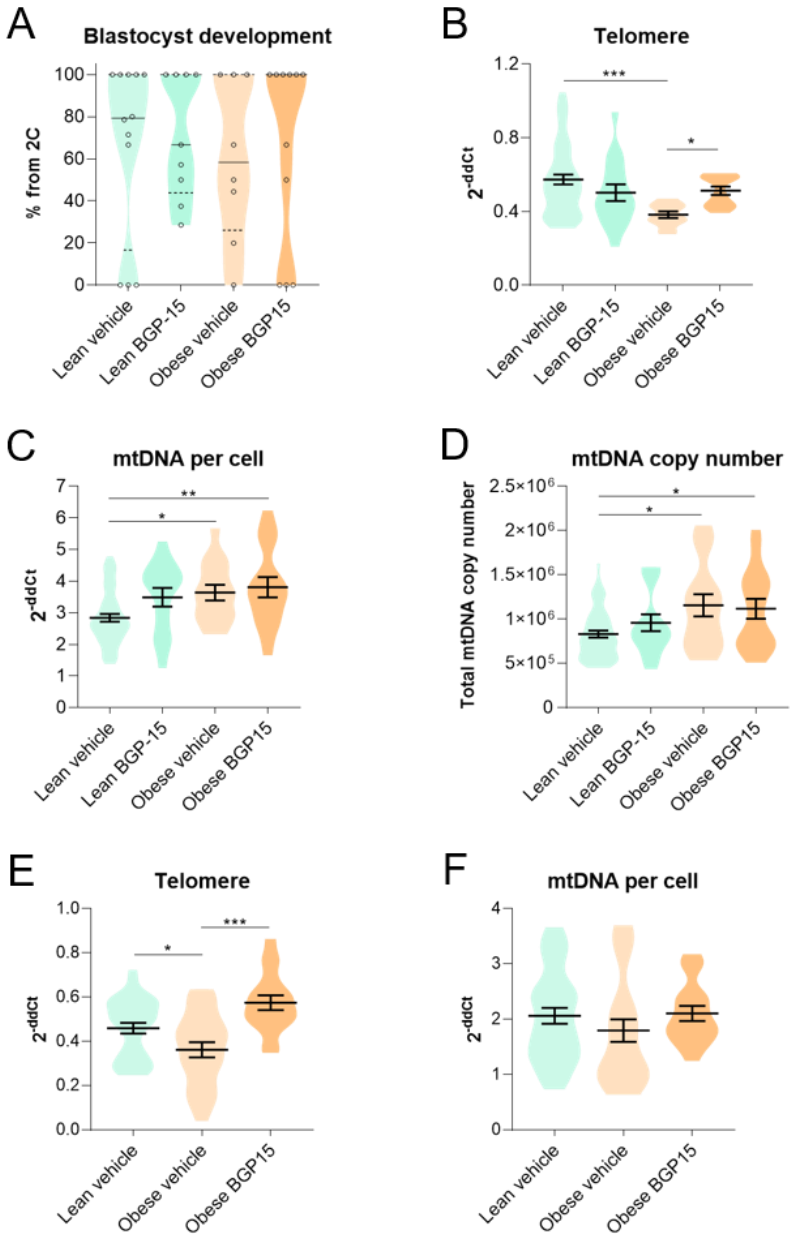


Figure 5.7. Obesity reduces blastocyst and ICM telomere length

Successful blastocyst development was scored 96 hours post fertilisation (A) and whole blastocysts and isolated ICMs were individually analysed using the Triple Test for telomere content (B & E), mtDNA per cell (C & F), and total mtDNA copy number (D). For embryo development n=12 lean vehicle, n=9 lean BGP-15 treated, n=8 obese vehicle, and n=16 obese BGP-15 treated mice. For Triple Test n=53 lean vehicle, n=16 lean BGP-15 treated, n=15 obese vehicle, and n=16 obese BGP-15 treated blastocysts. Blastocyst development (A) and log transformed data (B-F) analysed using one-way ANOVA, * $p<0.044$, ** $p=0.0063$, *** $p=0.0007$. Shaded areas represent the population distributions, while horizontal lines represent mean ± SEM.

5.3.5 Advanced maternal age reduces oocyte telomere length and mtDNA copy number

To examine the effects of advanced maternal age on telomere and mtDNA dynamics in oocytes and throughout embryo development, reproductively old (12 months old) and young (3-4 months old) females were administered daily injections for four days of 100mg/kg BGP-15 or the equivalent volume of saline, with PMSG and hCG stimulation according to body weight (5IU/12g) (see Fig 5.1). COCs were collected 15 hours after hCG administration for *in vitro* fertilisation (IVF), and oocyte quality was assessed four hours after fertilisation (Fig. 5.8). The total number of oocytes ovulated was counted at this time with old mice, as expected, ovulating fewer oocytes than young mice (Fig. 5.8 A). Treating old mice with BGP-15 for four days increased ovulation compared to old untreated mice, however this was still reduced compared to young mice. To determine if BGP-15 treatment was resulting in more aged mice ovulating, the percentage of mice that successfully ovulated was compared (Fig. 5.8 B). The proportion of ovulating mice was decreased in old mice compared to young controls, however BGP-15 treatment did not result in an increase in the percentage of aged mice that ovulated. Thus, as many aged mice failed to ovulate, the total number of oocytes from ovulating females only was evaluated (Fig. 5.8 C). Consistent with total ovulation, the number of oocytes from aging mice that ovulated was less than that from young mice, and BGP-15 treatment resulted in an increase in the number of oocytes ovulated per mouse. Taken together, these results suggest that BGP-15 treatment enabled more oocytes to be ovulated from mice that retained the capacity to ovulate, rather than stimulate ovulation from mice that were otherwise anovulatory. Ovaries from anovulatory mice were sectioned and examined histologically. It was noted that, surprisingly, a number of large follicles were present in these ovaries (Fig. 5.8 D) and thus the number of pre-ovulatory follicles, classed as a large antral follicle with a COC visible in at least one section, were counted. The number of pre-ovulatory follicles in each ovary per mouse (Fig. 5.8 E, left y-axis), and therefore the total number per mouse indicated an increase in the number of pre-ovulatory follicles in ovaries from anovulatory aged mice that had been treated with BGP-15 (Fig. 5.8 E, right y-axis), indicating that BGP-15 treatment stimulated follicle growth at least to the pre-ovulatory stage.

Following oocyte collection, viability was assessed based on morphology (Fig. 5.8 F). Maternal age was not associated with adverse impacts on oocyte viability, and BGP-15 treatment did not change these proportions in young or aged mice. Further classification of live oocytes based on their maturity showed maternal aging was not associated with an increase in abnormal maturation (based on polar body extrusion), and maturation was not affected by BGP-15 treatment (Fig. 5.8 G)

MII oocytes from young and aged control mice were denuded and individually analysed using the Triple Test (Fig. 5.9). Due to the lack of improvement to oocyte telomere lengths with BGP-15 treatment in obese females, this was not assessed in oocytes from aged females. Advanced maternal age resulted in oocytes with markedly shorter telomeres (Fig. 5.9 A) and reduced total mtDNA copy number (Fig. 5.9 B)

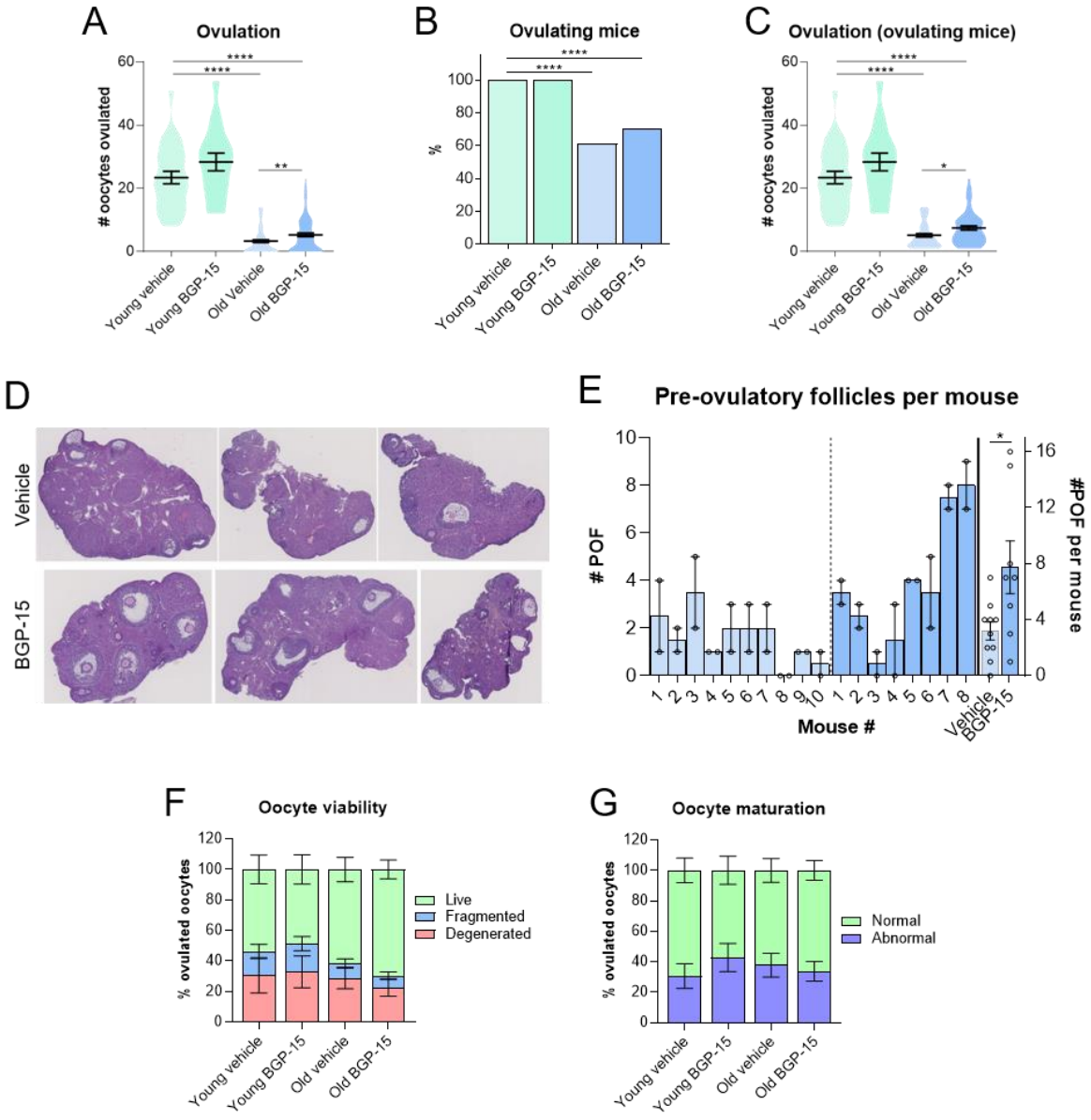

A
Ovulation
oocytes ovulated
Young vehicle
Young BGP-15
Old Vehicle
Old BGP-15
B
Ovulating mice
%
C
Ovulation (ovulating mice)
D
Vehicle
BGP-15
E
Pre-ovulatory follicles per mouse
POF
#POF per mouse
Mouse #
Vehicle
BGP-15
F
Oocyte viability
% ovulated oocytes
Live
Fragmented
Degenerated
G
Oocyte maturation
Normal
Abnormal

Figure 5.8. Advanced maternal age reduces ovulation numbers but does not impact oocyte viability or maturation

COCs were collected 15 hours after hCG administration and fertilised via IVF. Four hours after fertilisation, the total oocytes ovulated were counted (A). The proportion of mice that successfully ovulated from each cohort was compared (B) as was the number of oocytes ovulated only from those mice (C). Whole ovaries from aged mice that did not ovulate were fixed in 4% PFA at 4°C overnight, transferred into PBS, embedded in paraffin wax and sectioned at 5µM thickness. Every 5th slide was stained with H&E (Histology Services, Adelaide University) and imaged using a Nanozoomer Digital Slide Scanner (Adelaide Microscopy) (C). Pre-ovulatory follicles were defined as large antral follicles with a COC visible in at least one section. 12-18 sections were counted per ovary, and both ovaries from 8-10 mice per group were assessed. Follicle counts are shown as the number of follicles counted in each ovary per mouse (D, left y-axis), and the total follicles per mouse, per group (D, right y-axis). Oocytes and presumptive zygotes were scored for viability (live, fragmented or degenerated, D) and maturity (presence of at least one polar body, E). For total ovulation counts, n=26 young vehicle, n= 16 young BGP-15, n=87 old vehicle, and n=91 old BGP-15 mice. For % of mice that successfully ovulated n=11 for young vehicle, old vehicle, and old BGP-15 and n=5 for young BGP-15. For oocyte number in ovulating mice, n=26 young vehicle, n=16 young BGP-15, n=55 old vehicle, and n=65 old BGP-15 mice. For viability and maturity assessments, n=12 young vehicle, n=11 young BGP-15, n=26 old vehicle, and n=30 old BGP-15 mice. Data analysed using one-way ANOVA (A, C, F, G), or Chi-squared test (B), or unpaired t-test (E, right y-axis), * p=0.0125, ** p=0.0069, *** p=0.0001, **** p<0.0001. For A, and C, shaded areas represent the population distributions, while horizontal lines represent mean ± SEM.

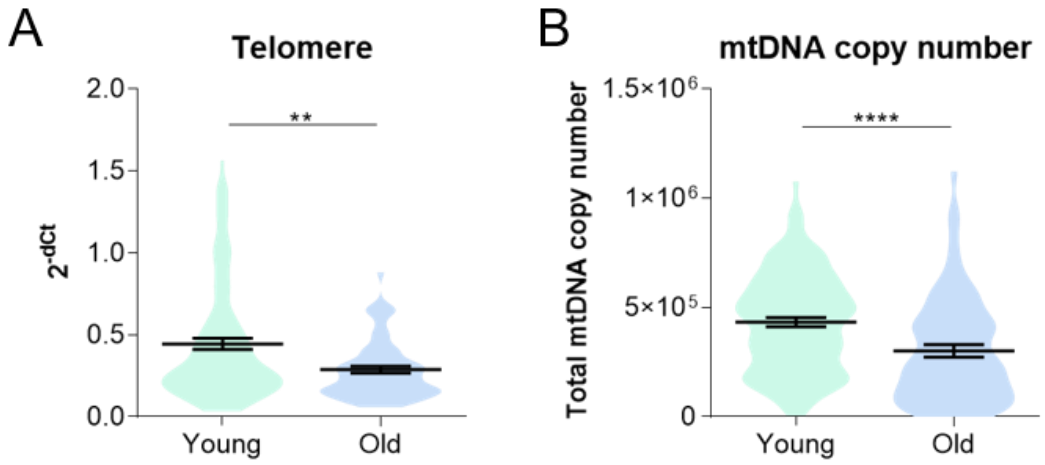


Figure 5.9. Advanced maternal age is associated with reduced telomere length in MII oocytes

Fully denuded MII oocytes were individually frozen for Triple Test analysis. Relative telomere length (A) and total mtDNA copy number (B) were compared between oocytes from young or aged mice. n=109 young and n=69 old MII oocytes. Log transformed data analysed using one-way ANOVA ** p=0.011, **** p<0.0001. Shaded areas represent the population distributions, while horizontal lines represent mean ± SEM.

5.3.6 Advanced maternal age results in perturbations to zygotic epigenetic reprogramming

Zygotes derived from young, aged, or aged females that had been treated with BGP-15 were assessed for the global methylation status of the maternal and paternal pronuclei using antibodies specific to 5mC and 5hmC (Fig. 5.10 A). Analysis of pronuclei size showed established differences, with the paternal pronuclei being larger in size than the maternal, however this difference was not as pronounced in zygotes from old mothers (Fig. 5.10 B).

In zygotes from young females, the maternal pronucleus displayed higher levels of 5mC fluorescence than the paternal pronucleus, however there was no differences between pronuclei of zygotes from aged females (Fig. 5.10 C). Treatment of aged females with BGP-15 saw a restoration of this difference between the maternal and paternal pronuclei (Fig. 5.10 C). When comparing fluorescence of the maternal or paternal pronuclei between groups, there were no differences in fluorescence levels between paternal pronuclei across groups, however the maternal pronucleus of zygotes from aged females displayed lower levels of fluorescence than the maternal pronucleus from young females or those treated with BGP-15 (Fig. 5.10 C). This indicates that treating aged females with BGP-15 may rectify defects seen in maternal pronuclei epigenetic reprogramming in aged females, to similar levels seen in zygotes from young females. When comparing the ratio for fluorescence between the paternal and maternal pronuclei, the levels were more similar between zygote pronuclei from aged females than those from young ($p=0.0751$), and this difference was restored when comparing to the ratio from old mothers that had undergone BGP-15 treatment (Fig. 5.10 C, right y-axis).

The paternal pronucleus had higher levels of 5hmC than the maternal pronucleus in all groups (Fig. 5.10 D), as expected. When comparing fluorescence intensities in the respective pronuclei across groups, maternal pronuclei in zygotes from aged females that had undergone BGP-15 treatment were higher than those from young or aged females (Fig. 5.10 D), indicating that BGP-15 treatment may elevate 5hmC levels in the maternal pronucleus to above that of controls. This was reflected in comparison of the fluorescence ratio between parental pronuclei from each group, where zygotes from aged BGP-15 treated females had a lower ratio than those from aged females,

however there was no difference between zygotes from young females and those from the BGP-15 treated aged females (Fig. 5.10 D, right y-axis).

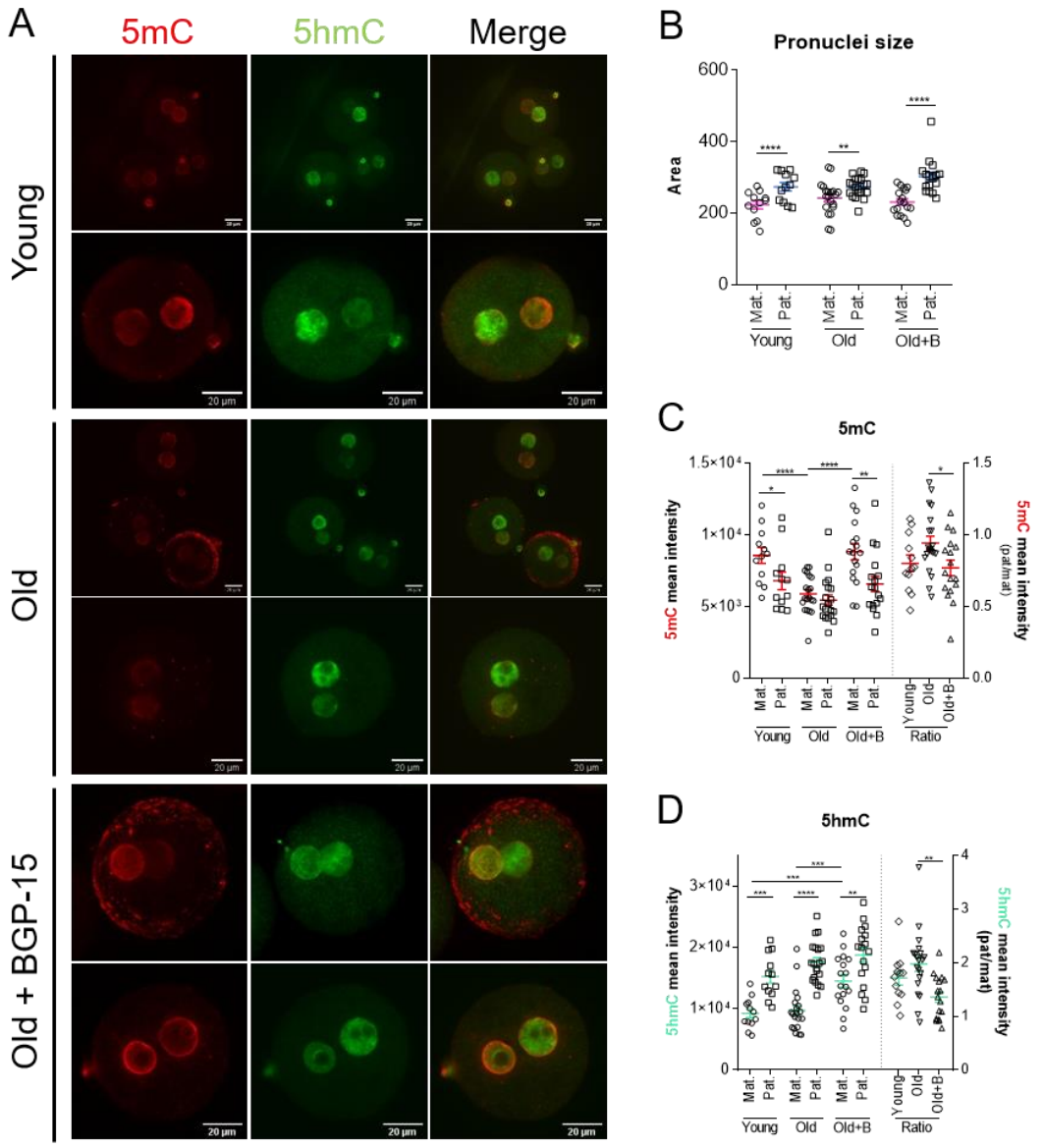


Figure 5.10. Advanced maternal age alters zygotic epigenetic reprogramming events that is partially restored by BGP-15 treatment

Zygotes from young, old, and old females treated with BGP-15 (Old+B) were collected 6 hours after *in vitro* fertilisation and co-stained with anti-5mC (red) and anti-5hmC (green) antibodies (A). Pronuclei size was measured (B) and signal intensity fluorescence levels were quantified for 5mC (C) and 5hmC (D) in maternal and paternal pronuclei. Data presented as signal intensity for maternal (Mat.) and paternal (Pat.) pronuclei on the left axis, and the ratio of the signal for paternal to maternal fluorescence on the right axis. Data analysed using paired t-test for comparisons between maternal and paternal pronuclei of the same zygote, and one-way ANOVA for pronuclei comparisons and ratio comparisons between groups, * $p<0.03$, ** $p<0.005$, *** $p=0.0001$, **** $p<0.0001$.

5.3.7 Advanced maternal age does not impact on-time embryo development but results in shorter telomeres in blastocysts

Presumptive zygotes were assessed 24 hours after fertilisation for successful 2C development (Fig. 5.11 A), and a further 32 hours later for on-time 8C development (Fig. 5.11 B). Advanced maternal age did not result in perturbations to embryo development at either stage and BGP-15 treatment did not alter these development rates either, attesting to the importance of high-quality culture conditions in supporting successful embryo development.

On-time 8Cs were subjected to individual Triple test analysis for relative telomere content and total mtDNA copy number (Fig. 5.11 C & D). Fascinatingly, telomere length was not different between 8C embryos derived from young or aged females, regardless of treatment (Fig. 5.11 C), suggesting that embryos from aged females are able to recover the shortfall in telomere length seen in MII oocytes (Fig. 5.9 A). Assessment of total mtDNA copy number revealed that, unlike in MII oocytes, there was no difference in total mtDNA copy number in 8C embryos from aged females to those from young females (Fig. 5.11 D). mtDNA copy number in 8C embryos from aged females that were treated with BGP-15 was less than those from untreated aged females but was not different to those from young females.

Successful blastocyst development was scored on day five of culture and this was not affected by maternal aging, similar to the normal 2C and on-time 8C development (Fig. 5.12 A). Analysis of individual blastocysts using the Triple Test revealed that, despite having no detectable differences in 8C telomere length, blastocysts derived from aged females had shorter telomeres than those from young females (Fig. 5.12 B). BGP-15 treatment of aged females resulted in an increase in blastocyst telomere length when compared to aged controls, however telomeres in these embryos were still shorter than those from young females. Likewise, relative mtDNA normalised to nuclear gene intensity was reduced in blastocysts from aged females, and BGP-15 treatment resulted in mtDNA level indistinguishable from blastocysts from young females (Fig. 5.12 C). However, total mtDNA copy number was not found to be different between blastocysts (Fig. 5.12 D), suggesting differences in cell numbers in blastocysts derived from young females, aged females, and aged females treated with BGP-15. Analysis of the ICM cell population, revealed consistent decreases in telomere length when

ICMs were derived from aged females (Fig. 5.12 E). Maternal BGP-15 treatment again resulted in substantial increases in telomere lengths, and appeared to have an enhanced effect in the ICM by restoring telomere lengths such that they were indistinguishable to those derived from young females. Unlike whole blastocysts, differences in mtDNA per cell were not apparent in the ICM lineage (Fig. 5.12 F).

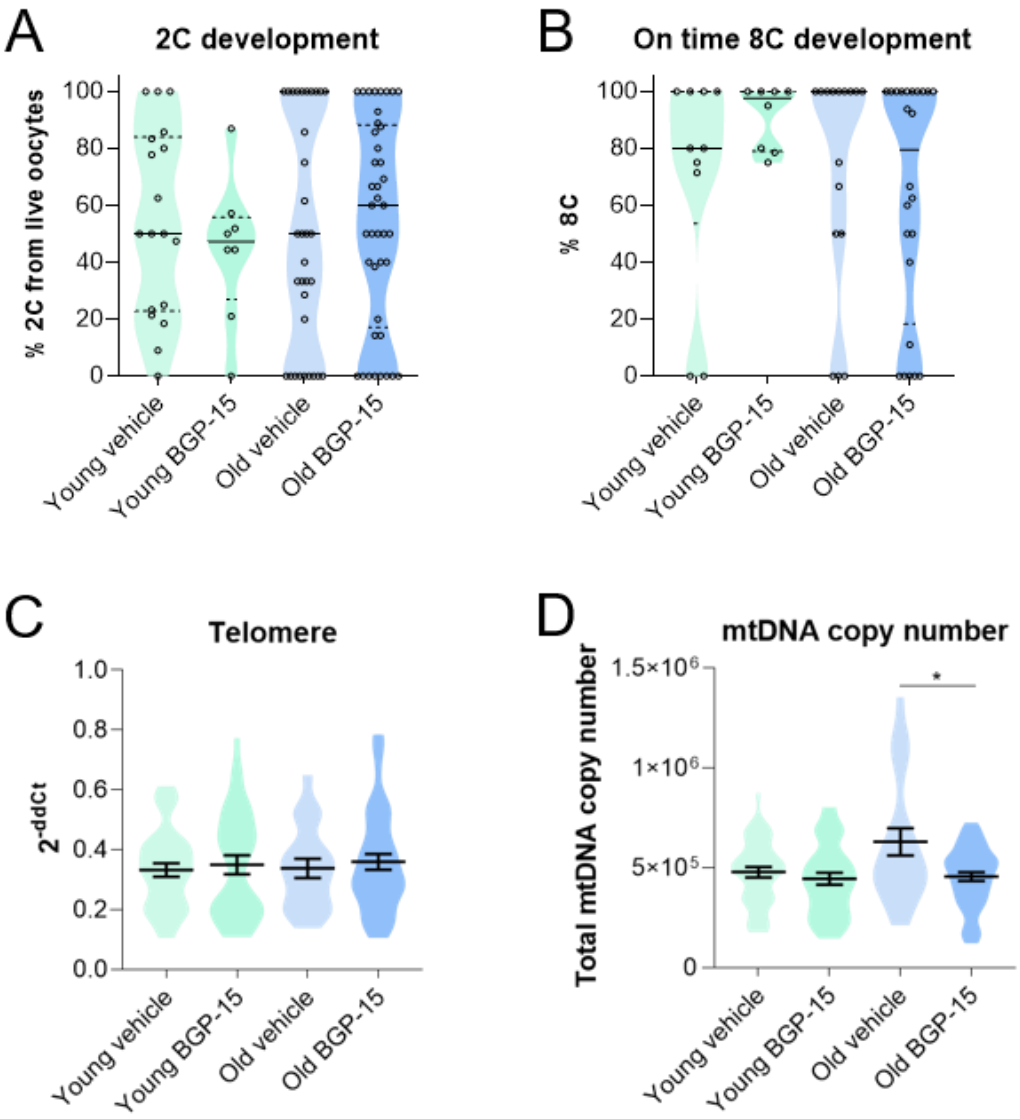


Figure 5.11. Advance maternal age does not impact embryo development or 8C telomere lengths

Oocytes were fertilised via IVF and scored 24 hours later for successful development to the 2C stage (A) and a further 32 hours later for on time development to the 8C stage (B). 8C embryos were collected and individually analysed for telomere length (C) and total mtDNA copy number (D) using the Triple Test. For embryo development n=10-18 young vehicle, n=8 young BGP-15 treated, n=16-33 old vehicle, and n=24-41 old BGP-15 treated mice. For Triple Test n=38 young vehicle, n=35 young BGP-15 treated, n=20 old vehicle, and n=47 old BGP-15 treated 8C embryos. Development data (A, B) and log transformed telomere (C) and mtDNA copy number (D) data analysed using one-way ANOVA, * p=0.03. Shaded areas represent the population distributions, while horizontal lines represent mean ± SEM.

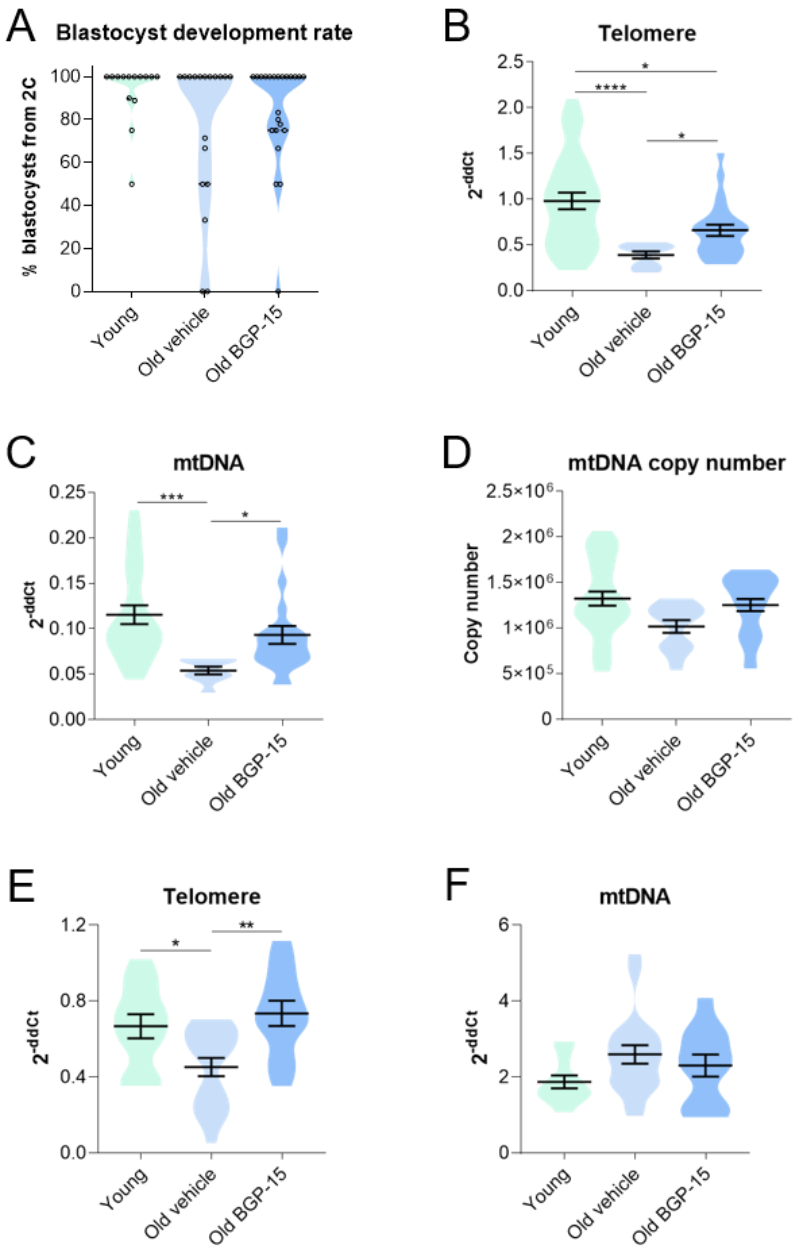


Figure 5.12. Advanced maternal age reduces blastocyst telomere length and mtDNA copy number that is reversible by treatment with BGP-15

Successful blastocyst development was scored 96 hours post fertilisation (A) and whole blastocysts and isolated ICMs were individually analysed using the Triple Test for telomere content (B & E), mtDNA per cell (C & F), and total mtDNA copy number (F). For embryo development n=14 young, n=18 old vehicle, and n=23 old BGP-15 treated mice. For Triple Test n=31 young, n=10 old vehicle, and n=24 old BGP-15 treated blastocysts, and n=12 young, n=19 old vehicle, and n=12 BGP-15 treated ICMs. Blastocyst development (A) and log transformed data (B-F) analysed using one-way ANOVA, * $p<0.05$, ** $p<0.0084$, *** $p=0.0009$, **** $p<0.0001$. Shaded areas represent the population distributions, while horizontal lines represent mean ± SEM.

5.4 Discussion

The combined results of this study further support the hypothesis of oocyte mitochondrial function being a key regulator of telomere elongation during pre-implantation embryo development. Oocytes from female mice that are either obese or reproductively aged are known to have mitochondrial deficiencies and the results from this chapter show that these oocytes give rise to embryos with shorter telomeres than lean young controls (see Fig. 5.13). Further, treatment of mice with BGP-15, which has been shown to increase oocyte mitochondrial activity (Wu et al., 2015 and unpublished data) reversed the telomere elongation deficiency in both aged and obese model systems, thereby further implicating mitochondrial function as a key mediator of early telomere elongation.

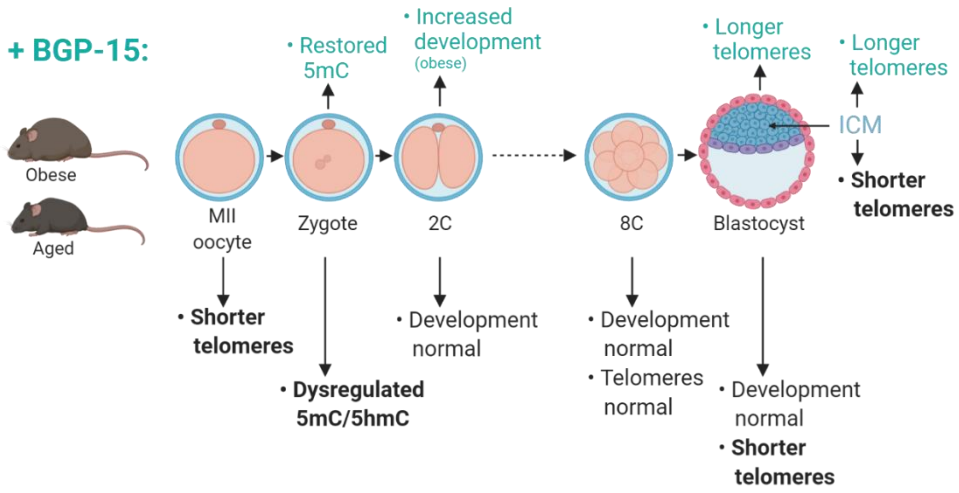


Figure 5.13. Maternal obesity and age disrupt telomere elongation events

Maternal obesity and age perturbed several oocyte and embryo measures (bold text) that were able to be restored by BGP-15 treatment (green text). Embryo development rates in either category were not affected when compared to controls, likely the result of high quality culture conditions used to better support development. Both obesity and aging perturbed zygotic reprogramming events. Obesity resulted in a smaller paternal pronucleus, and aging similarly abolished the differential 5mC. Most remarkably, both obesity and aging resulted in identical effects on telomere length kinetics during development. Both resulted in shorter oocyte telomeres, which were not different from controls at the 8C stage, but were again shorter than normal at the blastocyst stage, specifically in ICMs. BGP-15 treatment was able to restore the 5mC differential in zygotes, and resulted in longer telomeres in whole blastocysts and the ICM.

Maternal obesity and aging similarly impact pre-implantation telomere elongation and reprogramming

Telomere elongation

Oocytes from both categories of females had reduced telomere lengths when compared to controls, and importantly, this is the first evidence that maternal obesity results in shorter oocyte telomeres. While it is likely that short oocyte telomeres from obese females are due to an induced stress state and mitochondrial dysfunction in oocytes from obese females (Han et al., 2018; Wu et al., 2015, 2010), it is hard to speculate whether the decrease in aged oocyte telomere lengths is solely due to mitochondrial dysfunction, or the culmination of the oocytes being exposed to a lifetime's worth of stressors. A somewhat surprising finding, although consistent with the previously investigated rotenone-induced mitochondrial dysfunction model (see Chapter 4), was that 8C telomere lengths were not different to controls, adding further support to the hypothesis that mitochondrial function is not a determining factor in pre-compaction telomere elongation processes. By the blastocyst stage of development however, telomere lengths were demonstrably reduced in embryos derived from obese and aged females. More specifically, this reduction in length was evident in the ICM population, which may result in biologically older offspring and have implications for their health- and life-span. Further, these results indicate a common pathway that leads to reduced telomere lengths during post-compaction development. Given that oocytes from obese, aged, and rotenone-exposed females (see Chapter 4) all present with mitochondrial dysfunction, this provides additional support to mitochondria being a critical regulator of telomere elongation during this time.

Epigenetic reprogramming

Another critical early reprogramming event that was altered to a similar degree by both maternal obesity and aging was the establishment of epigenetic asymmetry between the maternal and paternal pronuclei of zygotes. In both circumstances, the difference in size between pronuclei was not as pronounced as with controls, and 5mC fluorescence intensity difference between pronuclei of the same zygote was also lost. This suggests that gene expression in these embryos may be altered due to global changes in repressive chromatin mark levels, which can potentially have further downstream consequences and requires further investigation. Specifically, the immunofluorescence assay used is a simplistic measure of methylation, and any

potential differences detected should be further validated with more quantifiable assays, such as amplicon bisulfite sequencing using next-generation sequencing (NGS) (The BLUEPRINT consortium, 2016). Further, alterations to 5mC and 5hmC patterns may impact genomic imprinting, as pronuclei epigenetic asymmetry is believed to be an important step in establishing parent-specific developmental programmes (Mayer et al., 2000a). The observation that the size of the paternal pronucleus is affected in the studied models (being smaller in zygotes from obese mice than lean, and the size differential not being as pronounced in zygotes from aged females) likely alludes to deficiencies within the oocyte. Formation of the paternal pronucleus occurs about 1-1.5 hours earlier than the formation of the maternal pronucleus in mouse zygotes (Howlett and Bolton, 1985), and is characterised by decondensation of the chromatin (replacement of protamines with histones). This process is largely controlled by oocyte factors, therefore delays in pronucleus formation highlight further intrinsic problems in oocytes from obese and aged females, possibly by reduction of oocyte capacity to synthesise glutathione, which has been shown to be critical for decondensation and paternal pronucleus formation (Perreault et al., 1988; Wiesel and Schultz, 1981). Glutathione is an important intracellular antioxidant, with critical roles including maintenance of the redox state, and protection from damage by free radicals and peroxides. While glutathione is produced exclusively in the cytosol, it is imported into the mitochondria, where it plays a key defence role against ROS (reviewed in Ribas et al., 2014). A lack of sufficient glutathione in oocytes, and therefore zygotes, from obese and aged females to facilitate timely sperm decondensation may also reflect decreased mitochondrial glutathione levels, thereby leading to decreased embryonic defences against ROS, and allowing cellular damage and dysfunction to occur, as mouse cleavage embryos have limited capacity to synthesise glutathione and are susceptible to conditions that deplete glutathione (Gardiner and Reed, 1995). The results from the obesity model agree with previous work done in a high fat diet-induced obesity model (Han et al., 2018), which also used a similar assay methodology, where maternal obesity resulted in more similar levels of both 5mC and 5hmC between the maternal and paternal pronuclei than in controls, where the differential was much more pronounced. Pronuclei size was not compared in the previous study (Han et al., 2018), and it is important to note that some differences are more pronounced in the previous study than the current study as zygotes were analysed in this study at the PN3 stage, whereas the previous study

analysed PN4 stage zygotes (Han et al., 2018). To my knowledge, this is also the first demonstration that maternal aging can disrupt this epigenetic reprogramming process.

Mitochondrial DNA

Interestingly, blastocysts derived from obese females exhibited more mtDNA per cell than those from lean females, however this difference was not apparent in the ICM population. In contrast, whole blastocysts derived from aged females displayed decreased mtDNA copy number per cell compared to those derived from young females, however this was again not apparent in the ICM population. Taken together, this suggests that there are perturbations in the trophectoderm population in these embryos. This may stem from premature trophectoderm proliferation in obese blastocysts, possibly resulting from mitochondrial dysfunction causing early loss of pluripotency in these cells as mitochondria are key for maintaining pluripotency and regulating differentiation (Seo et al., 2018), and delays in trophectoderm proliferation in embryos from aged females (Velazquez et al., 2016). Quantification of blastocyst cell populations in this model of aging would provide further insight into this difference as a previous study did not find a difference in ICM cell numbers with advanced maternal age (Velazquez et al., 2016).

Treatment with BGP-15 improved several outcomes

BGP-15 is a novel insulin sensitiser drug and is currently in phase II clinical trials for treatment of insulin resistance and type II diabetes mellitus, and is also showing promise in other pre-clinical trials involving animal models of disease (reviewed in Pető et al., 2020). While BGP-15 was initially established as a stimulator of heat shock protein expression, several studies have highlighted beneficial effects of this compound on mitochondrial-stress-related diseases. BGP-15 treatment has protective effects against oxidative stress, can reduce mitochondrial ROS production and thereby improve cell survival (Sumegi et al., 2017; Szabados et al., 2000), as well as prevent mitochondrial depolarisation (Nagy et al., 2010). BGP-15 can also prevent mitochondrial fragmentation, stabilise mitochondrial membranes, and promote mitochondrial fusion in a model of pulmonary arterial hypertension (Szabo et al., 2018). BGP-15 treatment of obese females increased oocyte mtDNA copy number, increased TFAM and DRP1 (mitochondrial replication factors) abundance in oocytes, and restored fetal mtDNA tissue content (Wu et al., 2015). Therefore, there is a

growing body of evidence that BGP-15 has both protective, and stimulative effects on mitochondria in stress situations.

Consistent with previous reports, BGP-15 treatment increased mtDNA copy number in oocytes from obese mice when compared to both obese and lean controls (Wu et al., 2015). Strikingly, treatment of obese and aged females with BGP-15 was able to restore telomere length deficits seen in both whole blastocysts, and excitingly, the ICM lineage too. Importantly, the effect of BGP-15 treatment in aged females on telomere length was more pronounced in the ICM lineage than the whole blastocyst, as whole blastocyst telomeres were still shorter than those from young females, while ICM telomere length was indistinguishable. The restoration of telomere lengths following treatment of females with a compound that is known to enhance oocyte mitochondrial function adds another layer of compelling evidence to the theory of mitochondria being a key regulator of post-compaction telomere elongation events. Mitochondrial function is well established as a major influencer of oocyte developmental competence and therefore subsequent embryo development, as their dysfunction results in many deficiencies. Due to this relationship it is certainly conceivable that telomere elongation is another embryonic factor that is compromised by mitochondrial dysfunction. The recognised relationship between mitochondrial dysfunction and telomere length is that mitochondrial dysfunction results in accelerated shortening of telomeres, however the notion that mitochondrial function may be a key regulator of telomere elongation events, as shown here, is not a previously described phenomenon. This poses an exciting new role for mitochondria and warrants further investigation into how this modulation of elongation occurs.

Treatment with BGP-15 appeared to restore other deficits seen in the key reprogramming event of pronuclear epigenetic asymmetry establishment. The loss of 5mC fluorescence intensity asymmetry associated with maternal obesity and age was re-established following BGP-15 treatment, which may rescue any associated gene expression or imprinting alterations and requires further investivation. This data agrees with extensive evidence that mitochondria are a key regulator of epigenetic reprogramming events in early embryogenesis (extensively reviewed by Harvey, 2019), and importantly, that their influence is modifiable, thus enabling rectification of these processes in situations of mitochondrial stress or dysfunction.

Epidemiological and public health perspectives

The results of this study have major implications for the understanding the developmental programming of lifespan. Epidemiological studies have linked maternal obesity during pregnancy with premature mortality from cardiovascular events in adult offspring (Reynolds et al., 2013), and maternal age at conception showing and inverse relationship with offspring lifespan (Gavrilov and Gavrilova, 2012). Furthermore, maternal obesity has been directly linked to decreased telomere lengths in offspring cord blood and placenta (Martens et al., 2016), while children of women who had metabolic syndrome during pregnancy had shorter telomeres than those born to mothers that did not have metabolic syndrome during pregnancy (McAninch et al., 2020).

This study has revealed the likely origin point of shorter telomeres observed in children from obese mothers (Martens et al., 2016; McAninch et al., 2020) and the decreased offspring life spans associated with maternal obesity and age (Gavrilov and Gavrilova, 2012; Reynolds et al., 2013). Here, it has been shown that these telomere length deficits originate in the blastocyst, and more specifically, the ICM lineage which directly gives rise to the foetus.

Telomere length is known to decrease with age, and as such serves as a biomarker of aging. Due to the difficulty of analysing telomere length in humans throughout their lifespan as a consequence overall longevity, many assessments of telomere length and lifespan have been carried out in animals. Studies of zebra finches, wild purple-crowned fairy-wrens, and *Caenorhabditis elegans* found that early life telomere length was a predictor of lifespan, with those in possession of the longest telomeres having the longest lifespan (Eastwood et al., 2019; Heidinger et al., 2012; Joeng et al., 2004). Interestingly, early life telomere length was also a positive predictor of breeding duration and lifetime reproductive success in wild purple-crowned fairy-wrens (Eastwood et al., 2019). As the cells of the embryo that directly give rise to the foetus contain shorter telomeres when derived from obese or aged females, this provides a reasonable explanation for the reduced lifespan seen in these offspring. Further, this study provides critical new evidence that the peri-conception window is a fundamental determinant for the developmental programming of offspring lifespan.

In addition, this study highlights concerning implications for future population health and longevity, as rates of global obesity are increasing at a worrying pace, and shifts in societal trends are seeing women delaying childbearing until later in life.

Summary and future directions

The results from this study demonstrate many parallels between maternal obesity and advanced maternal age, such as decreased ovulation, as well as MII oocytes, blastocysts and ICM populations having decreased telomere lengths compared to controls. Together, these results indicate that maternal obesity induces premature hallmarks of reproductive aging. Further to this, treatment of both obese and reproductively aged females with the mitochondrial activator BGP-15 restored telomere lengths in blastocysts and ICMs. This exciting finding builds on previous results using a rotenone-induced mitochondrial dysfunction model to implicate mitochondrial function in oocytes as a key regulator of second-phase telomere elongation events. Overall, therapeutic modulation of oocyte mitochondrial function appears to be a promising candidate for correcting adverse phenotypes associated with maternal age and BMI at conception, such as reduced offspring life-span. To further build on this work, generation of offspring from each of these models for assessment and monitoring is essential.

5.5 References

Catalano, P., deMouzon, S.H., 2015. Maternal obesity and metabolic risk to the offspring: why lifestyle interventions may have not achieved the desired outcomes. International Journal of Obesity 39, 642–649. https://doi.org/10.1038/ijo.2015.15

Cimadomo, D., Fabozzi, G., Vaiarelli, A., Ubaldi, N., Ubaldi, F.M., Rienzi, L., 2018. Impact of Maternal Age on Oocyte and Embryo Competence. Frontiers in Endocrinology 9. https://doi.org/10.3389/fendo.2018.00327

Eastwood, J.R., Hall, M.L., Teunissen, N., Kingma, S.A., Hidalgo Aranzamendi, N., Fan, M., Roast, M., Verhulst, S., Peters, A., 2019. Early-life telomere length predicts lifespan and lifetime reproductive success in a wild bird. Molecular Ecology 28, 1127–1137. https://doi.org/10.1111/mec.15002

Gardiner, C.S., Reed, D.J., 1995. Synthesis of Glutathione in the Preimplantation Mouse Embryo. Archives of Biochemistry and Biophysics 318, 30–36. https://doi.org/10.1006/abbi.1995.1200

Gavrilov, L.A., Gavrilova, N.S., 2012. Biodemography of Exceptional Longevity: Early-Life and Mid-Life Predictors of Human Longevity. Biodemography and Social Biology 58, 14–39. https://doi.org/10.1080/19485565.2012.666121

Ghosh, S., Feingold, E., Chakraborty, S., Dey, S.K., 2010. Telomere length is associated with types of chromosome 21 nondisjunction: a new insight into the maternal age effect on Down syndrome birth. Human Genetics 127, 403–409. https://doi.org/10.1007/s00439-009-0785-8

Glastras, S.J., Chen, H., Pollock, C.A., Saad, S., 2018. Maternal obesity increases the risk of metabolic disease and impacts renal health in offspring. Bioscience Reports 38. https://doi.org/10.1042/BSR20180050

Grodstein, F., Goldman, M.B., Cramer, D.W., 1994. Body Mass Index and Ovulatory Infertility: Epidemiology 5, 247–250. https://doi.org/10.1097/00001648-199403000-00016

Han, L., Ren, C., Li, L., Li, X., Ge, J., Wang, H., Miao, Y.-L., Guo, X., Moley, K.H., Shu, W., Wang, Q., 2018. Embryonic defects induced by maternal obesity in mice derive from Stella insufficiency in oocytes. Nature Genetics 50, 432–442. https://doi.org/10.1038/s41588-018-0055-6

Harvey, A.J., 2019. Mitochondria in early development: linking the microenvironment, metabolism and the epigenome. Reproduction 157, R159–R179. https://doi.org/10.1530/REP-18-0431

Heidinger, B.J., Blount, J.D., Boner, W., Griffiths, K., Metcalfe, N.B., Monaghan, P., 2012. Telomere length in early life predicts lifespan. Proceedings of the National Academy of Sciences 109, 1743–1748. https://doi.org/10.1073/pnas.1113306109

Henderson, S.A., Edwards, R.G., 1968. Chiasma Frequency and Maternal Age in Mammals. Nature 218, 22–28. https://doi.org/10.1038/218022a0

Howlett, S.K., Bolton, V.N., 1985. Sequence and regulation of morphological and molecular events during the first cell cycle of mouse embryogenesis. J Embryol Exp Morphol 87, 175–206.

Joeng, K.S., Song, E.J., Lee, K.-J., Lee, J., 2004. Long lifespan in worms with long telomeric DNA. Nature Genetics 36, 607–611. https://doi.org/10.1038/ng1356

Kameyama, Y., Ohnishi, H., Shimoi, G., Hashizume, R., Ito, M., Smith, L.C., 2010. Asymmetrical allocation of mitochondrial DNA to blastomeres during the first two cleavages in mouse embryos. Reproduction, Fertility and Development 22, 1247. https://doi.org/10.1071/RD10076

Krisher, R.L., 2019. Maternal age affects oocyte developmental potential at both ends of the age spectrum. Reproduction, Fertility and Development 31, 1. https://doi.org/10.1071/RD18340

Ma, R.C.W., Gluckman, P.D., Hanson, M.A., 2020. Maternal obesity and developmental priming of risk of later disease, in: Obesity and Obstetrics. Elsevier, pp. 149–163. https://doi.org/10.1016/B978-0-12-817921-5.00016-3

Mania, A., Mantzouratou, A., Delhanty, J.D.A., Baio, G., Serhal, P., Sengupta, S.B., 2014. Telomere length in human blastocysts. Reproductive BioMedicine Online 28, 624–637. https://doi.org/10.1016/j.rbmo.2013.12.010

Martens, D.S., Plusquin, M., Gyselaers, W., De Vivo, I., Nawrot, T.S., 2016. Maternal pre-pregnancy body mass index and newborn telomere length. BMC Med 14, 148. https://doi.org/10.1186/s12916-016-0689-0

Mayer, W., Niveleau, A., Walter, J., Fundele, R., Haaf, T., 2000. Demethylation of the zygotic paternal genome. Nature 403, 501–502. https://doi.org/10.1038/35000656

McAninch, D., Bianco-Miotto, T., Gatford, K.L., Leemaqz, S.Y., Andraweera, P.H., Garrett, A., Plummer, M.D., Dekker, G.A., Roberts, C.T., Smithers, L.G., Grieger, J.A., 2020. The metabolic syndrome in pregnancy and its association with child telomere length. Diabetologia 63, 2140–2149. https://doi.org/10.1007/s00125-020-05242-0

Menken, J., Trussell, J., Larsen, U., 1986. Age and infertility. Science 233, 1389–1394. https://doi.org/10.1126/science.3755843

Morea, M., Miu, N., Morea, V.F., Cornean, R., 2013. Maternal obesity - a risk factor for metabolic syndrome in children. Clujul Medical (1957) 86, 259–265.

Nagy, G., Szarka, A., Lotz, G., Dóczi, J., Wunderlich, L., Kiss, A., Jemnitz, K., Veres, Z., Bánhegyi, G., Schaff, Z., Sümegi, B., Mandl, J., 2010. BGP-15 inhibits caspase-independent programmed cell death in acetaminophen-induced liver injury. Toxicology and Applied Pharmacology 243, 96–103. https://doi.org/10.1016/j.taap.2009.11.017

Page, K.A., Luo, S., Wang, X., Chow, T., Alves, J., Buchanan, T.A., Xiang, A.H., 2019. Children Exposed to Maternal Obesity or Gestational Diabetes Mellitus During Early Fetal Development Have Hypothalamic Alterations That Predict Future Weight Gain. Diabetes Care 42, 1473–1480. https://doi.org/10.2337/dc18-2581

Perreault, S.D., Barbee, R.R., Slott, V.L., 1988. Importance of glutathione in the acquisition and maintenance of sperm nuclear decondensing activity in maturing hamster oocytes. Developmental Biology 125, 181–186. https://doi.org/10.1016/0012-1606(88)90070-X

Pető, Á., Kósa, D., Fehér, P., Ujhelyi, Z., Sinka, D., Vecsernyés, M., Szilvássy, Z., Juhász, B., Csanádi, Z., Vígh, L., Bácskay, I., 2020. Pharmacological Overview of the BGP-15 Chemical Agent as a New Drug Candidate for the Treatment of Symptoms of Metabolic Syndrome. Molecules 25, 429. https://doi.org/10.3390/molecules25020429

Ray, A., Hong, C.-S., Feingold, E., Ghosh, Papiya, Ghosh, Priyanka, Bhaumik, P., Dey, S., Ghosh, S., 2015. Maternal Telomere Length and Risk of Down Syndrome: Epidemiological Impact of Smokeless Chewing Tobacco and Oral Contraceptive on Segregation of Chromosome 21. Public Health Genomics 19, 11–18. https://doi.org/10.1159/000439245

Reynolds, R.M., Allan, K.M., Raja, E.A., Bhattacharya, S., McNeill, G., Hannaford, P.C., Sarwar, N., Lee, A.J., Bhattacharya, S., Norman, J.E., 2013. Maternal obesity

during pregnancy and premature mortality from cardiovascular event in adult offspring: follow-up of 1 323 275 person years. BMJ 347, f4539–f4539. https://doi.org/10.1136/bmj.f4539

Ribas, V., GarcÃ-a-Ruiz, C., FernÃ¡ndez-Checa, J.C., 2014. Glutathione and mitochondria. Frontiers in Pharmacology 5. https://doi.org/10.3389/fphar.2014.00151

Robker, R.L., 2008. Evidence that obesity alters the quality of oocytes and embryos. Pathophysiology 15, 115–121. https://doi.org/10.1016/j.pathophys.2008.04.004

Seo, B., Yoon, S., Do, J., 2018. Mitochondrial Dynamics in Stem Cells and Differentiation. International Journal of Molecular Sciences 19, 3893. https://doi.org/10.3390/ijms19123893

Sharma, R., Biedenharn, K.R., Fedor, J.M., Agarwal, A., 2013. Lifestyle factors and reproductive health: taking control of your fertility. Reproductive Biology and Endocrinology 11, 66. https://doi.org/10.1186/1477-7827-11-66

Sumegi, K., Fekete, K., Antus, C., Debreceni, B., Hocsak, E., Gallyas, F., Sumegi, B., Szabo, A., 2017. BGP-15 Protects against Oxidative Stress- or Lipopolysaccharide-Induced Mitochondrial Destabilization and Reduces Mitochondrial Production of Reactive Oxygen Species. PLOS ONE 12, e0169372. https://doi.org/10.1371/journal.pone.0169372

Szabados, E., Literati-Nagy, P., Farkas, B., Sumegi, B., 2000. BGP-15, a nicotinic amidoxime derivate protecting heart from ischemia reperfusion injury through modulation of poly(ADP-ribose) polymerase. Biochemical Pharmacology 59, 937–945. https://doi.org/10.1016/S0006-2952(99)00418-9

Szabo, A., Sumegi, K., Fekete, K., Hocsak, E., Debreceni, B., Setalo, G., Kovacs, K., Deres, L., Kengyel, A., Kovacs, D., Mandl, J., Nyitrai, M., Febbraio, M.A., Gallyas, F., Sumegi, B., 2018. Activation of mitochondrial fusion provides a new treatment for mitochondria-related diseases. Biochemical Pharmacology 150, 86–96. https://doi.org/10.1016/j.bcp.2018.01.038

Tarín, J.J., Pérez-Albalá, S., Cano, A., 2002. Oral antioxidants counteract the negative effects of female aging on oocyte quantity and quality in the mouse: EFFECT OF ANTIOXIDANT DIET ON MOUSE OOCYTES. Molecular Reproduction and Development 61, 385–397. https://doi.org/10.1002/mrd.10041

Treff, N.R., Su, J., Taylor, D., Scott, R.T., 2011. Telomere DNA Deficiency Is Associated with Development of Human Embryonic Aneuploidy. PLoS Genetics 7, e1002161. https://doi.org/10.1371/journal.pgen.1002161

Velazquez, M.A., Smith, C.G.C., Smyth, N.R., Osmond, C., Fleming, T.P., 2016. Advanced maternal age causes adverse programming of mouse blastocysts leading to altered growth and impaired cardiometabolic health in post-natal life. Human Reproduction 31, 1970–1980. https://doi.org/10.1093/humrep/dew177

Wiesel, S., Schultz, G.A., 1981. Factors which may affect removal of protamine from sperm DNA during fertilization in the rabbit. Gamete Research 4, 25–34. https://doi.org/10.1002/mrd.1120040105

Wu, L.L., Russell, D.L., Wong, S.L., Chen, M., Tsai, T.-S., St John, J.C., Norman, R.J., Febbraio, M.A., Carroll, J., Robker, R.L., 2015. Mitochondrial dysfunction in oocytes of obese mothers: transmission to offspring and reversal by pharmacological endoplasmic reticulum stress inhibitors. Development 142, 681–691. https://doi.org/10.1242/dev.114850

Wu, L.L.-Y., Dunning, K.R., Yang, X., Russell, D.L., Lane, M., Norman, R.J., Robker, R.L., 2010. High-Fat Diet Causes Lipotoxicity Responses in Cumulus–Oocyte Complexes and Decreased Fertilization Rates. Endocrinology 151, 5438–5445. https://doi.org/10.1210/en.2010-0551

Zhang, J.-J., Liu, X., Chen, L., Zhang, S., Zhang, X., Hao, C., Miao, Y.-L., 2020. Advanced maternal age alters expression of maternal effect genes that are essential for human oocyte quality. Aging 12, 3950–3961. https://doi.org/10.18632/aging.102864

CHAPTER 6

SUMMARY AND FUTURE DIRECTIONS

6.1. Summary and future directions

Pre-implantation embryogenesis is a complex and highly dynamic time of development in which many aspects of lifelong health trajectories are set within a very short window of time. Critical events during this period include epigenetic reprogramming and telomere length re-setting, which are essential for normal embryo development, successful pregnancy, and offspring health- and life-span.

Summary

This work within this thesis firstly established a novel, highly sensitive qPCR assay, named the 'Triple Test', which precisely quantifies three outcomes (two genomic DNA sequences - telomere and *Rn18S* as the reference, and mitochondrial DNA) in individual oocytes and embryos. This assay was carefully validated and shown to overcome major flaws in previous methods that resulted in false readings, loss of mitochondrial DNA, and required large input DNA amounts from pooled samples. The Triple Test was invaluable throughout this thesis, enabling the natural variability in telomeric DNA and mtDNA between individual oocytes and embryos to be revealed, and enables robust measurements in physiological contexts where sample availability is greatly limited. This assay was then utilised to conduct a thorough examination of changes in telomere content relative to nuclear DNA throughout pre-implantation embryogenesis, from oocyte maturation through to blastocyst cell populations. This work revealed that telomere elongation routinely occurs during post-compaction development, however elongation patterns during pre-compaction development are subtly different depending on the genetics of the embryo.

The major finding of this work was that mitochondrial function was revealed as an important regulatory factor influencing post-compaction telomere elongation, through the use of oocyte-specific mitochondrial inhibition with rotenone. Additionally, telomere elongation was sensitive to several stressors that impact mitochondrial activity, including culture in super-physiological 20% oxygen, which is known to negatively impact mitochondrial function. This same perturbation to post-compaction elongation was also observed in two examined biological scenarios of oocyte mitochondrial dysfunction *in vivo*; specifically, maternal obesity and advanced age. Further solidifying the importance of mitochondria for telomere elongation, treatment of obese or aged females with the mitochondrial activator compound BGP-15 was able to

restore telomere lengths in blastocysts, and importantly within the ICM lineage, to where these were indistinguishable from controls.

Novel findings in telomere biology

An overarching aim of this thesis was to provide further insight into the patterns of, and mechanisms controlling telomere elongation during mouse pre-implantation embryogenesis. Firstly, I have provided a much more in-depth and robust characterisation of elongation trends than previous reports. Of interest is that telomere elongation occurred by the 8C stage in 3 out of 5 embryo strains analysed, and occurred from the 8C to blastocyst stage in all of them. This enabled the categorisation of elongation into two phases, the earliest during pre-compaction development (MII-8C) and the second occurring during post-compaction development (8C to blastocyst), which was critical for analysis of telomere elongation in induced- and biological-contexts of mitochondrial dysfunction.

Interestingly, the extent of elongation during pre- and post-compaction development was strain dependent. This indicates that the pre-compaction phase of elongation, possibly the result of Alternative Lengthening of Telomeres (ALT) action, does not occur in all contexts of embryo development. ALT-mediated elongation during the early embryonic cleavages, prior to telomerase upregulation, has widely become accepted as dogma. The findings of this thesis suggest that the ALT mechanism is not a consistent occurrence in pre-implantation embryogenesis and may only occur in some contexts.

Due to this discrepancy, an important next step for work on telomere elongation events is to investigate different species. Embryo telomere elongation patterns appear to differ between mice and bovine (Gilchrist et al., 2015; Iqbal et al., 2011; Liu et al., 2007; Meerdo et al., 2005; Wang et al., 2013), therefore it is crucial to elucidate these trends in other species as telomere elongation may not be universally conserved between mammals. Given that telomere elongation during the supposed ALT-stage of embryogenesis occurred in hybrid and outbred mouse strains, this mechanism might be expected to occur in human embryos due to their genetic diversity, which is absent in inbred laboratory mouse strains.

The ultimate aim of this research going forward is to elucidate these mechanisms in normal human embryogenesis to then enable interrogation of whether these are

perturbed in situations of sub- or in-fertility, as well as the potential effects on lifespan and healthspan in children. A logical first step is to analyse telomere elongation in non-human primate (NHP) species. Primate and murine embryogenesis are known to differ in several important aspects. For example, primates have protracted pre-implantation embryogenesis (Boroviak and Nichols, 2017; Ross and Boroviak, 2020), including later embryonic genome activation, which occurs at the 4-8C stage in humans (Braude et al., 1988), but at the 2C stage in mice. In addition to this, compaction occurs later in primate embryos than murine (16- to 32-cell stage (primates) compared with 8-16-cell (mouse)). As primate and murine pre-implantation embryogenesis show many distinct differences at key events, it is likely that telomere elongation during this time may also vary between the species. As such, telomere elongation in pre-implantation embryogenesis should first be characterised as a priority in NHPs as this would be directly relatable to human embryos. Human and NHP embryos show many similarities that are distinct from murine embryos, including unique hallmarks of pluripotency, and striking morphological similarities between common marmoset, rhesus macaque, and human implantation stage embryos (reviewed in Boroviak and Nichols, 2017). Therefore pre-implantation embryo telomere elongation patterns in NHPs should be relatively translatable to human embryos, and provide a strong knowledge base for subsequent exploration into human embryos. It is crucial to elucidate these mechanisms in human embryos in order to understand the developmental origins and programming of lifespan, health, and disease in our own species and maximise the opportunities to extend healthspan in clinical contexts.

A novel functional role for mitochondria

A major outcome of this research is the discovery that mitochondria play a role in the telomere elongation mechanisms that occur during embryogenesis. Each model of mitochondrial dysfunction that was analysed (rotenone-induced, maternal obesity, and advanced maternal age) consistently presented MII oocytes with shorter telomeres. Interestingly, embryos from each of these models as well as embryos cultured in super-physiological oxygen, exhibited unperturbed elongation up to the 8C stage, yet shortened telomeres in blastocysts and the ICM lineage. In maternal obesity and advanced age models, maternal treatment with the novel therapeutic BGP-15, which has been shown to have many protective effects on mitochondria in stress situations, for four days prior to oocyte collection and IVF, was able to restore telomere lengths

in blastocysts and ICMs. This adds another compelling layer of evidence for this novel role of mitochondria in telomere elongation.

Mitochondrial stress responses have been well established as a mediator of telomere shortening, however the findings of this thesis indicate a novel and exciting role for mitochondria as a mediator of telomere elongation. This thesis supports the concept that two telomere elongation mechanisms occur during pre-implantation development, and one remarkable insight is that these are differentially regulated by mitochondrial function. Firstly, it is clear that pre-compaction telomere elongation is not regulated by mitochondrial activity. Secondly, the use of multiple models consistently showed that post-compaction telomere elongation is sensitive to mitochondrial perturbations (see Fig. 6.1). Therefore, this work provides never-before documented insights into the complex relationship between mitochondria and telomeres.

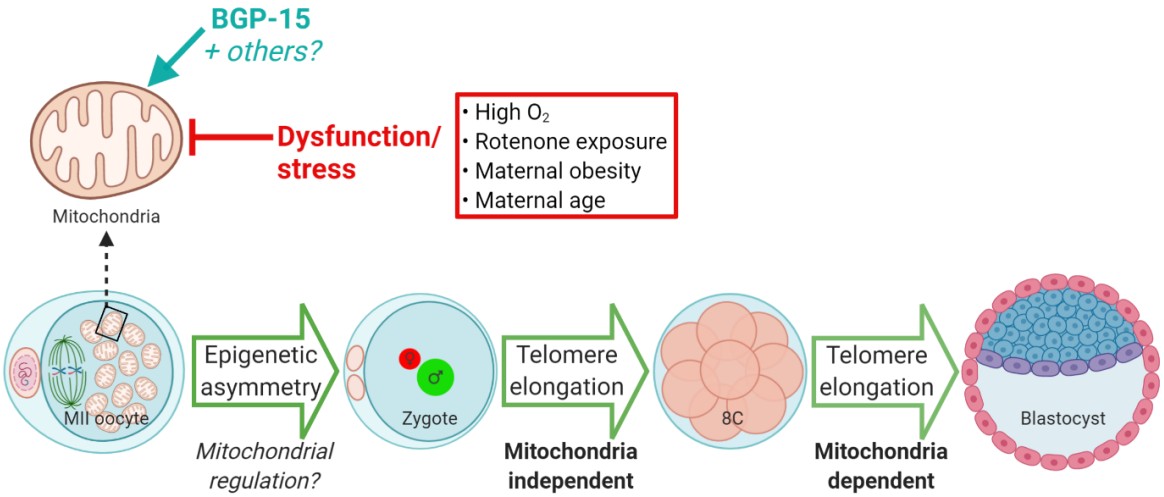


Figure 6.1. Novel findings of mitochondrial influence on early reprogramming events

Oocyte mitochondrial function was found to be a major factor influencing early reprogramming events, as evidenced by models of mitochondrial dysfunction, including high oxygen culture, rotenone exposure, maternal obesity, and advanced reproductive age, while enhancement of mitochondrial function via maternal BGP-15 treatment was able to restore normal events. The perturbed events include loss of epigenetic asymmetry between the maternal and paternal zygotic pronuclei, and impaired telomere length resetting from the 8C to blastocyst stage (including in the ICM lineage, specifically).

This new role for mitochondria, uncovered in this thesis, brings to light a key question for further understanding the relationship between mitochondrial function and telomere elongation that requires extensive investigation: By what mechanism(s) do mitochondria influence telomere elongation? The cellular processes regulated by mitochondria are numerous, and while their primary role is ATP production, other functions include but are not limited to metabolite synthesis, lipid, carbohydrate, and amino acid metabolism, apoptosis, calcium homeostasis, stem cell regulation, and senescence. Given the wide-ranging roles of mitochondria, there are several possibilities by which they could modulate telomere elongation. First, telomeres are

known to be highly susceptible to damage and shortening from exposure to reactive oxygen species, which are produced in excess by mitochondria under stress or dysfunction situations; therefore mitochondrial ROS production may lead to attrition of newly synthesised telomeric DNA, resulting in shorter telomeres. Secondly, many enzymes that deposit or remove epigenetic chromatin marks require mitochondrial-produced metabolites as essential cofactors for their function. Thus, mitochondrial metabolites, such as a-ketoglutarate for instance, may be required for appropriate expression or activity of the telomere elongation machinery during embryogenesis. Further, mitochondrial dysfunction could alter metabolite availability and potentially modify cellular epigenetic state, which was indicated as a possibility here through observed disruptions to epigenetic asymmetry establishment in zygotes from mitochondrial dysfunction models (see Fig. 6.1). An important next step for elucidating the validity of this suggested mechanism is to first analyse changes in global gene expression, and further validate this by high-resolution analysis of chromatin and histone epigenetic depositions. Alterations to a cell's epigenetic state may result in repressed expression of telomerase components, thereby culminating in decreased rates of telomere elongation. As telomeres are also epigenetically modified sequences, alterations to metabolite availability could impact the establishment or maintenance of telomeric epigenetic marks, thereby altering the epigenetic state of the telomeres themselves, which may impede access to telomere elongation machinery. Other possibilities include direct interactions between mitochondria and the telomere elongation machinery. For example, under situations of oxidative stress in cultured cells, telomerase (particularly the TERT component) moves from the nucleus and localises to mitochondria (Ahmed et al., 2008). TERT localisation to mitochondria was associated with prevention of mtDNA damage and superoxide production, and increased mitochondrial membrane potential (Ahmed et al., 2008), thereby suggesting a possible mechanism where telomere elongation could be sacrificed to preserve embryo survival. The exact mechanism for mitochondrial modulation of telomere elongation may lie outside of any of the suggested possibilities, or even be a combination of several, but the foundational observations of this thesis certainly open up exciting new possibilities for future investigation.

Implications for the developmental programming of lifespan

A major finding of this thesis that has significant clinical and public health implications is that both maternal age and obesity similarly perturbed telomere length reprogramming to result in blastocysts with shorter telomeres than those derived from young and lean females. Further, treatment of females with the mitochondrial activator BGP-15 was able to restore telomere lengths, indicating that this perturbation to telomere elongation is modifiable and able to be recovered. Importantly, this pattern of shorter telomeres with mitochondrial dysfunction and restoration with treatment of BGP-15 was observed specifically in the inner cell mass population of blastocysts. This has profound implications for the offspring as the ICM goes on to form the foetus.

A necessary aspect of future investigation is to determine the effects of decreased telomere length on offspring health- and life-span. Towards this, embryos from both obese and reproductively aged females, with and without BGP-15 treatment, should be implanted into surrogate mothers (to isolate the effects of the embryo phenotype and remove potential confounding systemic factors) and extensive assessments conducted on the offspring. In addition to this, embryos derived from females treated with rotenone should be implanted into surrogate females and undergo the same offspring assessments as those from obese or aged females to definitively demonstrate the extent to which oocyte mitochondrial dysfunction contributes to unfavourable postnatal and adult health outcomes seen in offspring from obese and aged females. Another important avenue of future investigation would be to treat obese and aged females with other compounds that are known to have beneficial effects on mitochondrial function to determine if these other therapies enhance oocyte mitochondrial function and have similar favourable outcomes on ICM telomere length as with BGP-15 treatment, and promote offspring health.

As women are increasingly delaying parenthood, and with obesity becoming more prevalent in young women, there is greater imperative now than ever to understand the mechanisms underlying the decline in oocyte and embryo quality that is known to lead to decreased fertility and poorer offspring health in these contexts. The adverse impacts of maternal obesity and advanced maternal age extend well beyond fertilisation and pre-implantation embryo development and lead to increased risk of detrimental pregnancy outcomes. Health trajectories also tend to be less favourable for children born to older and obese mothers. These include shortened lifespan,

adverse cardio-metabolic, respiratory, and cognitive-related outcomes, and increased BMI, blood pressure, insulin levels, and diagnosed health conditions (Gaillard et al., 2016, 2014; Galtier-Dereure et al., 2000; Gavrilov and Gavrilova, 2012; Myrskylä and Fenelon, 2012; Ng et al., 2014; Reynolds et al., 2013), thus furthering the adversities experienced by children born to older or obese mothers. My work furthers our understanding of the origins of these disorders by implicating mitochondrial dysfunction and shortened telomeres as a key cause of sub-optimal embryo quality that stems from advanced maternal age or maternal obesity.

In parallel, development of therapies to rescue adverse oocyte and embryo phenotypes to allow higher rates of successful embryo development, and to enable offspring the best chance at a long health-span and life-span are of utmost importance. Such interventions might include other mitochondria-targeted therapies such as metformin, MitoQ, and NAD+ boosters that are known to improve mitochondrial function and are emerging as potentially beneficial for fertility. Aside from therapeutics, lifestyle modifications including diet and exercise may also prove effective at restoring adverse oocyte and embryo phenotypes. These are important areas for future clinical investigation. Therefore, development of safe, therapeutic interventions to improve oocyte and embryo quality, and ultimately pregnancy outcomes and offspring health, have the potential to lessen potential adverse outcomes in children.

Conclusion

This research extends our understanding of the patterns of telomere elongation during pre-implantation embryogenesis and identifies how telomere length is compromised in situations of perturbed fertility. Further, models of inhibition and promotion of mitochondrial bioenergetics elucidates a mechanism by which telomere elongation is regulated by mitochondrial function, thereby discovering a novel relationship between mitochondria and telomere biology. This work has broadened our understanding of the roles of mitochondrial function in early embryogenesis, and how this is linked with telomere elongation. Further, the identification of new strategies to positively modulate telomere elongation during development holds promise for improving the healthspan and extending lifespan of future generations.

6.2 References

Ahmed, S., Passos, J.F., Birket, M.J., Beckmann, T., Brings, S., Peters, H., Birch-Machin, M.A., von Zglinicki, T., Saretzki, G., 2008. Telomerase does not counteract telomere shortening but protects mitochondrial function under oxidative stress. Journal of Cell Science 121, 1046–1053. https://doi.org/10.1242/jcs.019372

Boroviak, T., Nichols, J., 2017. Primate embryogenesis predicts the hallmarks of human naïve pluripotency. Development 144, 175–186. https://doi.org/10.1242/dev.145177

Braude, P., Bolton, V., Moore, S., 1988. Human gene expression first occurs between the four- and eight-cell stages of preimplantation development. Nature 332, 459–461. https://doi.org/10.1038/332459a0

Gaillard, R., Santos, S., Duijts, L., Felix, J.F., 2016. Childhood Health Consequences of Maternal Obesity during Pregnancy: A Narrative Review. Annals of Nutrition and Metabolism 69, 171–180. https://doi.org/10.1159/000453077

Gaillard, R., Steegers, E.A.P., Duijts, L., Felix, J.F., Hofman, A., Franco, O.H., Jaddoe, V.W.V., 2014. Childhood Cardiometabolic Outcomes of Maternal Obesity During Pregnancy: The Generation R Study. Hypertension 63, 683–691. https://doi.org/10.1161/HYPERTENSIONAHA.113.02671

Galtier-Dereure, F., Boegner, C., Bringer, J., 2000. Obesity and pregnancy: complications and cost. The American Journal of Clinical Nutrition 71, 1242S-1248S. https://doi.org/10.1093/ajcn/71.5.1242s

Gavrilov, L.A., Gavrilova, N.S., 2012. Biodemography of Exceptional Longevity: Early-Life and Mid-Life Predictors of Human Longevity. Biodemography and Social Biology 58, 14–39. https://doi.org/10.1080/19485565.2012.666121

Gilchrist, G., Kurjanowicz, P., Mereilles, F., King, W., LaMarre, J., 2015. Telomere Length and Telomerase Activity in Bovine Pre-implantation Embryos *In Vitro*. Reproduction in Domestic Animals 50, 58–67. https://doi.org/10.1111/rda.12449

Iqbal, K., Kues, W.A., Baulain, U., Garrels, W., Herrmann, D., Niemann, H., 2011. Species-Specific Telomere Length Differences Between Blastocyst Cell Compartments and Ectopic Telomere Extension in Early Bovine Embryos by Human

Telomerase Reverse Transcriptase. Biology of Reproduction 84, 723–733. https://doi.org/10.1095/biolreprod.110.087205

Liu, L., Bailey, S.M., Okuka, M., Muñoz, P., Li, C., Zhou, L., Wu, C., Czerwiec, E., Sandler, L., Seyfang, A., Blasco, M.A., Keefe, D.L., 2007. Telomere lengthening early in development. Nature Cell Biology 9, 1436–1441. https://doi.org/10.1038/ncb1664

Meerdo, L.N., Reed, W.A., White, K.L., 2005. Telomere-to-Centromere Ratio of Bovine Clones, Embryos, Gametes, Fetal Cells, and Adult Cells. Cloning and Stem Cells 7, 62–73. https://doi.org/10.1089/clo.2005.7.62

Myrskylä, M., Fenelon, A., 2012. Maternal Age and Offspring Adult Health: Evidence From the Health and Retirement Study. Demography 49, 1231–1257. https://doi.org/10.1007/s13524-012-0132-x

Ng, S.-K., Cameron, C.M., Hills, A.P., McClure, R.J., Scuffham, P.A., 2014. Socioeconomic disparities in prepregnancy BMI and impact on maternal and neonatal outcomes and postpartum weight retention: the EFHL longitudinal birth cohort study. BMC Pregnancy and Childbirth 14. https://doi.org/10.1186/1471-2393-14-314

Reynolds, R.M., Allan, K.M., Raja, E.A., Bhattacharya, S., McNeill, G., Hannaford, P.C., Sarwar, N., Lee, A.J., Bhattacharya, S., Norman, J.E., 2013. Maternal obesity during pregnancy and premature mortality from cardiovascular event in adult offspring: follow-up of 1 323 275 person years. BMJ 347, f4539–f4539. https://doi.org/10.1136/bmj.f4539

Ross, C., Boroviak, T.E., 2020. Origin and function of the yolk sac in primate embryogenesis. Nature Communications 11. https://doi.org/10.1038/s41467-020-17575-w

Wang, F., Pan, X., Kalmbach, K., Seth-Smith, M.L., Ye, X., Antumes, D.M.F., Yin, Y., Liu, L., Keefe, D.L., Weissman, S.M., 2013. Robust measurement of telomere length in single cells. Proc. Natl. Acad. Sci. U.S.A. 110, E1906-1912. https://doi.org/10.1073/pnas.1306639110